NEW ELEMENTS AND RESPONSE MODES

IN FLAME PHOTOMETRY

by

Xunyun Sun

Submitted in partial fulfilment of the requirements
for the degree of Ph.D. in chemistry

at
Dalhousie University
Halifax, Nova Scotia

February, 1993

ISBN 0-315-87498-8

Canada

Name XUNYUN SUN

Dissertation Abstracts International is arranged by broad general subject categories Please select the one subject which most nearly describes the content of your dissertation Enter the corresponding four digit code in the spaces provided

ANALYTICAL CHEMISTRY
SUBJECT TERM

0486
SUBJECT CODE

U·M·I

Subject Categories

THE HUMANITIES AND SOCIAL SCIENCES

COMMUNICATIONS AND THE ARTS
- Architecture 0729
- Art History 0377
- Cinema 0900
- Dance 0378
- Fine Arts 0357
- Information Science 0723
- Journalism 0391
- Library Science 0399
- Mass Communications 0708
- Music 0413
- Speech Communication 0459
- Theater 0465

EDUCATION
- General 0515
- Administration 0514
- Adult and Continuing 0516
- Agricultural 0517
- Art 0273
- Bilingual and Multicultural 0282
- Business 0688
- Community College 0275
- Curriculum and Instruction 0727
- Early Childhood 0518
- Elementary 0524
- Finance 0277
- Guidance and Counseling 0519
- Health 0680
- Higher 0745
- History of 0520
- Home Economics 0278
- Industrial 0521
- Language and Literature 0279
- Mathematics 0280
- Music 0522
- Philosophy of 0998
- Physical 0523
- Psychology 0525
- Reading 0535
- Religious 0527
- Sciences 0714
- Secondary 0533
- Social Sciences 0534
- Sociology of 0340
- Special 0529
- Teacher Training 0530
- Technology 0710
- Tests and Measurements 0288
- Vocational 0747

LANGUAGE, LITERATURE AND LINGUISTICS
- Language
  - General 0679
  - Ancient 0289
  - Linguistics 0290
  - Modern 0291
- Literature
  - General 0401
  - Classical 0294
  - Comparative 0295
  - Medieval 0297
  - Modern 0298
  - African 0316
  - American 0591
  - Asian 0305
  - Canadian (English) 0352
  - Canadian (French) 0355
  - English 0593
  - Germanic 0311
  - Latin American 0312
  - Middle Eastern 0315
  - Romance 0313
  - Slavic and East European 0314

PHILOSOPHY, RELIGION AND THEOLOGY
- Philosophy 0422
- Religion
  - General 0318
  - Biblical Studies 0321
  - Clergy 0319
  - History of 0320
  - Philosophy of 0322
- Theology 0469

SOCIAL SCIENCES
- American Studies 0323
- Anthropology
  - Archaeology 0324
  - Cultural 0326
  - Physical 0327
- Business Administration
  - General 0310
  - Accounting 0272
  - Banking 0770
  - Management 0454
  - Marketing 0338
- Canadian Studies 0385
- Economics
  - General 0501
  - Agricultural 0503
  - Commerce Business 0505
  - Finance 0508
  - History 0509
  - Labor 0510
  - Theory 0511
- Folklore 0358
- Geography 0366
- Gerontology 0351
- History
  - General 0578
  - Ancient 0579
  - Medieval 0581
  - Modern 0582
  - Black 0328
  - African 0331
  - Asia, Australia and Oceania 0332
  - Canadian 0334
  - European 0335
  - Latin American 0336
  - Middle Eastern 0333
  - United States 0337
- History of Science 0585
- Law 0398
- Political Science
  - General 0615
  - International Law and Relations 0616
  - Public Administration 0617
- Recreation 0814
- Social Work 0452
- Sociology
  - General 0626
  - Criminology and Penology 0627
  - Demography 0938
  - Ethnic and Racial Studies 0631
  - Individual and Family Studies 0628
  - Industrial and Labor Relations 0629
  - Public and Social Welfare 0630
  - Social Structure and Development 0700
  - Theory and Methods 0344
- Transportation 0709
- Urban and Regional Planning 0999
- Women's Studies 0453

THE SCIENCES AND ENGINEERING

BIOLOGICAL SCIENCES
- Agriculture
  - General 0473
  - Agronomy 0285
  - Animal Culture and Nutrition 0475
  - Animal Pathology 0476
  - Food Science and Technology 0359
  - Forestry and Wildlife 0478
  - Plant Culture 0479
  - Plant Pathology 0480
  - Plant Physiology 0817
  - Range Management 0777
  - Wood Technology 0746
- Biology
  - General 0306
  - Anatomy 0287
  - Biostatistics 0308
  - Botany 0309
  - Cell 0379
  - Ecology 0329
  - Entomology 0353
  - Genetics 0369
  - Limnology 0793
  - Microbiology 0410
  - Molecular 0307
  - Neuroscience 0317
  - Oceanography 0416
  - Physiology 0433
  - Radiation 0821
  - Veterinary Science 0778
  - Zoology 0472
- Biophysics
  - General 0786
  - Medical 0760

EARTH SCIENCES
- Biogeochemistry 0425
- Geochemistry 0996
- Geodesy 0370
- Geology 0372
- Geophysics 0373
- Hydrology 0388
- Mineralogy 0411
- Paleobotany 0345
- Paleoecology 0426
- Paleontology 0418
- Paleozoology 0985
- Palynology 0427
- Physical Geography 0368
- Physical Oceanography 0415

HEALTH AND ENVIRONMENTAL SCIENCES
- Environmental Sciences 0768
- Health Sciences
  - General 0566
  - Audiology 0300
  - Chemotherapy 0992
  - Dentistry 0567
  - Education 0350
  - Hospital Management 0769
  - Human Development 0758
  - Immunology 0982
  - Medicine and Surgery 0564
  - Mental Health 0347
  - Nursing 0569
  - Nutrition 0570
  - Obstetrics and Gynecology 0380
  - Occupational Health and Therapy 0354
  - Ophthalmology 0381
  - Pathology 0571
  - Pharmacology 0419
  - Pharmacy 0572
  - Physical Therapy 0382
  - Public Health 0573
  - Radiology 0574
  - Recreation 0575
  - Speech Pathology 0460
  - Toxicology 0383
- Home Economics 0336

PHYSICAL SCIENCES

Pure Sciences
- Chemistry
  - General 0485
  - Agricultural 0749
  - Analytical 0486
  - Biochemistry 0487
  - Inorganic 0488
  - Nuclear 0738
  - Organic 0490
  - Pharmaceutical 0491
  - Physical 0494
  - Polymer 0495
  - Radiation 0754
- Mathematics 0405
- Physics
  - General 0605
  - Acoustics 0986
  - Astronomy and Astrophysics 0606
  - Atmospheric Science 0608
  - Atomic 0748
  - Electronics and Electricity 0607
  - Elementary Particles and High Energy 0798
  - Fluid and Plasma 0759
  - Molecular 0609
  - Nuclear 0610
  - Optics 0752
  - Radiation 0756
  - Solid State 0611
- Statistics 0463

Applied Sciences
- Applied Mechanics 0346
- Computer Science 0984
- Engineering
  - General 0537
  - Aerospace 0538
  - Agricultural 0539
  - Automotive 0540
  - Biomedical 0541
  - Chemical 0542
  - Civil 0543
  - Electronics and Electrical 0544
  - Heat and Thermodynamics 0348
  - Hydraulic 0545
  - Industrial 0546
  - Marine 0547
  - Materials Science 0794
  - Mechanical 0548
  - Metallurgy 0743
  - Mining 0551
  - Nuclear 0552
  - Packaging 0549
  - Petroleum 0765
  - Sanitary and Municipal 0554
  - System Science 0790
- Geotechnology 0428
- Operations Research 0796
- Plastics Technology 0795
- Textile Technology 0994

PSYCHOLOGY
- General 0621
- Behavioral 0384
- Clinical 0622
- Developmental 0620
- Experimental 0623
- Industrial 0624
- Personality 0625
- Physiological 0989
- Psychobiology 0349
- Psychometrics 0632
- Social 0451

I faithfully dedicate this thesis to the Sun family.

Table of Contents

List of Figures

List of Tables

Abstract

The non-linear (approximately quadratic) response has been the one major impediment to the use of the flame photometric detector (FPD) for the gas chromatography (GC) of organosulfur compounds. Two and half decades after the introduction of the GC-FPD, a *linear* sulfur emitter has finally been found, and is introduced in this thesis The new emitter produces a linear response over four orders of magnitude. The minimum detection limit reaches 7×10^{-13} mol S/s at S/N = 2

In this thesis, a variety of organometallic compounds containing transition metals — Ru, Ni, Mn, Fe, Os, Re, Mo and Co — have been determined by GC-FPD The responses have been optimized for individual elements In a filte-less mode, and at optimized conditions, the detection limits (S/N = 2) range from 2 pg or 1×10^{-15} mol/s for ruthenocene to 5 ng or 3×10^{-12} mol/s for cobaltocene All these transition elements respond in a linear manner. The elemental selectivities *vis-à-vis* carbon in the filter-less mode range from 4×10^{5} (for ruthenium) to 1.5×10^{2} (for cobalt) The quenching effects caused by co-eluting hydrocarbon compounds are negligible The FPD spectra of these transition metals, some main-group elements, and several types of carbon compounds are obtained at analytical conditions A variety of atomic (as opposed to molecular) transitions are found to occur from levels as high as 3.6 eV above ground state.

The selectivities of various transition elements against hydrocarbons have been defined in (1) single-channel filter-less, (2) single-channel filter, and (3) dual-channel differential modes The metal-carbon selectivities are improved by one to two orders of magnitude by operating the detector not in the conventional single-channel filter mode but in the dual-channel differential mode The latter mode makes it possible to increase the selectivity of one hetero-element over the other, and to distinguish between two hetero-elements by oppositely directed peaks in a matrix of carbon compounds

A further dual-channel selective mode - conditional access (CONDAC) chromatography - has also been developed and tested CONDAC is able to generate chromatograms which are nominally specific (infinitely selective) for any chosen FPD-active element

Abbreviations

AAS: Atomic Absorption Spectroscopy (1)

AFID: Alkali Flame Ionization Detector (13)

AW: Acid Washed (23)

BC: Baseline Correction (41)

BP: BandPass (148)

CHROM: CHROMatograms (a computer program name) (35)

CONDAC: CONditional ACcess (14)

cw: complex wide (140)

ECD: Electron Capture Detector (1)

EDF: Exponential Dilution Flask (28)

FID: Flame Ionization Detector (3)

FPD: Flame Photometric Detector (1)

FTIR: Fourier Transform Infrared (14)

GC: Gas Chromatography (1)

i.d.: inner diameter (23)

ICP: Inductively Coupled Plasma (2)

IUPAC: International Union of Pure and Applied Chemistry (50)

LP: Long-Pass (interference filters) (70)

MDA: Minimum Detectable Amount (11)

MECA: Molecular Emission Cavity Analysis (151)

MIP: Microwave Induced Plasma (1)

MMT: Methylcyclopentadienyl Manganese Tricarbonyl (109)

MS: Mass Spectroscopy (1)

PMT: PhotoMultiplier Tube (2)

RC: Resistor Capacitor (29)

RRC: Response Ratio Chromatogram (39)

S_A: Slope in channel 1 (38)

S_B: Slope in channel 2 (38)

S/N: Signal/Noise (22)

SP: Short-Pass (interference filters) (70)

SR: Slope Ratio (38)

Acknowledgements

I am deeply indebted to my supervisor Dr. Walter A. Aue for his valuable and intelligent direction and supervision for the research that this thesis is based on. I wish to thank Brian Millier; without his assistance some of the results of this thesis would have been impossible to achieve.

Many thanks go to Dr. Youzhi Tang, Kevin Thurbide, Hameraj Singh, Nancy Lowery, and Jennifer Gebhardt for their assistance in the laboratory. I am grateful to the members of my supervisory committee Professors Amares Chatt, Robert D. Guy, Jim A. Pincock and Roger Stephens for reading and correcting this thesis. I should also like to acknowledge Wayne LeMoine, Christopher Wright, Jürgen Müller, Rick Conrad, the stock room staff and the departmental secretaries for their various forms of assistance during my pleasant years in the Chemistry Department.

I wish to thank the Chinese Authorities for their financial support during my first year at Dalhousie, and Dalhousie University for my graduate fellowship. This research was supported by NSERC grant A—9604.

Chapter 1. INTRODUCTION

Gas chromatography (GC) is well known for its high efficiency of separation and great accuracy of detection. It is one of the most successful new analytical techniques developed in the last few decades, not only for its powerful and unique analytical capability but also for its wide recognition. The technique has become indispensable in all analytical laboratories where isolation and detection of organic sample components (sometimes even inorganic) is practiced.

While the chromatographic column carries out the separations in a GC system, the detector(s) signals the presence of analytes in column effluents quantitatively and/or qualitatively. There exist, in general, two types of GC detectors: universal and selective detectors. A genuine selective detector should provide not only sensitive and quantitative detection, but - sometimes more importantly - qualitative information according to the analyst's interest. The latter is met by the detector's ability of accentuating the response to important analytes, and of diminishing the response to unimportant matrix components. Because of this unique feature, selective detection of GC column effluent has been one of the most active research areas since the first important selective detector — the electron capture detector (ECD) — was built in 1960. Today, there are many excellent selective detectors commercially available (including those in "hyphenated" techniques such as GC-MS, GC-AAS, GC-MIP *etc.*). The flame photometric detector (FPD) is one of them.

Since its commercial inception, the flame photometric detector has become very important for monitoring sulfur, phosphorus and many other elements of concern. Besides the high sensitivity and selectivity, its simplicity, stability, ease of

operation and comparatively low price all contribute to its great popularity.

The FPD employs a cool air-rich hydrogen/air diffusion flame as its emission source. The light detecting system normally consists of a photomultiplier tube (PMT) and a band-pass filter. The detector seems extremely simple compared to some spectrometers with modern excitation sources, *e.g.* microwave induced plasma (MIP), inductively coupled plasma (ICP), *etc.* However, as in many areas, simplicity has helped, not hindered, its further development over the years. The detector's history reveals not only the problems it suffered but also the developments it experienced.

1.1 Problems, Solutions and Further Developments — A Brief History of the Flame Photometric Detector

The principle of the FPD is that a sulfur (or phosphorus) containing compound produces blue (or green) chemiluminescence in a small, fuel-rich hydrogen/air flame. This chemiluminescent phenomenon has been known since more than 100 years, and a detector based on the phenomenon was built in 1962[1] for detecting sulfur and/or phosphorus from air. In 1966, Brody and Chaney[2] successfully adapted the detector to gas chromatography. It became known as the first-generation FPD ("Melpar"). The detector provided highly selective and sensitive detection for sulfur and phosphorus following GC separation. In that first report[2], the researchers successfully demonstrated the flame photometric detection of sulfur compounds from gasoline, and pesticide residues from vegetables.

Since then, several versions of the detector, designed by different manufacturers, became commercially available. Although two and half decades have passed, the detection limits for sulfur (1×10^{-10} g/s) and phosphorus (1×10^{-12} g/s)

reported by the Brody and Chaney[2], have not improved much. Still, many other modifications have been made that are truly remarkable.

In the Brody and Chaney model, a mirror was placed behind the flame because it was thought necessary to increase light input to the PMT. However, it was found later that the reflector made no contribution at all to the detector's detection limits (*i.e.* the signal/noise ratio remained the same with or without the mirror). Bowman and Beroza[3] constructed the first dual-channel FPD by replacing the mirror with a second filter/photomultiplier combination. The dual-channel flame photometric system made simultaneous determination of sulfur and phosphorus possible. From the response ratio of phosphorus to sulfur, the atomic ratio of the two elements in a molecule could be estimated. This dual-channel construction can now be found in many commercial detectors.

If the flame in the FPD plays the role of a heart (a metaphor used in the literature), then the detector suffered severe heart attacks in its youth. The injected solvent (1 μL or more) would easily extinguish the flame. To solve the problem, several remedies were suggested. Most directly, Watts[4] simply vented part of the solvent before it entered the detector to protect the flame. Obviously, the ventilation process caused a time delay. Winnett[5] renovated an electrical igniter to restore the flame after the solvent had passed the detector burner. The igniter made the detector workable, but it did not prevent extinction of the flame. Burgett and Green[6,7] simply switched the detector's hydrogen and air inlets, *i.e.* hydrogen (instead of air) was premixed with the column effluent and going through the outer path. This new configuration produced a so-called oxygen-hyperventilated flame, which was similar to that of the conventional flame ionization detector (FID). Surprisingly, this minor change made the detector withstand solvent injections as large

as 50 μL. The detection limits with this new flow arrangement were also slightly improved. Most (if not all) of the commercial FPD's have followed this simple yet extremely beneficial switch in design. It was noticed that the dual-flame detectors[8,9] did not suffer from flame extinction at all, although the dual flames were not initially designed for this purpose.

Once the traditional single flame was replaced by a dual-flame system[8,9], the detector displayed better selectivity, less quenching effect, and less dependence of sulfur response on structure. However, dual flames were somehow less sensitive than the single one. The designers[8,9] described the role of the first (lower) flame, which is hydrogen-rich, to decompose samples, and the second (upper) flame to produce light emission from S_2 and HPO. Despite the advantages reported by the inventors, the dual-flame FPD is still seeking general acceptance.

The inefficiency of the initial air-cooled heat sink, which was designed to protect the photomultiplier tube from being over-heated, limited the detector to temperatures below 200 °C. Dale and Hughes[10] modified the Melpar FPD with a water-cooled coil, which was inserted between the photomultiplier tube and the flame area. This modification allowed the detector to operate at temperatures as high as 250 °C. Although certain later research[11] showed that the detector was somewhat more sensitive to sulfur at low temperatures, the high temperature at least helped to prevent formation of residues in the detector.

The non-linear nature of sulfur response is one of the most difficult FPD problems to solve. The early approaches to the dilemma essentially focused on correcting the response by algorithmic or electronic means. Attar and co-workers[12] established a two-parameter calibration model to minimize the errors caused by non-linearity. As reported, the method produced better results than the normal calibration

method, but the precision could still be affected by sample size, column temperature, rate of temperature programming, *etc.*. The relationship between the FPD output and the concentration of sulfur could be linearized[9] with the aid of an electronic device, provided the exponential response factor was known. However, that factor is subject to change due to a variety of reasons. The electronic methods often suffered tremendously from this uncertainty of the non-linearity factor, since the techniques did not solve the problem of sulfur's second-order emission. In other words, the radiation remained non-linear. Aue and Flinn[13] tackled the problem chemically by making use of the second-order kinetics. They reported that the detector could produce a linear response to sulfur by simply doping the flame with a volatile sulfur compound, which created a constant background of sulfur emission and rendered the analyte signal pseudo first-order. A better detection limit for sulfur was simultaneously obtained.

Another inherent problem of the FPD is that the response to hetero-atoms (especially sulfur) can be quenched by co-eluting and/or background (*e.g.* column bleed) hydrocarbon compounds, or even by the carbonaceous part of the sulfur compound itself. Many studies[14-17] have investigated the nature of quenching and its mechanism, but none has developed an effective way to prevent the quenching from happening. However, Patterson[9] claimed that the quenching problem could be eliminated by his dual-flame FPD. More recently, Liu and Fu[18] proposed a critical way of evaluating the quenching effects.

Other major modifications of the FPD included different flame burner designs[19], interference filter removal[20], various flame chimney constructions[21] (which favour surface luminescence), pulsed flame[22], *etc.*

1.2 Response Characteristics of Sulfur and Phosphorus

The GC-FPD system has been successfully applied to detecting sulfur and phosphorus from pesticide residues, air pollutants, petroleum related products, *etc.* Theoretical studies concerned with the luminescence mechanism, spectrum interpretation, response optimization, *etc*, have all been undertaken.

1.2.1 Sulfur

In photometric detection, a spectrum provides important information in two aspects: (1) from the band (or line) wavelengths, the emitting species might be identified and thereby knowledge regarding the emission mechanism(s) may possibly be gained; (2) by locating the most intense emission bands, optimization can be carried out in terms of the best sensitivity and/or selectivity. The spectrum of sulfur in the FPD flame was therefore measured as soon as the detector was invented[2]. The electronic S_2 spectrum, with its typical pattern of vibrational levels, consists of a large number of approximately equally-spaced sharp bands from about 300 to 500 nm. The most intense band is found between 390 and 400 nm, and so a 394 nm band-pass filter is usually associated with the FPD for isolating sulfur's major emission. This extensive spectral feature of S_2 often causes sulfur interference to the detection of phosphorus and other FPD-active elements.

Information obtained from laser fluorescence[23] about sulfur chemistry in fuel-rich hydrogen/air flames supported the chemiluminescent mechanisms proposed by Sugiyama and co-workers[15,24]. The main reactions involved in the emission processes were described by the authors as follows:

$$\text{SULFUR COMPOUND} \rightarrow H_2S \qquad (1.1)$$

$$H_2S + H \rightleftharpoons HS + H_2 \qquad (1.2)$$

$$HS + H \rightleftharpoons S + H_2 \quad (1.3)$$

$$S + S + M \rightarrow S_2^* + M \quad (1.4)$$

$$S_2 + H + H \rightarrow S_2^* + H_2 \quad (1.5)$$

$$S_2^* \rightarrow S_2 + h\nu \quad (1.6)$$

where M is a third body.

Although knowledge concerning these and other possible processes is still incomplete, it is believed that S_2^* is the predominant emission species at wavelengths from 300 to 450 nm[2]. Other species such as SO^* and SH^* may be responsible for the minor bands of the spectrum. This assignment can easily explain the approximately quadratic sulfur response. Note that the term "quadratic response", used in the literature, indicates the relationship of analyte concentration with quadratic detector signal. "Quadratic" means a simple square function (n = 2); it is not derived from the "quadratic equation" with its additional constant and linear terms.

While the diatomic nature of the predominant emitter S_2 suggests bimolecular kinetics, the apparent reaction order varies. Most values of the response exponent fall between 1.8 and 2.2[25], but the total observed spread is much wider[12,26-28]. The reasons for deviation from the theoretical value include non-optimum flame conditions, compound-dependent decomposition, competitive flame reactions, non-Gaussian sample introduction, quenching effects, *etc.* This handicap of non-linear response can easily impair precision, and it has therefore limited the detector considerably in quantitative determination of sulfur-containing compounds. The current enigmas and practical usage of the FPD in sulfur mode have recently been well reviewed by Farwell and Barinaga[29].

To optimize the FPD response, hydrogen and air flow rates (or H_2/air ratio), carrier gas flow rate, detector temperature, voltage applied to the PMT's, and interference filter specifications are usually the parameters to consider. "Optimization" is an equivocal expression here, because operational conditions for the best detection limit may be, and often are, different from those for the best selectivity. Also, optimum conditions may be different for detectors made by different manufacturers. Although the definition of "optimum conditions" is rather ambiguous, and there are no conditions suitable for all detectors, a rough range of specifications of the detector reflecting the performance of the sulfur mode can be summarized from the literature. The minimum detectable mass flow rates range from about 5×10^{-11} to 2×10^{-12} g/s of sulfur. A linear range of about two orders of magnitude can be obtained from the sulfur-doping operation. The selectivity depends on the amount of sulfur introduced (due to the quadratic response), and varies from 10^3 gC/gS at low sulfur amounts to greater than 10^6 gC/gS at high sulfur amounts.

1.2.2 Phosphorus

The phosphorus spectrum is simple compared with that of sulfur. It consists of three main bands. The most intense one is located between 520 and 530 nm. Therefore, a 526 nm band-pass filter is often considered the "typical" phosphorus filter. The emitter has been identified as HPO^*. The phosphorus compounds first decompose to PO in the flame, then HPO^* is formed through the reaction

$$PO + H + M \rightarrow HPO^* + M,$$

as proposed by Syty and Dean[30]. Gilbert[31], however, assumed another reaction:

$$PO + OH + H_2 \rightarrow HPO^* + H_2O$$

Both reactions were based on the assumption of chemiluminescent mechanisms. Many people believed that other types of reactions might also be involved in the chemiluminescent processes.

The HPO^* emission mechanism suggests a linear dependence of response on the amounts of phosphorus. Numerous experiments have proved this expectation correct. The FPD's flow conditions in the phosphorus mode are usually different from those in the sulfur mode. It was reported[8], however, that the optimized flow rates of hydrogen and oxygen (or air) for both operational modes were identical for a dual-flame detector. Typical phosphorus detection limits range from 2×10^{-12} gP/s to 1×10^{-13} gP/s, which are about one order of magnitude better than those for sulfur. The linear range usually exceeds 3 orders of magnitude. The selectivity of phosphorus against carbon can be greater than 5×10^5 gC/gP.

1.3 Other Uses of the FPD

The FPD is based on the chemiluminescence of sulfur and phosphorus and was originally dedicated to detecting these two elements. Can elements other than sulfur and phosphorus produce analytically useful chemiluminescence in the small fuel-rich hydrogen/air flame? Researchers have wondered this since the detector was first developed. The answer is clearly in the affirmative. Boron was found to respond with useful sensitivity in the FPD as early as 1971[32]. Two years later, Ross and Shafik[33] reported the flame photometric detection of chromium from physiological fluids. In the same year, Aue and Hastings[20] found that many organometallic compounds were potentially detectable in their filter-less FPD.

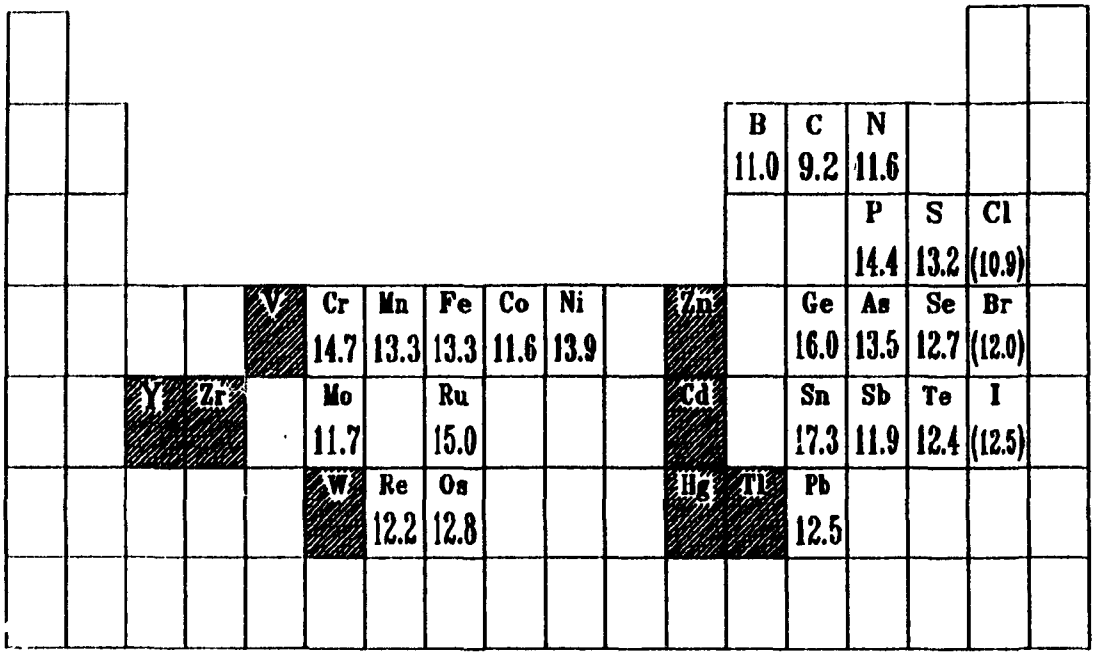

Figure 1.1 *Approximate overview of "best" FPD detection limits in -log(mole of element per second) at S/N = 2. Halogens: as copper or indium halides. Hatched rectangles: no significant response (own experiments).*

More recently, the FPD responses of tin, germanium, selenium, and many other elements have been characterized. Some of them are even more sensitive than phosphorus. (In fact, tin produces the strongest emission among the known FPD-detectable elements.) Figure 1.1 summarizes the FPD detection limits for elements whose responses have been optimized. All the data were taken from the literature available at the time of writing this thesis. Estimates were made on the few elements where the original literature did not report detection limits in gram or mole per second. Note that the Table includes some already published data from this thesis.

1.3.1 Tin and Germanium

A series of studies, conducted by Aue and Flinn[21,34-37] showed that the FPD was extremely sensitive to tin and germanium. The tin emissions had been classified as so called "gas phase" luminescence and "surface" luminescence. In a conventional FPD, a red emission from SnH^* (at 610 nm) and a green emission from SnO^* or $SnOH^*$ takes place in the flame region. If the normal or modified quartz chimney surrounding the flame provides an extremely clean surface, a blue emission will be observed from the quartz surface. The emitter(s) remains unidentified. The surface mode has better sensitivity for tin compounds, despite the peak tailing observed in most cases. The minimum detectable amount (MDA) is as low as about 0.1 picograms of tetrapropyltin. This surprisingly low MDA has made tin the most sensitive species in the FPD.

The response characteristics of germanium were found similar to those of tin. Both "gas phase" and "surface" luminescence were observed from the detector flame and from the walls of the quartz chimney. As mentioned above for tin, the germanium emission from the quartz surface was more intense than that from the gas phase. The detector responded to both tin and germanium in a linear fashion.

1.3.2 Selenium and Tellurium

Similar to sulfur, selenium and tellurium[38] had approximately quadratic response in the FPD. The spectra displayed dominant Se_2 and Te_2 emission bands. The detector performances for Se and Te were fully optimized. Sub-nanogram detection limits of the test compounds were obtained for both elements. Aue and Flinn[13] also established and explained a chemical method to linearize the response of these three chalcogens (S, Se and Te) simultaneously.

1.3.3 Boron, Chromium and Arsenic

The FPD response to boron hydrides was characterized by Sowinski and Suffet[32,39]. A hot flame, with approximately stoichiometric proportions of hydrogen and oxygen, was employed to improve sensitivity. The emitting species was believed to be mainly BO. The 546 nm band was chosen for further optimization. The detection limit was reported as 0.71 ng of $B_{10}H_{14}$. The detector displayed a linear response to boron.

Ross and Shafik[33] adapted a Melpar FPD for responding to chromium. Their work was aimed at applying the FPD to detect organochromium compounds in physiological fluids. A 425.4 nm band-pass filter was selected arbitrarily (arbitrarily, because no FPD spectrum of Cr at the *analytical* conditions was then reported) to favour the chromium response. Burgett and Green[7], however, monitored the chromium emissions at 520 nm in a hot H_2/O_2 flame, and claimed a much better detection limit of about 2×10^{-15} mole/s. No identification was made as to the emitting species. It should be mentioned that chromium was the only transition metal whose FPD response had been optimized and used at the commencement of this thesis project.

The arsenic emission was first used by Zado and Juvet[40] for detecting $AsCl_3$ in a lab-developed flame photometric device coupled to a GC system. More typically, Kapila and Vogt[19] reported GC flame photometric detection of arsenic in a conventional FPD. Sub-nanogram detection for triphenylarsenic was obtained, its response was linear over more than three orders of magnitude, and selectivity versus carbon was greater than 10^3. The emitters were not fully identified, but the authors implied that AsO was responsible for the spectral continuum.

1.3.4 Halogen Compounds

Halogen compounds, by themselves, do not produce analytically significant emissions in the FPD flame. However the emissions can be intensified tremendously by the presence of indium or copper. Usually, indium and copper are present in the shape of a foil, which is in close proximity to the flame. In the copper sensitised mode[41,42], the emitters were identified as CuOH, CuO, CuH, and copper halides. The response was found to be nonlinear. It was linearized by doping the flame with small amounts of the responding element (with copper present) by Tang and Aue[43]. In this doping mode, the detector sensitivity was dramatically increased as well.

The indium-induced emissions were those of indium halides. The dual-flame FPD[44,45] was believed most suitable as an indium-sensitized halogen detector. The compounds first decomposed in the lower flame, then the fragments reacted with indium to form indium halides in between the two flames, where an indium-coated copper tube was positioned. The emissions were viewed in the upper flame. This detection mode provided very good detection limits (1×10^{-11} g/s for Cl), selectivity (10^3 — 10^4 gC/gCl) and linear responses for chlorine, bromine and iodine. Versino and Rossi[46] have investigated the possibility of simultaneously detecting sulphur and/or phosphorus from the first flame, and organochlorine from the second flame.

The sodium emission in an alkali flame ionization detector (AFID) could be affected by combustion of a halogen compound in the flame. Aue and Moseman[47] found that the signals, corresponding to atomic sodium emission, could be either positive or negative. The latter (inverted peaks) could, as concluded by the authors, be used in qualitative analysis. From a quantitative viewpoint, this "sodium

FPD" was found to have a good linear range and sub-nanogram sensitivity to halogen-containing compounds[48].

1.3.5 Others

In a "filter-less" mode FPD, Aue and Hastings[20] examined the behaviour of Fe, Sb, Pb and Bi together with some of the above-mentioned elements. Although the responses were unoptimized because of the common conditions, the capability of the FPD to respond to those elements was clearly shown.

To complete the literature review, it should be mentioned that the FPD's response to Fe, Ru, Os, Mn, Ni, Re, Mo and Co have recently been examined, optimized and reported[49-52] by our group. As far as sensitivity is concerned, nickel was close to, and ruthenium even better than phosphorus. Two novel computer-assisted techniques for operation of the FPD — the differential mode[52], and the conditional access mode[53] (CONDAC) — have been established; and the selective detection of methylcyclopentadienyl manganese tricarbonyl, and phosphorus and lead containing compounds, from gasoline have demonstrated the potential of these techniques. As part of this thesis, details will be discussed later.

1.4 Objectives

The flame photometric detector is known as a conventional GC detector. It is referred to here as "conventional", because it is widely used, handy, rugged, inexpensive and simple. It seems that this conventional GC technique has matured. In fact, a lot of attention has recently been paid to the much more complex GC-spectrophotometric detection techniques, such as GC-AAS, GC-MIP, GC-ICP, GC-FTIR, *etc.* No doubt, those frontier instruments frequently provide very good selective and sensitive detection for a variety of elements. However, those detection

devices are actually *not dedicated* to gas chromatography. The systems are often costly (because the "detector" costs much more than the GC unit), and possibly time consuming (because sometimes coupling the instruments is up to the operator). This is especially frustrating for certain types of analysis demanded of lab technicians. It would therefore be extremely valuable to make the existing, conventional FPD more competent.

To make the FPD accept new challenges, the detector has to be modified at least in two aspects: it has to respond to more elements, and it has to do so more selectively. This thesis project is particularly designed with these two goals in mind. (Note that sensitivity is another important factor which needs to be improved. However, sensitivity is of an intrinsic nature. It basically depends on the nature of the source (the small fuel-rich hydrogen/air flame), and on the light detection system. It is not included in the scope of this study except for routine flow optimization.)

1.4.1 Choice of Elements

In present and future analysis, knowledge is often required not only on the total amount of an element but also on its "speciation". The latter provides information about the element's form (species) in the samples. Such information may be of vital importance to toxicologists, biologists, clinicians, *etc.*. It has been proven that the GC-FPD system is a sensitive and selective speciation tool for sulfur and phosphorus. One of the objectives of this study is to investigate the possibility that the FPD may respond to several more elements. Although every element in the periodic table needs appropriate methods of analysis, in practice speciation of certain elements needs to be investigated much more urgently than others. In choosing

elements for this study, priority is given to those which are analytically important, and whose compounds are commercially available and readily chromatographable.

From the preceding literature review, we know that the FPD has essentially been confined to determining main-group elements. The only transition metal for which, over the years, the FPD has provided analytical trace methodology, is chromium (as the trifluoroacetylacetonate[7,33]). That is not surprising since transition metals are typically determined by emission spectrometry, which usually involves thermal excitation of atomic lines. In contrast, the FPD method involves chemiluminescence produced from a cool fuel-rich hydrogen/air flame.

However, in 1973 Aue and Hastings[20] found, by using a filter-less FPD for a general survey, that many organometallics were potentially detectable. It would seem profitable, therefore, to optimize the FPD conditions for those organometallics, and to find further transition metals that respond to the FPD with analytically interesting sensitivity.

The immediate question would be: how well can the GC system deal with the organometallic derivatives of transition metals? Transition metals occur in a wide variety of biochemical, industrial and environmental key compounds. While few of these are amenable to gas chromatography, some can be converted into volatile derivatives. More importantly, the flame photometric detector is no longer restricted to conventional gas chromatographic effluents, but is increasingly being used with capillary liquid chromatography and supercritical fluid chromatography. Both techniques are capable of dealing with analytes of low volatility.

So far, there exists no logical basis on which to predict whether a particular element will or will not respond in the FPD. Therefore, the first step of the investigation is to make injections of the test compound at common GC conditions

to see if the detector's response to the organometallic is significantly more intense than its (estimated) response to the hydrocarbon portion of the compound. Once an interesting response is obtained, flow optimization should be carried out. Following that, the spectrum is scanned at analytical conditions if the radiation is strong enough. Finally, the quenching effect caused by hydrocarbons will be examined. It should be pointed out that, in the first step of this procedure, the compound may have decomposed before reaching the detector. This is obvious if the expected peak fails to appear. However, it would be rather confusing if a peak of the carbon portion of the compound were to appear, because such a peak could have conceivably been caused by a non-metallic product from the decomposing analyte.

Some main group elements, whose responses have already been characterised, will be only involved in spectral measurements, because the spectral information, at analytical conditions, is vital for the next goal of this study — selectivity improvement.

1.4.2 Demand and Possibilities for Selectivity Improvement

Spectral interference from sulfur in detecting phosphorus was observed in the early stages of the FPD's development. The interference is caused by the extensive nature of the sulfur spectrum. Joonson and Loog[54] eliminated this spectral cross-talk by means of electronic compensation. The sulfur signal in the phosphorus channel was, as reported, reduced by a factor of 10^3.

As the knowledge of further FPD-active elements has increased, so has the awareness that one element could possibly be mistaken for another. The danger is particularly acute in highly complex, environmental samples of largely unknown composition. This is but one of several reasons why improved understanding and

control of selectivity ratios is needed - not just for each element against carbon, but for each element against all the others.

It is usually assumed that the FPD's selectivity is gained from spectral discrimination by the interference filters. However, due to the nature of their typically wide bandpass (*ca.* 10 nm), the spectral resolution of the interference filter-PMT assembly is notoriously low. In fact, selectivity in the FPD is primarily related to the respective photon yield from different elements. For instance, it has been proved that the selectivity of hetero-elements against carbon in a filter-less mode is very close (if not equal) to that in the dispersive mode. In contrast, selectivity in conventional emission spectrometry is essentially a function of spectral resolution and background correction. It could be reasonably speculated that there would be little if any selectivity in a monochromator-less mode of a conventional spectrometry source. In the FPD, the inherently low intensity of the chemiluminescence has limited further enhancement of spectral resolution. Another fact is that the FPD often monitors broad molecular bands superimposed on continua. Therefore, a narrow bandpass filter will decrease the sensitivity, rather than increase the selectivity.

It appears to be a challenge to increase selectivity on a spectrometric device with a light source that faint and a spectral resolution that low.

However, one can reason that the response of the two FPD channels, which monitor different wavelengths, must contain different spectral information. In other words, the intensity difference between the two channels should be specific for each element being scanned. This specific difference is potentially useful in identifying elements. Of course, if any two spectra happen to have the same intensity ratios at the chosen wavelengths, the identification will be impossible. But this is far from reality.

To describe the principle in detail: One channel monitors the wavelength at which the desired element responds best, but at which response from carbon compounds (or other elements) are also seen; the other monitors a wavelength where carbon responds well but response from the element-of-interest is weak (or, preferably, absent). One of the amplified outputs is then attenuated such that the carbon responses in the two channels match. The carbon response will thus vanish when one channel is subtracted from the other.

Another possible approach to improve the selectivity reverses this case with the help of a computer: If the outputs of the two channels match, they are accepted; if not, they are rejected. The total output of this algorithm would be peaks (where accepted) or a straight (zero information) baseline (where rejected). By this "conditional acceptance", specificity (*i.e.* infinite selectivity) could hopefully be obtained.

Chapter 2. EXPERIMENTAL

The basic chromatography unit used through-out this study was a Shimadzu gas chromatograph (GC 4BMPF) equipped with a dual-channel flame photometric detector.

2.1 Shimadzu FPD

Figure 2.1 is a detailed diagram of the Shimadzu dual-channel flame photometric detector. Air (or oxygen) flows through the inner tube while hydrogen, mixed with the column effluent, flows through the outer path. A flame shield (a piece of stainless steel tube) is attached on top of the burner for blocking background emissions from the flame base. The shield height is adjustable. The cylindrical quartz surrounding the flame functions as a chimney to conduct the combustion wastes, to possibly confine the luminescence region, and to physically isolate the flame. The quartz windows on both sides separate the flame chamber from the light paths, and therefore protect the interference filters and the photomultiplier tubes from the flame gases. Optical filters can be inserted between the quartz windows and photomultiplier tubes. The water cooling system guards the PMT's from being over-heated.

2.2 Detector Hardware Modifications

The analytes' luminous shape in the FPD flame was observed by dark-adapted naked eye. It was found that the strongest emissions took place at the lower part of the flame for most (if not all) of the organometallics. This observation lead to removal of the original flame shield with small but noticeable beneficial effects. (Remember that the blue sulfur luminescence takes place at the space above the flame,

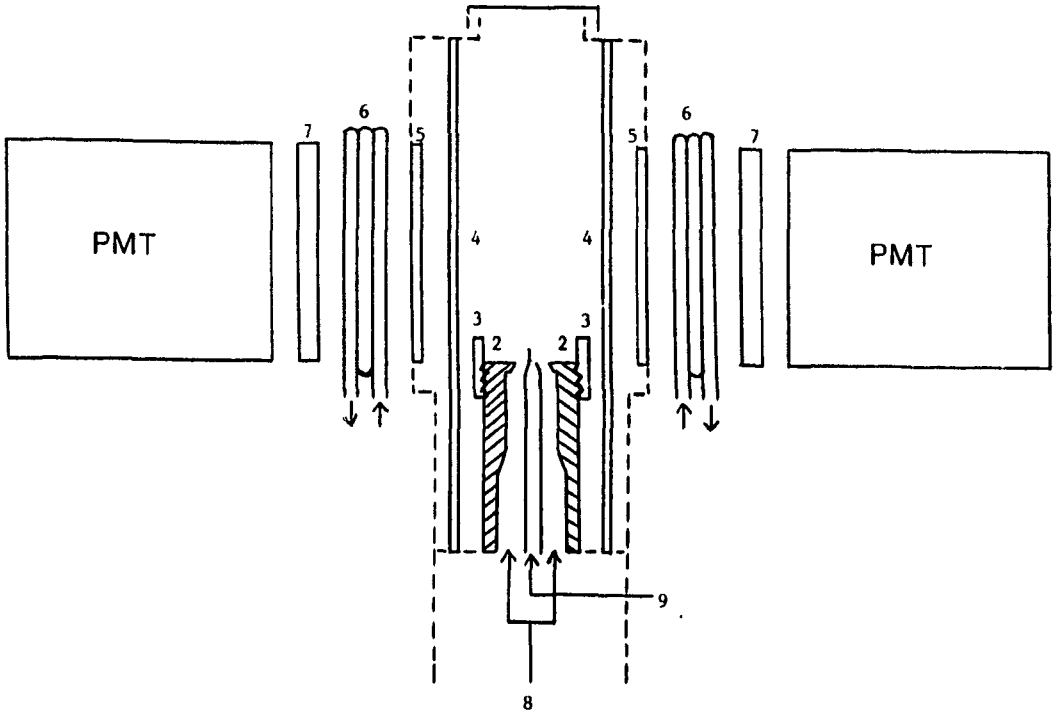

1. Burner inner nozzle; 2. Burner outer nozzle; 3. Adjustable flame shield; 4. Quartz chimney; 5. Quartz windows; 6. Water cooling coils; 7. Optical filters; 8. Hydrogen and column effluent; 9. Air (and/or oxygen)

Figure 2.1 *Detailed diagram of Shimadzu FPD.*

and fills up the quartz chimney. In such a case, the flame shield blocks off some (maybe most) background emission from the flame without reducing the radiation from the analyte.)

The quartz chimney was also removed in the optimization processes, because the unconfined flame somehow gave a better signal/noise (S/N) ratio and a more stable baseline. An additional nitrogen flow (usually from 10 to 25 mL/min)

was introduced into the flame via the hydrogen path for most of the experiments. This extra nitrogen did both increase the signal and decrease the noise slightly, but the reason for this remains unknown.

2.3 General Chromatographic Conditions

Three different packed columns were used to carry out chromatographic separation tasks for various situations. (A): 100 × 0.3 cm i.d. borosilicate glass column packed with 5% OV—101 on 100/120 mesh Chromosorb W AW; (B): the same as (A), but 5% Carbowax 20M; (C): 50 × 0.3 cm i.d. borosilicate glass column filled with 5% Carbowax 20M on 60/80 mesh Chromosorb W. Column A, with the best separation efficiency, was packed for chromatographing gasolines and complex organometallic mixtures. Column B, which provided a different stationary phase and therefore a different retention index from column A, was prepared for general use. Column C, very short and porous, and therefore well suited to very short retention time, was designed for thermally unstable organometallics such as $Ni(C_5H_5)_2$, and for less volatile compounds such as $As(C_6H_5)_3$.

The carrier gas (pre-purified nitrogen) flow varied between 13 and 40 mL/min. Together with a suitable column temperature, this flow variation was intended to control the isothermal retention time at about 2 minutes for different, singly injected analytes. This two-minute retention did not carry any special meaning in a chromatographic sense, but it ensured the complete separation of the analyte from the solvent with a reasonable peak width for the former. The same retention times gave approximately the same peak widths for different analytes, and this offered the possibility of direct comparison for measuring the minimum detectable flows of various analytes.

The temperature of the flame chamber (which was heated by an electrical cartridge) was controlled at about 200 °C throughout the experiments. The temperatures at the detector base and the injection port were usually the same, and at least 30 °C (in most cases) higher than that of the column.

Two types of PMT's (Hamamatsu Corp., Middlesex, N.J.) were used for different purposes. R-268: bialkali, 300 - 650 nm, maximum response at 420 nm, for general use, *e.g.* flow optimization and calibration curves. R-1104: multialkali, 180 - 850 nm, maximum response at 420 nm, most sensitive and red-extended, used essentially for scanning spectra. R-374: the same as R-1104, but less sensitive, used for monitoring compounds with strong emissions in the far red/near infrared.

2.4 Chemicals and Materials

All the chemicals used in this project were commercial products and used without further purification or tests for purity. They were labelled 95% or better. The standard organometallics were from various suppliers, including Alfred Bader Library of Rare Chemicals, Div. of Aldrich Chemical Company, Milwaukee, Wis.; Fluka Chemical Corp., Ronkonkana, N.Y.; K&K Laboratories, Div. of ICN Biomedical Inc., Plainview, N.Y.; Pfaltz and Bauer Inc., Stamford, Conn.; Polyscience Inc., Warrington, Pa.; Roc/Ric Inc., Orange, Ca.; Ventron Alfa Inorganics, Danvers, Ma., and Strem Chemicals Inc., Newburyport, Ma. The common organic compounds and solvents were from Aldrich Chemical Company and the Organic Mini-Stockroom (Model 0-1000A) of Chem-Service, West Chester, Pa. The various gasoline samples were collected from Halifax local gas stations. Most of the chromatographic materials were purchased from Chromatographic Specialties

Ltd., Brockville, Ontario. The sampling syringes were Hamilton products.

The nitrogen gas (used as carrier and additional gas) was the "pre-purified" product of Linde Union Carbide Canada Ltd., Toronto, Ont., with a minimum purity of 99.998%, and 5 ppm of moisture and 3 ppm of oxygen. Prior to the column, the carrier nitrogen passed through a particle, hydrocarbon and moisture trap of activated charcoal, molecular sieve 5A and silica gel (Guild Corporation, Bethel Park, Pa.), and through a Supelco oxygen purifier (Supelco Inc., Bellefonte, Pa.).

The detector used Linde prepurified hydrogen (minimum purity of 99.99%) and extra dry air (maximum moisture of 10 ppm). Both were filtered by a charcoal, molecular sieve 5A and silica gel filter before entering the detector. The methane gas was an "ultra-high purity" product of Matheson Gas Products, Toronto, Ont. The sum of N_2, O_2, CO_2, C_2H_4, C_3+ and H_2O was less than 300 ppm.

The optical filters (long-pass, short-pass, band-pass, wide-band and neutral) were bought from Ditric Optics Inc., Boston, Ma. The central wavelength and band-pass of the interference filters were checked in the laboratory with the help of a spectrometer. Most of them exhibited the nominal wavelengths, while a few were off. The wavelengths cited in this thesis are the lab-estimated ones.

2.5 Response Optimization and Calibration

The main variables involved in the process of optimization were hydrogen and air flows, PMT voltages, wavelengths of interference filters, *etc.* To optimize the flows, hydrogen varied between about 30 and 300 mL/min, while air flow was fixed at a common flow rate, say, 60 mL/min; then the hydrogen variation was repeated while air flow was set at another level. This process continued until all

possible hydrogen-air flow combinations were well covered. The plots of S/N ratio versus flows that resulted from this scanning experiment usually contained several maxima. The optimum flow conditions were chosen from the best S/N ratio. This type of experiments also produce plots of signal only *vs.* flow. The signal pattern of flow dependence sometimes provides useful information in judging the origin of the luminescence (*e.g.* one emitter or more.)

The cathode voltage was optimized for each PMT being used. The voltage varied between -400 and -800 V while certain amounts of a phosphorus-containing standard were repeatedly injected. The optimum voltage was chosen in terms of the S/N ratio (here noise is the peak-to-peak chromatogram baseline fluctuation). Surprisingly, the optimum voltage for all the PMT's was around -600 V. That was about 100 V lower than the detector manufacturer's recommended voltage. No doubt, the optimum voltage would depend, to some degree, on the intensity of the flame background. The extent to which the S/N ratio benefits from a 100 V drop might be slight, but the PMT's life times should improve. The modified (by B. Millier) Shimadzu high voltage source (HVS-5P) allowed the potential to vary continuously from -300 to -900 V.

The spectral optimization, *i.e.* the filter selection, was carried out according to the corresponding spectrum. A narrow band-pass (6-12 nm) interference filter was usually employed for isolating the sharp bands (or lines). In a case of overlapping spectra, a long-pass (or short-pass occasionally) filter would be used to include the analyte emission and to exclude the carbon emission (mainly at 430 nm), or luminescence from other FPD-active elements, as much as possible. A wide-band filter (*ca.* 40 nm bandpass) was often chosen for broad emission bands. All these

filter modes were chosen due to selectivity considerations. As far as sensitivity was concerned, an open mode (no optical filters) was favoured for most of the investigated species.

Once the operational conditions were chosen, calibration curves were made for determining the detection limits and linear ranges. The curves started from the amount from which the response could be reasonably determined, and ended at a point where they obviously bent off linearity. For most elements, more than one compound (if available) was tested to confirm the reproducibility of response, and to reveal any structural effects. The calibration curves of aliphatic and aromatic compounds (usually dodecane and naphthalene) were also established under the same conditions. These curves were used for determining selectivity of the analyte *vs.* hydrocarbon compounds.

2.6 Spectrum Determination

In order to scan the analytes' spectral features from the FPD flame, one of the photomultiplier channels was replaced by a Jarrell-Ash model 82-415 quarter-meter monochromator with a 1180 groves/mm grating blazed for 500 nm, a pair of slits (either 0.5 or 2.1 mm) and an R-1104 photomultiplier tube. If the radiation was too faint to be scanned that way, a filter monochromator (Oriel model 7155, range 400 to 750 nm), with slit options of 1, 2, 4 and 6 mm, would be used. This low resolution device gave a higher light input to the attached PMT. An infrared absorbing filter (Oriel 7165) was placed in front of the monochromator to block off the side bands (800-1400 nm) of the monochromator's interference filters. Analytes in amounts corresponding to the upper end of their linear ranges were repeatedly injected while the wavelength drive was being manually advanced. Some

spectra were made by automatic continuous scanning. In such a case, the analyte was first coated onto Chromosorb W, then the packing was filled into a glass column, and heated to a temperature that produced the desired constant level of the analyte in the carrier gas. The light produced from the constant analyte stream was then scanned by the motor-driven monochromator.

In cases where the second order spectra could be possibly recorded, a suitable cut-on (long-pass) filter was placed in front of the PMT to block off the second-order light derived from the monochromator's grating.

Note that the spectra were not corrected for the PMT's response profile. According to the manufacturer's information, the Hamamatsu R-1104 PMT has a fairly flat response between 200 and 600 nm. Thus, the uncorrected spectra should be largely consistent with the true emission features. However, we should distrust the recorded spectral features recorded beyond, say, 800 nm.

2.7 Quenching Tests

The quenching effect to the analyte radiation caused by co-eluting hydrocarbons was tested by doping methane (as a simple hydrocarbon-type quencher) into the flame. The quencher was introduced to the hydrogen line through either a fine valve (Nupro) or an exponential dilution flask (EDF) purged by hydrogen. The output concentration (C_i) of the EDF was calculated through:

$$C_i = C_0 e^{-\left(\frac{F}{V} t\right)}$$

where C_0 is the original quencher concentration in the flask; F the flow rate of the flushing hydrogen; V the flask volume; and t the flushing time. The EDF used in this experiment had a volume of 180 mL, so that the equation becomes:

$$C_i = C_0 e^{-0.0056Pt}$$

The test results were displayed by either a simple curve of relative response *vs.* quencher concentration in the flame or by a Stern-Volmer plot.

2.8 Flame Temperature Measurements

The temperature distribution in the flame chamber was estimated by thermocouple-temperature measurements. The measuring device consisted of a 0.2 mm diameter fine-wire iron-constantan thermocouple and a simple amplifier (Omega OMNI-AMP II-A). The measurements were double-checked with a 0.4 mm diameter iron-constantan wire dipped into phosphoric acid prior to use. The two thermocouples gave essentially the same readings.

2.9 Initial Design of Differential Interfaces

To generate a differential signal, a simple interface between the electrometers and the chart recorder was constructed on a piece of prototype board. As shown in Figure 2.2, one channel was adjustable through a 500 Ω potentiometer. If the signal of carbon (or of any other unwanted element) from one channel was adjusted to match that from another channel, the output of the recorder would be null since the two equal signals were fed into the same recorder channel and thus cancelled. This simple subtraction circuit was designed to suppress the matrix hydrocarbons (*e.g.* hydrocarbon components in gasolines). Preliminary sampling was required in order to match the two channels. The resistor-capacitor (RC) combination in Figure 2.2 functioned as an electronic filter to remove the high-frequency noise.

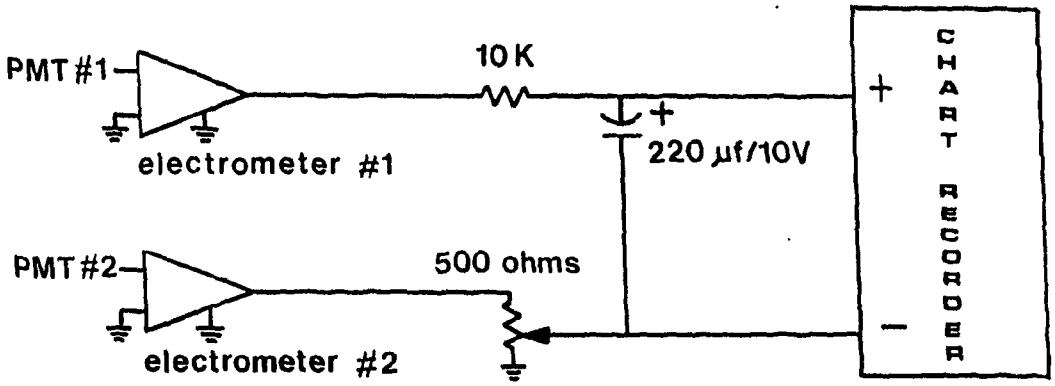

Figure 2.2 *Original design of analog interface circuit for differential operation.*

2.10 Improved Design of Differential Interfaces

The original circuit worked well, but the simple RC filters were too rough, and it was a time-consuming job to match the two signals precisely. A commercial-looking interface was built by the departmental electronic shop (B. Millier) to allow further exploration. It is an analog "front-end" circuit (shown in Figure 2.3). It consists of an input attenuator — a ten-turn potentiometer with vernier dial — and a three-pole active filter. This circuit is duplicated for the second channel, and a simple switching circuit selects either the intact two channels or their subtraction signal for output to the recorder. The potentiometers offer calibrated attenuation for each channel, and a choice of cut-off frequencies is available via independent switches. In addition, an optional capacitor coupling on the output of each channel guards against excessive drift of the chromatographic background signal.

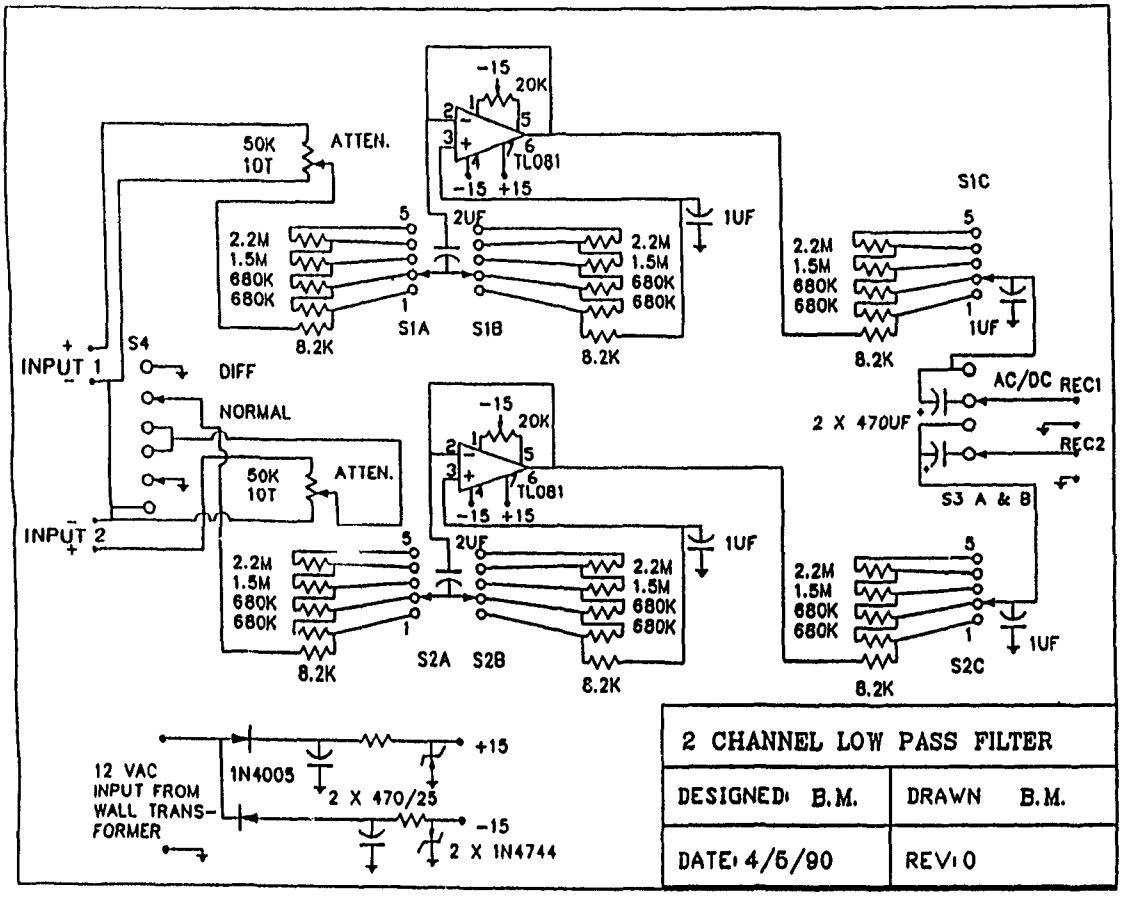

Figure 2.3 *Analog interface for manipulation and recording of independent or dual-channel differential chromatograms.*

2.11 Computer System

The above-mentioned two interfaces were simple analog circuits, and they were limited to the subtraction operations. Also, obviously, the electronic circuits did not have memories, so that one injection was just for one try. Sometimes tens of programmed-temperature chromatographic runs were required to make a good differential match. For efficient operations, the data from one chromatographic run were therefore stored in a computer for different types of manipulation, and for later reference. The computer, which was dedicated to this particular GC-FPD system, was a 12 MHz AT-compatible processor. To provide for a data display of satisfactory appearance and reasonable operating speed, the hardware configuration includes one megabyte memory, 40 Mb hard disk, 80287 math coprocessor, VGA display adapter and Multi-Sync monitor.

2.11.1 GC-FPD/Computer Interface

For digital data processing the "integrator" outputs of the two Shimadzu electrometers are connected to the AT computer through an interface. This interface is built (by B. Millier) around an IBM PC Prototype card, the schematic for which is available in the IBM PC Technical Reference Manual, publication 6025005. The schematic for the custom part of the circuit ("2-channel chromatographic interface") is given in Figures 2.4A and 2.4B.

The circuit consists of two identical channels. A simple RC filter at the input blocks high-frequency noise. This is necessary as any noise with frequencies above 1/2 the computer sampling rate (10 Hz) must be removed prior to sampling and converting the analog detector output to a digital value; otherwise aliasing noise will be present in the digital data. A voltage-to-frequency converter is

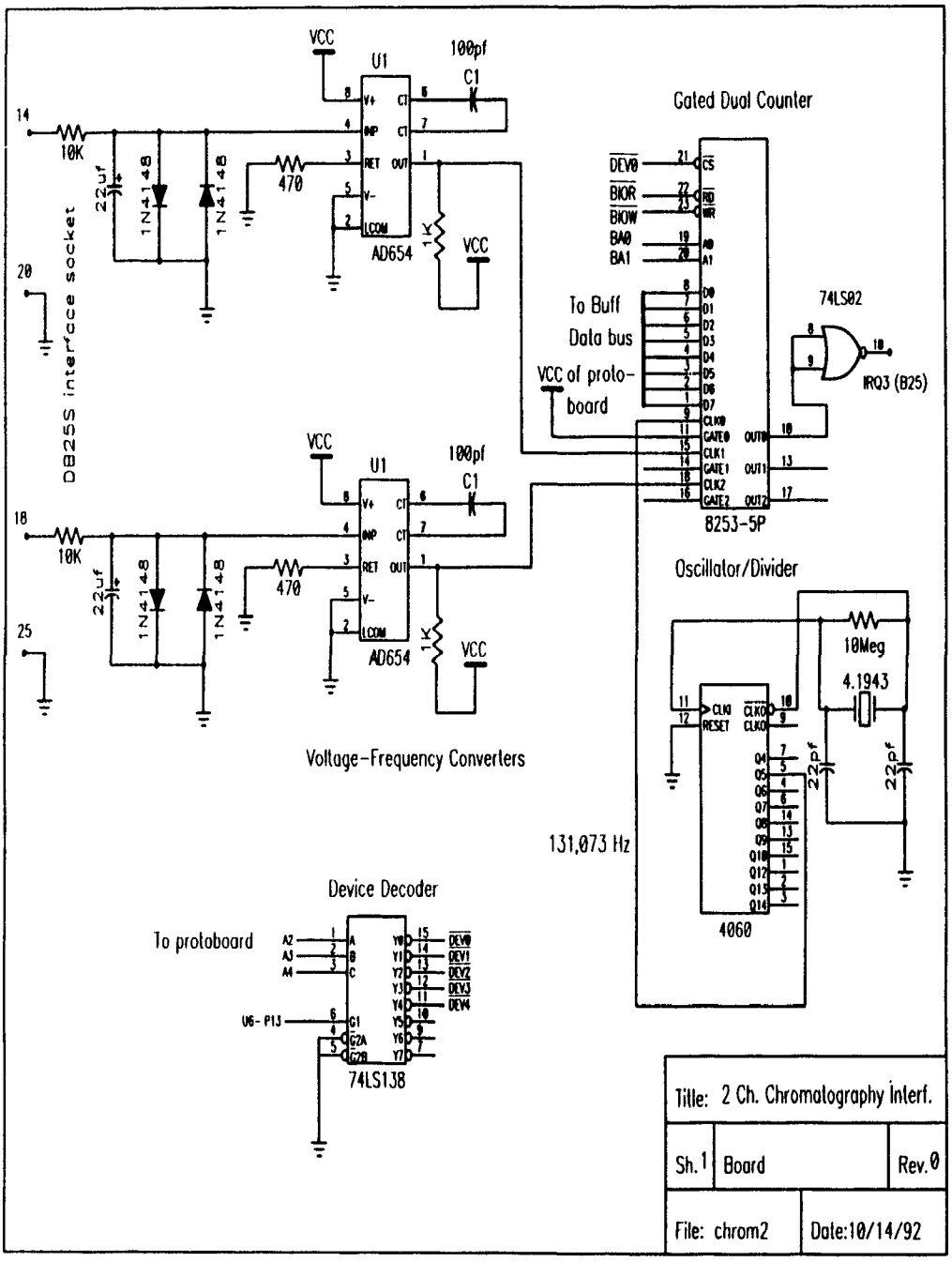

Figure 2.4A *Part of "Computer system" interface for computer input and output of dual-channel chromatograms.*

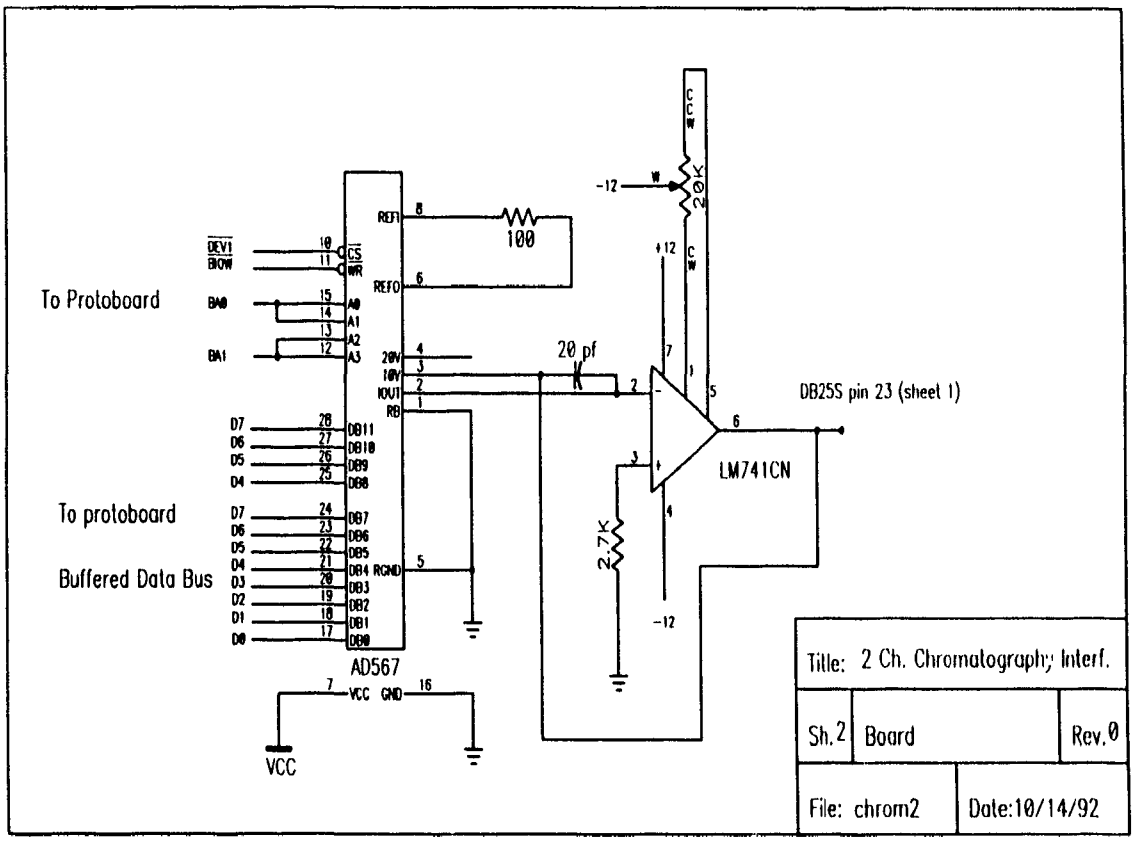

Figure 2.4B *Part of "Computer system" interface for computer input and output of dual-channel chromatograms.*

used to transform the signal to a digital pulse train, and a counter accumulates these pulses over 0.1 second intervals. A full-scale input signal will produce a digital count value of 16,000, providing resolution about equal to a 14-bit analog-to-digital converter. The input voltage to this circuit, required to produce full-scale digital output, is about 200 millivolts. The Shimadzu electrometers' "integrator" outputs had

been slightly modified to provide the computer with a signal 10 times the amplitude of that sent to the recorder. Therefore the computer offers a 2:1 over-ranging capability compared to the recorder, assuming the latter is operated on its 10 millivolt scale.

An Analog Devices AD567 digital-to-analog converter generates an analog signal that is fed to a strip chart recorder for hard-copy output of computer manipulated/generated chromatograms. Since the DAC output is 0 - 10 volts, that strip chart recorder operates on its 10 volt range.

2.11.2 Computer Program #1 — CHROM

CHROM was written (by B. Millier) in compiled Quick Basic which generates reasonably fast code. The following is a brief description of the main features of the programme.

1 Acquisition and Display

All data acquisition is performed by assembly language routines using interrupts for timing accuracy. However, due to the large amounts of data collected per run, a math coprocessor is needed to allow data manipulation such as filtering and scaling at an acceptable speed.

The program samples the two channels every 0.1 seconds and provides up to 1600 seconds (26 min 40 s) readout on the screen. The sample injection is marked and two vertical or two horizontal cursors appear for manipulation of the two chromatograms. The vertical cursors define the time section to be worked on; the horizontal cursors set the baselines and allow the approximate measurement of peak heights in subsequent routines.

2 Zoom

Zoom is designed to select a certain section of the chromatograms to work with. In typical operation, a time window, which contains the peak(s) of interest, is selected, and all the data between the vertical cursors will be expanded horizontally to fill the display screen area. To work on the zoomed section (instead of the whole chromatogram) can save enormous time in operations such as filtering, subtraction, correlation, *etc.*

3 Digital Filtering

Probably the first step to run the programme is to remove the high-frequency noise from the raw data to ease the further manipulations. The programme provides a digital low pass filtering routine. There is an option of three taps (32, 64 and 128) to choose from. The higher the number selected, the higher the order of the analog filter that will be digitally simulated. The operator is also able to set a cut-off frequency. Any noise with frequency higher than that will be filtered off.

4 Matching

To execute the differential (subtraction) or CONDAC (correlation) routines, the peaks of interest from the two channels must be matched in advance. The matching factor for channel 2 can be selected either by typing in the value (if known) or by graphically defining peaks in both channels. In the graphic process, one peak is selected (and zoomed) from the chromatogram as a tuning standard for cancellation of its congeners; *e.g.* dodecane may be selected for cancelling aliphatics. The programme measures the peak heights as the user moves the horizontal cursor from the bottoms to the tops of the peaks. Then, the computer calculates the matching factor, scales one of the whole chromatograms, and displays both.

5 Subtraction

The roughly matched peaks can be cancelled out by the subtraction routine. The resulting chromatogram can be fine tuned by the user. The programme proceeds through several user-prompted interactions in which the two-channel intensity ratio is changed by small increments. The visually "best" iteration is then selected to scale all of the data. (This final magnification factor can be employed directly in further computer runs and/or it can be manually transferred to the "analog interface". For analytes contained in complex matrices, this routine serves well in obtaining the best overall discrimination against the background.) Note that the updated version of the subtraction program also takes response ratios of the two channels directly from another sub-routine ("Slope Ratios"). The program uses these ratios to match the two channels. This new feature obviously bypasses the "Matching" routine and hopefully saves time. The final differential chromatogram (plus magnification factor) can, as all chromatograms, be stored on hard disc. It can also be subjected to other routines (*e.g.* digital filtering).

6 Correlation

This algorithm correlates the slopes of data trains from two channels that had been previously adjusted by the matching routine for equal response of a hetero-element standard (see above). Its main operating principle is "conditional acceptance" or "conditional access" (CONDAC): data are accepted by the algorithm, and can access the final read-out routine, only on the condition that the slopes S_a (*i.e.* $\Delta R_a/\Delta t$) and S_b of the two chromatographic responses do not differ from one another by more than an analyst-chosen fraction f of their value — otherwise the data are rejected and a flat baseline is drawn. If accepted, *i.e.* if S_b is located within the

tolerance band of width $2f \times S_a$, each data pair is summed (and the result halved for display convenience) to produce the final response. Note that the algorithm also accepts a user-entered slope ratio (SR), S_a/S_b, which can be obtained from another sub-routine. The acceptance condition is: $(S_a - f \times S_a) < S_b \times SR < (S_a + f \times S_a)$.

Data preliminarily accepted in this manner gain access to final read-out only after further tests against statistical and chromatographic criteria, of which two more have threshold values set by the user. First, a minimum percentage of positively correlated data pairs must be obtained and, second, this extent of positive correlation has to be maintained over a specified time. The particular settings of these thresholds may vary widely depending on the type, operating conditions, and quality of the chromatographic separation; on the kind of sample; on the signal/noise level; and on the objectives of the analyst. For general purposes, the user may want to choose the most narrow threshold definition that still allows all peaks of a chosen element to be recognized.

Approximate usage ranges are: maximum slope tolerance $f = 0.\text{x}$ to 0.1; minimum number of positively correlated data pairs = 50 to 90%; minimum correlated time = 1 to 4 standard deviations of the average Gaussian peak.

7 Slope Ratios

To provide response ratios for the correlation and subtraction algorithms, a sub-routine is used to calculate the slope ratios (SR's) in the conjugated peaks of the two FPD channels according to the formula:

$$\overline{SR} = \frac{\sum \left| \frac{S_a^2}{S_b} \right|}{\sum |S_a|}$$

The programme computes (averaged) slope ratio values for all, or for a defined ("zoomed") range of peaks from a dual-channel chromatogram in "manual", "split-peak" and "whole-peak" modes, and forwards the results to screen, recorder and printer (the manual mode activates the screen only).

The numerical result of this calculation is displayed on the screen in the "manual" mode. In the continuous "split-peak" and "whole-peak" modes it is forwarded to a printer, while both screen and recorder show in log scale the "response ratio chromatogram" (RRC). (Note: since the FPD-RRC is designed as a "chromatographic" representation in the true sense of the word, it also follows the same time scale as the conventional chromatogram.) On the screen this representation is superimposed on the two original chromatograms; on the recorder it is preceded by a staircase calibration with steps at $\log(\overline{SR}) = 1.5, 1.0, 0.5, 0, -0.5, -1.0$, and -1.5. When no peak is present (*i.e.* when S_A or S_B or both are essentially zero), or when no peak is recognized by the computer, the RRC retreats to a "no information" line that is arbitrarily drawn at $\log \overline{SR} = 0$, *i.e.* that coincides with $\overline{SR} = 1$.

For the continuous modes, two further parameters need to be defined by the operator. The first prompt requests a numerical value for "n", the number of 0.1-second intervals to be included in the slope calculation for each data point. Thus the slope is calculated from time $(i - n/2)$ to time $(i + n/2)$; with i being the data point under consideration. Note that, in this procedure, the time ranges for sequential slope calculations overlap, since data points are also established every 0.1 seconds. Reasonable values for n are thus small even integers. For instance, this study used most often $n = 2$ or 4. Broader peaks would typically demand larger values.

The second prompt asks how many sequential slope ratio values have to be of same sign (positive or negative) before the algorithm decides, retroactively, that the ascending or descending portions of a peak have begun or ended, and that cut-on or cut-off commands are to be issued. (Typical values in our studies ranged from 1 to 4 depending on the noise level.)

The two prompts are meant to add reliability to peak definition; they help to distinguish a true peak from the mere puff of the flame. Answering them should be done with some caution and the particular type of chromatogram in mind. In this they are similar to parameters used in the (here also available) digital filtering routine: too little filtering or damping can render the subsequent calculation technically impossible, too much can render it analytically unreliable.

8 Statistics

This sub-routine is designed to calculate the standard deviation (σ) of the baseline fluctuation and, furthermore, the signal over noise ratio. The user first positions the two vertical cursors to define the baseline segment for which the sigma value is to be calculated. The programme then smoothes this segment by the filtering routine. The straightened line is then taken as the "true" baseline, and the original noise is imposed on it. The noise is defined as the baseline fluctuation from the "true" baseline. The programme samples data points every 0.1 second. These data are then used to calculate the standard deviation σ in the conventional manner:

$$X = \frac{\sum_{1}^{i} x_i}{i}$$

$$\sigma = \sqrt{\frac{\sum_{1}^{i} (X_i - \bar{X})^2}{(i - 1)}}$$

9 Plotting

The program offers a feature to plot the original, differential, correlation, and response ratio chromatograms on a chart recorder. This is useful for publication, documentation, and more importantly, comparison with conventional chromatograms. The output can be magnified by any factor. The user has the choice of time indicators superimposed on the plots.

10 Auxiliary Features

The programme contains many handy operational features. They are: saving and retrieving data, swapping channels, toggling between displays, restoring raw data, displaying retention times, file directory, *etc.*

2.11.3 Computer Program #2 — BC

An separate programme, BC, is written for baseline correction. If the baseline drifts severely during a programmed-temperature run, the subtraction and correlation routines may have difficulty in processing the data. Unfortunately this often happens. BC provides a cubic-spline correction (adopted from the common domain by B. Millier) for a severely drifting background.

The user has a star cursor to define a maximum 30 "correct" baseline points. Then the computer will draw a new baseline (a cubic-spline approximation) through those points. If the user is satisfied with this computer-generated line, BC

will accept it as the chromatogram's new baseline. The offset of the chromatogram is also adjusted by this operation. The chromatogram with the new baseline can be retrieved by CHROM to proceed to further manipulations.

The source codes of "CHROM" and "BC" are presented in Appendices I and II.

Chapter 3. LINEAR SULFUR RESPONSE IN THE FLAME PHOTOMETRIC DETECTOR

3.1 Introduction

As reviewed in Section 1.2, the one major impediment to the use of the flame photometric detector for organosulfur compounds[2,25,29,31,55] is its non-linear signal. The FPD's sulfur response is roughly exponential, and different exponents obtain for different compounds. While the diatomic nature of the predominant emitter, S_2, suggests bimolecular kinetics, the apparent reaction order varies. Most values of the response exponent ("n") fall between 1.8 and 2.2 [25], but the total observed spread is much wider. To aggravate the problem, the lowest section of the calibration curve often turns linear (*c.f.* [2]), with the extent of such linearity depending on the presence of extraneous sulfur[13]. The current state of knowledge (or lack thereof) has been well documented[25,29,31,55].

Its many problems notwithstanding, the FPD remains the workhorse of choice for the determination of volatile organosulfur compounds. This is due in part to its simplicity, durability and low cost; and in part to the large demand for organosulfur analysis. Sulfur compounds play major roles and pose major problems - analytical and otherwise - in biological, environmental and industrial chemistry. For instance, many important components of aromas and fuels, and quite a few pesticides and pollutants, contain sulfur.

This situation has spawned or at least spurred the development of more complex analytical devices, capable of detecting sulfur in chromatographic effluents. For instance, the "sulfur chemiluminescence detector" is based on the conversion of sulfur compounds to sulfur monoxide in an FID, followed by ozone oxidation of SO

to electronically excited SO_2 [56,57]. As another example, the (multi-element) "atomic emission detector" relies on the 180.7 nm sulfur line emitted from a microwave-powered, doped helium plasma contained in a cooled quartz capillary[58]. Both instruments exhibit linear response. They have recently been subjected, side by side, to various tests of analytical performance[59].

Still, the comparative simplicity, reliability and economy of the FPD make it highly desirable to "linearize" its response to sulfur. Electronic means[60] and chemical means (*e.g.* [13]) have been employed to this end. However, neither has found general acceptance. It may indeed prove more rewarding for the analyst to abandon the roughly quadratic S_2 emission and search for an alternative sulfur emitter with conventional first-order kinetics, as has been suggested in a frequently-cited review. This review concludes that further research into the S_2 mode should be encouraged but that "the development of a simple and sensitive sulfur-selective detector with a linear response should receive even higher priority"[29].

Owing to a stroke of luck in the study of spectral response ratios[61] (see the discussion about response ratios in Chapter 7), we became aware of just such an emitter. Figure 3.1 shows the results of the seminal experiment. The response ratio for sulfur in two FPD channels (the numerator channel with a 420 nm long-pass, the denominator channel with a 540 nm short-pass filter) increases as the injected amount of the analyte di-*tert*-butyldisulfide decreases. That suggests the presence of a linear emitter situated toward the red, whose contribution in the numerator channel is masked at higher sulfur concentrations by the (approximately quadratic) S_2 emission; and which, for the very same reason, would not be easily detected by conventional, *i.e.* high-concentration, spectral scans. Although the identity of the linear emitter is at present unknown - and may remain so for a while - its analytical performance

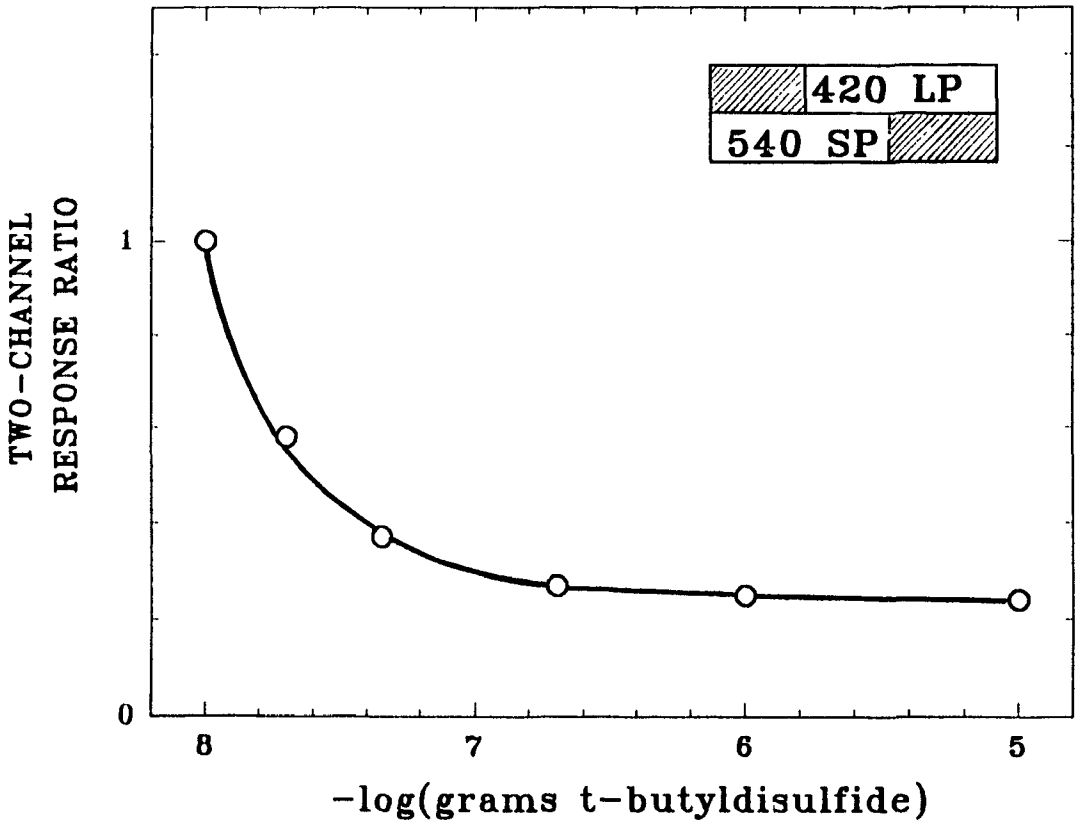

Figure 3.1 *Sulfur response ratio from different concentrations of di-tert-butyldisulfide in a dual-channel FPD. First channel: 420 nm long-pass filter; second channel: 540 nm short-pass filter; both channels with R-268 photomultiplier tubes; quartz chimney removed. Flows:* H_2 *= 300, air = 40,* N_2 *= 20 mL/min.*

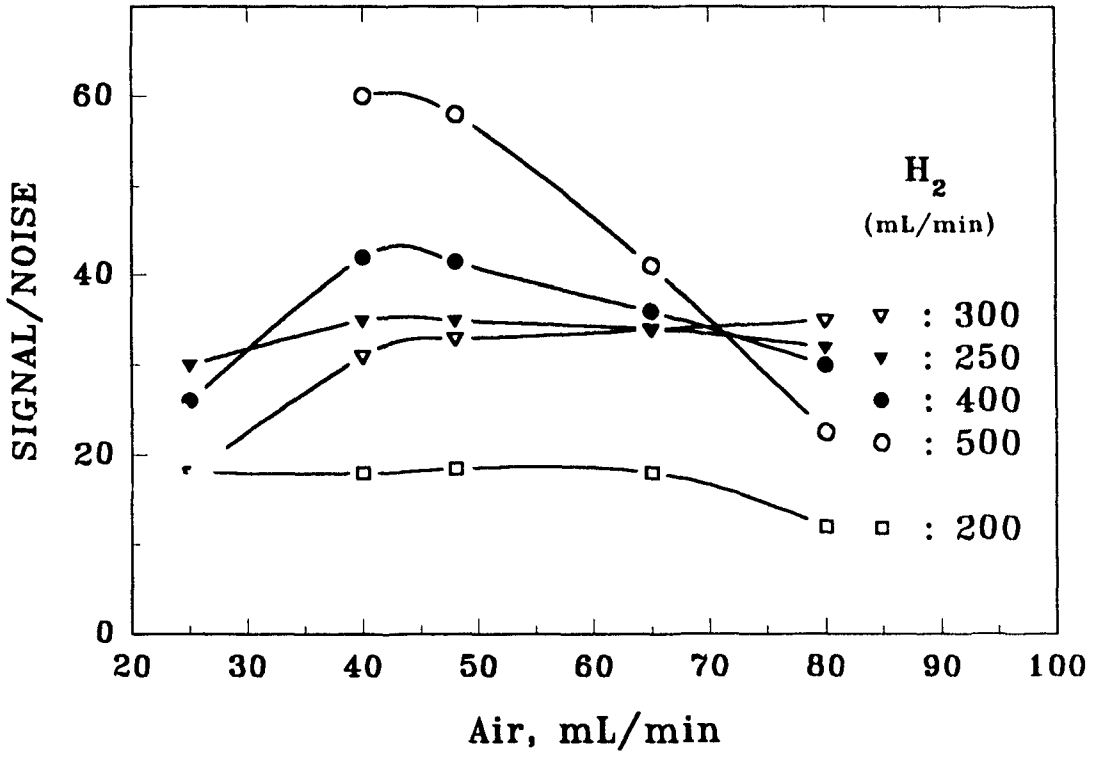

Figure 3.2 *Signal/noise vs. hydrogen and air flows. Conditions: 600 nm long-pass filter, quartz chimney absent and R-374 PMT. 20 ng of thianaphthene injected.*

qualifies it as a serious contender for the determination of sulfur-containing peaks in gas chromatographic effluents.

3.2 Linear Range and Detection Limit of the New Linear Sulfur Mode

There is little doubt that the emitter monitored for the linear sulfur mode is not the commonly observed S_2. This point is made here because, under particular circumstances, S_2 *can* produce a linear calibration curve. For instance, a sulfur-containing analyte will respond linearly when superimposed on a massive sulfur background[13]. Also, the S_2 emission will become linear if all analyte sulfur is converted to S_2 [62]. Note that the S_2 bands stretch into the red, although rather feebly. However, the possibility that S_2 might in some way be responsible for the observed effect, is clearly ruled out by the simultaneous observation of both quadratic and linear calibration curves.

Since the S_2 bands are strong and stretch right into the red end of the spectrum, the first challenging task is to isolate the new emissions from S_2. A series of calibration curves are made with different long-pass filters (from 550 to 650 nm) to characterize any contribution of the S_2 response. A 600 nm long-pass filter is found to generate a linear calibration curve with maximum response purely (within error limits) from the new emitter. Therefore, the optimization of the gas flows is carried out with the 600 nm long-pass filter.

Figure 3.2 shows the variation of the S/N ratio in accordance with hydrogen and air flow rates. In Figure 3.2 (and flow-optimization Figures for other elements), each data point is the average of at least three samplings. The standard deviation of the S/N ratio caused by the injections is never bigger than 4% of the S/N ratio values. Error bars with such small values would not show up in the Figure. From Figure 3.2, the operational conditions for the FPD's linear sulfur mode are chosen as: 500 mL/min H_2, 40 mL/min air, a 600 nm long-pass filter, and no quartz chimney. (Note: the curve with 500 mL/min of hydrogen appears to stop at its

maximum. This is because the air flow becomes too low to sustain the flame at such a high hydrogen flow.)

Figure 3.3 shows the familiar quadratic response resulting from S_2 chemiluminescence and, measured from the very same injections in the second FPD channel, the new linear response. The conditions for this experiment are those that favor the linear emission: primarily a high hydrogen flow rate in the absence of the conventional quartz chimney. One channel monitors the commonly used S_2 band at 394 nm (or, in other cases, the entire blue region plus adjoining UV); the other the red region (plus adjoining infrared). Also shown in Figure 3.3 are the calibration curves of a standard alkane for visually presenting the selectivity of sulfur against hydrocarbons.

The response measured with the conventional 394 nm interference filter displays the typical behaviour of S_2: a mostly quadratic (slope 2) calibration curve with a linear (slope 1) section at the base. In contrast, the response measured with a 600 nm long-pass filter is purely linear. It spans a range of about four orders of magnitude, and bends off at the same analyte level as the S_2 emission. Under this set of conditions, the linear response is the stronger of the two at low concentrations. The atomic selectivity S/C (S as in thianaphthene, C as in dodecane) exceeds three orders of magnitude.

While Figure 3.3 establishes the presence of an emitter other than S_2 in a spectrally motivated experiment, it does not provide an analytically fair comparison between the two emission modes. One set of conditions had to be chosen for this experiment and the choice, for obvious reasons, fell upon the set favorable to the linear sulfur emission. In contrast, the S_2 chemiluminescence is normally measured off a flame that uses a much lower hydrogen flow and burns inside a quartz chimney.

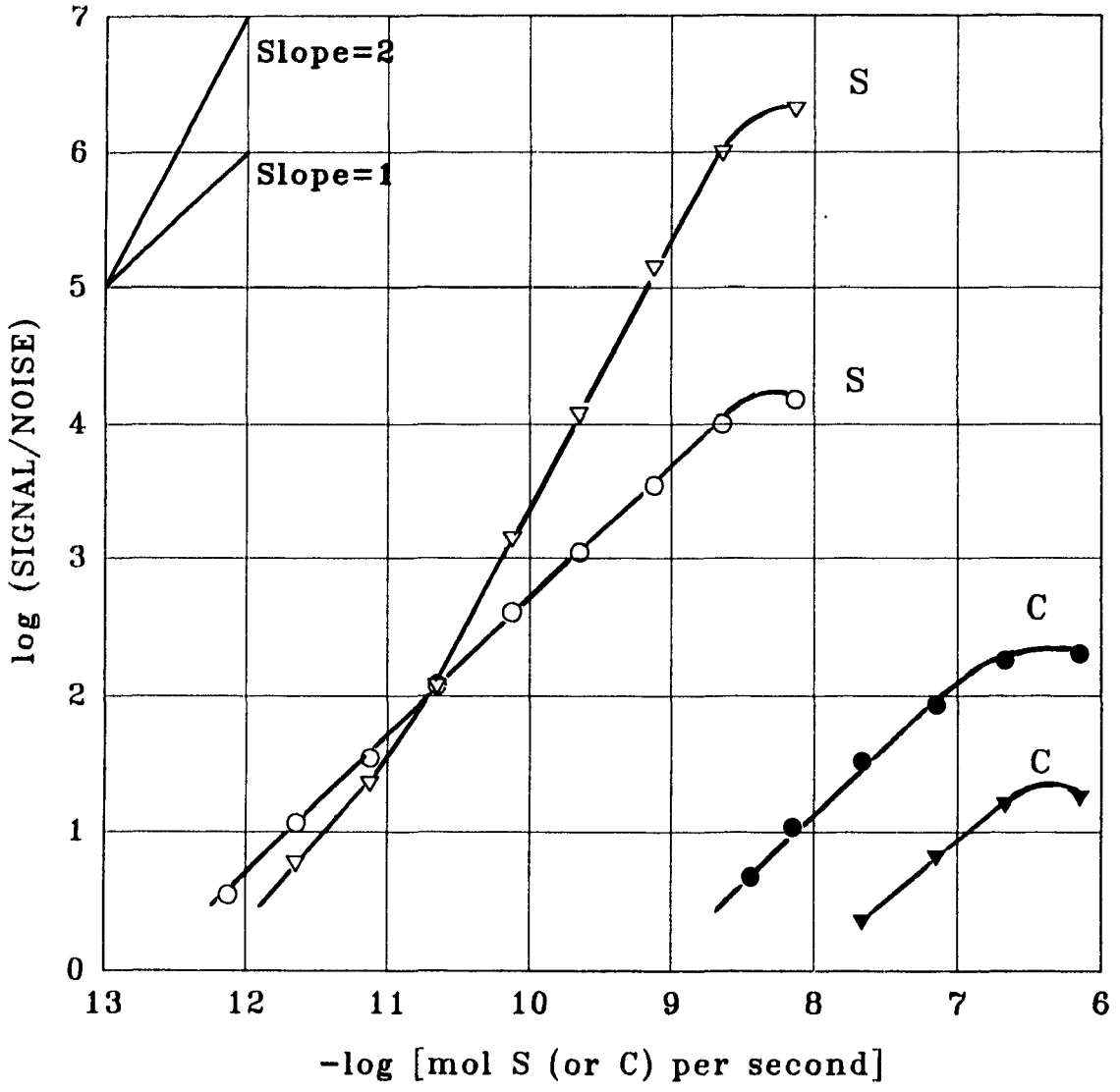

Figure 3.3 *Calibration curves of thianaphthene (empty symbols) and dodecane (filled symbols) in a dual-channel FPD. Both channels with R-374 PMT's. The flow conditions are those of the linear sulfur mode: 500 mL/min hydrogen, 40 mL/min air.*

○ ● *channel 1, 600 nm long-pass filter.*
▽ ▼ *channel 2, 394 nm band-pass filter.*

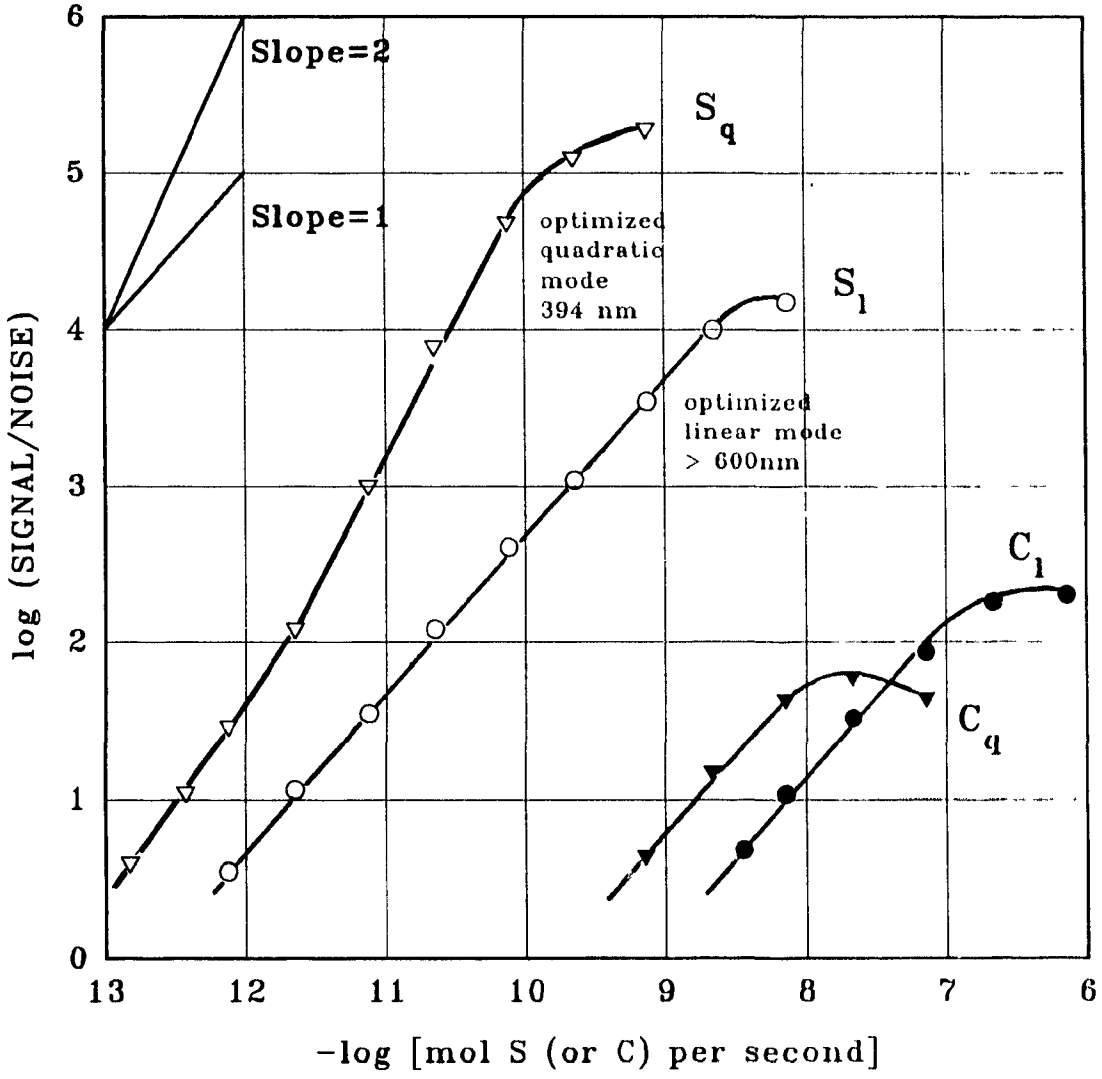

Figure 3.4 *Calibration curves of thianaphthene (empty symbols) and dodecane (filled symbols). Both channels with R-374 PMT's. Flow and spectral conditions:*

○ ● *"linear mode" optimized for sulfur: 600 nm long-pass filter; 500 mL/min hydrogen; 40 mL/min air.*

▽ ▼ *"quadratic mode" optimized for sulfur: 394 nm band-pass filter; 50 mL/min hydrogen; 40 mL/min air.*

To account for that, Figure 3.4 presents a comparison of the two emission modes under individually optimized circumstances. The linear calibration curve is essentially a repeat of that shown in Figure 3.3. Its sensitivity is now worse than that of the conventional quadratic calibration curve. A comparison of Figures 3.3 and 3.4 shows that the relative effect of flow conditions and the presence/absence of the quartz chimney amounts to only one order of magnitude.

Though small, this effect is important. The stronger the S_2 emission (relative to the linear one), the stronger will be the influence of its bands that stretch into the red; consequently, the longer will have to be the wavelength of the cut-on filter needed to keep the new response purely linear, and the poorer will be the sensitivity. (The wavelengths of cut-on filters tested in this study ranged from 550 to 650 nm.)

The minimum detectable quantity of sulfur was determined separately by following the IUPAC-recommended criterion $S/\sigma_N = 3$ via an algorithm that determined σ_N, by a least-squares fit (provided by Professor C. Warren) to a normal (Gaussian) distribution. The result was 2×10^{-13} mol S/s. (For easy comparison with values arrived by other common definitions, that value translates into 6×10^{-12} g S/s or 2.5×10^{-11} g thianaphthene/s; or, at the $S/N_{p\text{-}t\text{-}p} = 2$ limit, 7×10^{-13} mol S/s or 2×10^{-11} g S/s or 1×10^{-10} g thianaphthene/s.) For visual evaluation, Figure 3.5 shows a 2 ng peak of thianaphthene in the linear mode (the peak width at half height is about eight seconds). Figure 3.6 provides the distribution of noise, and its approximation by a Gaussian, in the baseline exhibited in Figure 3.5.

As has been amply demonstrated in the literature, the performance of the FPD is strongly dependent on its dimensional construction and operational condition. This may also apply to the new linear emission and its intensity relative to

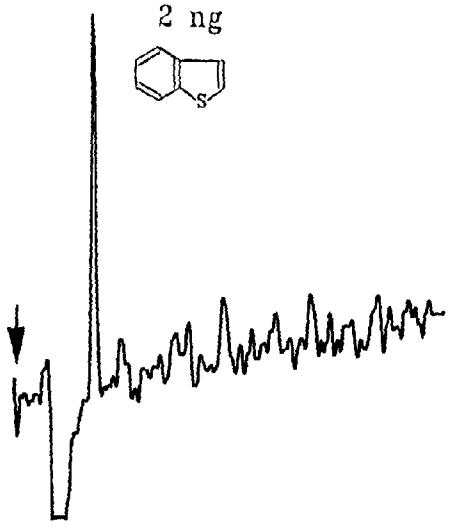

Figure 3.5 *Typical peak of 2 ng thianaphthene (benzo(b)thiophene) in the linear sulfur mode near the detection limit. 600 nm long-pass filter. 500 mL/mn hydrogen. 40 mL/min air. R-374 PMT.*

S_2. Accordingly, different FPD models may require different flow and spectral settings for optimal linear response.

In the Shimadzu FPD used in this study, the new mode offers an attractive alternative for the determination of sulfur compounds. At low concentrations, its selectivity against alkanes and its detection limit are only slightly worse than those of the quadratic mode. In return - and this is far more important for analytical practice - its calibration curve for sulfur is inherently linear.

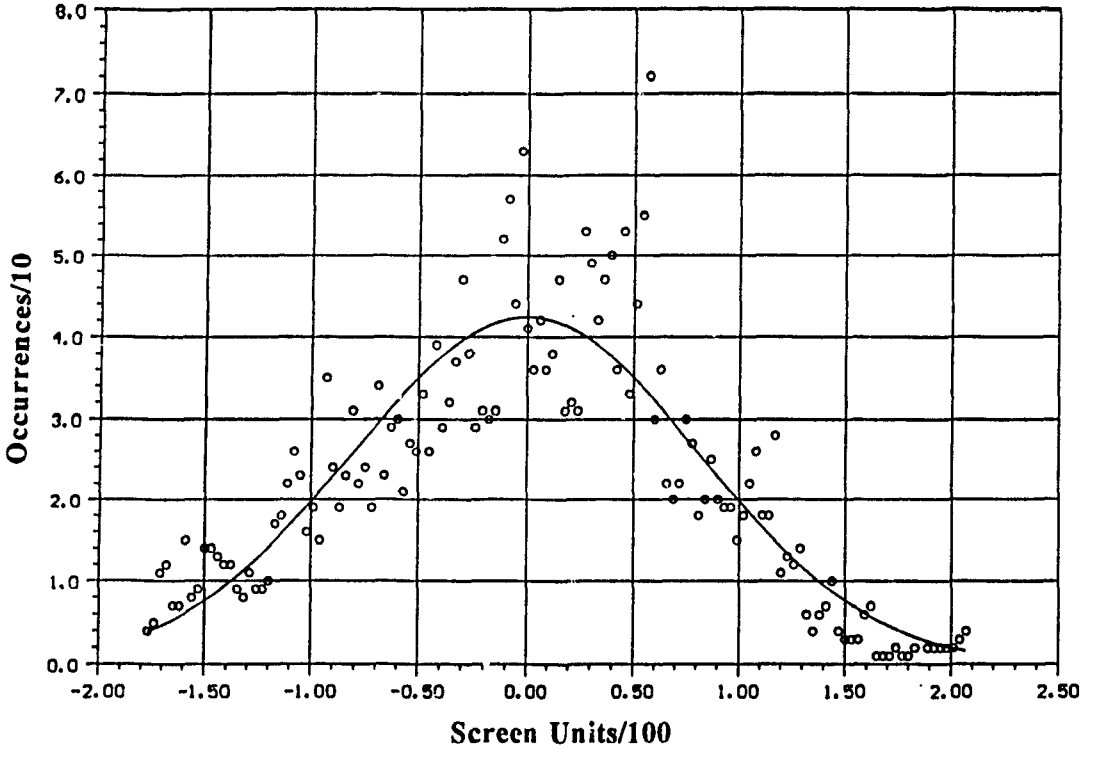

Figure 3.6 *Least-squares Gaussian fit of the baseline fluctuation shown in Figure 3.5 and used in calculating the detection limit.*

Since this new linear sulfur mode attracts some interest, a more detailed assessment of its spectral and analytical properties appears warranted.

3.3 Spectrum of Linear Sulfur Emission

At this stage of the study the most obvious and urgent questions are: What is the spectrum of the linear emission? Can it be attributed to one or more of the many known sulfur systems? Can the knowledge about the linear spectrum (if the

search for the spectrum is successful) be used to improve selectivity *vis-à-vis* other elements that luminesce in the FPD? Two aspects make the quest for the linear sulfur spectrum particularly difficult.

On one hand, and common to all elements responding in the FPD, the spectrum of the emitter has to be determined under typical operating conditions. Otherwise, analytical relevance may be lost[63,64]. That means making do with the low spectral resolution imposed by a feeble luminescence; it also means remaining within the linear range of analyte concentration.

On the other hand, and peculiar to sulfur, the S_2 bands arise from a second-order reaction[29,31]. Hence, as these bands stretch from the ultraviolet to the infrared[65], they tend to overwhelm any first-order reaction at the high analyte concentrations that have to be used for spectral assignments. The S_2 bands are extremely prominent in the feeble, cool, and hydrogen-rich flame of the FPD, and optimizing the conditions for the competitive linear emission detracts but little from that prominence. Still, some spectral characterization of the linear emitter must be obtained, if only for the optimization of analytical performance.

The S_2 bands have been repeatedly exhibited in the literature. Figure 3.7 displays them as they appear in this Shimadzu FPD under "conventional" conditions. This spectrum makes it clear why the linear sulfur emission has remained hidden for so long. On the chosen intensity scale, no further emissions appear beyond 520 nm (except for the S_2 bands in second order).

Even without the quartz chimney, at a higher hydrogen flow, and with an order-sorting filter - as well as a much higher gain - it is difficult to recognize the linear emitter. Figure 3.8 shows the crucial region - on the top in automatic scanning, on the bottom in manual injection mode. The latter was used for spectrally

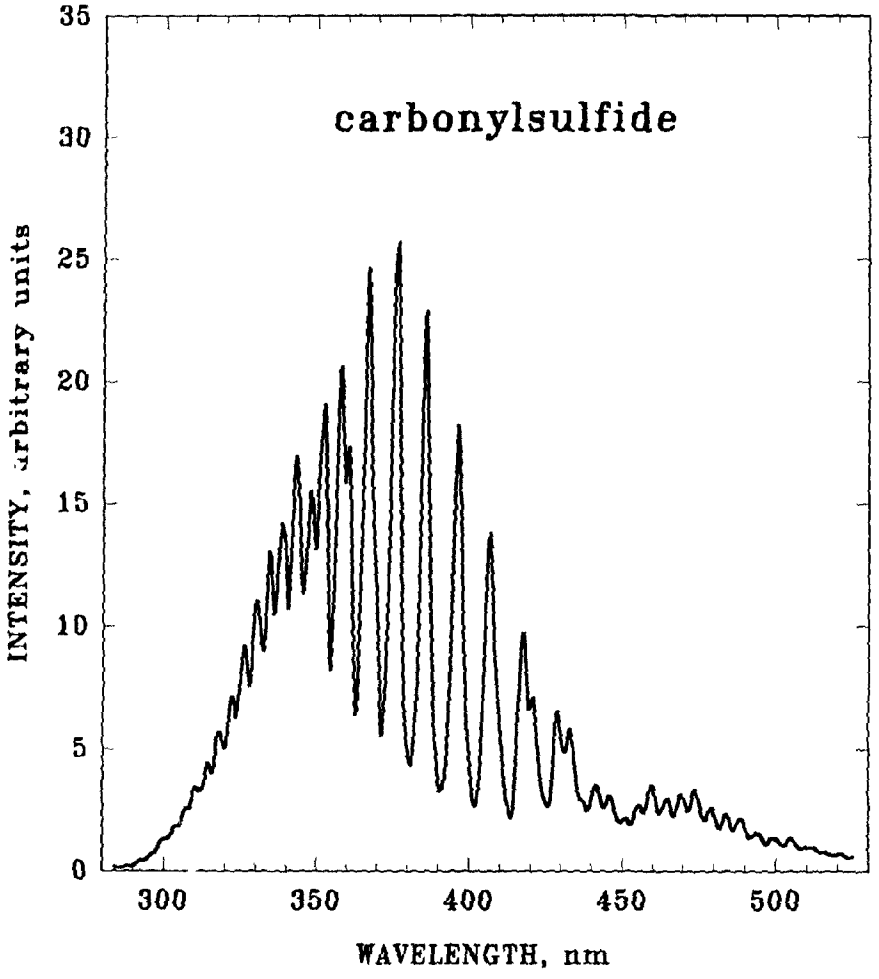

Figure 3.7 *S_2 luminescence (obtained from continuous introduction of COS) in the quadratic mode: 50 mL/min hydrogen, 40 mL/min air, quartz chimney, 1/4 meter grating monochromator equipped with 2 mm slits and R-374 PMT. Bandpass ca. 6.7 nm.*

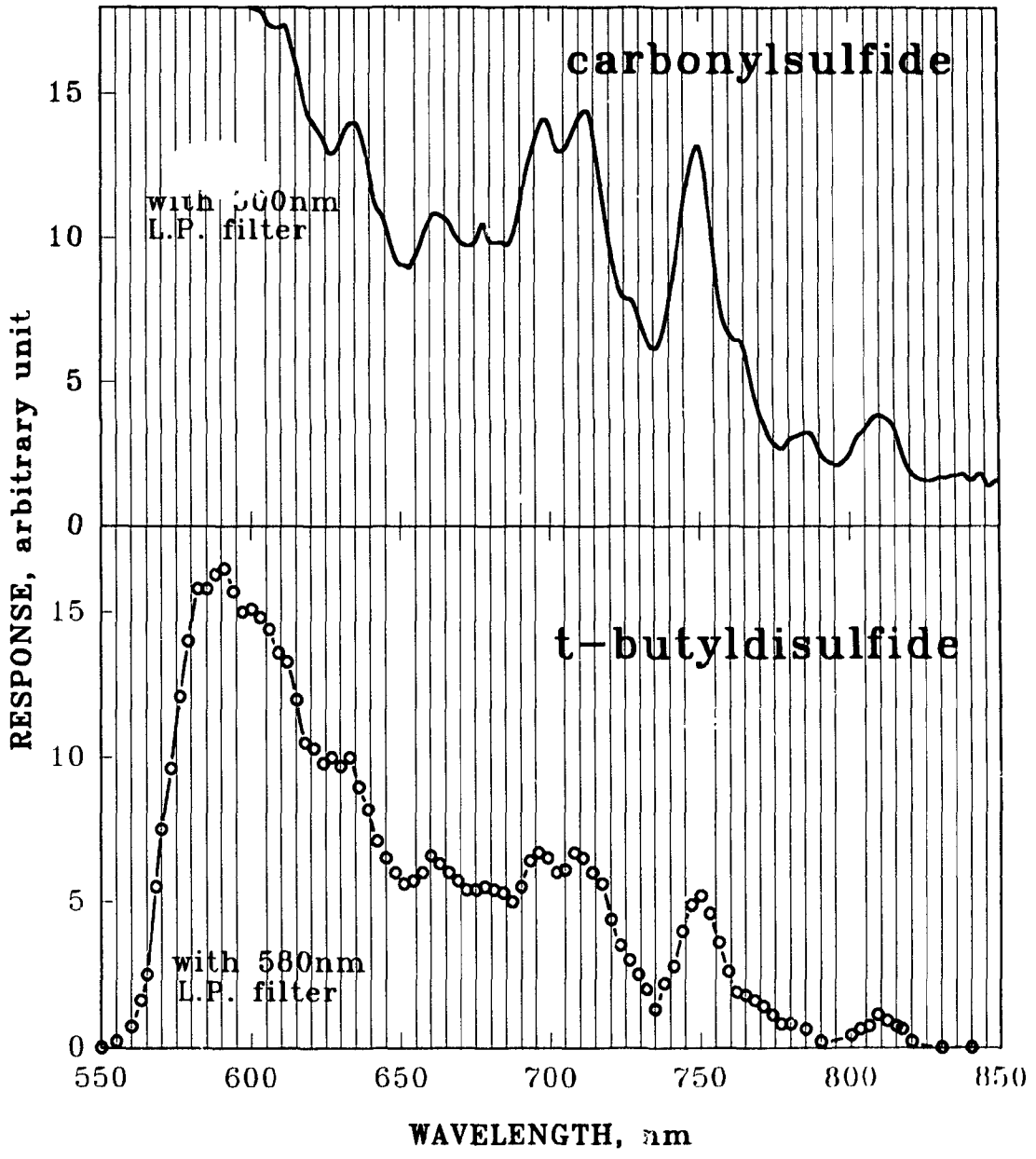

Figure 3.8 *Luminescence obtained by continuous introduction of COS (above) and repeated injection of* $(t\text{-}C_4H_9)_2S_2$ *(below) in the linear mode: 500 mL/min hydrogen, 40 mL/min air, no quartz chimney, 1/4 meter grating monochromator equipped with 2 mm slits and R-374 PMT. Bandpass ca. 6.7 nm. Long-pass (order-sorting) filters: 500 nm (above) and 580 nm (below).*

confirmative replication, for clearer definition of possible continua, and for circumvention of conceivable background features. The automatic mode represents conventional procedure; the manual approach resembles analytical practice. Fortunately, the two produce very similar spectra - spectra that are clearly not part of the S_2 system.

The emitter they represent remains unknown; none of the emission systems of sulfur[65] could be assigned to it. The spectra of Figure 3.8 must also include some overlapping S_2 bands and, because of this, it is still unclear where the strongest bands of the linear emission(s) lie. In our case, a 600 nm cut-on filter will produce a purely linear calibration curve; a 550 nm cut-on filter will come close to that. The most pronounced feature in Figure 3.8 is the band located at *ca.* 750 nm. This isolated band is potentially useful in selectivity enhancement.

3.4 Selectivities in Linear and Quadratic Modes of Sulfur Response

With a 750 nm band-pass filter, sensitivity will clearly be lower, but selectivity generally higher, than with, say, a 600 nm cut-on filter. To determine the selectivity of sulfur against other FPD-active elements in the "linear" mode is interesting and indeed necessary; it has been done for both optical conditions. Note, however, that the conditions of the linear mode had originally been set according to sensitivity, not selectivity; *i.e.* according to the highest S/N ratio for sulfur, not the various highest selectivity ratios *vis-à-vis* other elements.

It is also interesting, as well as necessary for assessing the relative merits of the two techniques, to determine the selectivity ratios of sulfur against other FPD-active elements in the quadratic mode, and to compare these numbers with those of the linear mode. To remain analytically relevant, the comparison needs to be

carried out with each mode under its own, individually S/N-optimized conditions. Yet the comparison will still be restricted in application: it applies to only one level of sulfur. Higher sulfur levels increase, lower sulfur levels decrease the single-value selectivity ratios in the quadratic mode. (Very rough estimates of the selectivity ratios at higher or lower levels of sulfur can be obtained by assuming the response to be proportional ω the square of the sulfur concentration; however, the exponential factor often differs from the ideal value of 2 and, furthermore, often approaches 1 in the low concentration range of the "quadratic" calibration curve.)

Although the quadratic sulfur mode has been in worldwide use for several decades, published information on sulfur selectivity ratios is largely restricted to the selectivity of sulfur versus carbon (really: versus the particular hydrocarbon that serves as a carbon standard in the selectivity ratio measurement). Recently, selectivity ratios of quadratic sulfur against various other elements were reported[64], but these values pertain to open (filter-less) operation at a generalized (as opposed to a sulfur-optimized) set of conditions. Thus the values of Table 3.1 may be helpful to users not only of the linear but also of the quadratic mode.

With the above in mind we can examine the compilation of experimentally determined selectivity ratios in Table 3.1 - first for each mode on its own, then for the two modes in comparison. The ratios of the conventional quadratic mode show the expected higher selectivity conferred by the 394 nm narrow-band interference filter (versus open, *i.e.* filter-less operation) in all but four cases. However, the increase in selectivity, which comes at some decrease in sensitivity, is small (a factor of 5 on average). This is in agreement with earlier data on the generally minor effect various interference filters bring to FPD selectivity[14,66].

For obvious reasons the linear sulfur mode cannot be run "open", *i.e.* it cannot be observed unless a filter is used that cuts off most of the S_2 bands. Still, similar comments as above can be made about the comparison of the *ca.* 730-770 nm range monitored through the 750 nm wide-band interference filter, with the much wider 600-850 nm range admitted by the 600 nm long-pass filter. Not surprisingly, the increase in selectivity due to optical discrimination is even smaller in the linear mode.

Perhaps more important than these intramodal relationships is the direct confrontation of the quadratic with the linear mode. The 750 nm linear mode shows selectivity ratios that are better in four and worse in nine cases than the 394 nm quadratic mode. This seems reasonable if one considers the decidedly greater intensity of the S_2 emission overall. At higher sulfur levels than those used in Table 3.1, the selectivity ratios of the quadratic mode would increase, tilting the comparison still further in its favor. An advantage of the linear mode, on the other hand, is that the response of hydrocarbons is generally negative (peaks are inverted), thereby providing a qualitative distinction between compounds that contain sulfur and those that contain only carbon and hydrogen. (It may be noted that in the comparison with selenium, the S/Se selectivity ratios depend strongly not only on the injected amount of sulfur but also on the injected amount of - similarly quadratic - selenium.)

Finally, it should be noted that all analytes were used in this experiment "as received". Table 3.2 charts them according to FPD-active element and lists the amounts in which the compounds were injected for the determination of selectivity ratios in Table 3.1. Knowing the injected amounts is particularly important for elements whose response is non-linear.

Table 3.1 MOLAR SELECTIVITY[a] FOR SULFUR AGAINST OTHER ELEMENTS IN TWO FPD RESPONSE MODE

Group	Element (X)	Quadratic Sulfur Mode[b]		Linear Sulfur Mode[c]	
		394 nm	Open[d]	600 LP	750 WB
3A	B	6×10^{2}	2×10^{2}	3×10^{3}	$>10^{4}$
4A	C	2×10^{4}	2×10^{4}	1×10^{3}*	6×10^{3}*
4A	Sn	1×10^{-1}	5×10^{-2}	3×10^{-2}	7×10^{-1}
4A	Pb	2×10^{2}	4×10^{1}	7×10^{-2}	1×10^{-1}
5A	N	7×10^{2}	1×10^{2}	1×10^{2}*	1×10^{2}*
5A	P	1×10^{1}	1×10^{-1}	2×10^{-1}	5×10^{-1}
5A	As	3	4	5×10^{-2}	1×10^{-1}
6A	Se	8	6	7	5×10^{1}
6B	Cr	3×10^{1}	2	5×10^{-2}	1×10^{-1}
7B	Mn	2×10^{1}	7	8×10^{-2}	2×10^{-1}
8B	Fe	5	5	9×10^{-2}	2×10^{-1}
8B	Ru	4×10^{-1}	9×10^{-2}	2×10^{-1}	1
8B	Os	6	3×10^{-1}	8×10^{-2}	1×10^{-1}

* *Peak direction is reversed for compounds containing these elements.*

[a] *The selectivity of sulfur against element X, $S_{S/X}$, is calculated as*

$$S_{S/X} = \frac{R_{(S)}}{R_{(X)}} \times \frac{mol\ X/s}{mol\ S/s}$$

where $R_{(S)}$ is the peak height response at unit attenuation of thianaphthene, and $R_{(X)}$ is the same for a compound of element X (see injection amounts from Table 3.2); while mol X/s and mole S/s are the molar flows per second at peak apex of element X and sulfur.

[b] *50 mL/min H_2, 40 mL/min air and 22 mL/min carrier N_2; with quartz chimney; Hamamatsu R-374 PMT.*

[c] *500 mL/min H_2, 40 mL/min air and 22 mL/min carrier N_2; without quartz chimney; Hamamatsu R-374 PMT.*

[d] *No optical filter used.*

Table 3.2 AMOUNTS OF COMPOUNDS USED FOR DETERMINING SELECTIVITY RATIOS IN TABLE 3.1

Group	Element	Compound	Amount Injected (ng)			
			Quadratic		Linear	
			394nm	Open	600LP	750WB
3A	B	*o*-carborane $1,2\text{-}H_2C_2B_{10}H_{10}$	50	50	2,000	2,000
4A	C	dodecane $n\text{-}C_{12}H_{26}$	2,000	2,000	1,000	3,000
4A	Sn	tetrabutyltin $(n\text{-}C_4H_9)_4Sn$	0.5	0.5	2	100
4A	Pb	tetraethyllead $(C_2H_5)_4Pb$	200	200	2	10
5A	N	tributylamine $(n\text{-}C_4H_9)_3N$	2,000	2,000	1,000	5,000
5A	P	tributylphosphite $(n\text{-}C_4H_9O)_3P$	20	20	5	20
5A	As	triphenylarsine $(C_6H_5)_3As$	50	50	2	10
6A	Se	diphenylselenide $(C_6H_5)_2Se$	5	5	100	1,000
6B	Cr	chromiumhexacarbonyl $(CO)_6Cr$	50	50	1	10
7B	Mn	MMT $C_5H_4CH_3Mn(CO)_3$	30	30	2	10
8B	Fe	ferrocene $(C_5H_5)_2Fe$	20	20	2	10
8B	Ru	ruthenocene $(C_5H_5)_2Ru$	1	0.2	3	30
8B	Os	osmocene $(C_5H_5)_2Os$	5	2	3	3
6A	S	thianaphthene C_8H_6S	3	3	3	10

3.5 Structural Effect of Sulfur

Conflict exists in the literature about the dependence of the FPD's S_2^* response on compound structure. Do structurally different compounds produce different responses per gram of sulfur in this Shimadzu FPD? Do they do that under the particular conditions used? If so, how large is the effect in the linear as compared to the conventional (quadratic) mode? It is no overstatement to say that this project would remain incomplete without an answer to these fundamental questions.

Experimentally, the linear mode shows very little, if any, dependence of sulfur response on compound structure. There can obviously be no dependence of measured sensitivity on analyte concentration or retention time (as it occurs in the quadratic mode). Any difference observed between the sensitivities of various compounds is thus directly attributable to differences in photon yield per sulfur atom (given the absence of impurities, degradation and quenching, of course).

Figure 3.9 shows the linear calibration curves of seven disparate sulfur compounds, plotted on a "per gram sulfur" basis. Their responses vary by less than a factor of two. Given (a) the experimental error band (injection, flow and temperature control, *etc.*) for each individual sulfur compound; (b) the always possible and often present perturbations caused by impurity, premature decomposition or irreversible absorption of the analyte; and (c) the non-avoidable quenching that occurs internally (by analyte carbon) or externally (by column bleed and/or co-eluting compounds); a factor of two is small enough to allow sulfur response to be indeed considered independent of molecular structure. For purpose of analytical response estimates, therefore, a rough sulfur equivalency can be assumed for the linear mode. Note, however, that the range of compounds tested here is limited, and that the above assumption thus remains subject to change.

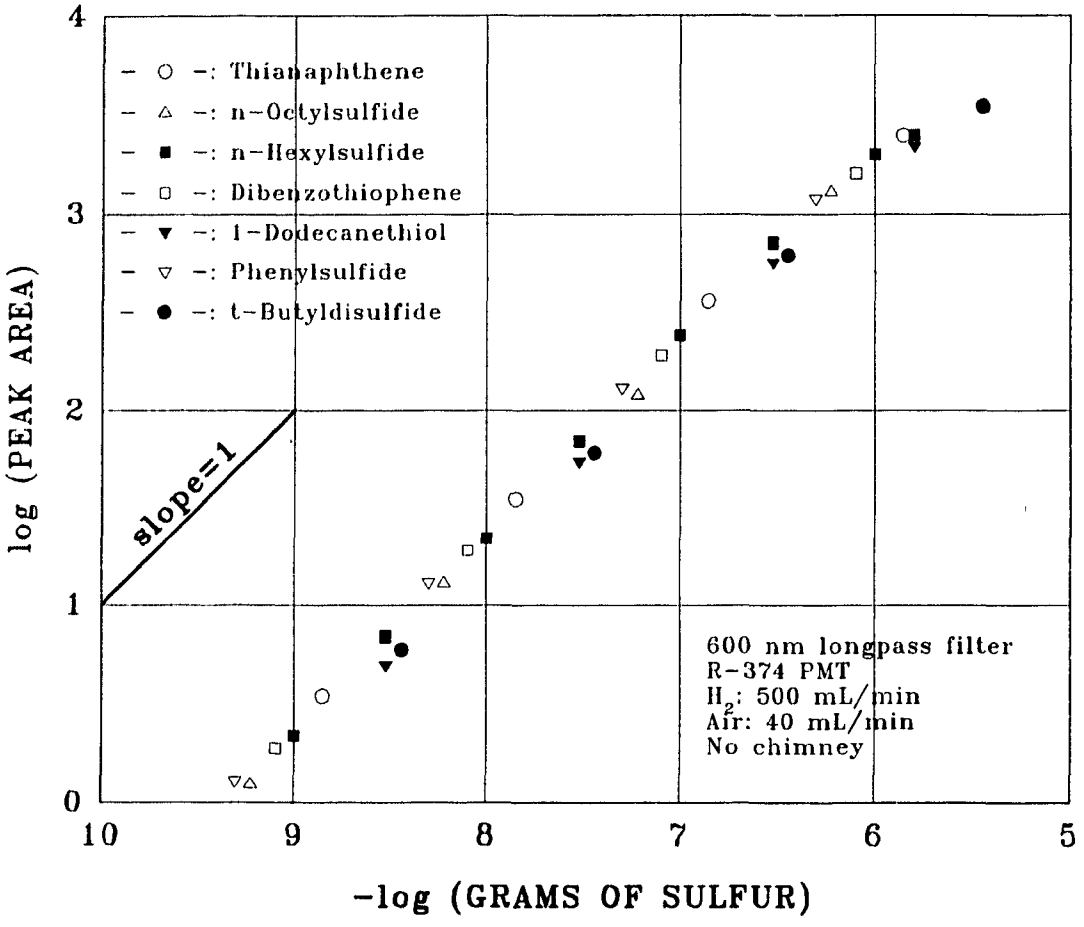

Figure 3.9 *Calibration curves for seven sulfur compounds in the linear sulfur mode. Filter: 600 nm long-pass. Hydrogen: 500 mL/min. Air: 40 mL/min. PMT: R374.*

What about sulfur equivalency in the quadratic mode? Figure 3.10 exhibits the "quadratic" calibration curves of the same compounds as used earlier in producing Figure 3.9. Response among the seven analytes varies here by a factor of just less than five. That is clearly more than a factor of two for the linear mode but,

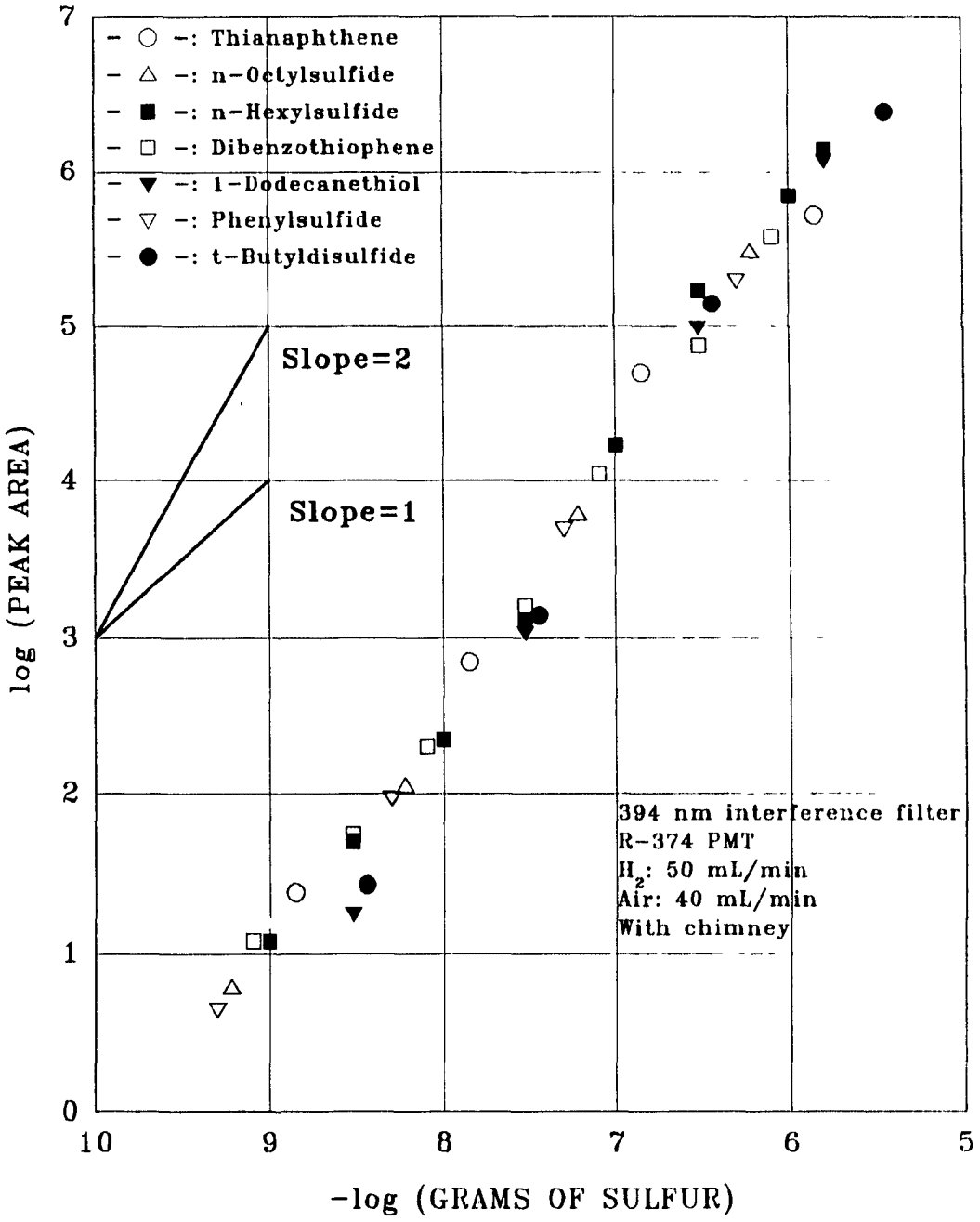

Figure 3.10 *Calibration curves for seven sulfur compounds in the quadratic mode. Filter: 394 nm band-pass. Hydrogen: 50 mL/min. Air: 40 mL/min. PMT: R-374.*

while analytically relevant, this comparison is not fair. A quadratic emitter will respond to any structure-related difference in the second power. A mechanistically fairer approach is to use the square root of response or, more simply, to compare the *amounts* of compounds that respond with equal intensity in the two modes. If this is done, the variation in the quadratic mode is only slightly larger than a factor of two, *i.e.* it does not appear to differ significantly from the variation in the linear mode.

If such narrow variation ranges should prove typical of a more extensive and variegated future roster of sulfur compounds, it would suggest that the *quadratic* mode may be independent of molecular structure as well.

3.6 Quenching Effect on Sulfur Response

3.6.1 Introduction

Hydrocarbons quench the response of sulfur in the flame photometric detector[155]. This effect is troublesome to analytical chemists, particularly those concerned with petroleum products, air pollutants, pesticide residues, and food aromas. Considerably effort has therefore been expended to elucidate the quenching mechanism [reference 29 and studies cited therein]. Its most common description assumes collisional deactivation of electronically excited S_2 by CH compounds or their fragments[115].

In contrast, there exists no major study of quenching effects involving elements other than sulfur. The impression the reader may easily gain from the literature is that the quenching of sulfur luminescence is unique in extent if not in kind. The rather sporadic nature of references to the quenching of other elements only serves to strengthen this impression.

Currently, proposed quenching mechanisms for sulfur remain speculative and quenching data for other elements sparse, so that any further information should be of benefit. In particular, analysts might be interested in being able to predict the effects of peak overlap in multi-element samples. For analyzing such samples, the FPD conditions are typically chosen for the best response of some particular important element, say sulfur.

In this section, the following questions will be investigated: Is the response of sulfur in the linear mode less or more susceptible to quenching than in the quadratic mode? What happens to the response of other FPD-active elements under the quenching conditions of the linear sulfur mode? Under such conditions, does sulfur really behave differently from the other elements?

3.6.2 Quenching of Sulfur in Both Modes

Any quantitative definition of quenching effects in the new linear sulfur mode needs to include a comparison with the established quadratic mode, preferably carried out on the same instrument. Figure 3.11 shows in full symbols the quenching curve (the relative fractional response) of 8 ng di-*tert*-butyldisulfide against the methane concentration at the detector flow conditions of the quadratic mode, and with almost all of the S_2 luminescence admitted by the 500 nm short-pass filter. (Essentially the same curve, though at lower sensitivity, can be obtained by the traditional 394 nm interference filter.) The approximate shape and position of this curve is well known[14], although the conventional measurement involves an overlapping peak rather than, as here, a constant background of a quencher.

Given its typical (distorted) S-shape, a measure of quenching intensity may be reasonably and conveniently taken at half height, *i.e.* at the point where quenching has reduced a peak to 50% of its original height and $R/R_0 = 0.5$. This occurs in Figure 3.11 for the quadratic mode at a methane concentration (calculated on the total gas flow) of about 3.7×10^3 part per million (v/v), or a carbon flow of 3.4 microgram per second.

Figure 3.11 also includes a measurement of the red region with a 600 nm long-pass filter (empty symbols). The two curves were determined off the selfsame peaks, hence are exactly comparable. The 600+ nm region contains the spur of the S_2 bands plus the bands of the linear emitter, though at the flow conditions of the quadratic mode. It is nevertheless obvious that the linear emitter appears less susceptible to quenching than S_2^*. The effect is not large, about a factor of 2 at half height. The corresponding data for a tenfold amount of analyte - 80 ng di-*tert*-butyldisulfide - are very similar and, consequently, are not shown here.

Despite the exiguity of the effect when measured by the difference in quencher concentration for an equal extent of quenching, it can appear dramatic whe. measured by the ratio of relative peak heights for an equal - and very heavy - quencher concentration. This is demonstrated in Figure 3.12 (note its logarithmic ordinate). The response ratio of the two channels rises to more than 100 at the methane concentration of 16,000 ppm (which is a very heavy level for the quadratic moue). Although rare, such cases do occur in analytical practice.

It is obvious that the real quenching effect in the linear mode has to be assessed at its own operational conditions. Peaks obtained at the conditions of the linear mode (high hydrogen, no quartz chimney) are monitored by, again, two photomultiplier channels. The first channel, equipped with a 600 nm long-pass filter,

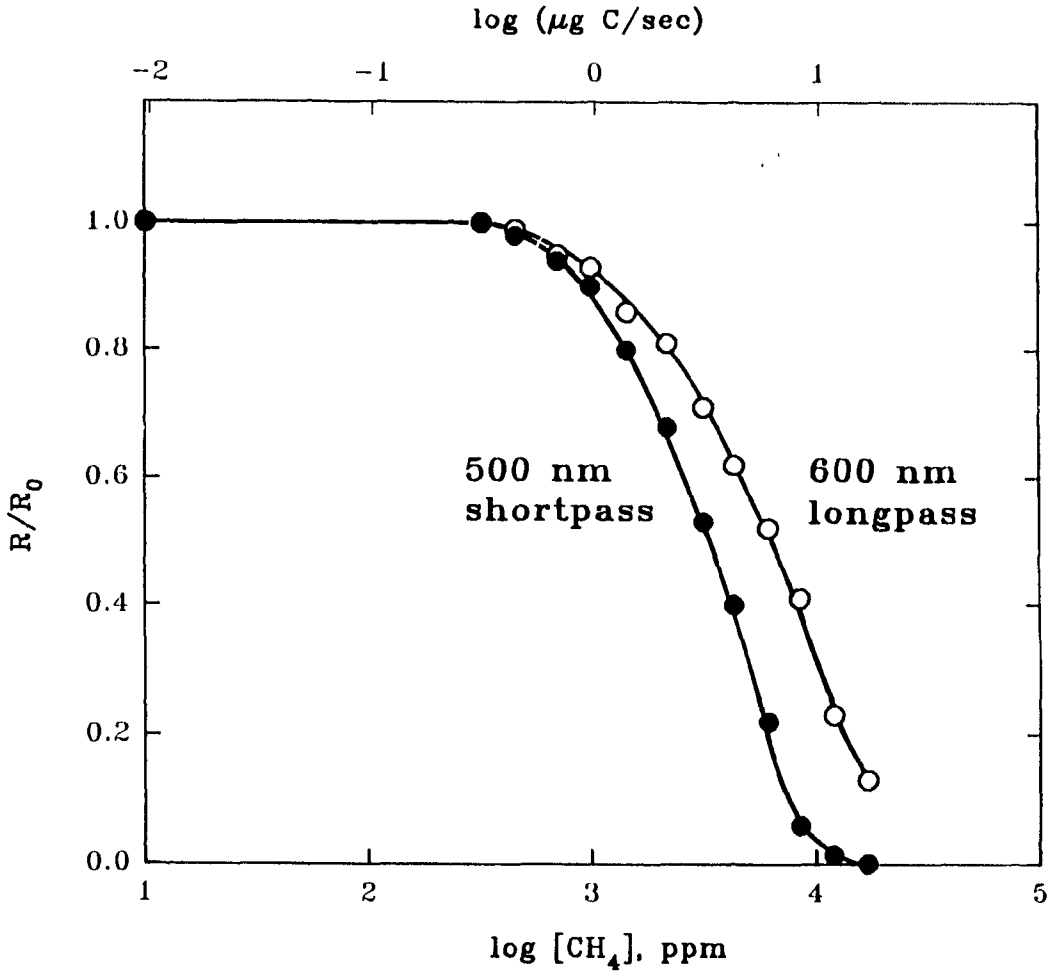

Figure 3.11 *Quenching of sulfur in the quadratic mode. Analyte: 8 ng of di-tert-butyldisulfide; Quencher: methane introduced from an exponential dilution flask into the hydrogen line. R: quenched response; R_0: unquenched response. 50 mL/min hydrogen, 40 mL/min air and R-374 PMT.*

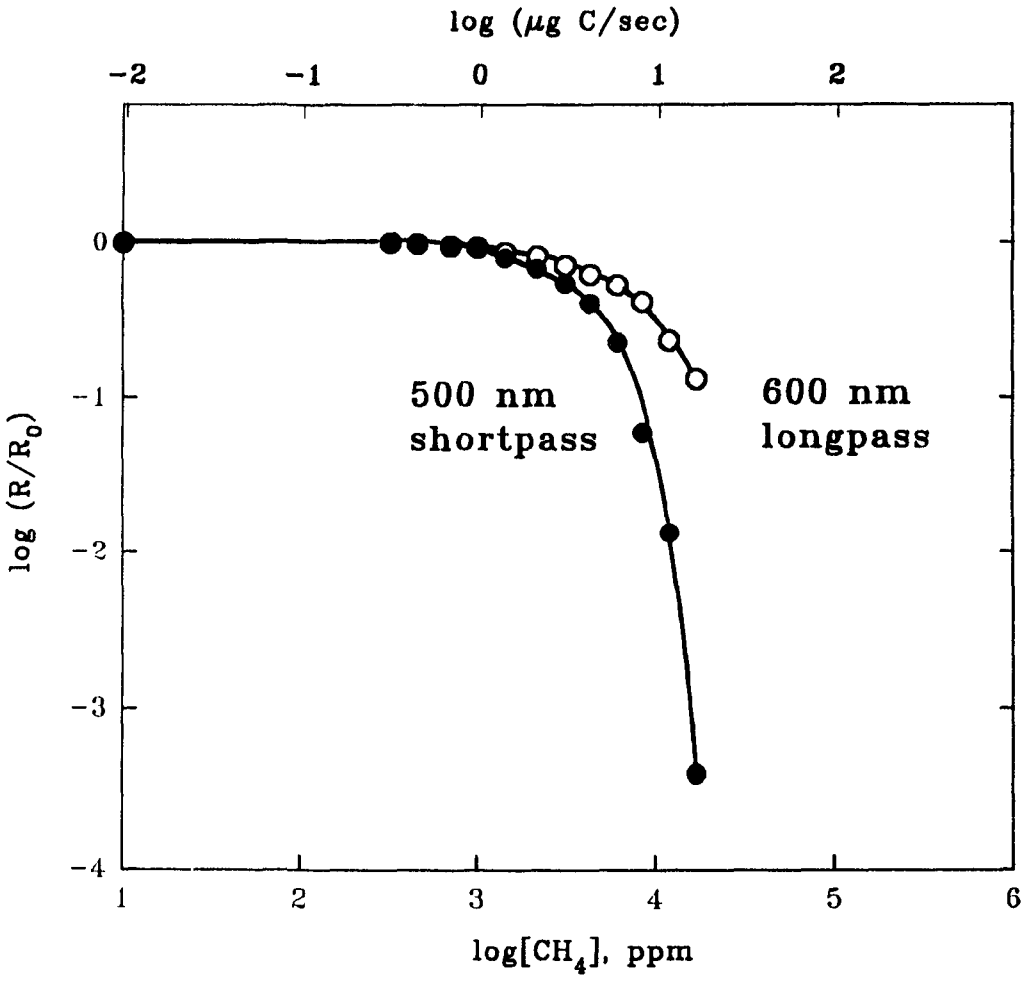

Figure 3.12 *Extreme quenching of sulfur in the quadratic mode. Similar to Figure 3.11 but with logarithmic ordinate to cover measurements extended to extremely severe quenching conditions.*

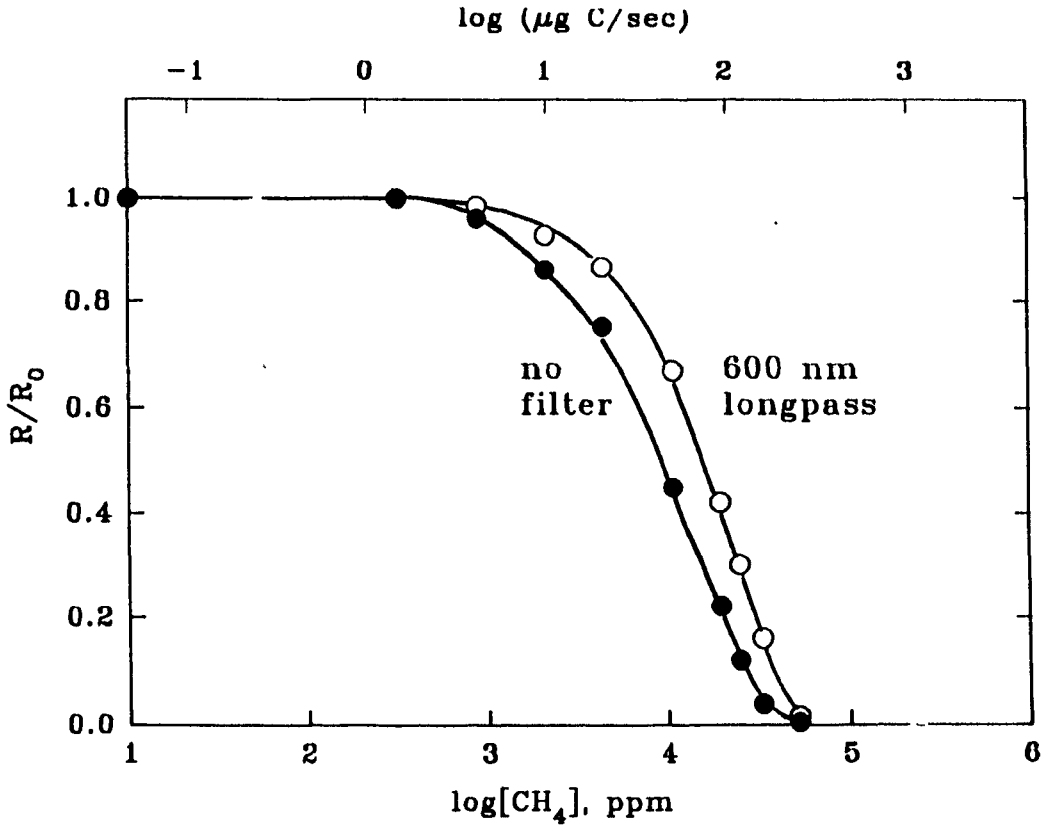

Figure 3.13 *Quenching of sulfur under the flow conditions of the linear mode. Analyte: 50 ng of thianaphthene. 500 mL/min hydrogen, 40 mL/min air and R-374 PMT.*

truly represents the linear mode: the calibration curves are purely first order. The second channel is "open" (filterless), *i.e.* it can potentially accept radiation from a 180 to 850 nm range. Calibration curves for sulfur in this channel are approximately quadratic: though weakened by the flow conditions, the S_2 bands still dominate.

Figure 3.13 shows the quenching curves for sulfur measured under the flow conditions of the linear mode. The methane levels for peak half height are about 9.6×10^3 ppm and 1.6×10^4 ppm (still calculated on the - now much larger - total gas flow) for the open and 600+ nm channels, respectively. The corresponding carbon flows are 43 and 73 µg C/s. Again, the difference between the two optical channels amounts to very roughly a factor of 2.

Much more important than the comparison of the two optical channels is, however, the comparison of the quadratic with the linear mode under individually optimized conditions (*i.e.* the 500 nm SP curve in Figure 3.11 *vs.* the 600 nm LP curve in Figure 3.13). Here is the interesting result: the linear mode can tolerate a methane flow that is roughly 4.4 times in ppm and 22 times in µg C/s *larger* than in the quadratic mode (the numbers are measured at a fifty percent reduction in peak height, but remain fairly constant over the whole analytically interesting quenching range). The former number represents the spectrochemically relevant one in that it addresses the flame composition; the latter, however, represents the chromatographically and analytically important one in that it predicts the relative intensity of quenching by an overlapping peak (or a heavy column bleed). This approximately twentyfold greater tolerance of the linear as opposed to the quadratic mode may prove decisive for the much demanded determination of sulfur compounds in complex hydrocarbon matrices.

A look at these numbers for sulfur reveals a surprising fact: it seems that they are not all that different from the numbers that characterize the extent to which the luminescence of some other elements is quenched. The literature contains some isolated examples of quenching beyond sulfur (and some of these measurements will be included in the next chapter). For instance: the total-flame methane

concentrations for a 50% reduction of peaks containing Fe[49], Ru[50], and Mn[52] are 4.8×10^3, 1.6×10^3, and 3.5×10^3 ppm (v/v), respectively. That is quite close to, say, the 3.7×10^3 ppm measured for sulfur in the quadratic mode. However, these measurements are taken at significantly different flow conditions (H_2 range 300 to 370, air range 60 to 80, N_2 range 44 to 55 mL/min, *i.e.* with generally higher air flows and hence at higher temperatures).

3.6.3 Comparison of the Quenching of Sulfur with Other Common FPD-Active Elements

What is obviously needed for a valid comparison is to examine all elements at the same approximate conditions ("approximate" because different temperatures for the chromatographic separation, hence slightly different column flows and bleed levels; as well as temporally, qualitatively, and quantitatively variable memory effects of the chromatographic system can never be completely ruled out). The common set of conditions which should be applied to all elements of this study will obviously be that of the linear sulfur mode.

Figure 3.14 shows the quenching data of the chosen five elements, plus sulfur, at the exact conditions of the linear mode. Figure 3.15 presents the very same peaks obtained from the second open (filter-less) channel. What is obvious but surprising in these Figures is that all curves huddle together, with sulfur right in their middle. No other curve is horizontally farther away from the sulfur curve than by a factor of 2 (Figure 3.15) or 3 (Figure 3.14). If all elements and both Figures are thrown together, the strongest quenching curve turns out to be no farther than a factor of four away from the weakest. This suggests that the behavior of all (so far tested) elements is similar and, hence, that the benavior of sulfur is not unique.

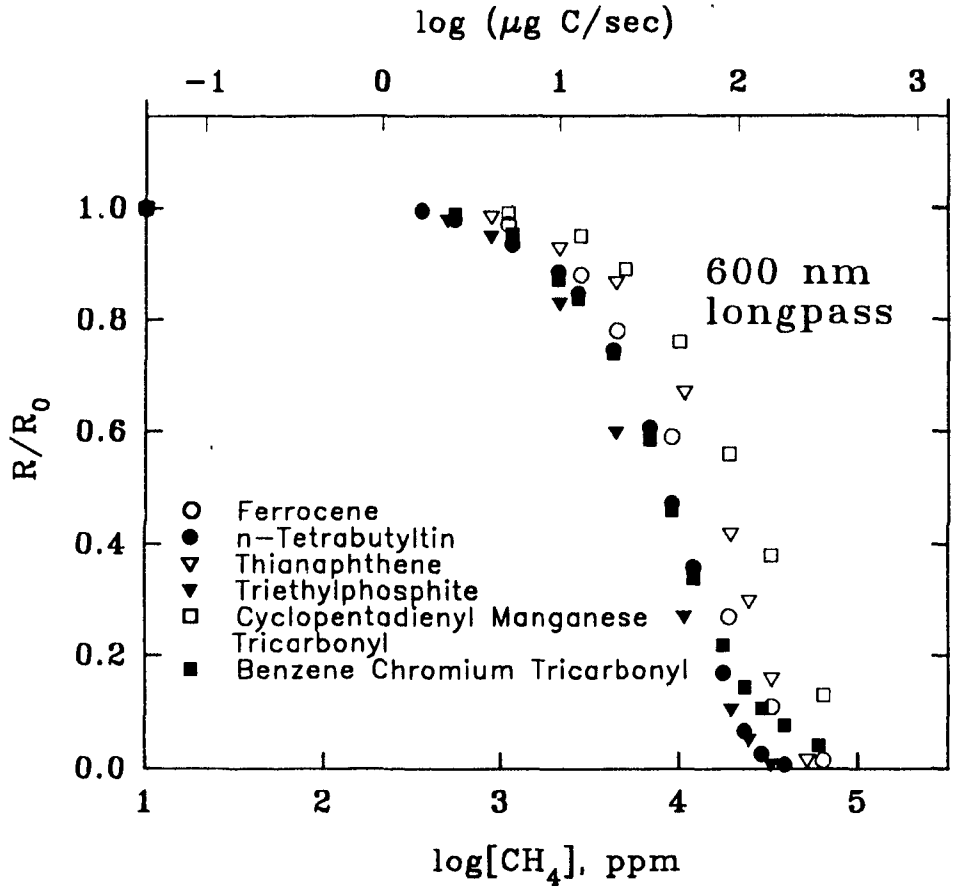

Figure 3.14 *Quenching of six elements in the linear-sulfur mode. Flow conditions: 500 mL/min hydrogen and 40 mL/min air. R-374 PMT. Curves not drawn for clarity.*

A further experimental question is whether the calibration curve under quenching conditions is linear and, if so, whether its linear range is comparable to that of the unquenched curve - as well as whether the parallelism of the two curves perhaps extends even beyond the end of their respective linear ranges.

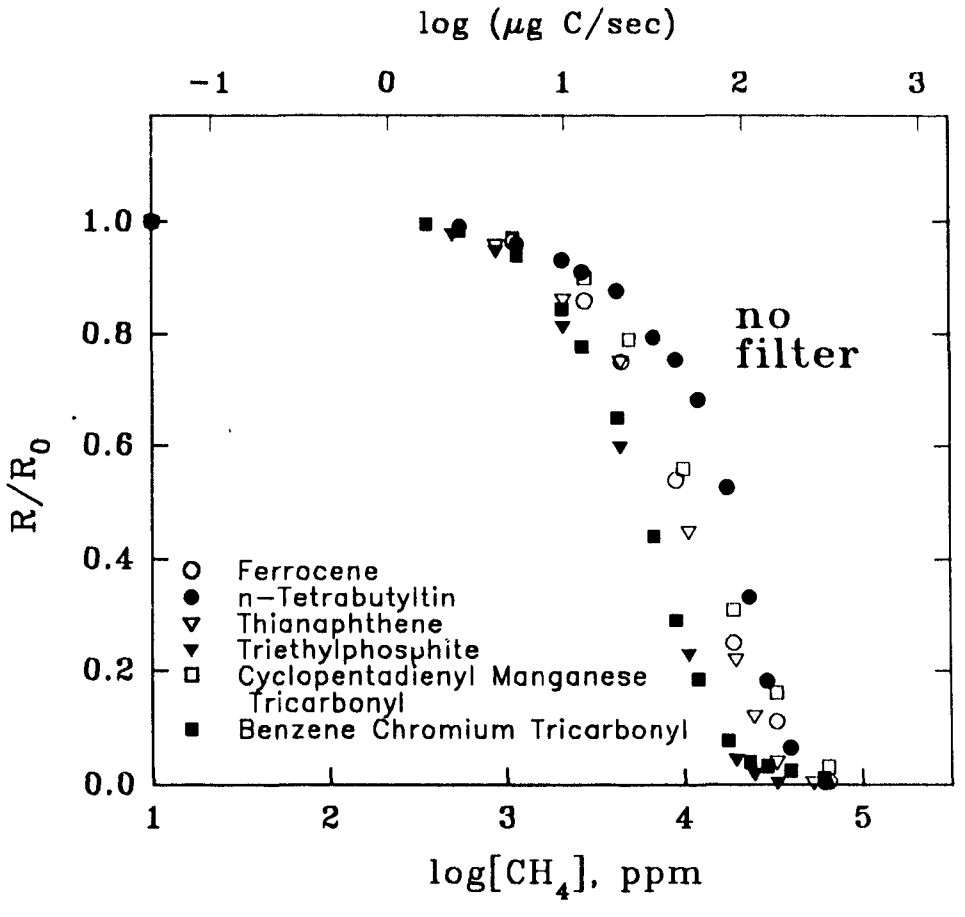

Figure 3.15 *Quenching of six elements in open mode. Simultaneous measurements from the experiment shown in Figure 3.14, but as seen through the second, filter-less FPD channel. R-374 PMT.*

The corresponding experiment measures a series of conventional log/log calibration curves for sulfur (and five other elements) - with *vs.* without methane, and for the full spectrum *vs.* just its linear portion. The results are presented as the ratio of the calibration curves (the fractional quenching) versus their

flow in log (mol X/sec), where X is the FPD-active element; and arrows are also included to point to the upper (-10%) end of the linear (or, in two cases involving sulfur, quadratic) response range of the unquenched curves. Figure 3.16 shows this for the 600 nm long-pass filter (*i.e.* the linear sulfur mode), Figure 3.17 for the corresponding filter-less mode. The choice of the individual quenching level of methane for each analyte is arbitrary; however, it generally ranges from 40% to 70% peak reduction so that any change in the relative quenching intensity would show up clearly in the Figures.

Figure 3.16 clearly establishes that quenching is independent of analyte concentration over almost the whole linear range (of the unquenched calibration curve under the flow conditions of the linear-sulfur mode). Even beyond the linear range, however, most deviations from this rule are relatively minor. Sulfur itself is certainly well-behaved in this regard.

In the *open* channel more emitters may be seen. For instance: tin will emit via SnOH, SnH and the blue surface emission on quartz[37]; some transition metals will radiate via atomic lines, molecular bands and continua[63], *etc.*. It could be argued that this should not influence the constancy of the response ratios, as long as all simultaneous emissions obey first-order kinetics. However, in the regions approaching and exceeding the end of the linear range, with different emitters of the same element perhaps experiencing different endpoints of linearity, the use of a wider optical range may cause a greater deviation from the "ideal" behavior.

This may indeed have been the case for some elements in the wide open range monitored for Figure 3.17, although none of the deviations is exorbitant and, for a case like tin, the deviation is even smaller than in the 600-850 nm region. The only strikingly deviant curve is that of sulfur, but that is mostly due to a

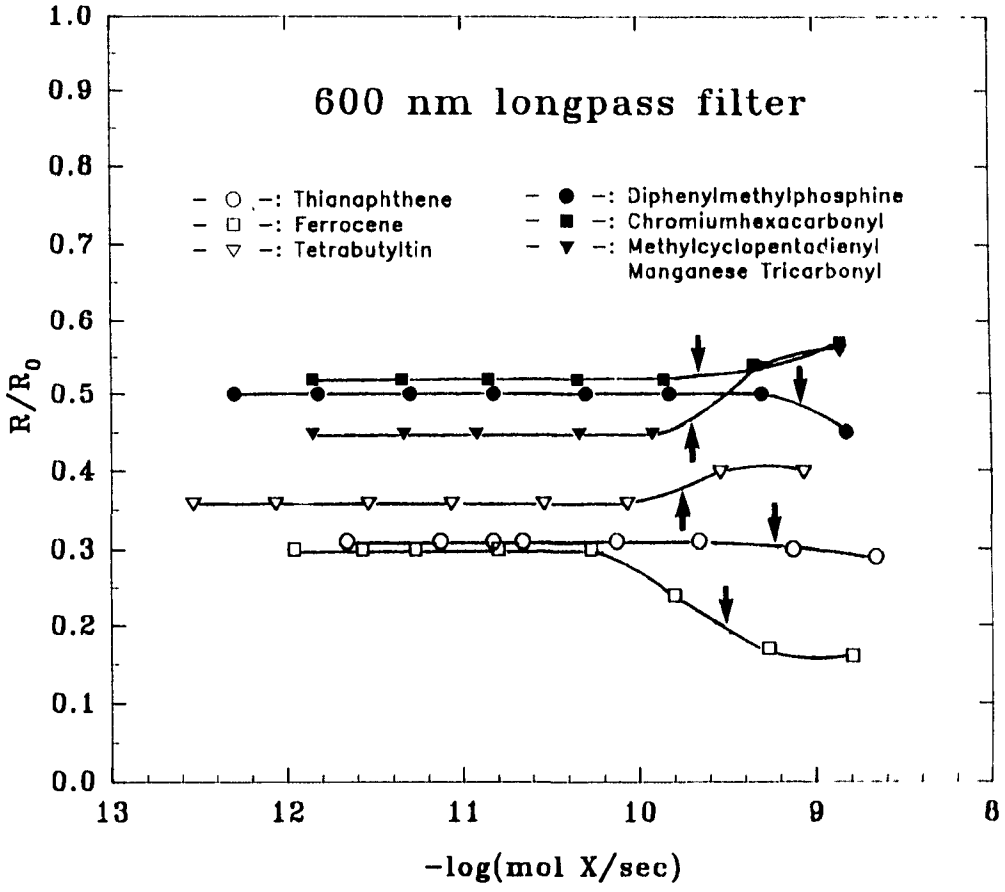

Figure 3.16 *Fractional response of six elements under constant quenching conditions in the linear-sulfur mode. 500 mL/min hydrogen, 40 mL/min air and R-374 PMT. X = FPD-active element. The arrows mark the end (10% deviation) of the linear, unquenched calibration curves.*

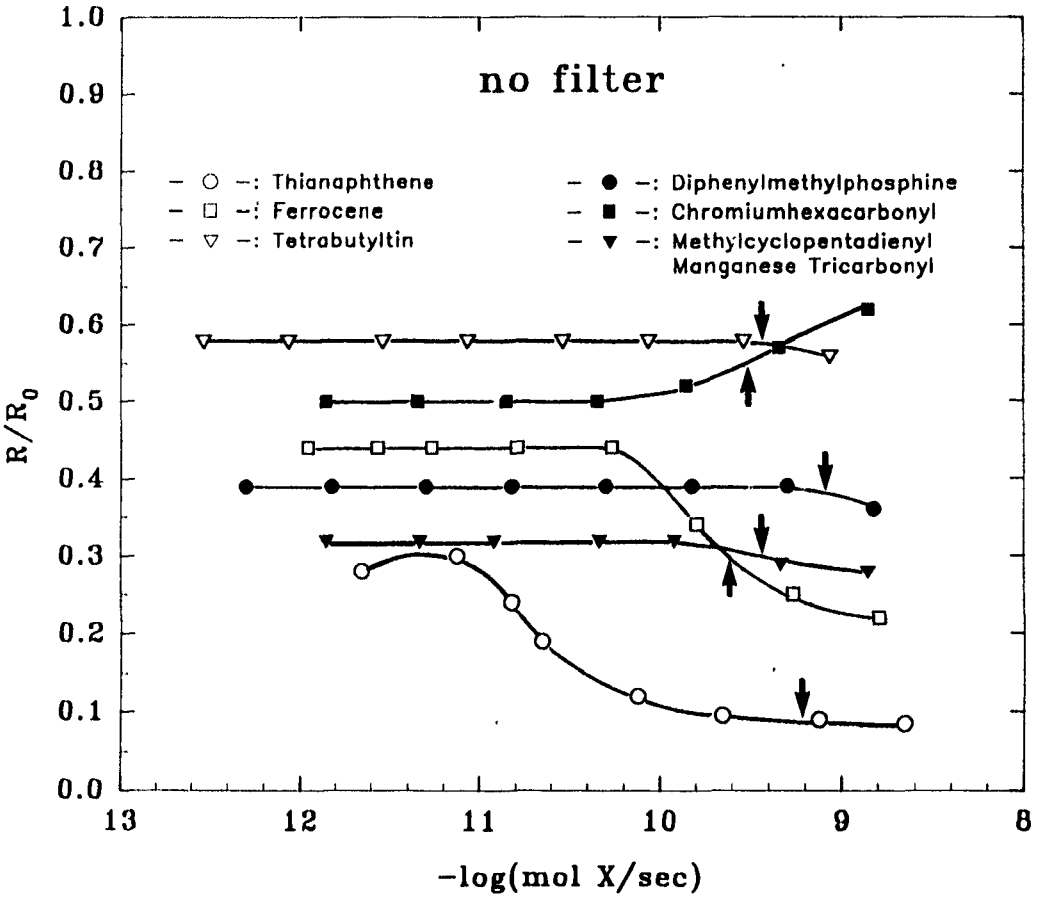

Figure 3.17 *Fractional response of six elements under constant quenching conditions in open mode. Simultaneous measurements of the experiment shown in Figure 3.16, but as monitored by the second, filter-less FPD channel. R-374 PMT.*

quadratic mixing up with a linear emitter. It would therefore seem that the rule of constant relative quenching could be extended even to very wide spectral regions (provided that all monitored emitters respond in linear fashion and remain in linear range).

Chapter 4. FLAME PHOTOMETRIC DETECTION OF TRANSITION METALS

4.1 Iron

4.1.1 Introduction

Ferrocene (dicyclopentadienyl iron) and many of its derivatives are stable, volatile compounds. They serve in a variety of roles, *e.g.* as additives to flames (antiknock compounds), as stabilizers of lubricants and polymers, as photosensitizers, *etc.*. Some have also insecticidal properties.

Volatile iron compounds have been analyzed by gas chromatography, almost from the inception of the technique, with non-selective monitors such as the thermal conductivity detector. For selective detection, the flame photometric detector was shown to respond to ferrocene[20]. The minimum detectable limit was then about 2 ng, and the linear range more than two orders of magnitude. However, that result was obtained in a survey of compounds containing a larger variety of hetero-elements. The detector conditions were uniform for all analytes, and the spectral features were not investigated.

This study was designed to optimize ferrocene response, map the spectrum of its luminescence, chromatograph additional iron compounds, establish calibration characteristics, and check for interference by hydrocarbons.

4.1.2 Optimization of the Ferrocene Response

Figure 4.1 shows a graph with typical data from one of the optimization runs. Here, the air flow, hence the flame temperature, is varied over a large range. The response — *i.e.* the luminescence emitted upon introduction of

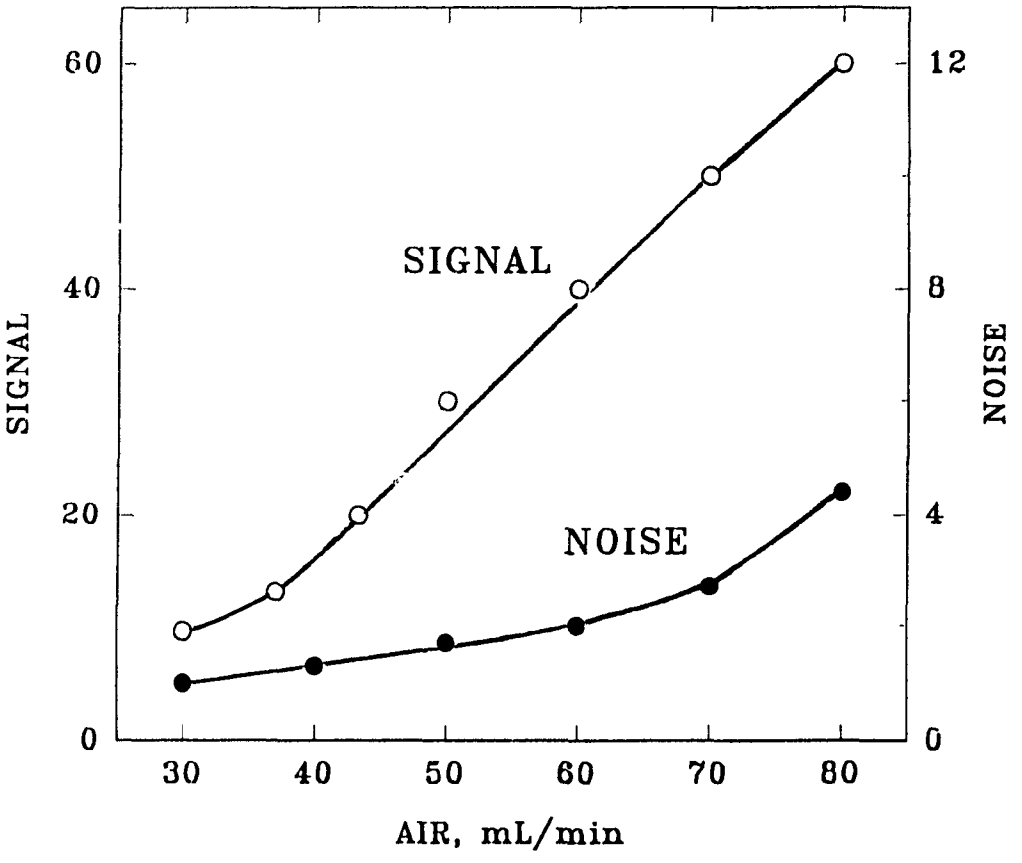

Figure 4.1 *Behaviour of signal and noise with increasing air supply. Analyte: ferrocene. Hydrogen flow rate: 250 mL/min. No quartz chimney, no flame shield, and no interference filter. R-268 PMT.*

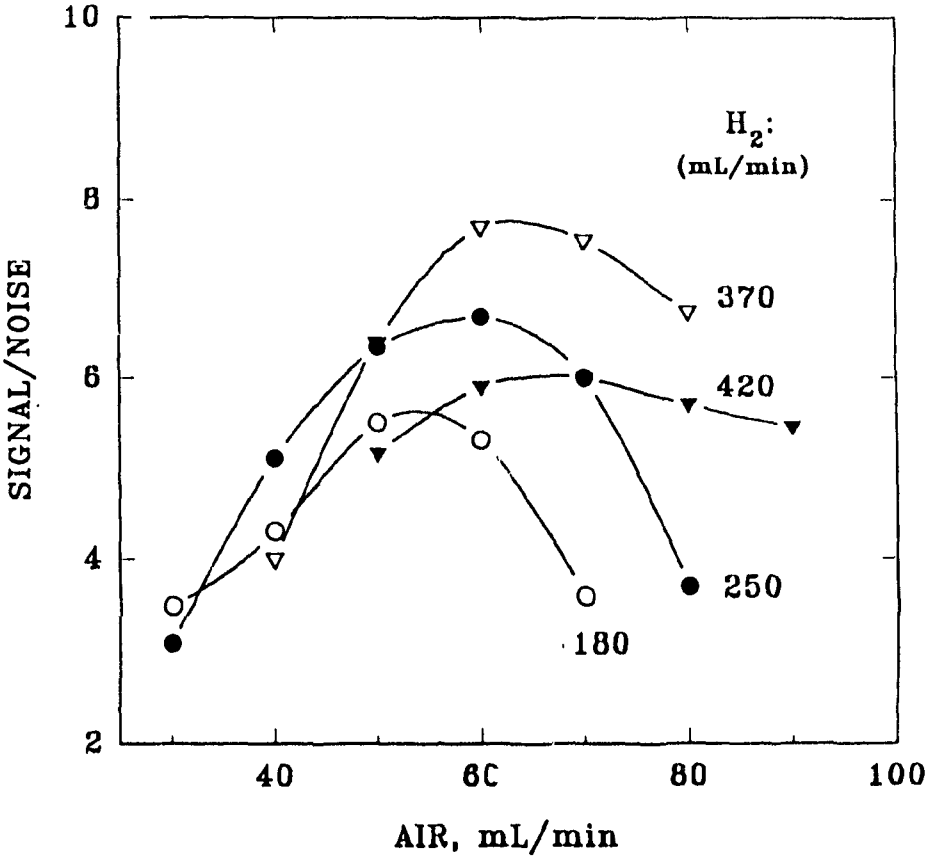

Figure 4.2 *Variation of the S/N ratio (from ferrocene injections) with varying air flow rate at four different hydrogen levels (as indicated by the numbers in the Figure). Other conditions as in Figure 4.1.*

ferrocene — increases steadily with the air flow. Unfortunately but not unexpectedly, the baseline noise also increases with increasing air flow-rate, *i.e.* with temperature and baseline current, and it does so in an apparently exponential fashion. This means that the S/N ratios will reach maxima, and a few of these maxima are shown in Figure 4.2. The highest S/N ratio is obtained at about 370 mL/min hydrogen and 60 mL/min air (plus 23 mL/min nitrogen added to the air supply, and 32 mL/min nitrogen from the column).

The optimum hydrogen flow-rate here is quite high for an FPD, but the optimum air flow-rate supplies only about 7% of the hydrogen that would be required for a stoichiometric flame. At these conditions, the maximum temperature measurable by the thermocouple is 570 °C at the base of the flame.

In the experiments relating to all the flow-optimization, quenching and calibration plots, multi-injections were made for each setting of conditions. This is necessary to ensure that the operational conditions (*e.g.* hydrogen or air flow) are stable, and that there is no mistake in injecting. The σ (standard deviation) values that resulted from multiple injections were never big enough to show up as error bars in the flow-optimization, quenching and calibration curves.

Other optimization strategies were pursued as well. The quartz chimney and the adjustable steel flame shield were removed, resulting in higher sensitivity. No changes were apparent on varying the injection port and detector base temperatures between 160 and 200 °C. This suggests that no significant premature decomposition of ferrocene occurred in the chromatographic system. Adding nitrogen (about 20 mL/min) to the air supply also improved performance, but larger amounts extinguished the flame.

4.1.3 Spectra and Interpretation

Figure 4.3 shows a spectral scan of luminescence from a ferrocene-doped flame under conditions close to the analytical optimum. The peak width is determined by the very wide 2.0-mm slits (bandpass 6.7 nm), but that is all the low intensity and the diffuse nature of the luminescence would permit. The wavelengths of the peaks suggest that they represent some of the commonly found atomic lines. For instance, in a copper arc, the three strongest lines for transitions to the $^5D_4$ ground state are, in order of their intensity, 371.994, 385.991 and 344.061 nm[67]. These numbers correspond, given our wide error limits, quite well to the peaks shown in Figure 4.3 (373, 387 and 345 nm), although the latter might include more lines than the three cited ones. The strongest line in the copper arc is located at 373.487 nm and it may also be present here, as well as become more prominent in the following spectra.

With slightly lower hydrogen and higher air supply rates, the spectrum changes (see Figure 4.4). The peak at *ca.* 373 nm increases; this may, but need not, be due to the emergence of the above-mentioned 373.487 nm line. Also, a broad feature is starting to emerge between about 400 and 600 nm.

In the next spectrum, shown in Figure 4.5, the hydrogen flow-rate has been dramatically decreased to the point that the flame is now approximately stoichiometric. The 0.5-mm slits can be used because of the vastly increased light level. Some of the atomic lines may still be present, but they are now dwarfed by other features. In the ultraviolet, some new peaks have come up at *ca.* 359 and particularly at 367 nm; those may be related to the two groups of FeOH bands as described by Gaydon[65]. Bands found in the hydrogen-air flame at *ca.* 344, 358, 383, 388 and 393 nm, and attributed to FeO[68], may also be present; however, these may

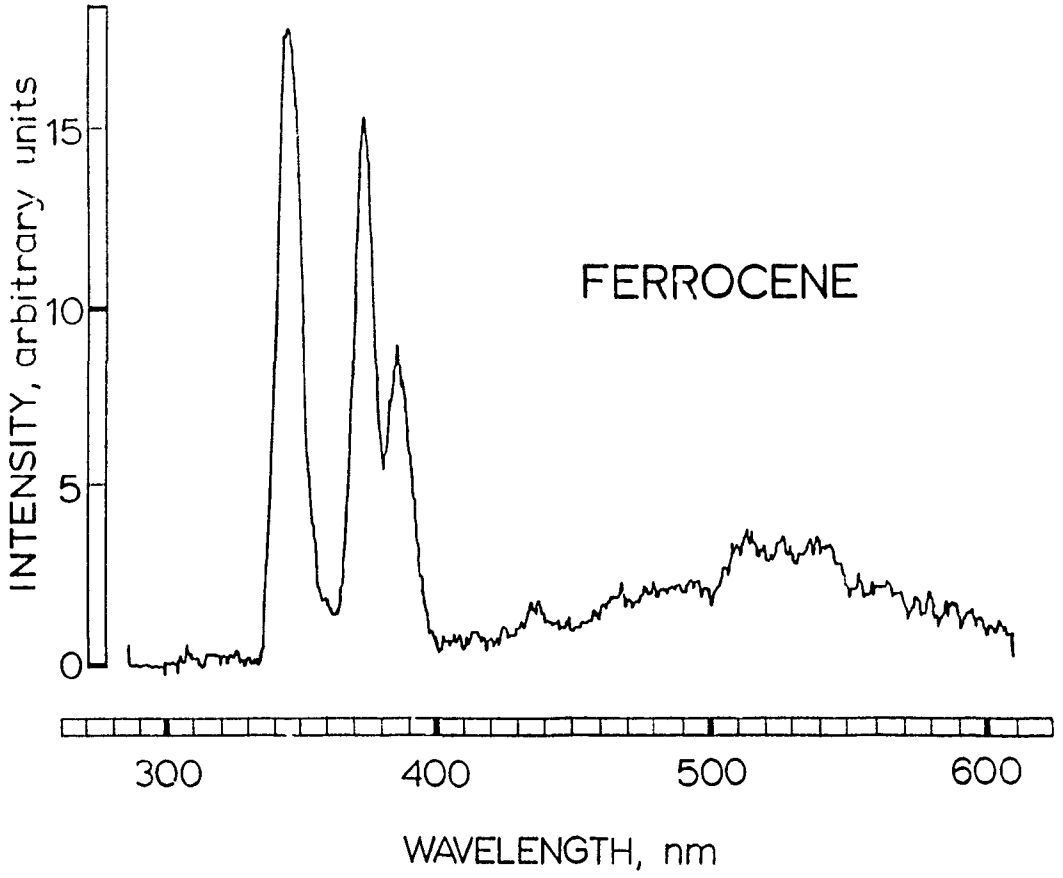

Figure 4.3 *Spectrum scan of a ferrocene-doped flame with conditions close to the optimal flows (slightly higher air flow rate, 80 mL/min). 1/4 meter grating monochromator with R-268 PMT. Slits: 2.0 mm. Bandpass: 6.7 nm.*

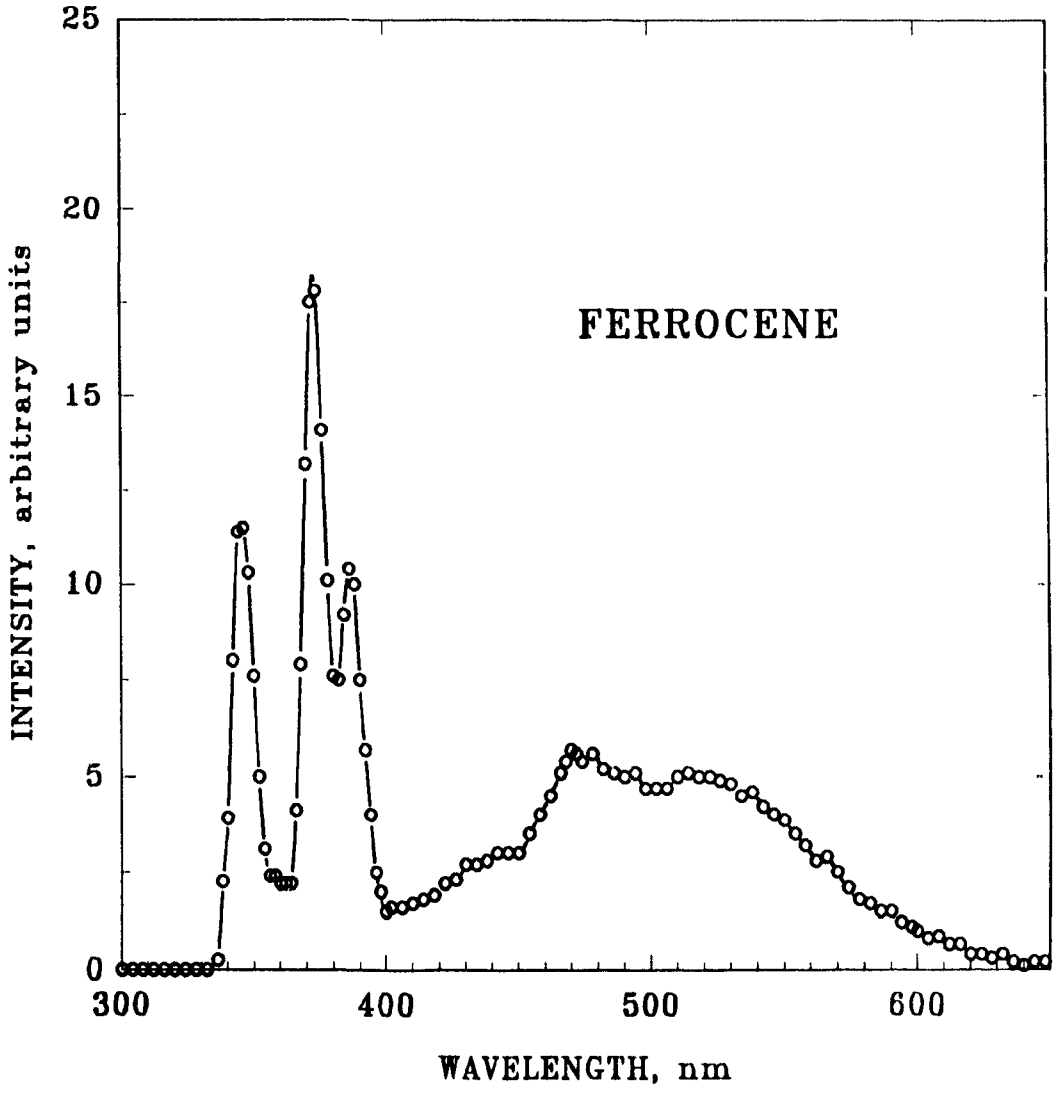

Figure 4.4 *Spectrum from ferrocene, hydrogen-poorer (260 mL/min) than at optimal conditions. 1/4 meter grating monochromator with R-268 PMT. Slits: 2.0 mm. Bandpass: 6.7 nm.*

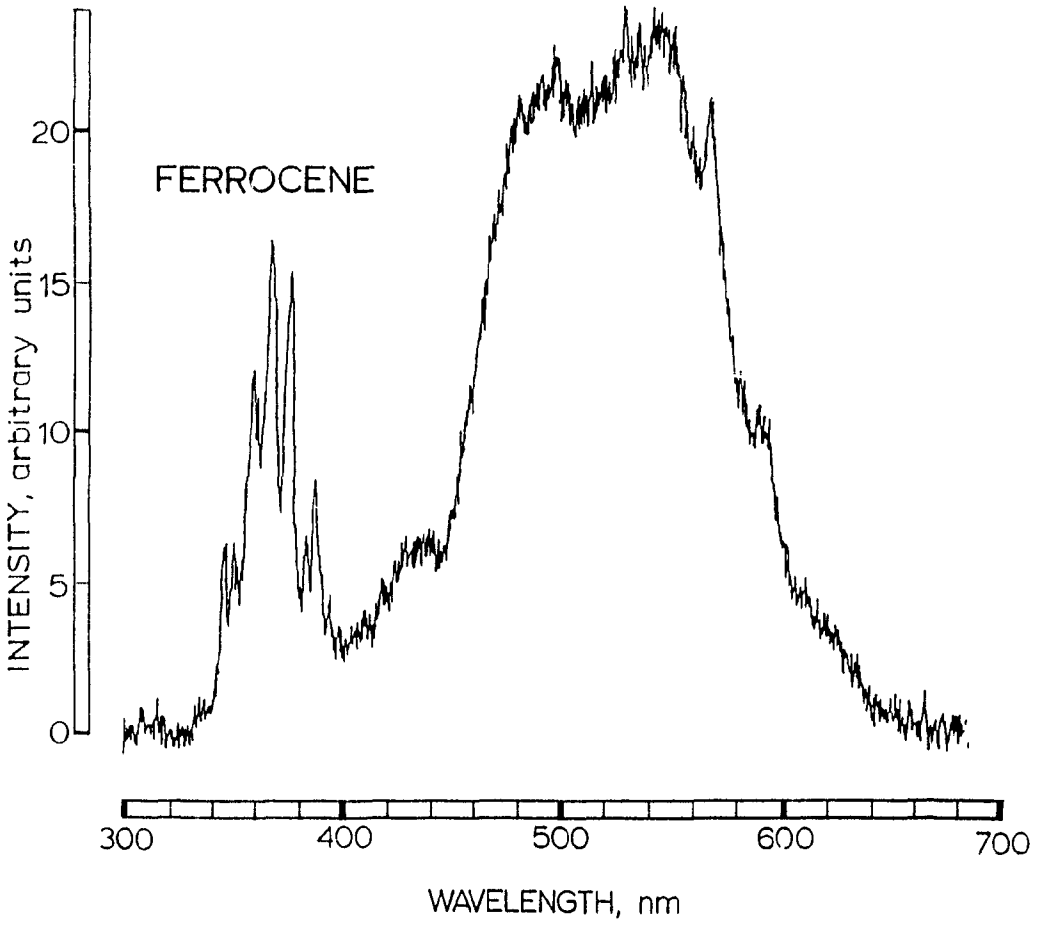

Figure 4.5 *Spectrum of ferrocene-doped flame, with conditions close to stoichiometric flame conditions. Hydrogen: 46 mL/min. Air: 75 mL/min. 1/4 meter grating monochromator with R-268 PMT. Slits: 0.5 mm. Bandpass: 1.7 nm.*

as well be due to prominent atomic lines originating from higher excited states of the iron atom. The large hump between 460 and 580 nm must remain unassigned.

Note that Figures 4.3 and 4.5 differ from Figure 4.4 in that the former were run with a constant input of ferrocene and automatic wavelength scanning. Figure 4.4, on the other hand, was determined by repeatedly injecting ferrocene while manually advancing the wavelength drive. Figure 4.4 thus recorded the pure response, while emissions other than those resulting from ferrocene could have shown up in Figures 4.3 and 4.5. However, scans of the blank flame in these cases confirmed that the luminescence from the flame itself was negligible.

For analytical selectivity, the line at 344 nm or the line at 372 — 374 nm (if these are indeed *lines*) would likely be the best for analysis with an interference filter. Another possibility may be to use a 400-nm cut-off filter, depending on what other FPD-active elements one wishes to guard against.

4.1.4 Response Characteristics

Figure 4.6 shows several calibration curves for iron-containing analytes; plus, for purpose of comparison, one for a sulfur and two for a couple of hydrocarbon compounds.

The calibration curve for ferrocene under optimized conditions (curve 1) ends at a minimum detectable amount (S/N = 2) of 100 pg, or 10 pg/s, or 54 fmol/s. This is one order of magnitude better than found in the earlier survey[20]. The linear range spans four orders of magnitude. The selectivity against dodecane (which appears here as an alkane standard) is about 1.1×10^3, or 1.5×10^4 on an elemental (mol Fe/mol C) basis. In terms of a sensitivity ranking for the FPD, this performance places iron in the vicinity of sulfur and chromium (with only

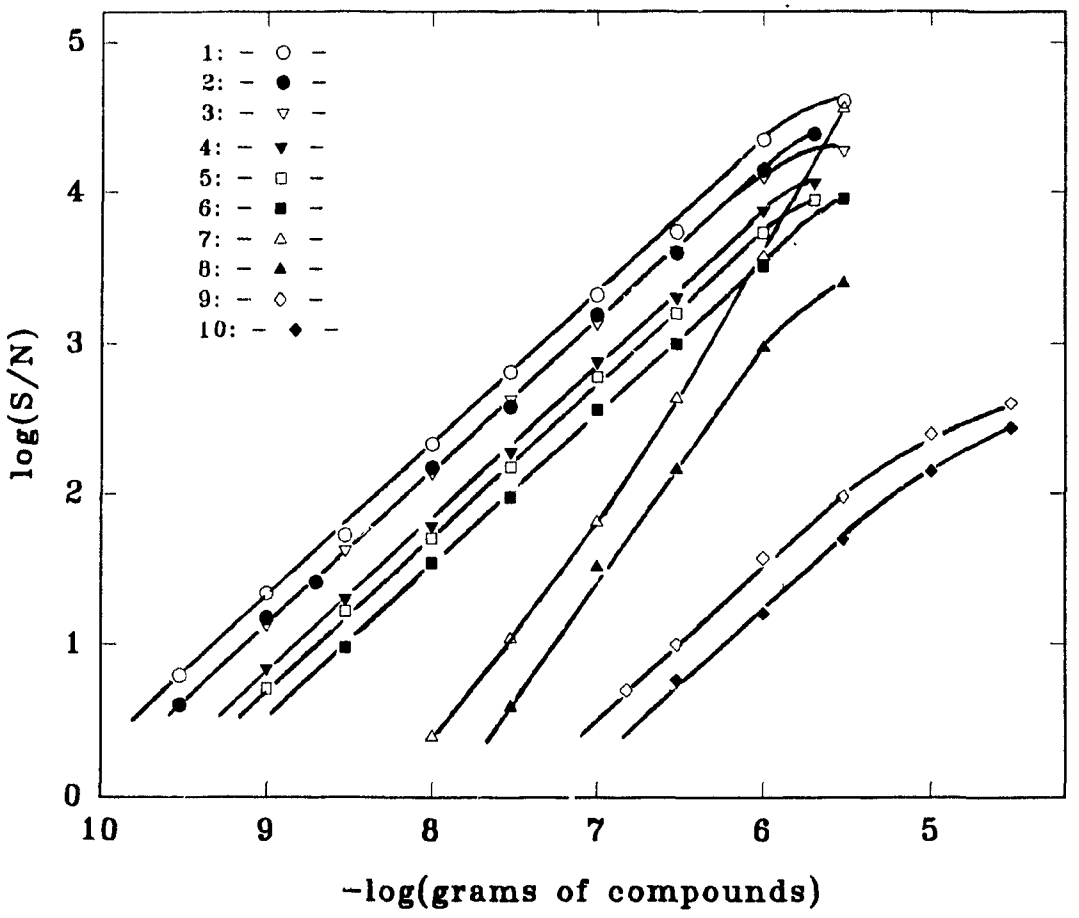

Figure 4.6 *Calibration curves: (1) Ferrocene at optimal conditions. Flow-rates in mL/min: 370 of hydrogen; 60 of air; 32 of carrier nitrogen; and 23 of additional nitrogen. Temperatures in °C: column, 130; injection port, 200; detector base, 170. No quartz chimney. (2) Ferrocene. Conditions as in curve 1, but no additional nitrogen. (3) Iron pentacarbonyl. Conditions as in curve 1, but carrier nitrogen 11 and additional nitrogen 25 mL/min; column 35, injector 80 and detector 80 °C. (4) Acetylferrocene. Conditions as in curve 1, but column temperature 180 °C. (5) Ferrocene. Conditions as in curve 1, but original quartz chimney present. (6) Cyclooctatetraeneiron tricarbonyl. Conditions as in curve 1, but column temperature 150 °C. (7) Di-tert-butyldisulfide. Conditions as in curve 1, but column temperature 150 °C. (8) Ferrocene. Conditions as in curve 1, but hydrogen 37 and air 83 mL/min (closer to stoichiometric); 460 nm long-pass and 580 short-pass filter. (9) Naphthalene. Conditions as in curve 1, but column temperature 125 °C. (10) Dodecane. Conditions as in curve 1, but column temperature 118 °C.*

phosphorus, ruthenium, germanium and tin above it; and with arsenic, selenium, boron and tellurium clearly below it)[37].

This does not mean that sulfur would show up equally well at conditions optimized for iron. In particular, the absence of the quartz chimney decreases sulfur (but increases iron) response. Curve 7 shows the calibration for di-*tert*-butyldisulfide, obtained under the same conditions as curve 1 for ferrocene. The selectivity of iron *vs.* sulfur, at conditions best for iron, is defined by the two curves.

Curve 2 shows the calibration curve for ferrocene, but without the additional 23 mL/min nitrogen diluting the air supply. The curve position (relative to curve 1) shows the decrease in S/N.

Curve 3, which coincides with curve 2 over most of the graph, is that of iron pentacarbonyl. This compound is an interesting analyte in its own right, but it also demonstrates that presence of the metallocene structure is not a necessary criterion for response. Two further iron compounds, acetylferrocene and cyclooctatetraeneiron tricarbonyl, are shown in curves 4 and 6, respectively.

Curve 5 shows the determination of ferrocene, with the original quartz tube of the Shimadzu FPD re-inserted. There is no cogent explanation to offer for the reduction in S/N ratio. Analytically, of course, the removal of the conventional quartz cylinder turns out to be highly beneficial.

Curve 8 shows the calibration of ferrocene under stoichiometric flame conditions, with cut-on and cut-off filters around the big amorphous feature shown in the spectrum of Figure 4.5. Note that response itself is higher, but that this response is analytically barren because of the concomitant high noise level.

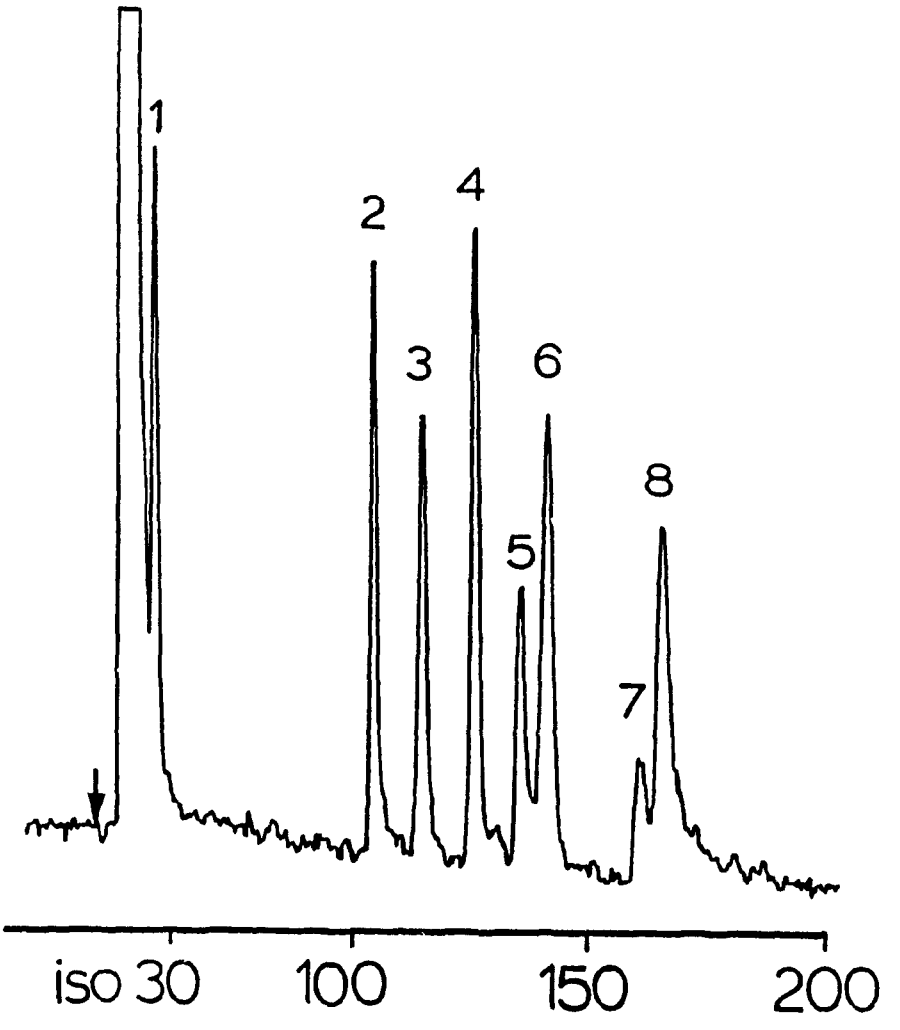

Figure 4.7 *Temperature-programmed chromatography at detector conditions optimal for ferrocene. Isothermal at 30 °C until $Fe(CO)_5$ elutes, then 18 °C/min till 100 °C, then 10 °C/min from 100 to 200 °C. Flow conditions: 370 mL/min hydrogen and 60 mL/min air. No interference filter. Peaks: #1 = 1 ng ironpentacarbonyl; #2 = 200 ng di-tert-butyldisulfide; #3 = 800 ng dodecane; #4 = 1 ng ferrocene; #5 = 0.5 ng 1,1-dimethylferrocene; #6 = 1 ng acetylferrocene; #7 = 0.5 ng ferrocene carboxaldehyde; #8 = 2 ng cyclooctatetraeneiron tricarbonyl.*

Curve 9 and 10 are those of an aromatic and an aliphatic hydrocarbon, which have been included here to characterize the behaviour of a possible hydrocarbon sample matrix. As is well known, aromatics produce somewhat higher light levels.

Figure 4.7 presents a temperature-programmed separation of six volatile iron compounds injected in 0.5 to 2 ng amounts. The chromatogram also shows 200 ng of a disulfide and 800 ng of a hydrocarbon, which produce peaks of comparable size. This demonstrates graphically that the normally large response of sulfur is diminished to a significant degree by the choice of conditions optimal for iron compounds. Besides selectivity, the chromatogram also illustrates the sensitivity with which iron compounds respond. Given that the separation has taken place on a short, low-resolution packed column, still higher sensitivities could be expected from peaks of higher chromatographic efficiency.

4.1.5 Quenching Evaluation

In flame photometric analysis, particularly when the flame is weak and cool, quenching can seriously reduce response. The classical example of this type of interference is the diminution of S_2 luminescence by co-eluting hydrocarbons. To test for the relative importance of quenching, Figure 4.8 shows the decrease in response of ferrocene and dodecane, as caused by increasing amounts of methane in the detector atmosphere. It may be worth noting that methane affects its homologue dodecane more strongly than it does ferrocene.

How serious is such quenching for the analyte ferrocene? It takes about 4.8×10^3 ppm methane in the total detector gases — corresponding to a carbon mass flow-rate of about 1 mg/min — to reduce the ferrocene peak by 50%. If

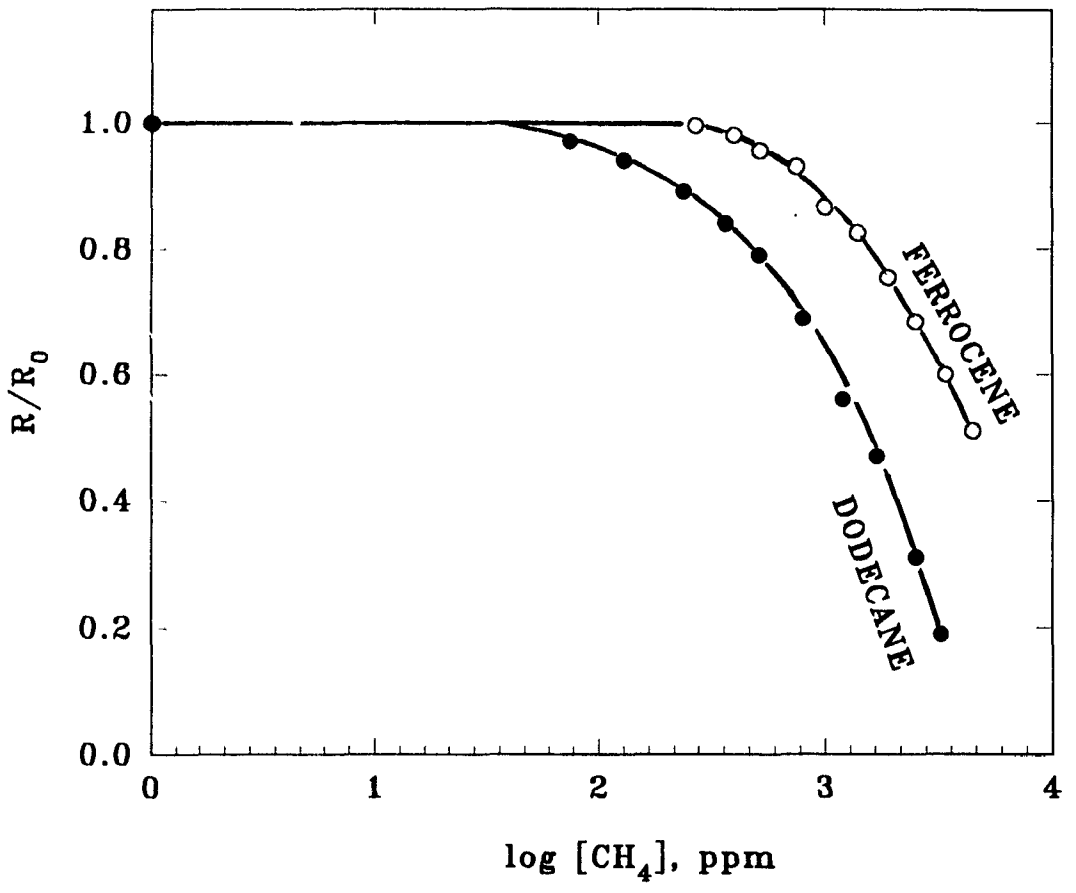

Figure 4.8 *Quenching of ferrocene and dodecane response by methane. Methane concentration given per total detector gas flow. Detector conditions optimal for ferrocen. 370 mL/min hydrogen. 60 mL/min air. No interference filter. R-268 PMT. R: quenched response.* R_0: unquenched response.

methane had been doped only into the column flow, the corresponding concentration there would have been about 7%. That is far larger than any likely continuous input due to contamination. If, on the other hand, the same level of interfering carbon compound had eluted as a peak of the same retention time as ferrocene, quenching

would have been observed only in the upper regions of the calibration curve. In its lower regions, the interferent would have added to the peak height by its own response. The large amounts of carbon necessary to produce a 50% reduction in ferrocene peak height suggest that quenching should not present a serious problem under conventional circumstances.

4.2 Ruthenium

The volatile and stable nature of ruthenocene [bis(cyclopentadienyl)ruthenium] makes it stand out as a suitable test compound for this study. This simple metallocene — as well as other, related ruthenium structures — is of interest in a variety of areas, *e.g.* in catalysis. It has been subjected to the GC technique before[69]; however, no conventional gas chromatographic detector is known to be selective to ruthenium.

The microwave-excited atmospheric pressure helium plasma has been used on ruthenocene (and many other organometallics) eluted from a capillary column. Spectrophotometric monitoring of the 240.3 nm Ru^{+} line yields a minimum detectable amount of 7.8 pg/s, an elemental selectivity against carbon of 1.34×10^{5}, and a linear range of 10^{3} [70].

The aim of this study is to use the existing FPD to detect organoruthenium. Fortunately, the FPD does respond in an analytically useful manner to ruthenium. The following presents the results of conditional optimization, spectral scans, evaluation of quenching behavor, *etc.*

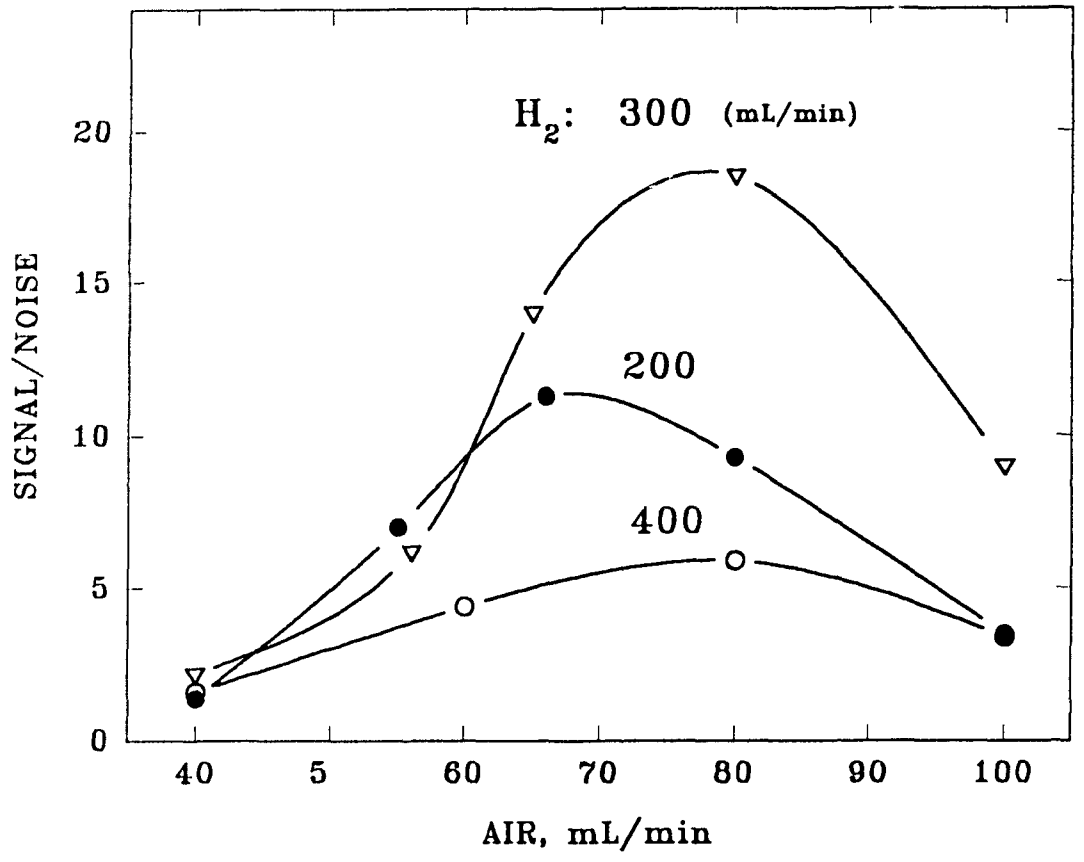

Figure 4.9 *Flow optimization curves for ruthenocene. Column temperature: 155 °C. Temperatures at detector base and at injection port: 180 °C. 20 pg ruthenocene injected. No interference filter. R-268 PMT.*

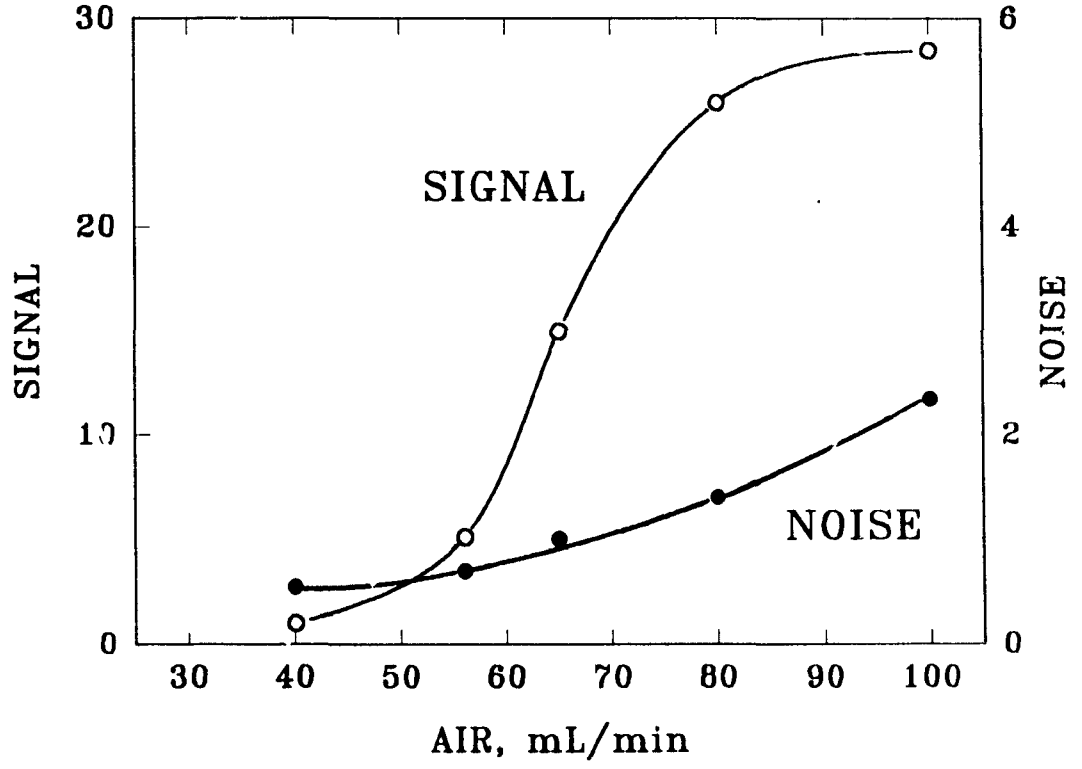

Figure 4.10 *One curve of Figure 4.9 (300 mL/min hydrogen), but plotted as signal (and noise) vs. air flow rate.*

4.2.1 Hydrogen and Air Flow Optimization

The variation of detector gas flow rates in Figure 4.9 shows that the highest S/N ratios are obtained around 300 mL/min of hydrogen and 80 mL/min of air (with "noise" defined as the peak to-peak baseline fluctuation). Visual observation of the ruthenocene peak was possible: the slim luminescence, green with an upper

bluish tinge, appeared strongest in the flame itself, diminished gradually above it, and vanished about halfway up the viewing area - without ever significantly spreading out to the sides. (The term "flame" refers here to the minute region where a very weak glow can be visually observed under no-analyte conditions.) Thus the visible luminescence did by no means fill the total accessible volume - as, for instance, low concentrations of sulfur would have done.

In the context of excitation mechanisms, it is interesting to know whether and to what extent emission increases with increasing air flow (flame temperature). Figure 4.9 displays only the S/N ratio and, while this criterion is of paramount importance in an analytical setting, the signal itself is of more interest in a spectral context. Figure 4.10 shows that the signal itself does not rise much anymore beyond the region where S/N reaches its maximum (in several cases involving other elements, both signal and noise kept right on rising with increasing air flow rates).

4.2.2 Spectrum from Ruthenium

Using the optimum flow rates, the spectrum of the luminescence was determined. It is shown in Figure 4.11. The emissions in the 350 to 400 nm range agree with the atomic Ru lines most prominently found, and most often used, in atomic spectroscopy[68]. They are all transitions to the ground state (a^5F_5) from $z^5G_6^0$ (349.9 nm), $z^5F_5^0$ (372.8 nm), and $z^5D_4^0$ (379.9 nm).

The atomic lines in the 350 to 400 nm region constitute, however, only a minor part of the observed total light intensity. The larger part of the spectrum consists of two similarly shaped, complex structures, whose dominant, sharp emissions are centred at approximately 484 and 528 nm. A search of the literature failed to locate that system (or systems). It should be noted that the peak width of the

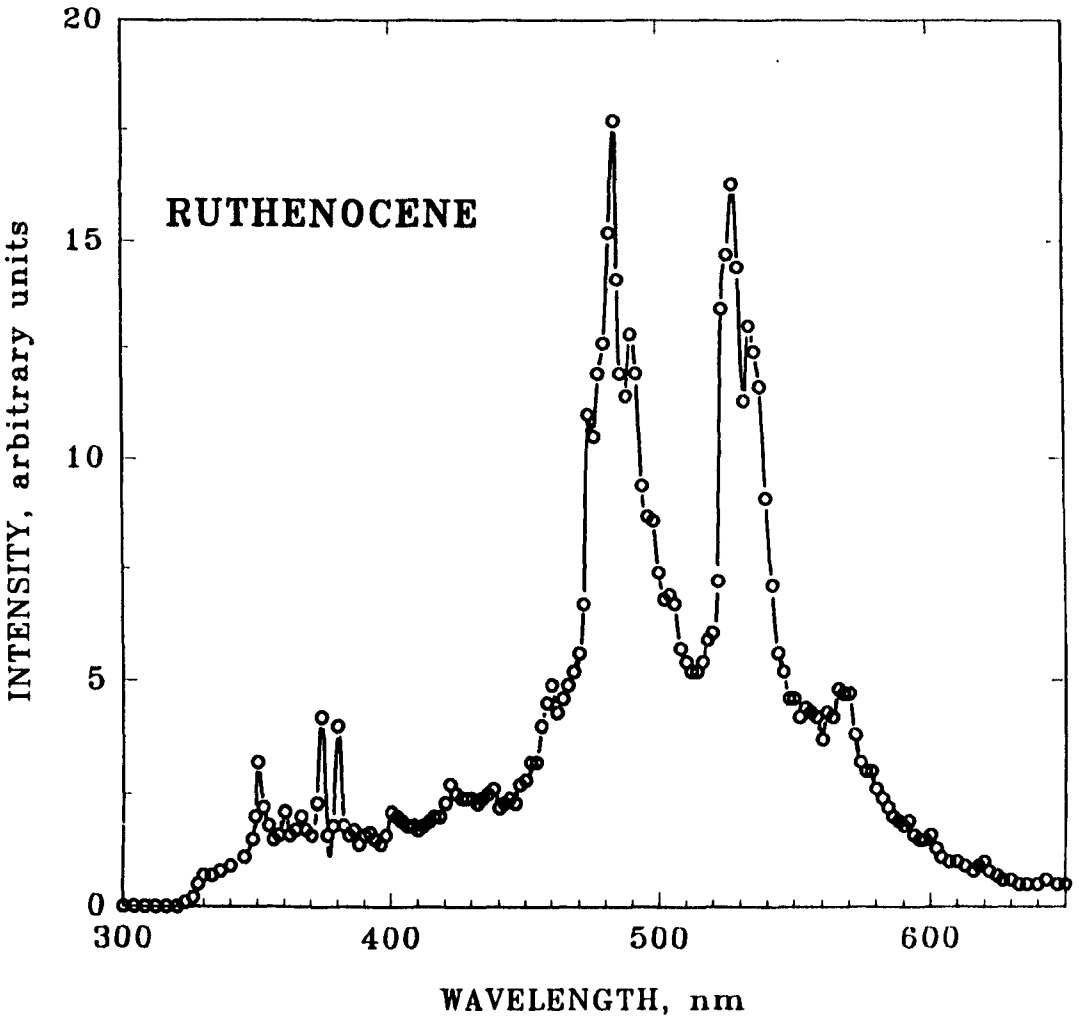

Figure 4.11 *Spectrum of ruthenocene. Hydrogen: 300 mL/min; air: 80 mL/min. 500 ng of ruthenocene repeatedly injected. 1/4 meter grating monochromator with R-268 PMT. Slits: 0.5 mm. Bandpass: 1.7 nm.*

484 and 528 nm bands as shown in Figure 4.11 is likely not the natural one but is determined by the 0.5 mm slit width (1.7 nm band pass).

4.2.3 Calibration Curves

The calibration curves are shown in Figure 4.12. Six are for ruthenocene and the other two for the hydrocarbon standard dodecane. The analytically "best" calibration curve — *i.e.* #1, the one farthest to the left — is obtained without interference filter and quartz chimney, and at optimized conditions. The minimum detectable amount of ruthenocene, as defined by an S/N ratio of two, is 2.2×10^{-12} g. On a peak with a base width of 20 seconds (2σ = 10 seconds), 2.2 pg translates to 2.2×10^{-13} g/s or 9.5×10^{-16} mol/s. (To compare: for the two most prominent analyte heteroatoms in the FPD, phosphorus and sulfur, Dressler reports a literature range of minimum detectable mass flow rates of 1×10^{-13} to 2×10^{-12} gP/s and 2×10^{-12} to 5×10^{-11} gS/s[55] — corresponding to 3×10^{-15} to 6×10^{-14} mol P/s and 6×10^{-14} to 2×10^{-12} mol S/s.)

The selectivity against dodecane, on an (atom Ru)/(atom C) basis — and measured at the same conditions as the "best" ruthenocene calibration curve — is 4.2×10^{5}. The calibration is linear over a range of 1 to 4×10^{4}.

The next best calibration curve (#2) is obtained at similar conditions, except that the additional 20 mL/min flow of nitrogen (piped into the detector's air supply) is shut off.

The next calibration curve (#3) uses a significantly smaller amount of air (50 instead of 80 mL/min). Despite the fact that the temperature measured (583 °C at the bottom to *ca.* 420 °C in the upper regions of the luminescence) is now considerably lower, the detector performance is only slightly diminished. This is

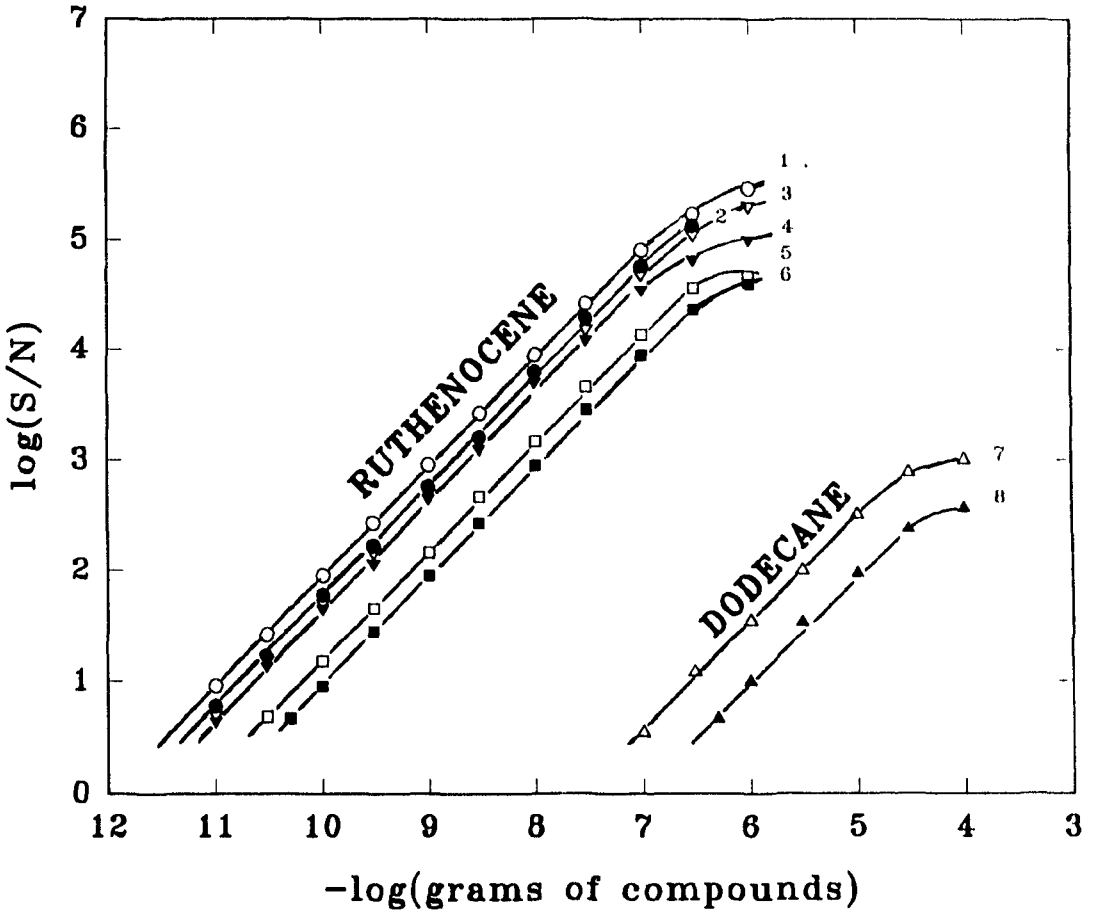

Figure 4.12 *Calibration curves for ruthenocene and dodecane at different conditions. (1) Ruthenocene response optimized for maximum S/N ratio; (2) as curve 1, but no nitrogen added to detector gases; (3) as curve 1, but air flow = 50 mL/min; (4) As curve 1, but 526 nm interference filter present; (5) as curve 1, but quartz chimney present; (6) as curve 1, but ca. 1600 ppm methane present in total detector gases; (7) dodecane response at conditions of curve 1; (8) dodecane response at conditions of curve 4.*

welcome in the analytical context of ruthenocene having to be determined in conjunction with other organometallic compounds, which may require different flame temperatures and/or compositions.

The next calibration curve (#4) is obtained at optimum conditions (like #1), but with a 521 nm interference filter of 4 nm bandpass at half-height. (Note that the filter came as part of the original Shimadzu FPD package, and was specified as the "phosphorus filter" with at least 75% maximum transmission at 526 nm and at most 6 nm bandpass). Not surprisingly, the curve takes a position much lower than Curve #1 since the filter is just sitting on the shoulder of the major band at 528 nm. However the selectivity against dodecane (by comparing curve #4 and #8) is now at a higher level, *i.e.* at 7.4×10^5.

The next ruthenocene calibration curve (#5) simply shows what happens when the original Shimadzu quartz chimney is being put back in: The S/N value drops to one sixth of optimum.

The last ruthenocene calibration curve (#6) employs optimum conditions (like #1), but with *ca.* 1600 ppm CH_4 (as an example of a quencher) added to the detector gases. This large amount of methane reduces the ruthenocene peak by about one half. The calibration curve, however, shifts to the right by about one full decade — owing to the effect of a drastic rise in baseline (background luminescence) on noise in the S/N measurement. Still, the calibration remains linear.

To demonstrate sensitivity and/or selectivity in a graphic manner, Figure 4.13 shows the chromatogram of ruthenocene in the company of other hetero-organics. The detector gas flows are roughly optimized according to the ruthenocene S/N ratio, hence the responses of other elements are depressed to varying extents, but the conditions are not optimal for obtaining the largest possible selectivity for

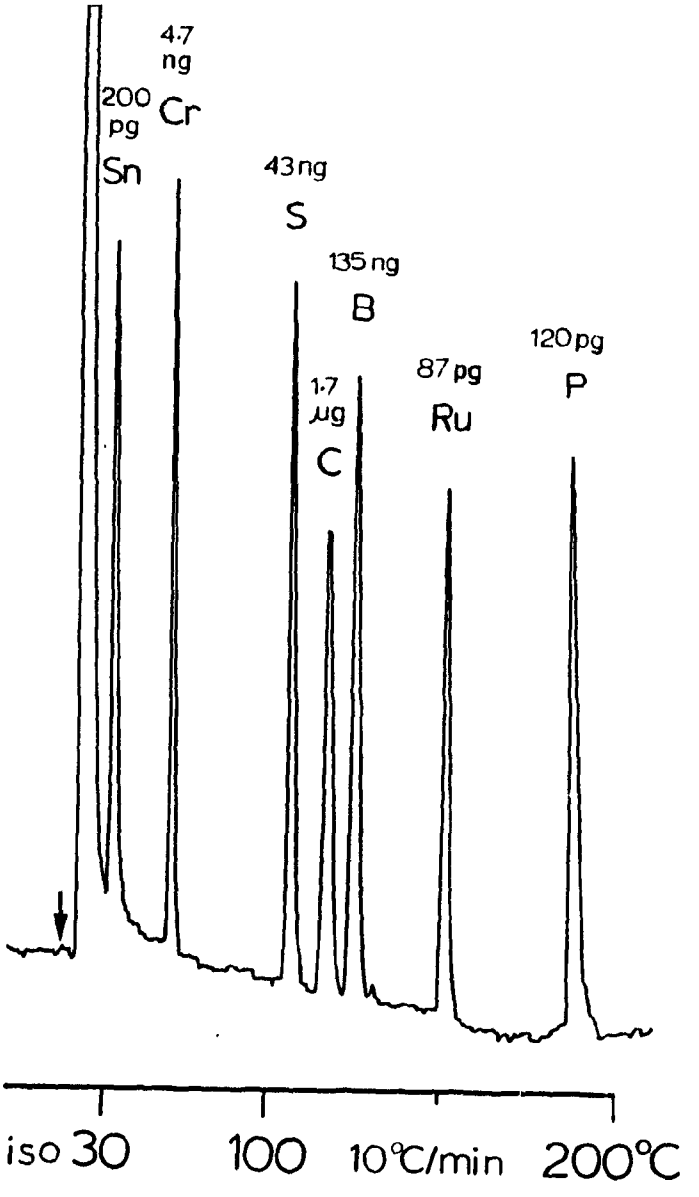

Figure 4.13 *Temperature-programmed chromatography of compounds containing various FPD-active elements. Amounts injected (in order of elution): 0.3 ng tetramethyltin, 20 ng chromium hexacarbonyl, 120 ng di-tert-butyldisulfide, 2 µg dodecane, 180 ng o-carborane, 0.2 ng ruthenocene, 1 ng tri-n-butylphosphate. Flows in mL/min: hydrogen 300, air 80, carrier nitrogen 25, additional nitrogen 23. Detector and injector temperature 200 °C. No interference filter. R-268 PMT.*

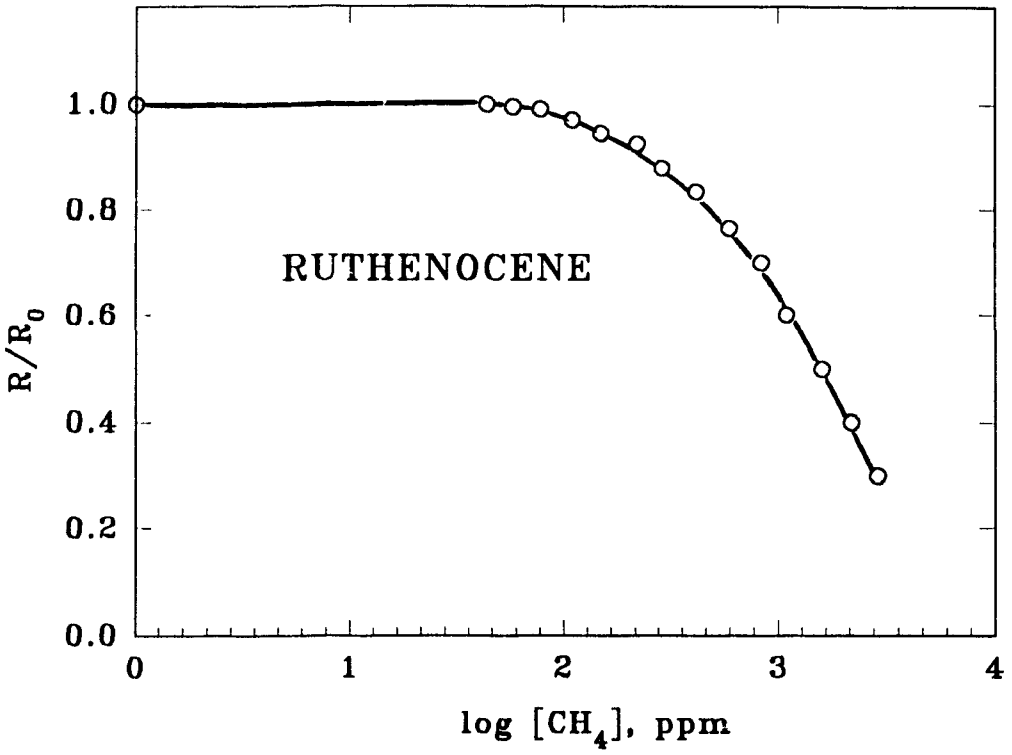

Figure 4.14 *Response of 3 ng ruthenocene at optimized conditions, but with varying concentrations of methane added to the hydrogen supply via an exponential dilution flask. Hydrogen: 300 mL/min. Air: 80 mL/min. R: quenched response.* R_0: unquenched response.

ruthenium *vis-à-vis* one or more of these other elements. Further improvements in single-channel selectivity can be achieved by adjusting flow conditions and by using various interference filters. The elemental responses in Figure 4.13, under those conditions and normalized to ruthenium on an atomic basis, are roughly Ru 1, Sn 0.6, P 0.3, Cr 1×10^{-2}, S 9×10^{-4}, B 8×10^{-5}, and C 5×10^{-6}. Note that these response ratios

are intended for determination of ruthenocene in the presence of other hetero-analytes: they should not be confused with a general FPD sensitivity ranking (for which each element is measured at its own, optimized conditions).

4.2.4 Quenching Effect

Figure 4.14 shows one of a series of experiments that use methane as a quencher and are designed to clarify the magnitude of the expected interference from a co-eluting hydrocarbon peak. (Note: methane is added to the hydrogen supply which, in turn, joins the column effluent prior to reaching the flame.) It takes about 500 ppm (v/v) of methane to reduce the peak height of ruthenocene by a mere 20%. To reduce the peak to one half of its former size requires about 1600 ppm CH_4.

Furthermore, the concentration of methane is calculated here on the total volume of detector gases (*ca.* 422 mL/min), not just on the nitrogen flow through the column. These 1600 ppm would correspond to about 3.1 volume percent, or 7.1×10^{-6} g/s, or 4.5×10^{-7} mol/s, of methane in the 22 mL/min of nitrogen carrier gas. That means that it takes a column flow of methane 3.6×10^{6} and 4.5×10^{7} times larger — on a weight and on a molar basis, respectively — than that of ruthenocene at its (quenched) minimum detectable limit, to reduce the ruthenocene peak by 50%. Thus, if the quencher behaves similarly to methane and is being continuously introduced (as are column bleed, carrier gas contamination, *etc.*) the quenching effect should be unobservably small in most practical cases.

4.3 Osmium

In the context of determining trace levels of metallocenes of the iron group by GC flame photometry, osmocene [bis(cyclopentadienyl)osmium] is the analyte with the heaviest atom. Osmocene takes gas chromatography well[69], and it

can be detected via the Os^+ line at 225.6 nm in a microwave-excited atmospheric pressure helium plasma (capillary GC-MED) with a detection limit of 6.3 pg/s, a selectivity against carbon of 5.00×10^4, and a linear dynamic range of 10^3[70]. Reported here is the sensitive and selective detection of osmocene by the conventional GC flame photometric detector.

4.3.1 Spectrum from Osmium

Figure 4.15 shows the spectrum obtained at roughly optimized flow conditions by repeated injections of osmocene at different wavelengths. The recorded fine structure is indeed present: Crucial injections were repeated to ensure that the various small peaks had not been caused by experimental perturbations. The width of most of these corresponds to the spectral bandpass (about 7 nm), *i.e.* their true width cannot be assessed from Figure 4.15. The only atomic line of osmium[67] (that may be) present in the spectrum is the lowest-energy transition to the ground state at 442.047 nm (about 2.8 eV or 271 kJ/mol). (Note that the injections began at 200 nm but that the results are shown only starting from the region where luminescence could be observed, *i.e.* from 400 nm on). In contrast, the response of ferrocene, at comparable flame conditions, is based mainly on *atomic* Fe emission. Ruthenocene, on the other hand, shows only very minor atomic contributions; its major system is of still unassigned origin. Furthermore, the spectrum obtained by injecting osmocene contains several small peaks whose wavelengths are spaced in apparent sequences, but an attempt at interpreting these without achieving a better resolved spectrum would be highly speculative. The main, broad emission continues strongly into the near infrared. (Note that the apparent end of the continuum is determined by the R-1104 phototube, which has a nominal upper wavelength limit of 850 nm.) The origin of

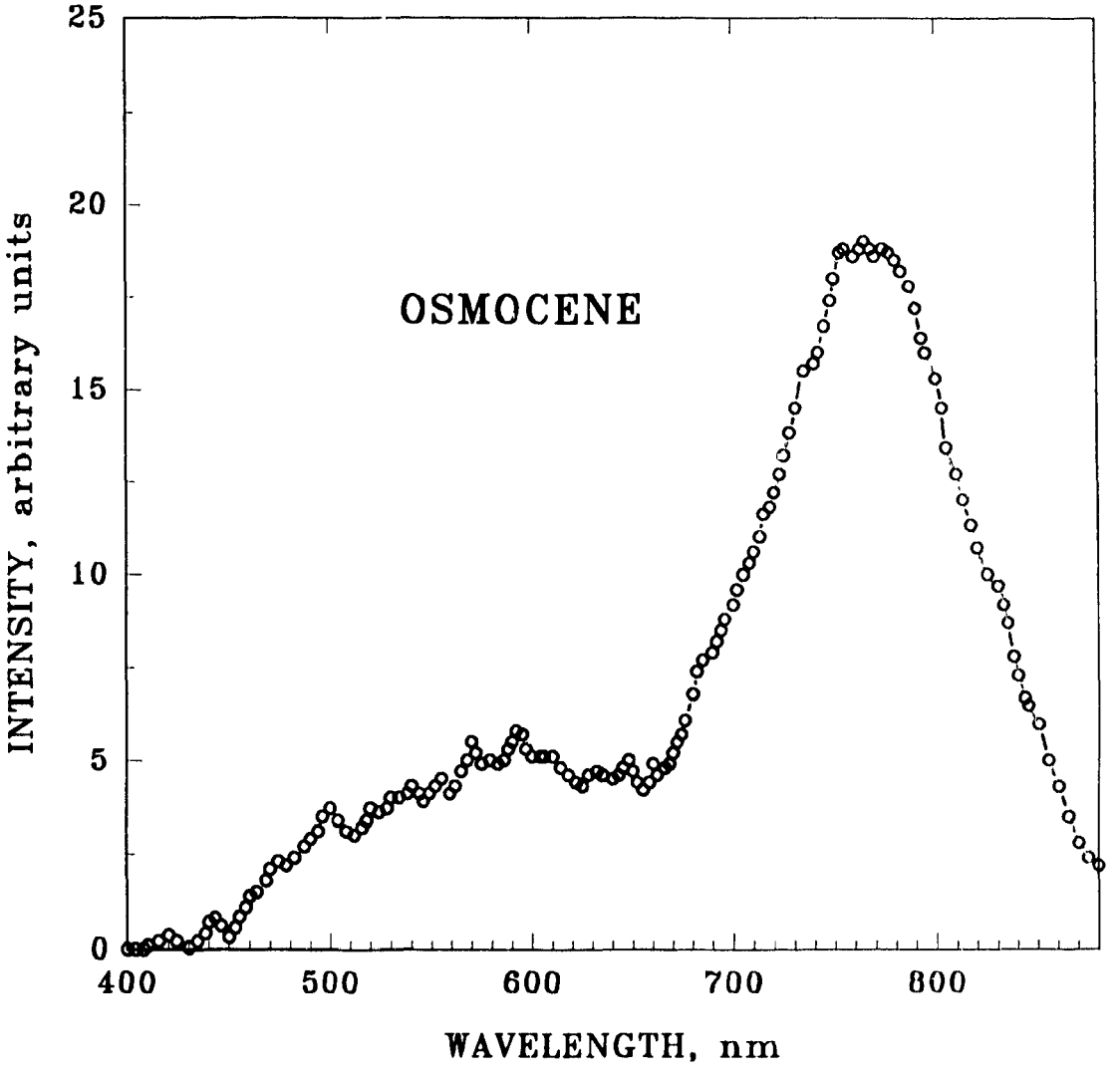

Figure 4.15 *Spectrum of luminescence obtained from osmocene. Hydrogen: 300 mL/min. Air: 60 mL/min. 1/4 meter grating monochromator with R-1104 PMT. Slits: 2.0 mm. Bandpass: 6.7 nm.*

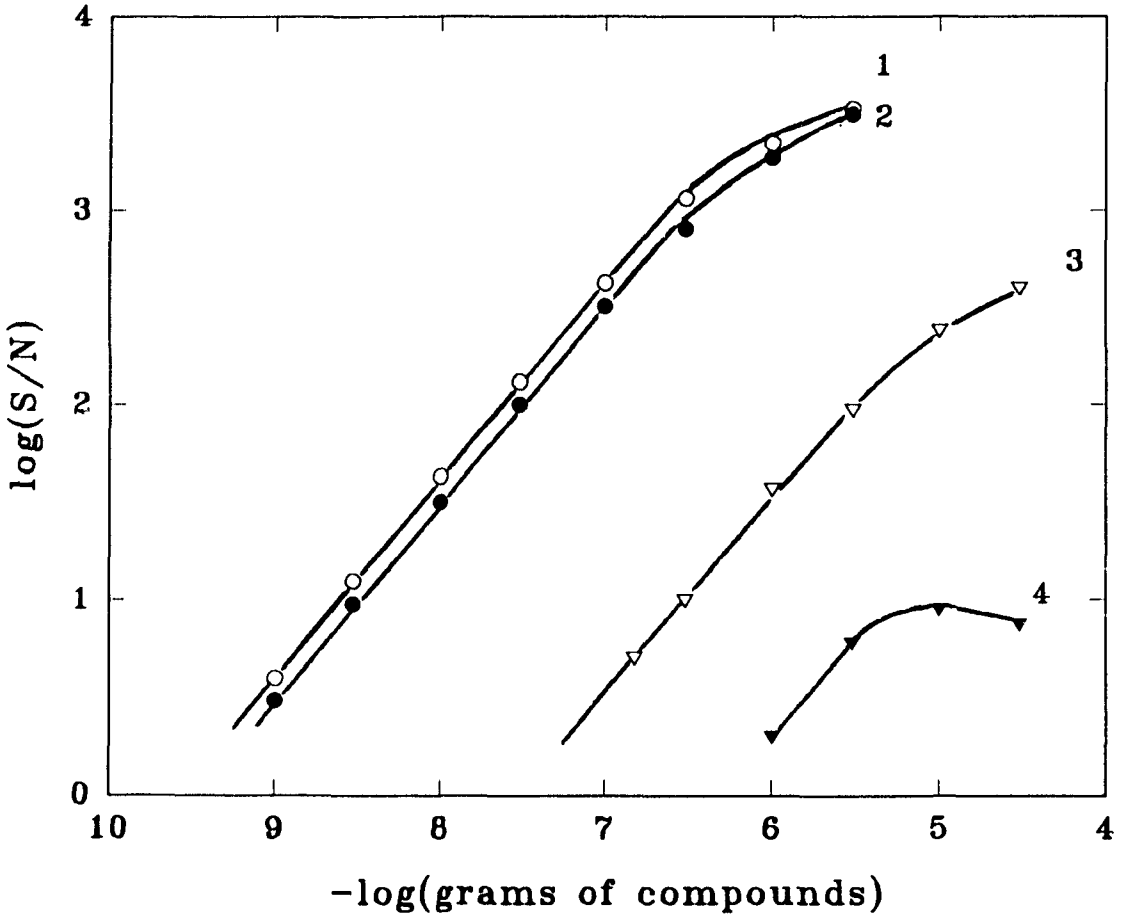

Figure 4.16 *Calibration curves of osmocene and naphthalene at approximately optimal conditions for osmocene. (1) Osmocene. Gas flows in mL/min: 300 of hydrogen, and 60 of air. Temperatures in °C: 170 at column oven, and 200 at detector and injector. No interference filter. No quartz chimney. (2) Osmocene. Same conditions as in curve 1, but 650 nm long-pass filter present. (3) Naphthalene. Same conditions as in curve 1. (4) Naphthalene. Same conditions as in curve 2.*

the continuum is unknown; it might even be due to particle formation.

4.3.2 Calibration Curves

The spectral features shown in Figure 4.15 suggest that in the wavelength region accessible to the red-extended photomultiplier tube either the whole luminescence or — if some discrimination against typical FPD-active elements or against carbon is desired — only the major, low-energy portion could be used. These two modes are compared in the calibration curves for osmocene shown in Figure 4.16.

Also included in Figure 4.16 are the data for naphthalene recorded under these two conditions. As is well known, aromatics produce stronger responses than aliphatics in the FPD, and naphthalene is used here to assess just how prominently matrix components might show up. Note that when the cut-on filter is used, the response of naphthalene is negative. Thus inverted peaks for compounds that contain only carbon and hydrogen and quench the background luminescence, could indeed be used to distinguish hydrocarbon components of a sample matrix from the true, osmium-containing analytes.

The term "negative response" is used here to describe a gas chromatographic peak that extends below — not, as usual, above — the baseline. That peak is therefore due to a decrease — not, as usual, an increase — in luminescence. The occurrence of such an "inverted" peak presumes the existence of a sizeable background emission when the analyte passes through the detector. The background luminescence of FPD's in general and of the present system in particular has not been characterized in detail as to its various origin(s); it would be expected to include typical emission bands from the flame gases — *e.g.* OH — as well as

emissions from column bleed or gas contaminants — *e.g.* CH, CC — and, finally, luminescence caused by residues from earlier injected compounds containing FPD-active elements.

The minimum detectable amount of osmocene, defined by a S/N ratio of two (with noise measured as the short-term, peak-to-peak fluctuation of the baseline), is 5×10^{-10} g, or about 5×10^{-11} g/s, or 0.15 pmol/s. When measured by the IUPAC definition $S/\sigma = 3$, the detection limit is about 0.2 ng. The linear range of osmocene spans close to three powers of ten. The selectivity against naphthalene, with the cut-on filter in place, is about 1.7×10^{3} on a weight basis (g osmocene/g naphthalene) or 4.3×10^{4} on an elemental basis (mol Os/mol C), these numbers being calculated as the ratio of minimum detectable concentrations. Clearly, selectivity could be further improved, with the choice of a filter depending on the particular analytical task. Note that even a simple cut-on filter at, say, 700 nm would exclude many of the FPD-active elements. It may also be possible to use IR-sensitive detection, *i.e.* with a charge coupled device, to some advantage.

On the other hand, when osmocene or its analogues have to be determined together with other volatile organometallics of the iron group, the detector needs to pick up a variety of emissions that differ greatly in wavelength among Fe, Ru and Os. Thus the open mode (no optical discrimination) is called for. Optimum flow conditions in this mode differ somewhat from Fe to Ru to Os, but quite adequate detection can be achieved at "average" detector settings. Such are chosen in Figure 4.17 for the demonstration chromatography of the three unsubstituted bis(cyclopentadienyl) derivatives. The magnitude of response varies among the three, as illustrated here by the different amounts that need to be injected in order to produce peaks of roughly equal size. The corresponding response ratios are,

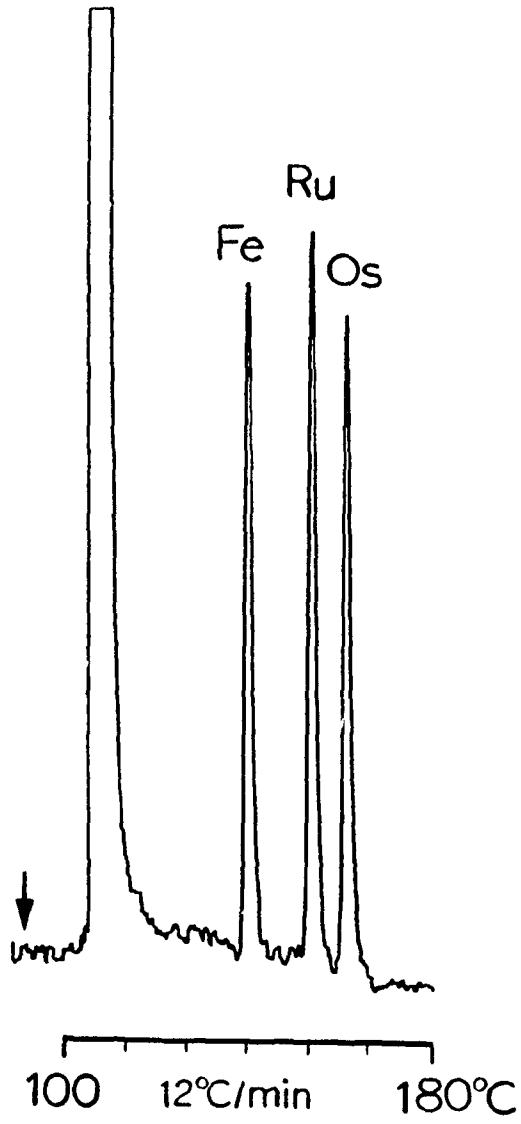

Figure 4.17 *Temperature-programmed chromatography of 1.5 ng ferrocene (Fe), 0.1 ng ruthenocene (Ru) and 8.0 ng osmocene (Os) in a mixture. Hydrogen: 300 mL/min; air: 65 mL/min; Carrier nitrogen: 25 mL/min; additional nitrogen: 20 mL/min. Temperature at detector base and injection port: 200 °C. No quartz chimney and flame shield. No interference filter. R-374 PMT.*

approximately, Fe : Ru : Os = 5 : 90 : 1 on a compound weight basis, or 3 : 60 : 1 on a molar basis. The S/N ratio of osmocene is slightly but not drastically reduced in comparison with that from a setting optimized for osmium.

4.4 Manganese

4.4.1 Introduction

The FPD response to manganese is characterized by examining the photometric behaviour of methylcyclopentadienyl manganese tricarbonyl (MMT). MMT is chosen as the representative because it is not only easy to deal with but it is also a very important gasoline additive (antiknock agent). A real-life GC-FPD determination of MMT from gasolines is also investigated by using a simple differential technique.

Considerable literature exists about the determination of this[71] and other gasoline additives. The methodologies range from simple analysis for total manganese[72] to sophisticated techniques of combining gas chromatography with emission or absorption plasma spectrophotometry. The most sensitive approach makes use of the hydrogen-atmosphere flame ionization detector, which can detect 1.7×10^{-14} g/s of manganese (and 7.2×10^{-12} g/s of lead), at selectivities against carbon compounds of four to five orders of magnitude[73]. Excellent performance has also been achieved with an atmospheric-pressure helium microwave plasma emission system coupled to a gas chromatograph: the minimum detectable flow of Mn was 0.25×10^{-12} g/s (that of Pb 0.49×10^{-12} g/s), with selectivities larger than six orders of magnitude[74]. Gas chromatographic separation may also precede atomic emission from a DC argon plasma (minimum detectable amount = 3 ng Mn)[75]; or atomic absorption in a slotted quartz tube atomizer (MDA = 0.2 ng Mn)[76]. Note that

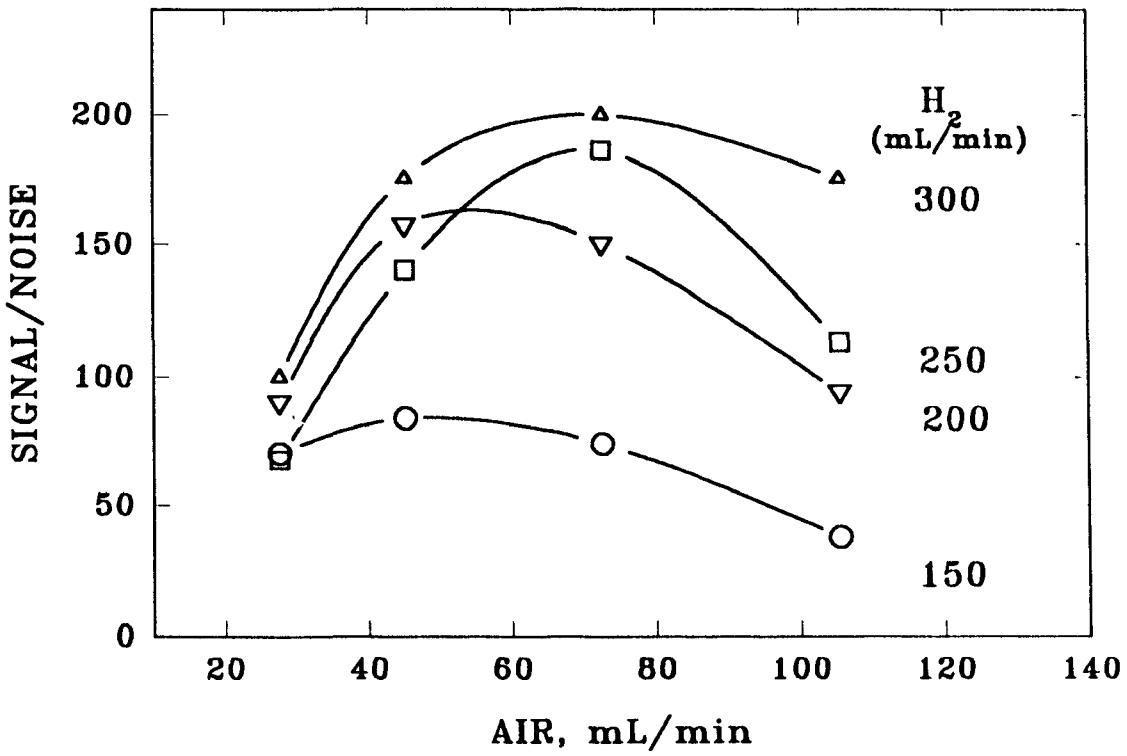

Figure 4.18 *Optimization curves (S/N ratio vs. air flow) of MMT. Column temperature 130 °C. Carrier N_2 22 and added N_2 18 mL/min. 405 nm interference filter present. R-268 PMT. 10 ng of MMT injected.*

minimum detectable amounts (or flows) are cited here solely to allow a limited comparison of different approaches. Detection limits are only one — and frequently not even the most important one — of analytical performance criteria. Beyond analysis, technical and environmental health aspects of manganese in general, and MMT in particular, have been covered well in the literature[77,78].

4.4.2 Optimization of Detector Gas Flows

Even the first experiments clearly established manganese as belonging to the roster of elements that produce analytically useful responses in the FPD. To locate the best S/N response, a conventional flow optimization routine is conducted. Figure 4.18 shows the results obtained with a 405 interference filter. From the graph, 300 mL/min of hydrogen and 70 mL/min of air are chosen as "regular conditions". However, as seen in the Figure, the S/N ratio still improves with hydrogen flows higher than 300 mL/min. Experiments show that if the hydrogen flow is double that of the "regular condition", the S/N ratio is increased by about a factor of two. Obviously, the detector's sensitivity is restricted to some degree by choosing those "regular conditions". On the other hand, this choice also reduces the potential hazard posed by the large amount of unconsumed hydrogen gas. To demonstrate the increased sensitivity, Figure 4.19 shows a chromatogram of 0.20 ng of MMT with a hydrogen flow twice as high as that in the "regular condition".

Figure 4.20 shows a separation of (nominally) three manganese compounds under "regular conditions" and at somewhat higher concentrations to demonstrate the applicability to other Mn-containing analytes. Note that one of the compounds, cymantrene, is commonly used as an internal standard for the gas chromatographic determination of MMT. However, in the present case MMT is analytically so well behaved that an internal standard is considered unnecessary.

4.4.3 Spectrum from Manganese

The spectral distribution of the luminescence originating from MMT, obtained by repeatedly injecting the analyte at different wavelengths, is shown in Figure 4.21. The emission at 403 nm corresponds to the two strongest arc lines of

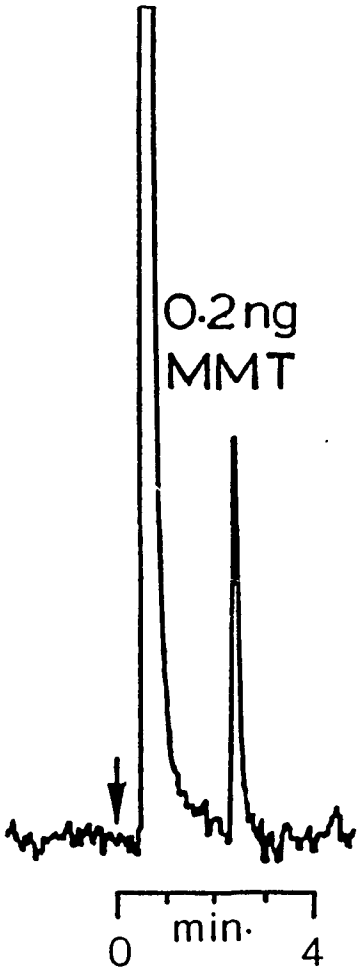

Figure 4.19 *Chromatogram of 0.2 ng MMT. Hydrogen flow ca. 600 mL/min. Single channel with 405 nm interference filter. R-268 PMT.*

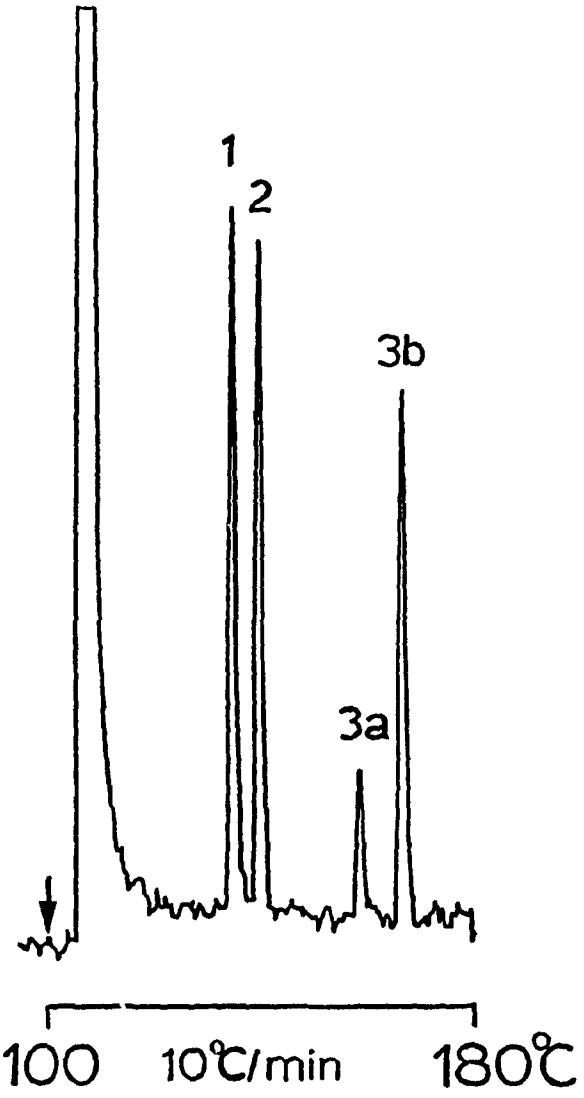

Figure 4.20 *Temperature-programmed chromatography of manganese compounds. (1) 1 ng cyclopentadienyl manganese tricarbonyl (cymantrene). (2) 1 ng MMT. (3a and 3b) 1.5 ng pentamethylcyclopentadienyl manganese tricarbonyl. Flow conditions: 300 mL/min hydrogen and 70 mL/min air. 405 nm interference filter. R-268 PMT.*

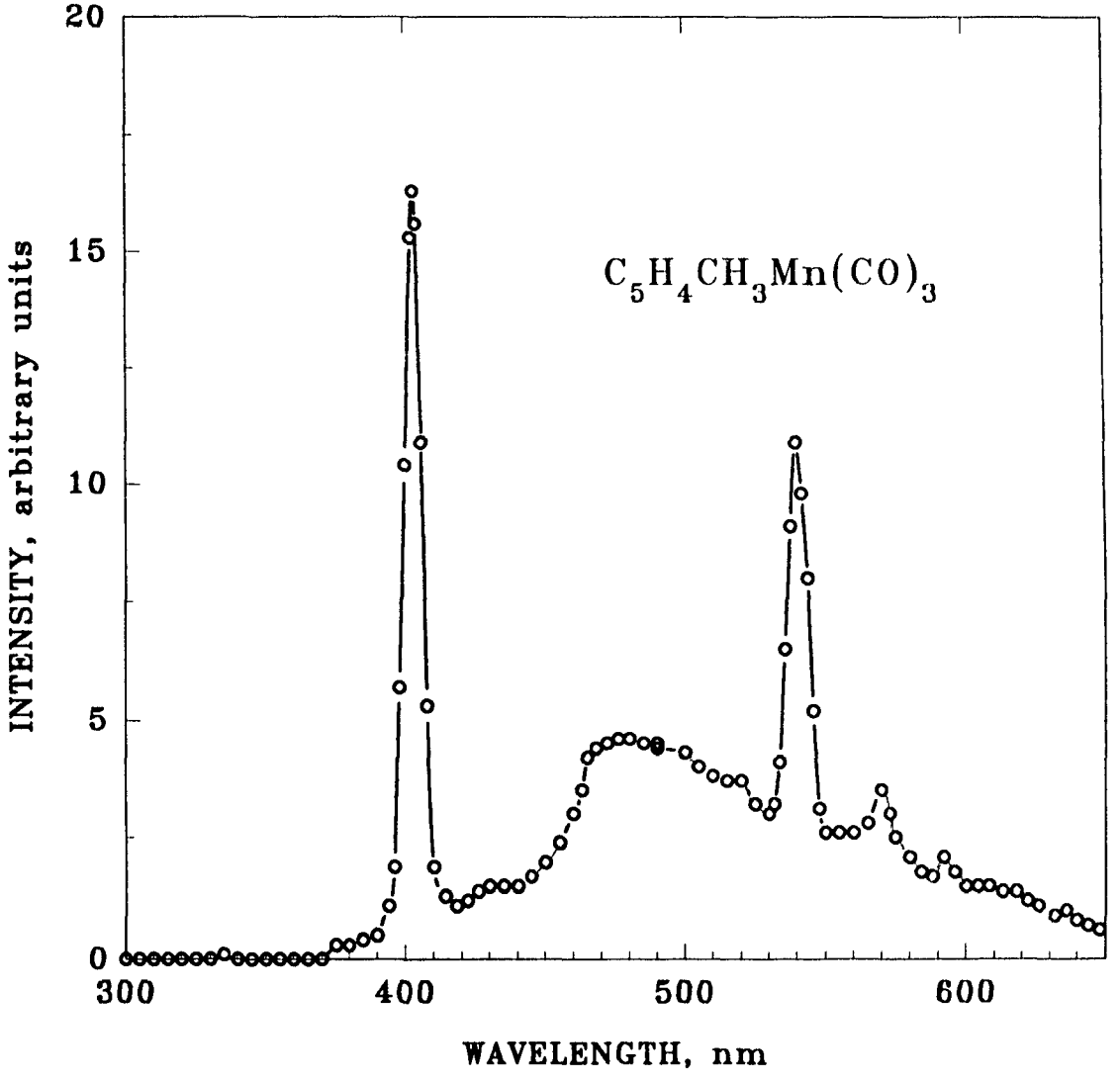

Figure 4.21 *Spectrum obtained by repeatedly injecting 2 μg of MMT. Hydrogen: 300 mL/min. Air: 55 mL/min. 1/4 meter grating monochromator with R-268 PMT. Slits: 2.0 mm. Bandpass: 6.7 nm.*

atomic manganese, found at 403.076 and 403.307 nm (also to the strong line at 403.449 nm). The emission at 540 nm may represent one or both of the 539.467 and 543.255 nm lines. While the latter are hardly visible in an arc, they share with the 403 nm lines the distinction of being transitions to the ground state[67].

The assumption that the 540 nm emission is atomic in origin is also supported by the fact that the 405 and 540 nm channels keep showing similar behaviour under the wide variation of hydrogen and air flows employed in optimization runs. For analytical purposes — such as improving the signal-to-noise ratio and discriminating against other FPD-active elements — the combined 403 nm lines offer the best performance (as they also do in conventional, high-temperature atomic emission from oxyhydrogen and oxyacetylene flames).

4.4.4 Calibration Curves

Figure 4.22 shows calibration curves measured at 405 nm for MMT and dodecane in acetone under "regular conditions". Also included is a calibration curve measured at 540 nm (the second strong Mn emission) and one that describes the differential response from a gasoline sample. "Differential" means, as described in Experimental (Section 2.9) that the response measured at 448 nm — after adjustment of amplitude for best overall suppression of gasoline constituents — is electronically deducted from the response at 405 nm, thereby yielding a single recorder trace. The differential calibration curves from acetone and gasoline solutions turn out to be virtually identical.

Using the most sensitive curve, the minimum detectable amount of MMT is determined as approximately 5×10^{-14} mol/s at S/N = 2 (or about 2×10^{-14} mol/s according to the more lenient $S/\sigma = 3$ IUPAC definition). The response

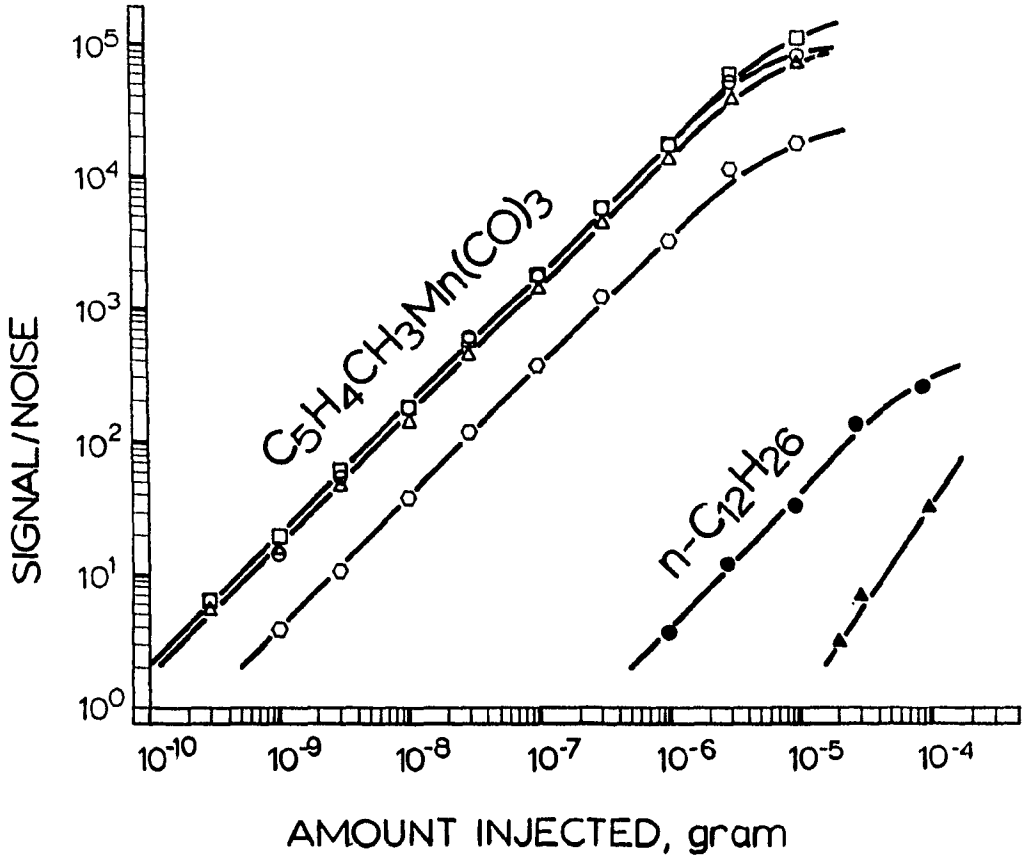

Figure 4.22 *Calibration curves.* —○—: *MMT in acetone, single channel at 405 nm, under "regular" flow conditions;* —□—: *as "—○—", but MMT in gasoline;* —△—: *as "—□—", but dual differential channel (405 - 448 nm, carbon suppressed);* —◇—: *as "—○—", but 540 nm.* —●—: *as "—○—", but dodecane in acetone;* —▲—: *as "—△—", but dodecane in acetone.*

selectivity for the manganese compound against a carbon standard (dodecane) on the single 405 nm channel is about 5×10^3 w/w (or 7×10^4 on a mol/s C *vs.* mol/s Mn basis) as determined from the minimum detectable amounts. This selectivity ratio improves slightly if the hydrogen flow is increased, and drastically if two channels are operated in the differential, carbon-suppressing mode. Nominally higher selectivities than the one shown in Figure 4.22 — *i.e.* higher than 1.5×10^5 w/w (or 2×10^6 mol/s C / mol/s Mn) — could be possibly achieved by exactly matching the response of the two channels for the very carbon standard used in the selectivity measurement. However, since different carbon compounds can differ in spectra and response (*e.g.* aromatics > aliphatics), the general setting chosen earlier for the best overall suppression of gasoline matrix peaks is maintained for the selectivity measurement.

The linear range for the manganese compound is 2×10^4 (4.3 orders of magnitude). This value does not vary significantly among single and double channel modes, or among samples dissolved in gasolines and in acetone. The minimum detectable concentration — at S/N = 2, with a 0.5 μL injection and without analyte enrichment — is about 0.6 ppm (weight MMT/weight gasoline). This lower limit could likely be improved by adding a preconcentration step or by using a capillary column. However, such seems hardly necessary for routine determination of the much higher MMT levels found in typical gasoline samples.

4.4.5 Quenching Effect and Spectral Interference

Quenching curves for MMT and a standard carbon compound are obtained by introducing varying levels of methane (as the quencher) through an exponential dilution flask. The result is presented in the form of relative response *vs.* logarithm of quencher concentration in Figure 4.32. Manganese response is slightly

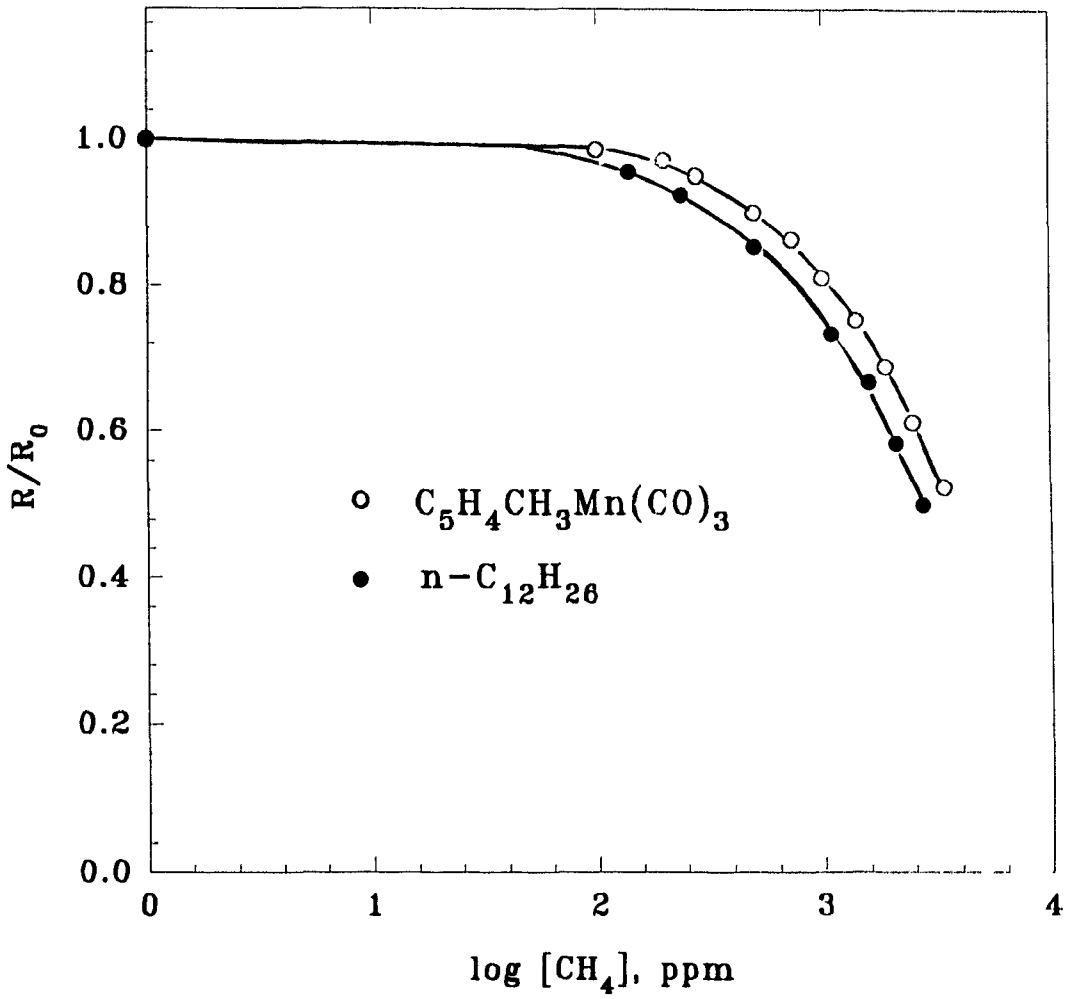

Figure 4.23 Quenching of luminescence from MMT and dodecane by methane present in the detector gases. R: response in the presence of quencher, R_0: response in the absence of quencher. Concentration of methane in ppm (v/v) of total detector gases. Flow conditions: 300 mL/min hydrogen, 55 mL/min air, 20 mL/min carrier nitrogen and 25 mL/min additional nitrogen. R-268 PMT.

less affected by the background presence of carbon (in methane) than is the response of the carbon standard itself. More importantly, it takes about 3,600 ppm (v/v) of methane in the detector atmosphere (which corresponds to 65,000 ppm if calculated on the nitrogen flowing through the column) to reduce the manganese peak by half. Thus, unless the manganese peak is subject to severe overlap by a very large carbon peak, interference originating from luminescence quenching can be considered negligible.

There are, however, other types of spectral interference that could assume importance in the flame photometric detection of manganese in gasoline (if not circumvented by chromatographic separation). Most importantly, the atomic emission of Mn at 403 nm is located very close to one of the major bands of S_2. The emission from lead stretches over that region as well. The HPO bands are far away but, for the analysis of an automotive product, it still would seem prudent to characterize the selectivity against phosphorus. Besides, the initial work on the FPD involved S and P compounds and these are often best determined in this manner. Finally, the luminescence from carbon compounds (as opposed to their quenching effect on Mn emission) is relatively strong at 403 nm.

Table 4.1 lists the molar selectivity ratios for manganese versus carbon, phosphorus and lead, under three increasingly selective spectral conditions. The last of these conditions refers to the so-called "differential" mode. The electronic circuit displayed by Figure 2.2 is used here to obtain differential selectivity against carbon response. In this particular case, channel 1 monitors 405 nm, which favors the manganese response, while channel 2 views 448 nm which is close to optimal for the carbon response. The carbon signals from channel 2 are so attenuated by the potentiometer that they match the ones from channel 1. The signals (of both

manganese and carbon) are then combined into *one* channel at the recorder. The carbon response is therefore subtracted while the manganese response remains almost intact. Thus, as shown in Table 4.1, higher selectivity of manganese versus carbon is gained. However, the manganese determination in this differential operation never reaches specificity (infinite selectivity).

Table 4.1 MOLAR SELECTIVITY RATIOS FOR MANGANESE[a]

Filter	Mn vs: C	P	Pb
None	9.7×10^{3}	0.6	7.4
405	7.1×10^{4}	2.2×10^{2}	2.0×10^{2}
405/448[b]	2.3×10^{6}	1.7×10^{3}	3.0×10^{2}

[a] *Formally calculated as the minimum detectable molar amount [signal/(peak-to-peak noise) = 2] of interfering element (C, P or Pb) per second, divided by the minimum detectable moles of Mn per second.*

[b] *Differential mode tuned for suppression of dodecane.*

Sulfur is even more likely than C, P and Pb to interfere in the determination of Mn, but its selectivity is more difficult to characterize because of the quadratic nature of its S_2-based response and its susceptibility to detector contamination (sulfur residues in the detector increase analyte sulfur response and linearize the calibration curve in the lower concentration range). The advantage of switching from single to differential channel operation for sulfur suppression is

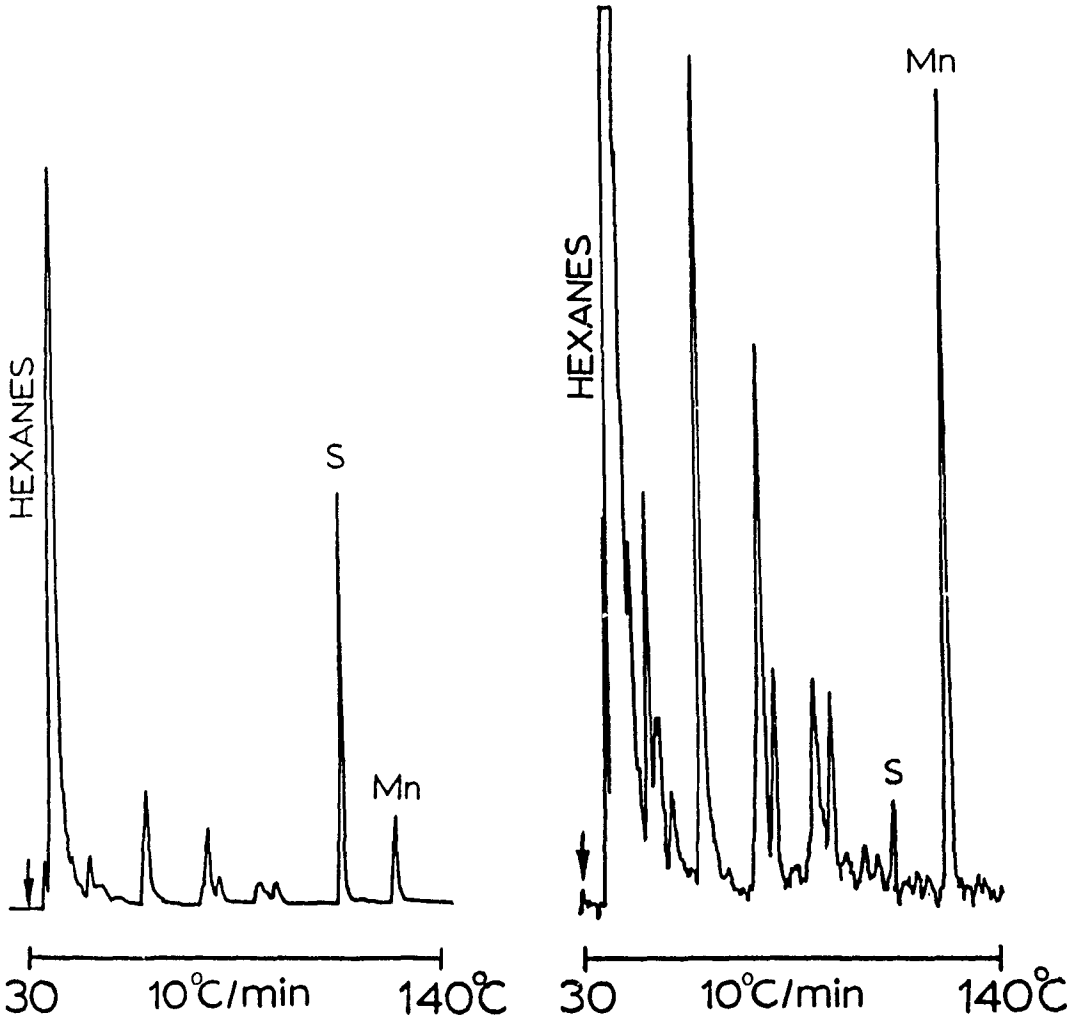

Figure 4.24 *Chromatography of 10-fold diluted, unleaded gasoline doped with a sulfur compound. Left: 405-nm filter, attn. 16, Mn peak height 126 pA. Right: 405/365-nm differential filters, attn. 2 (sulfur suppressed). "Mn": 1.5 ng of MMT; "S": 250 ng of di-tert-butyldisulfide.*

therefore illustrated here by chromatography of gasoline doped with a sulfur compound. Figure 4.24 shows the approximately fifty-fold gain in selectivity of Mn *vs.* S, which could be further improved by fine-tuning.

4.4.6 Determining MMT in Gasolines

Samples of premium unleaded gasolines bought from different companies in Halifax could, in fact, be analyzed for MMT (after a 10:1 dilution with hexanes) without having to resort to spectral discrimination at all, *i.e.* without the aid of an interference filter. The left chromatogram of Figure 4.25 shows such an analysis. For comparison, the middle and right-side chromatograms in Figure 4.25 show the same sample (at lower attenuation) as viewed through a 405 nm single channel and through 405/448 dual differential channels, respectively. The resulting increase in selectivity is large but, while important for trace work, is not really needed for the routine determination of MMT in gasolines. The amount of manganese as MMT in this sample is, incidentally, 7.0 mg Mn/L and thus at about half the legal upper limit.

The permissible concentration of Mn is 18 mg/L (approximately 80 ppm MMT by weight). To demonstrate the determination of a much lower concentration, 3 ppm of MMT was added to an old (practically MMT-free) unleaded gasoline. The resulting chromatograms, shown in Figure 4.26, provide a graphic demonstration how the 3 ppm peak of MMT, barely credible in open mode (upper left), becomes clearer in Mn single-channel mode (upper right) and, save for a sulfur containing matrix component, dominates the chromatogram in carbon-suppressed dual-channel differential mode (lower right). The sulfur-suppressed differential mode (lower left) establishes that the large peak marked "S" did indeed arise from a sulfur

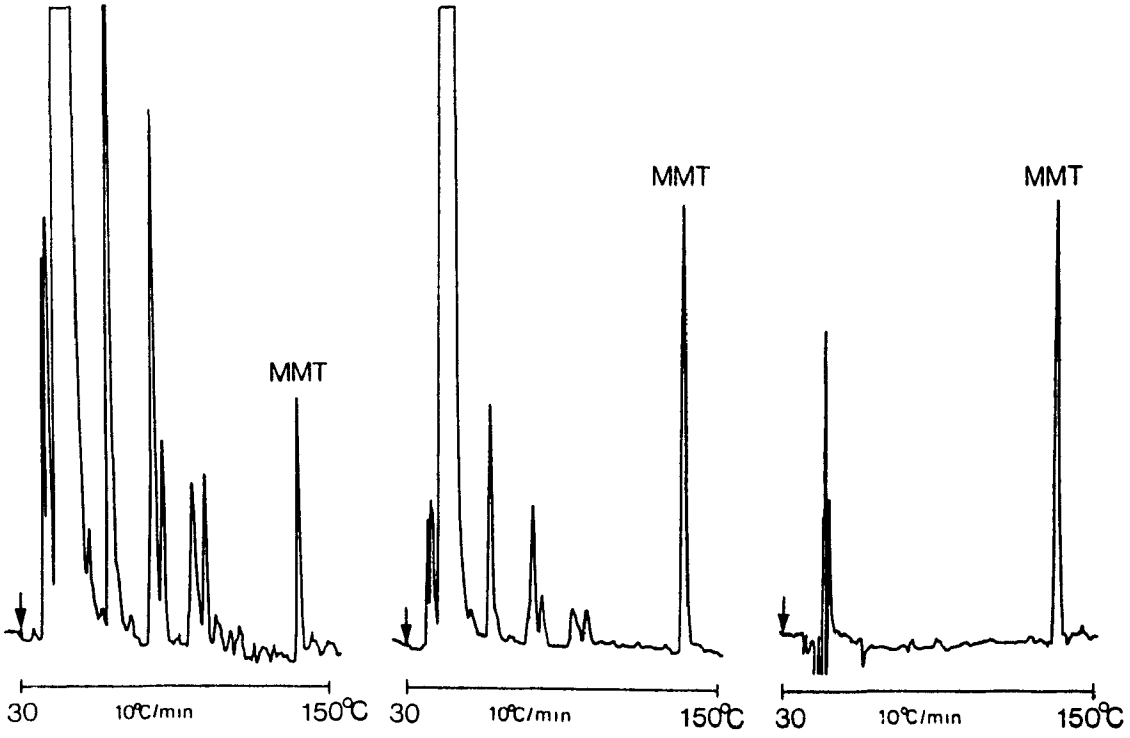

Figure 4.25 *Temperature-programmed chromatography of premium unleaded gasoline. Left: open (no interference filter, higher attenuation), MMT peak height 227 pA. Middle: 405-nm filter (for manganese). Right: 405/448-nm differential (carbon suppressed), MMT peak 189 pA.*

compound. A variety of different filters could be used to suppress sulfur efficiently; however, it should be noted that the extent to which carbon response is simultaneously changed does vary in accordance with the chosen wavelength.

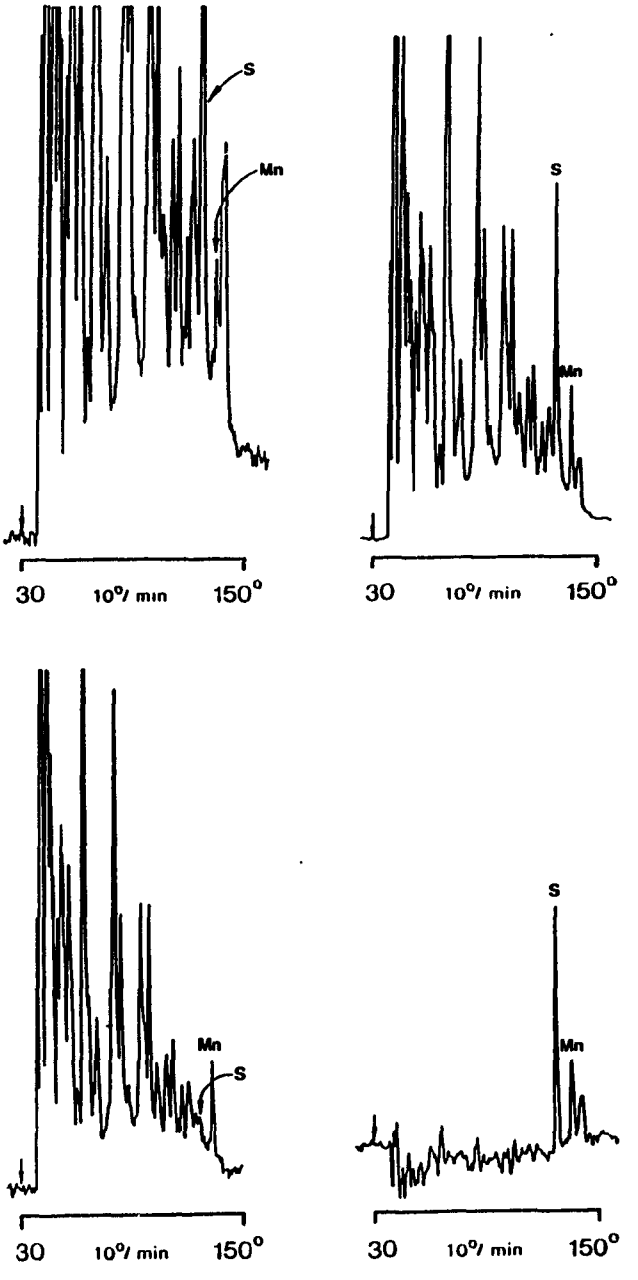

Figure 4.26 *Temperature-programmed chromatography of unleaded gasoline containing 3 ppm (w/w) of MMT. Upper left: open (no interference filter). Upper right: 405-nm filter (for manganese). Lower left: 405/365-nm differential (sulfur suppressed). Lower right: 405/448-nm differential (carbon suppressed). Mn peak heights in same sequence from upper left to lower right: 78.7, 47.2, 55.1, and 50.4 pA.*

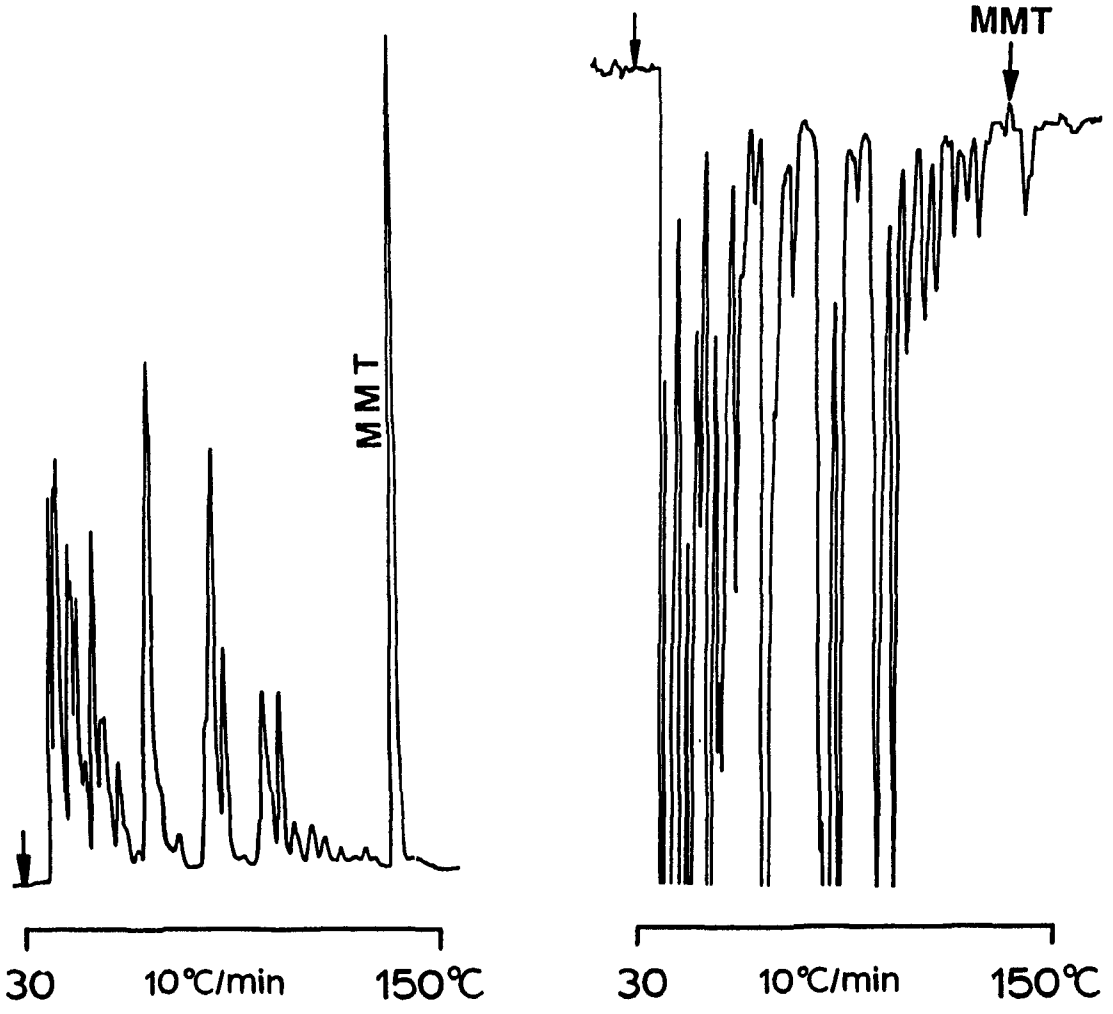

Figure 4.27 *Temperature-programmed chromatography of premium unleaded gasoline containing ca. 80 ppm (w/w) of MMT. Left: 405-nm filter, MMT peak height 1.26 nA. Right: 405/540 nm differential (MMT suppressed).*

Although a positive peak identification is not obligatory under routine circumstances, cases may arise where the identity and/or homogeneity of the MMT peak is truly in doubt. One way of narrowing down the alternatives is to suppress or cancel the interfering heteroelements while keeping the Mn response intact. The opposite approach is also possible: it depends on cancelling the Mn response itself. The disappearance of the suspected MMT peak then establishes its nature as a manganese compound. This is demonstrated in Figure 4.27 with a regular chromatogram on the left and a Mn-suppressed one on the right (in the latter case, carbon response is strong and inverted). Note that any element that should happen to have the same response ratio as manganese at the two wavelengths could theoretically produce the same effect; however, the probability of this occurring is remote. Beyond MMT in gasolines, such dual-channel differential methodologies can be used to analytical advantage in a wide variety of samples containing FPD-active elements.

4.5 Nickel, Chromium, Rhenium, Molybdenum and Cobalt

A survey of easily available and sufficiently volatile compounds of transition metals (besides Fe, Ru, Os and Mn) was carried out. Several produced luminescence that was substantially more intense than could be expected from the analytes' carbon content. These analytes were the simple bis(cyclopentadienyl) derivatives of nickel and cobalt, and carbonyls of rhenium and molybdenum. The metals are thus joining the roster of chromium[33], manganese[52], iron[49], ruthenium[50] and osmium[51], whose responses in the FPD have been previously described.

A variety of other transition metals produce only negligible response. (For this study, "negligible response" is roughly defined as less than ten times the expected carbon response.) This thesis regards such negative results - obtained from

compounds of Y, V, W, Zn, Cd, Hg, Zr and Tl - much less conclusive than the positive results on which it focuses. Conditions in the FPD may not have been suitable for these elements. Or some of the organometallics may have decomposed before reaching the detector. While the latter is immediately obvious when the expected peak fails to appear, the opposite effect - *i.e.* the presence of a peak commensurate with the carbon portion of the molecule - is ambiguous. Such a peak could have been caused by the formation of a non-metallic product from the decomposing analyte. Note that the lack of response from certain transition elements, as mentioned here, refers only to their behaviour in the cool and hydrogen-rich flame of the typical FPD. By no means does it imply that these metals would also fail to respond in, say, a conventional oxyhydrogen flame (which has occasionally been reviewed together with the FPD proper[55]).

Chromium will also be studied in this section. Although Cr was known to be one of the FPD-sensitive elements a long time ago[7,33], no spectral information under FPD conditions was reported. Without knowledge of the actual spectra under analytical circumstances, a rational choice of detector conditions — particularly for increasing the selectivity of one species over the other — would be difficult.

4.5.1 Calibration Curves

The most sensitive of the new analytes is nickel. This fact commands interest since nickel is an element of economic, environmental and medical importance. Industrially as well as analytically, it is easily transformed into its highly volatile (and highly toxic) tetracarbonyl[79,80]. Figure 4.28 shows the calibration curve of bis(cyclopentadienyl)nickel, a compound that is less stable but safer to handle under exploratory circumstances.

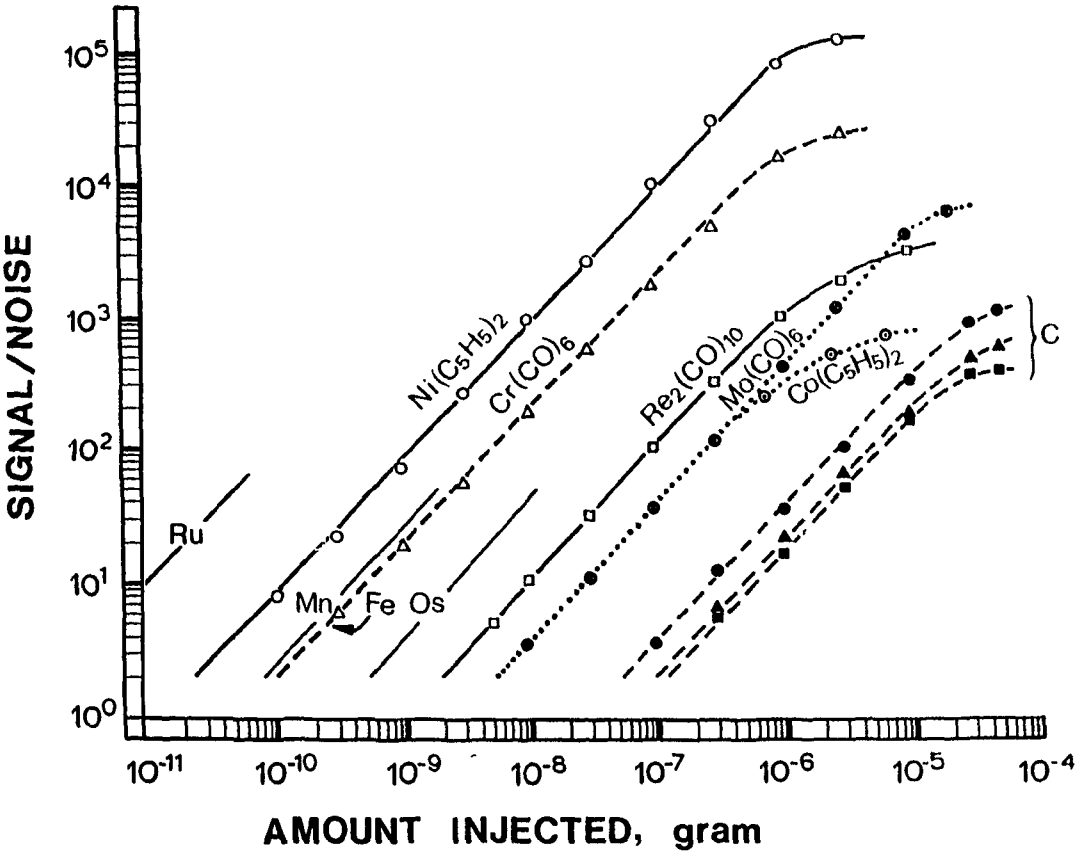

Figure 4.28 *Calibration curves (from left to right): (1) Nickelocene (solid line); (2) Chromium hexacarbonyl (dashed); (3) Dirhenium decacarbonyl (solid line); (4) Molybdenum hexacarbonyl (dotted); (5) Cobaltocene (dotted); (6) Naphthalene (dashed); (7) Dodecane (dashed); (8) Di-n-hexyl ether(dashed). All the curves made in open mode (no interference filters). Flow conditions: 300 mL/min hydrogen and 55 mL/min air for all the metals; 300 mL/min hydrogen and 60 mL/min air for the three carbonaceous compounds. The short lines at the bottom indicate the response intensities of Ru, Mn, Fe and Os, which have been discussed before.*

Figure 4.28 also includes the calibration curves of the other new transition metal analytes. Each is the result of an individual, coarse optimization of flow conditions. All measurements are made in the non-filter mode. In most cases - and particularly when the spectrum consists of broad bands of low intensity that stretch over an extended wavelength region - the open mode produces higher signal/noise ratios than the use of an interference filter.

Minimum detectable limits can be read directly from this graph: at an ordinate value of 2 for the conventional measurement, at an ordinate value of about 0.5 for the IUPAC definition $S/\sigma = 3$. Since the GC column temperature was so chosen that each analyte eluted at about 2 minutes with a σ_{peak} close to 10 seconds, these minimum detectable amounts, at the more conservative $S/N = 2$ definition (where "noise" is the short-term peak-to-peak fluctuation of the baseline) vary from 1×10^{-14} mol/s for nickel to 3×10^{-12} mol/s for cobalt. Table 4.2 lists these values together with column temperatures and detector conditions. Included in Table 4.2 are also data for typical carbon compounds, as well as literature references to other transition elements. The assumption inherent in accepting as elemental detection limits numbers that were determined using only one compound of a thermally and/or chemically labile nature, is that no significant decomposition occurred during gas chromatography. A further assumption is that the non-metal part of the analyte molecule did not significantly detract from, or contribute to, the response of the metal.

To allow a visual comparison without repeating information already in the literature, as well as to avoid cluttering up Figure 4.28, the relatively positions of Ru[50], Mn[52], Fe[49] and Os[51] responses are indicated at the bottom of the graph. The calibration curve for $Cr(CO)_6$ is shown in dashed form, since the flame photometric

Table 4.2 BEHAVIOUR OF TRANSITION METALS IN THE FPD*

Ele.	Compound	Col. Temp.	H_2 mL/min	Air mL/min	MDA[a] mol/s	Filter nm	Reference
Ru	$Ru(C_5H_5)_2$	155	300	80	1×10^{-15}	none	this work
Ni	$Ni(C_5H_5)_2$	130	300	55	1×10^{-14}	none	this work
Cr	$Cr(tfa)_3$	—	70	50(air) 50(O_2)	2×10^{-13} [b]	520	[7]
	$Cr(tfa)_3$	160	180	35(O_2)	2×10^{-11} [b]	425.4[c]	[33]
	$Cr(CO)_6$	60	300	55	5×10^{-13} [b]	none	this work
Mn	MMT	130	300	55	5×10^{-14}	405	this work
Fe	$Fe(C_5H_5)_2$	130	300	60	5×10^{-14}	none	this work
Os	$Os(C_5H_5)_2$	170	300	60	2×10^{-13}	none	this work
Re	$Re_2(CO)_{10}$	132	300	55	6×10^{-13}	none	this work
Mo	$Mo(CO)_6$	52	300	55	2×10^{-12}	none	this work
Co	$Co(C_5H_5)_2$	120	300	55	3×10^{-12}	none	this work
C	naphthalene	130	300	60	4×10^{-10}	none	this work
C	dodecane	130	300	60	7×10^{-10}	none	this work
C	di-n-hexyl ether	130	300	60	8×10^{-10}	none	this work

* *Shimadzu FPD without quartz chimney unless otherwise indicated.*

[a] *Minimum detectable amount in mole of element per second, at a S/N ratio of 2, where noise is the short-term peak-to-peak fluctuation of the baseline. Divide by two for a rough MDL estimate according to the* $S/\sigma_{noise} = 3$ *IUPAC definition.*

[b] *Moles of element at S/N = 2*

[c] *Melpar (Tracor) FPD*

detection of chromium, as $Cr(tfa)_3$, had been described in the literature many years ago. The present measurement is somewhat more sensitive than that found in the seminal work of Ross and Shafik (2.5 ng Cr at S/N = 6.0[33]). However, it falls short by about a factor of two when compared with the minimum detectable amount reported by Burgett and Green (79 pg Cr at S/N = 12.6[7]): in the units used by these authors, the minimum detectable amount of this thesis is 24 pg Cr at S/N = 2.

The calibration curves for $Mo(CO)_6$ and $Co(C_5H_5)_2$ are barely beyond this thesis's definition of significant metal response in the FPD, *i.e.* that of ten times the response expected from the carbon portion of the molecule. Analytically, they are thus of only marginal interest. Here they are shown in dotted lines, for reasons that relate mainly to their spectra.

4.5.2 Spectrum from Nickel

One of the definitely interesting transition metal spectra is that of nickel (nickelocene). It is shown in Figure 4.29. Unfortunately, most of its features must remain unassigned at this stage. This is due, in part, to the limited resolution available from an FPD emitter of only moderate strength. For reasons discussed earlier, the use of flame conditions optimized for spectral (as opposed to analytical) purposes, was considered inappropriate to this end.

The spectral feature centered at 345 nm, which appears to be slightly broader than the optical bandpass (6.7 nm), is likely due to an accumulation of atomic lines. Many prominent Ni lines occur between, say, 335 and 355 nm[67] - among them the strongest ones known from emission, absorption and fluorescence spectrophotometry[68]. If preference is given to strong transitions from/to the ground state - including states that exceed the ground state by no more than the ambient

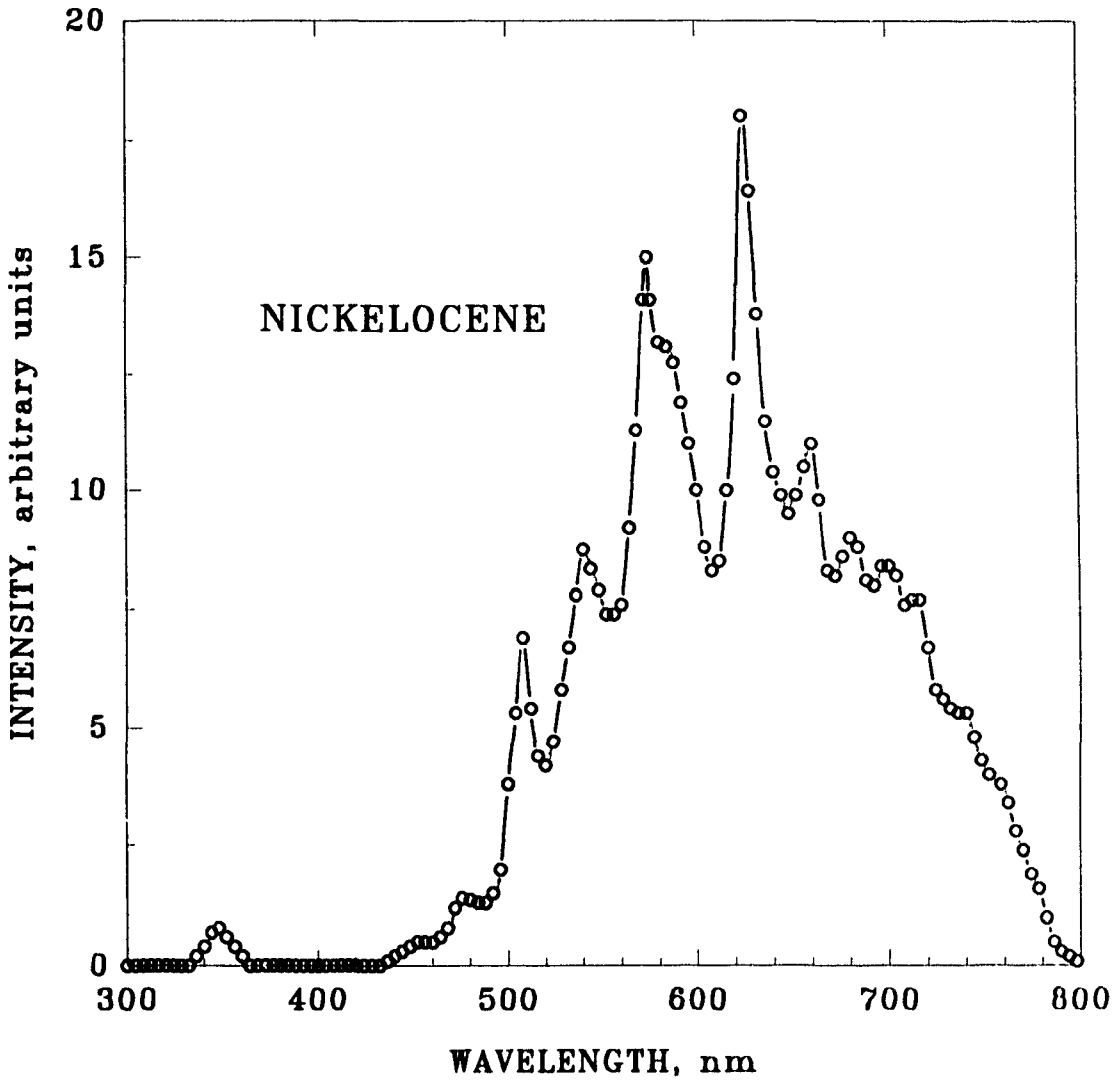

Figure 4.29 *Spectrum obtained by repeatedly injecting 500 ng of nickelocene under optimized gas flows (300 mL/min H_2 and 55 mL/min air). 1/4 meter grating monochromator with R-1104 PMT. Bandpass: 6.7 nm.*

thermal (kinetic) energy - then the roster includes such lines as 341.476 nm (205 - 29481 cm^{-1}), 352.454 nm (205 - 28569 cm^{-1}), 346.165 nm (205 - 29084 cm^{-1}), 336.957 nm (0 - 29669 cm^{-1}), 339.105 nm (0 - 29481 cm^{-1}) and 343.728 nm (0 - 29084 cm^{-1}). The upper state energies are 3.66 and 3.54 eV for the two first-cited lines, as well as 3.68 eV for the line of highest energy whose presence could not be reasonably excluded. (Chemical excitation, for which these numbers are of interest, will be discussed later.)

The much more intense system(s?) between about 500 and 750 nm is puzzling. The literature lists several systems of NiO that occur in this region. The 0,0 transitions of NiO Systems V and VI are given as 509.83 and 473.0 nm[65], *i.e.* at values close to two of the maxima shown in Figure 4.29. However, other wavelengths representing these systems are not found in the spectrum. Also, the overall appearance is quite different from such NiO spectra as, for instance, produced by the chemiluminescent reaction of $Ni(CO)_4$ with O_3 [80].

A quite plausible emitter for some of the sharper bands is NiH. Gaydon and Pearse list several systems. One of these, the "625.7 nm system", has strong 0,0 and 1,0 transitions that are close to the maxima of Figure 4.29 at 626 and 574 nm[65]. And the band shown at 507 nm may correspond to a NiH band mentioned by R. E. Smith[81]. While no definitive assignment can be made under the circumstances, we believe that NiH and (with less justification) NiO should be considered as candidates for producing much of the emission in the visible.

4.5.3 Spectrum from Chromium

The spectrum from chromium (chromium hexacarbonyl) was checked because, even though the FPD response of chromium compounds had been known for quite some time and had been claimed to be "specific" with the use of a 425.4 nm interference filter[33], the corresponding FPD spectrum has not been reported. Even if it had, the fact that earlier studies were carried out on a Melpar FPD - while this study used a Shimadzu FPD - would have mandated a re-measurement of the chromium spectrum to serve the envisioned experiments on selectivity. The choice of the 425.4 nm interference filter in the seminal FPD paper[33] was obviously based on chromium's strongest emission line at 425.435 nm (actually, on the triplet at 425.435, 427.480 and 428.972 nm, given the bandpass typical of interference filters). This wavelength had been used previously for monitoring Cr emission from an oxyhydrogen torch (*i.e.* from a hot, oxygen-rich flame of 5.7 L/min H_2 and 39 L/min O_2) connected to a gas chromatograph[82]. The choice of a 520 nm filter in the most sensitive FPD determination of Cr reported to date[7] may have been aimed at the strongest emission line in an air-hydrogen flame (520.604 nm[68]). Note, however, that this atomic transition (7593 - 26796 cm^{-1}), together with its triplet companions, does not involve the ground state and that, based on arguments made in this report, it is therefore unlikely to produce strong response in the FPD. (It is interesting to note, nevertheless, that its upper-level energy of 26796 cm^{-1} is lower than that of the most energetic line seen, *i.e.* 27935 cm^{-1} for the 357.869 nm line.)

The upper half of Figure 4.30 displays the spectrum obtained under regular operating conditions of our FPD. As expected it does not show the 520 nm line, but it does indeed include a distinct maximum centered at about 427 nm. This peak represents the earlier mentioned triplet, which is also easily observed in the

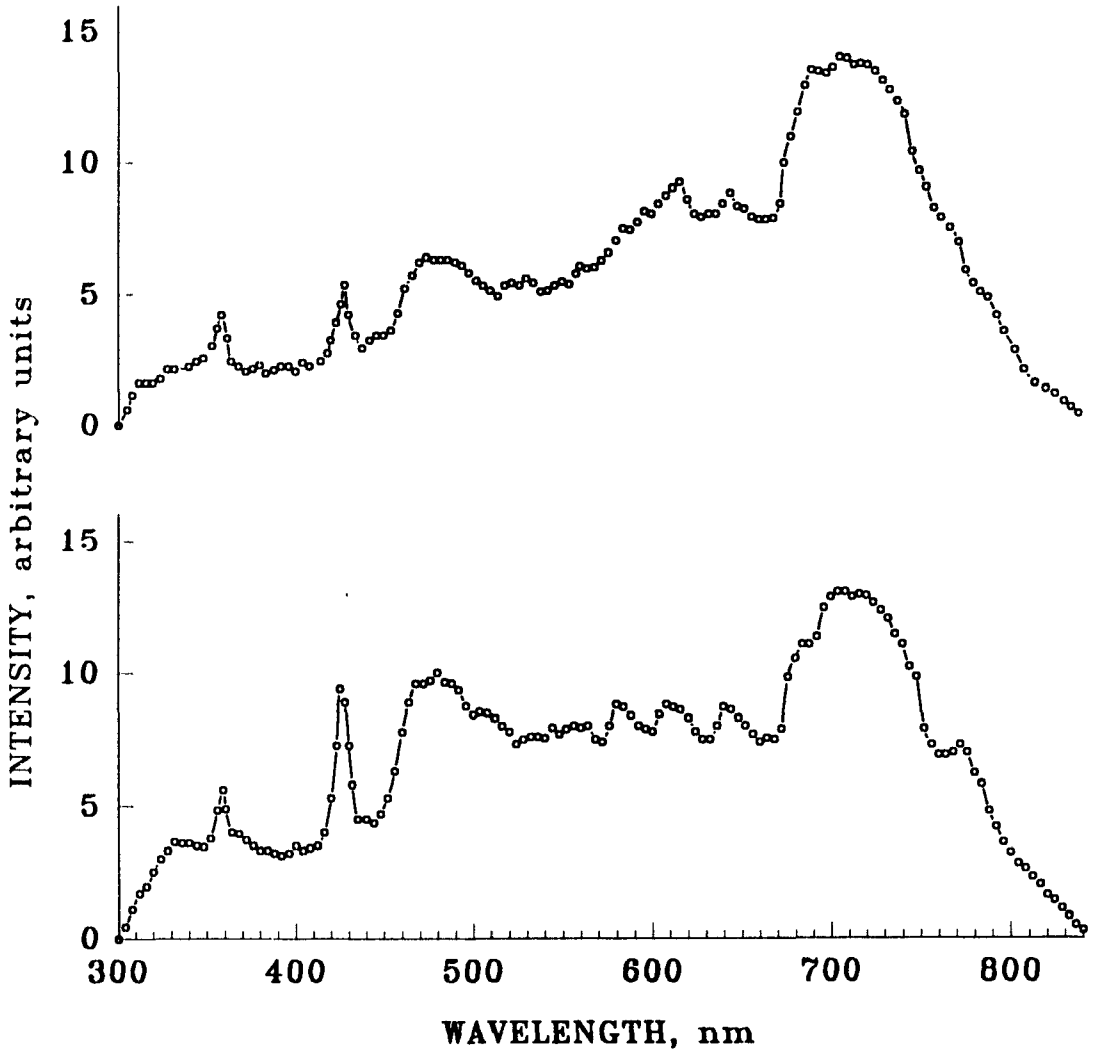

Figure 4.30 *Spectra from chromium hexacarbonyl with 6.7 nm bandpass. An order-sorting filter (500 nm long-pass) is placed in front of the monochromator from 600 nm on to avoid recording second-order spectral features. 1/4 meter grating monochromator with R-1104 PMT. Upper: spectrum from regular flame (300 mL/min H_2 and 55 mL/min air). Lower: spectrum from stoichiometric flame (50 mL/min H_2 and 125 mL/min air).*

conventional air-hydrogen flame[68]. Another combination of three strong emission lines occurs at 357.869, 359.349 and 360.533 nm, with the resulting peak centered in our spectrum at 359 nm (the CrH bands around 368 do not seem to show up). There are no clearly assignable lines at higher energy.

Aside from these atomic emissions, the spectrum is dominated by some broad features of unknown origin. Not surprisingly, then, the minimum detectable limit of chromium hexacarbonyl is considerably better when using the "open" (no interference filter) mode than when using an interference filter at 427 nm. Indeed, the most prominent spectral feature is located far away, *i.e.* between 670 and 750 nm (as seen by the red-extended phototube).

Aware of the case of iron[49], we became interested in possible spectral changes resulting from shifts in flame conditions. If such changes occur, the individual optimization of disparate emission features can serve purposes both analytical (*e.g.* increase selectivity) and spectral (*e.g.* yield information on the identity of the emitters).

In the case of chromium, however, the overall distribution of the spectrum changes but little - and that within a very wide range of flame conditions. To document this with one out of several runs, the spectrum shown in the lower part of Figure 4.30 was obtained from a stoichiometric flame. Not shown here, but in agreement with the conclusion given above, were runs with (a) a flame much hotter than usual - though still hydrogen-rich - and (b) a flame much cooler and so starved of oxygen as to hover near extinction. Note that the latter spectrum, because of its very low light level, had to be obtained within the much shorter range and lower resolution of a filter monochromator.

The benefits of having available an FPD spectrum valid at analytically relevant conditions (top of Figure 4.30) are obvious. It allows a reasonable choice of wavelength for optimization of response and, much more importantly, for optimization of selectivity *vis-à-vis* other FPD-active species[66]. In this context, the initial literature choice of 425.4 nm as the central wavelength of an interference filter for chromium (with a presumed bandpass around 10 nm) is interesting in light of the fact that the largest response of carbon compounds also occurs in that spectral window (*vide infra*). The "specific" response for chromium at 425.4 nm[33] against the background - presumably mainly carbon compounds - relies therefore on the innate difference in luminescence intensity rather than on the wavelength at which the two emissions are measured. In fact, in our system - and different FPD's can differ greatly in this regard - the open mode produces a higher selectivity for chromium against aliphatic carbon than if that analysis had been carried out with the 425 nm interference filter in place. The reason is obvious from the two spectra obtained at analytical operating conditions.

4.5.4 Spectrum from Rhenium

The spectrum of rhenium (dirheniumdecacarbonyl) under regular operating conditions is shown in Figure 4.31. Rhenium is not a particularly strong emitter in the FPD and, furthermore, its spectrum is essentially continuous: two characteristics that necessitate use of the more sensitive but less versatile filter monochromator. The spectrum differs from rhenium spectra found in the literature. It is known, for instance, that Re is a "flame-greening" element[31] (whereas Figure 4.31 suggests red). There is also little similarity between it and the continuum seen in a low-temperature hydrogen diffusion flame[82].

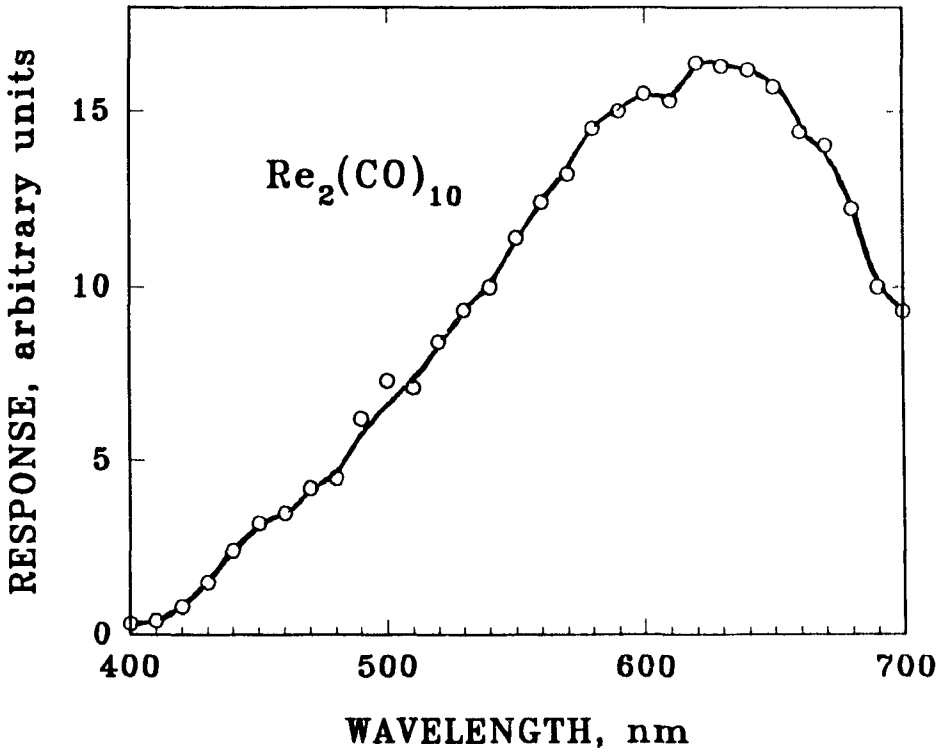

Figure 4.31 *Spectrum obtained from dirheniumdecacarbonyl. Filter monochromator with 4-mm slit and R-1104 PMT. Bandpass (specification) = 28 nm at 550 nm. Gas flows: 300 mL/min hydrogen and 60 mL/min air.*

For reasons discussed in the cases of chromium and iron, and for the chance to use the higher resolution and wider wavelength range of the grating monochromator, a variety of hotter flames were tried that, while still hydrogen-rich, contained less hydrogen and more oxygen than the analytically optimized setting. Figure 4.32 shows the case for Re. Not surprisingly for such a heavy atom (*c.f.* Os[51]), identifying features tend to be submerged in the broad continuum.

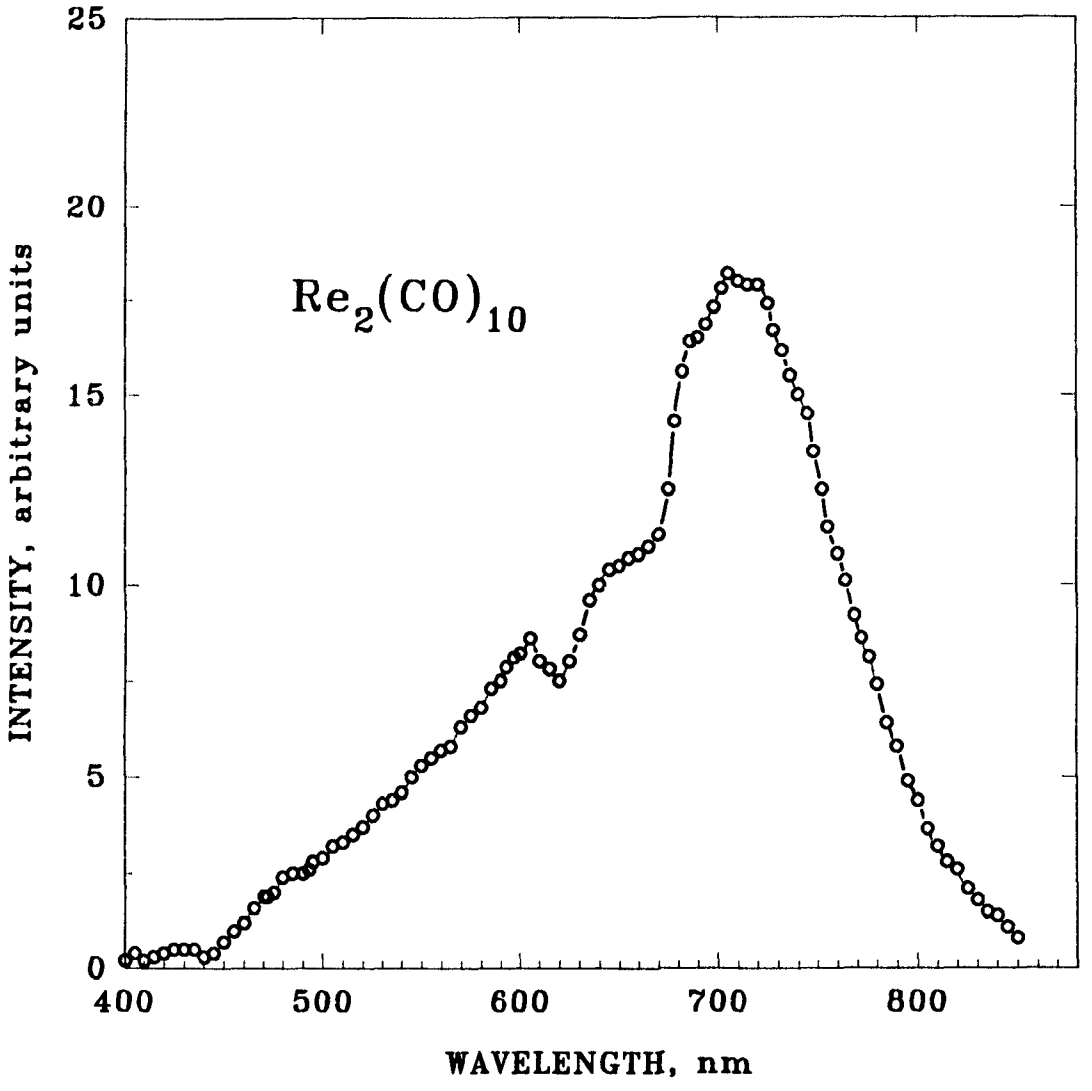

Figure 4.32 *Spectrum obtained from dirheniumdecacarbonyl in a hot flame. Hydrogen: 120 mL/min. Air: 125 mL/min. Photomultiplier tube: R-1104. 1/4 grating monochromator. Slits: 2.0 mm. Bandpass: 6.7 nm.*

The resonant line of Re at 346.047 nm (3.58 eV) is not seen in the spectrum. Note that the region from 300 to 400 nm was included in the measurement but proved blank. Either there are too few free atoms present in the first place, or they fail to undergo chemical excitation, or excited atoms are not formed in chemiluminescent processes from di- or triatomic species, or molecular excitation pathways are energetically favored. The only known atomic transitions from less than 3.58 eV to/from the ground state, are located at 488.914 nm (2.54 eV) and 527.556 nm. Both are characterized as "cw" (complex and wide) in an arc[67], but are the strongest lines seen in emission from an oxyhydrogen flame[68]. Both are absent from this spectrum; however, yet another spectrum from a still hotter flame (not shown here) contained, superimposed on the continuum, some very minor features at these two wavelengths.

4.5.5 Spectra from Molybdenum and Cobalt

Figures 4.33 and 4.34 show the spectra obtained from repeatedly injecting $Mo(CO)_6$ and $Co(C_5H_5)_2$. In the calibration curves presented in Figure 4.28, response from these two analytes is displayed by dotted lines. The reason for that visual caveat is the question whether the recorded spectra are, in fact, due to emission from species containing these metals. This scepticism is based not only on the weakness of response - which is relatively close to the response of carbon compounds - but also on certain spectral features.

The most prominent feature of the molybdenum spectrum shown in Figure 4.33 is the relatively sharp peak around 420 nm. There are two prominent atomic lines for Mo in the vicinity, *i.e.* at 414.355 and 418.832 nm. However, the energy levels for these transitions are apparently in question[67], and it is thus unlikely

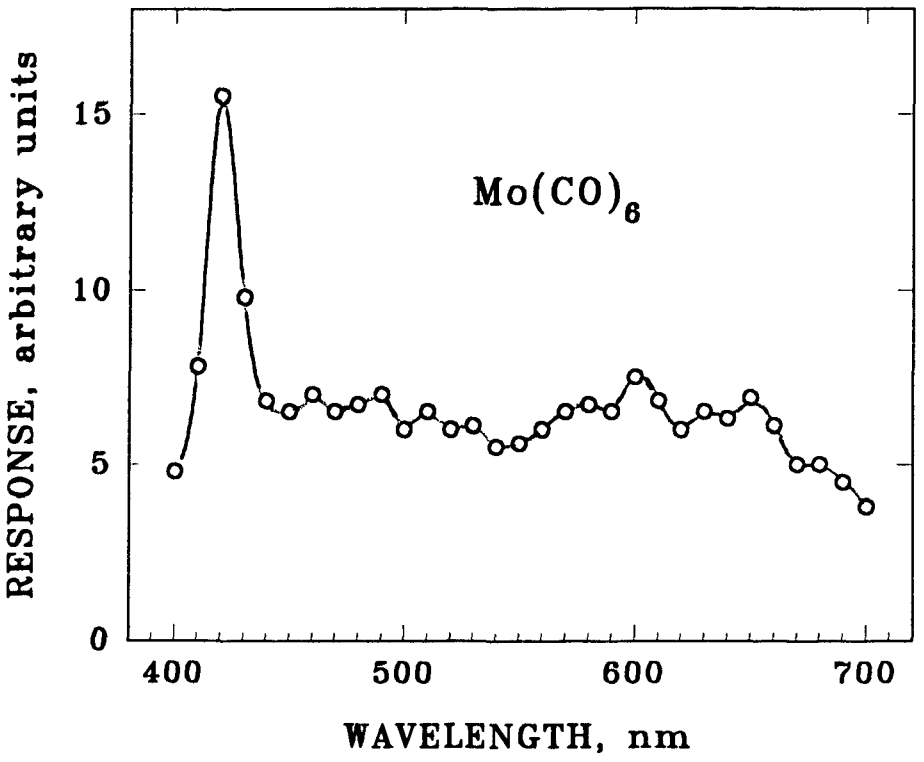

Figure 4.33 *Spectrum obtained from molybdenum hexacarbonyl, using a filter monochromator with 2 mm slit (corresponding to a 13 nm bandpass at 400 nm). Flame conditions: 300 mL/min H_2 and 80 mL/min air.*

that they represent transitions to/from the ground state. Also, MoO is very refractory. Owing to the prevailing low light level, we did not separately check for the possible presence of, for instance, the prominent lines 386.411 nm (0 - 25872 cm^{-1}, 3.21 eV) and 390.296 nm (0 - 25614 cm^{-1}).

A look at the calibration curves shows that, on a weight basis, the molybdenum compound is only about one order of magnitude larger in response than a typical aromatic carbon compound. However, the spectral measurements demonstrate that the luminescence from molybdenum hexacarbonyl at 420 nm is about ten times stronger than the luminescence obtained from a commensurate amount of naphthalene. Thus it appears that the spectrum shown does indeed contain most of the luminescence that established the calibration curve (note the difference in wavelength range between the calibration curve and the spectrum). However, the final possibility of carbonaceous emission being enhanced (catalyzed) by the presence of molybdenum is not precluded by the experiment.

Similar arguments can be made in the case of Co (here in the form of dicyclopentadienylcobalt) whose spectrum is shown in Figure 4.34. It is even more suggestive of an aromatic hydrocarbon (see below) than that of molybdenum. In the region of the blue maximum there are two cobalt lines involving the ground state, namely 419.071 nm (0 - 23856 cm^{-1}) and 423.400 nm (0 - 23612 cm^{-1})[67]. However, these lines are very weak in other systems and, furthermore, one would have expected that, if atomic excitation were occurring, the very strong lines around 350 nm[67,68] should have been observed in the form of a stronger overall response for Co (the lines are outside the range of the filter monochromator but are included in the open mode of the FPD calibration curve). It may also be mentioned that one of the R heads of CoH is situated at 419.45 nm (but the other, for the 0,0 transition, is located at 448.19 nm)[81]. More reasonable than to invoke such spectral features may be to assume that the emission observed within the 400 - 700 nm range of the filter monochromator is dominated by carbon-based response. If so, this would suggest either that there occurs significant luminescence from cobalt-containing species

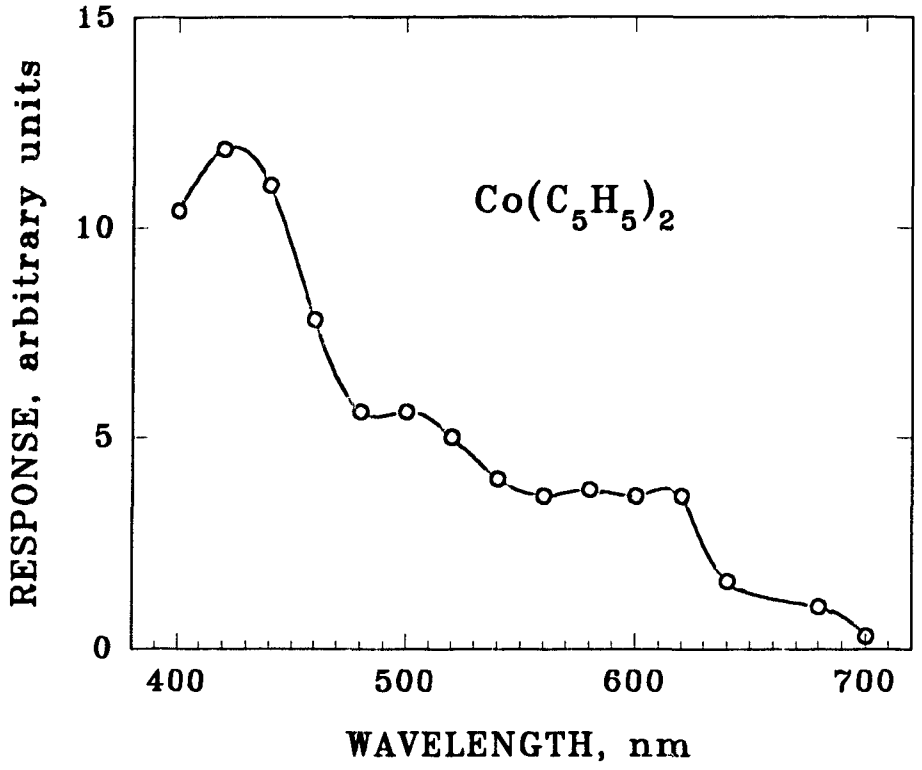

Figure 4.34 *Spectrum obtained from cobaltocene under flow conditions of 300 mL/min hydrogen and 55 mL/min air. The filter monochromator was used with a 6 mm slit. Bandpass = 27 nm at 400 nm.*

outside this range, or that the presence of cobalt somehow stimulates carbonaceous emission(s). A comparison of the absolute magnitude of suitable spectra suggests - but does not prove - the former alternative, *i.e.* that there may indeed exist further uncharted Co emissions.

Both cobalt- and molybdenum-derived emissions could be further investigated. However, because of their low sensitivity and hence minor analytical importance in the FPD, the matter was dropped.

Chapter 5. SPECTRA OF SOME MAIN-GROUP ELEMENTS IN THE FPD

5.1 Introduction

Besides sulfur and phosphorus, several other main group elements have shown analytically useful responses in the FPD. Most of these responses have been well studied - optimized, calibrated, spectrally characterized, *etc.*. However, some spectra of FPD-active main-group elements are still missing. This is because either the elements are analytically less important or the responses are not strong enough to be conveniently scanned by a conventional monochromator.

A known spectrum could make the task of wavelength selection so much easier - and such knowledge can be extremely helpful for designing solutions to various FPD selectivity problems. Also, certain spectral features, by virtue of not having been reported before, may attract the interest of the spectroscopist. As discussed in one of our papers[63], analytically reliable spectra should originate from the same detector as used in the actual analysis, running at the same operating conditions. Some such spectra - HPO, S_2, *etc.* - have been amply documented in the literature and will not be reproduced here. However, spectra of boron, lead, nitrogen, and antimony, which are not available from the FPD literature, will be presented in this chapter. Carbon spectra are also included here. This is not because carbon is important as an analyte in itself, but because carbonaceous materials make up the bulk of many biological or environmental samples. The information about carbon spectra is indispensable for a rational choice of detector conditions in the new selective FPD modes (Chapters 6 and 7). Note that the following spectra were obtained by repeatedly injecting the analyte while manually advancing the

monochromator's wavelength drive; they are hence free of flame background emissions.

The "common" conditions, which will be referred in the following context, mean the Shimadzu flame photometric detector is run with its quartz chimney normally left in place (in contrast to earlier work with transition metals, see Chapter 4); with its flame shield down for viewing the unshielded flame; and with 200 mL/min of hydrogen and 45 ml/min of air.

5.2 Boron

The green flame bands of boron have been studied for over one-and-a-half centuries, and much analytical work has been done with them[31]. Boron spectra are included here only because of the analytically as well as spectroscopically relevant presence in the FPD of *two* emitters; and because their relative contributions, not surprisingly so, change with the air flow. The two analytical studies[39,83] most closely related to the present context both mention the *ca.* 546 nm emission (and interference filters with central wavelengths of 550 and 546 nm, respectively); they attribute the band to BO. It is interesting to note that Braman and Gordon's "borane monitor" ran with a flame that was air-rich and much larger than that of a typical FPD. For sensitivity reasons, the monitor seems to have actually used a green glass filter[39]. Sowinski and Suffet's work on the Melpar FPD preferred an interference filter; their smaller flame - as judged by the conditions given for the calibration curve - was hydrogen-rich but just barely so[83]. Neither study shows a spectrum. Pearse and Gaydon[65] list the 546 nm band under "boric acid fluctuation bands, BO_2". They note that "BO bands are usually present as well" (the closest bands of the BO alpha system occur at 551 and 555 nm[65]).

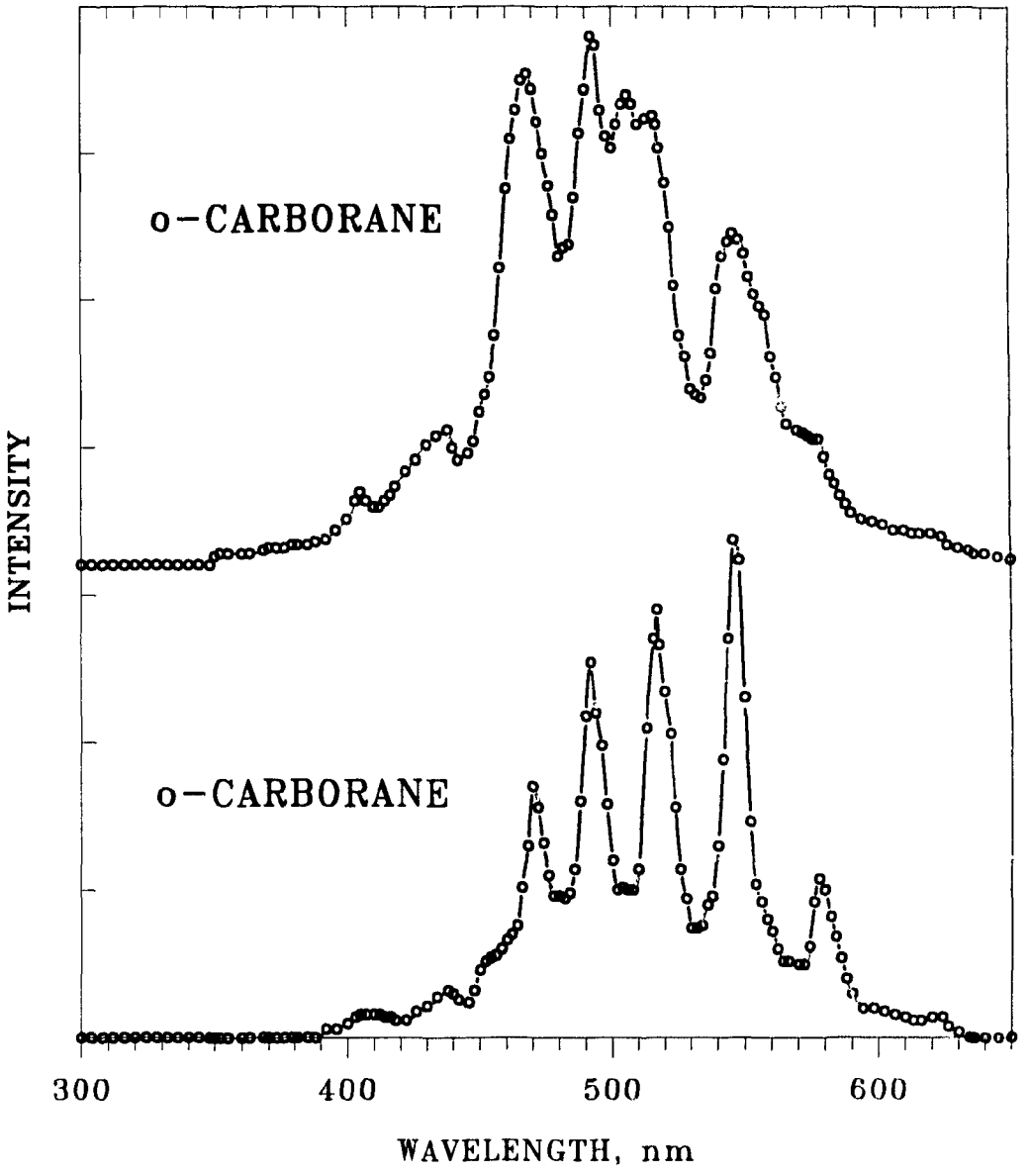

Figure 5.1 *Spectra from o-carborane. Grating monochromator, Hamamatsu R-1104 photomultiplier tube. Upper part: 200 mL/min hydrogen, 45 mL/min air, bandpass 6.7 nm. Lower part: close to stoichiometric conditions 47 mL/min hydrogen, 100 air, bandpass 1.6 mm.*

Indeed, the spectrum taken at the "common" FPD conditions (Figure 5.1, upper part) represents a mixture of systems. If the flame is changed to consume more air, almost up to stoichiometry, the spectrum (Figure 5.1, lower part) takes on the appearance of a single system whose bands coincide with those listed for BO_2[65], $A^2\Pi_u$ - $X^2\Pi_g$. The additional spectrum present in the upper part of Figure 5.1 is the alpha system of BO, $A^2\Pi$ - $X^2\Sigma^+$. A comparison of the two scans shown in Figure 5.1 provides an instructive example of the strong influence FPD flame conditions exert on the spectral distribution, hence the choice of wavelength (or *vice versa*, depending on the optimization mode). This is important not only for spectroscopic assignments but also for another objective of this thesis - selectivity improvement based on spectral differences among two channels: spectra representing more than one emitter alert the analyst to a likely change in the dual-channel response ratio with a change in detector gas flows.

5.3 Lead

Figure 5.2 shows the luminescence obtained from injections of tetraethyllead, at the "common" conditions. Some bands are superimposed on a continuum (whose relative contribution grows as the air flow is lowered - *i.e.* under those filter-less conditions that produce the maximum S/N value). The presence or absence of the quartz chimney seems to be of no importance. There is little, if any, evidence of the 405.8 nm line (*c.f.* ref. 63 for energy considerations) that has been used in the photometric detection of lead in gasoline samples fed to an oxyhydrogen flame[72]. The response of lead in a typical FPD has been mentioned before in the literature[20]; however, no spectral data were given there.

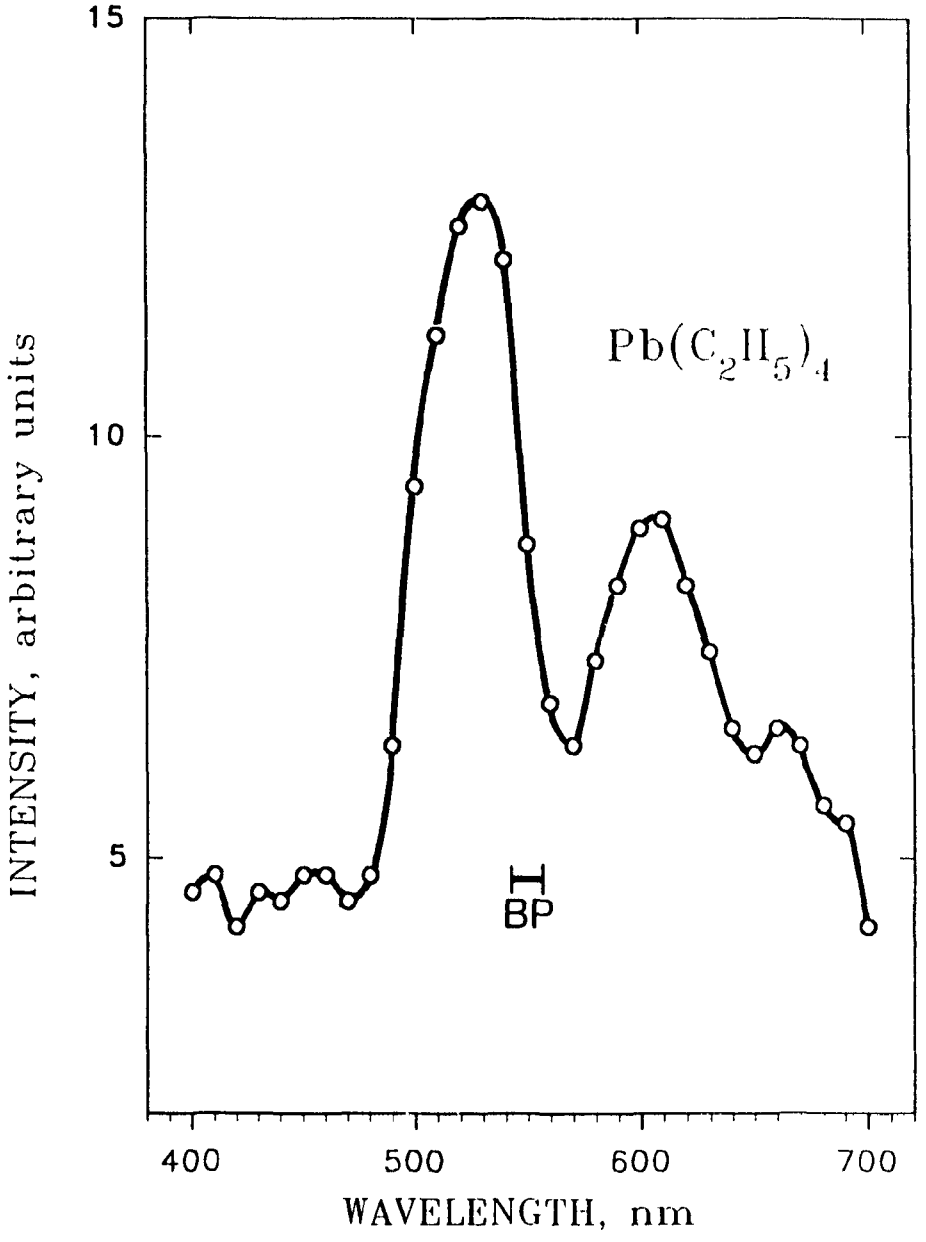

Figure 5.2 *Spectrum from tetraethyllead at flow conditions: 200 mL/min hydrogen, 45 mL/min air. Filter monochromator with R-1104 PMT. BP = bandpass (@ Oriel specification).*

The low light level (consequently the poor resolution) prevents a possible spectroscopic assignment. The PbH bands could be involved, but the B system of PbO also occurs in that region[65]. Analytically (not spectroscopically) interesting may be the fact that here the maximum luminescence of lead is located very close to that of phosphorus, which is conventionally monitored as HPO at 526 nm.

Note that most recently Jennifer A. Gebhardt (a graduate student in our group) has established favorable conditions for tetraethyllead on the very same detector. The sensitivity is improved by a factor of 10, so that a spectrum with higher resolution can be obtained. The new spectrum is quite different. Detailed results will appear in a future manuscript and J. A. Gebhardt's thesis.

5.4 Nitrogen

Figure 5.3 shows the flame luminescence due to the introduction of indole. There is no significant difference in the spectra taken with and without the quartz chimney. That this weak luminescence does not originate from the carbon part of the molecule is obvious from the fact that it can also be obtained from N_2O. The low intensity of organo-nitrogen response is probably the reason that it is not described by any detailed report in the FPD literature - despite the fact that nitrogen compounds are ubiquitous constituents of environmental and biological samples.

For the history of direct and indirect nitrogen emissions in flames, Gilbert's detailed account[31] should be consulted; cited here is only information of particular relevance to the FPD. The interference of nitrogen compounds in the "borane monitor" (a device related to the FPD) was attributed to the NH_2 alpha bands[83], and a later paper by the same author contains a spectrum and a comparison

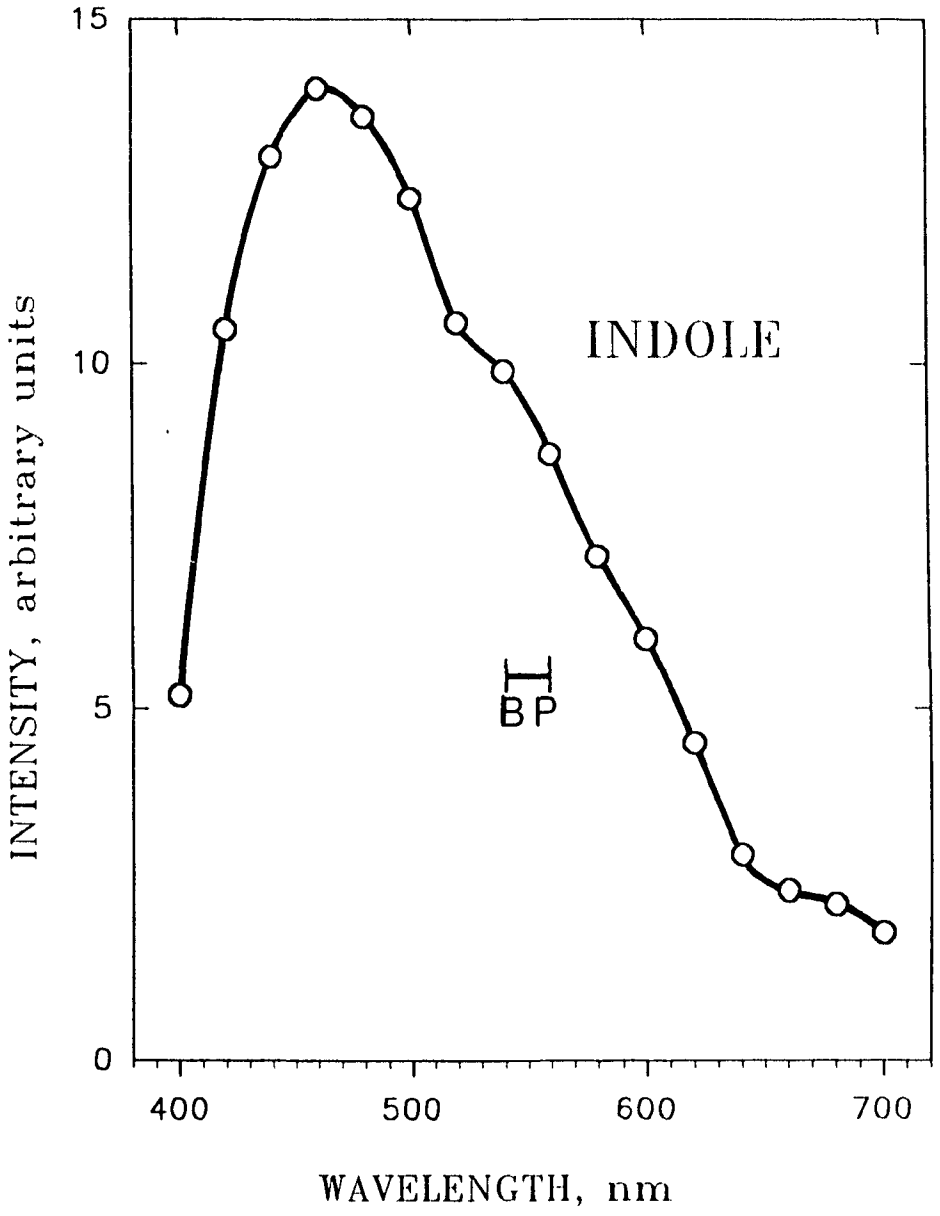

Figure 5.3 *Spectrum from indole at flow conditions: 200 mL/min hydrogen, 45 mL/min air. Filter monochromator with R-374 PMT.*

of the response of nitrogenous *vs.* carbonaceous compounds. The spectrum presented there for triethylamine[84] shows a certain similarity with the luminescence envelope of Figure 5.3; however, it is clearly located farther toward the red. The same is true of the spectrum shown for ammonia in a hydrogen-nitrogen diffusion flame[85]; and of the "bright, white" emission in the MECA oxy-cavity tentatively attributed to the NO-O continuum and monitored for analytical purposes at 500 nm[86]. Interestingly enough, the same study also contains the spectrum of a "faint blue" emission [ref. 87, Figure 1A], which was obtained in the absence of additional oxygen and closely resembles the one presented in Figure 5.3. In a hydrogen-nitrogen diffusion flame - where the 336 nm NH band was most prominent and was therefore used for the detection of ammonia - "the wavelength of maximum emission for the NH_2 band varied between 425 and 575 nm". Viewed on a long-slot burner, "a persistent blue emission" was observed at the base of the flame and (with larger amounts of ammonia) a "yellow emission" appeared above it[87].

Note that all these literature flames were oxygen (air) rich; and that, with the possible exception of the regular MECA cavity, they were much hotter than the puny, strongly hydrogen-rich flame of the FPD. Under the "common" conditions of this study, the highest temperature of the FPD flame - as suggested by the response of a thin-wire thermocouple - remained below 550 °C. Different emission behaviour is thus to be expected, although both hydrogen-rich and air-rich types of diffusion flames do, of course, contain all three of hydrogen-rich, stoichiometric and air-rich zones. Furthermore, the spectral distribution (wavelength of maximum emission) is likely to vary if two or more chemiluminescent emitters of roughly comparable strength are present.

It may be reasonably assumed that the weaker blue emissions referred to in references [86] and [87] came from cooler and more hydrogen-rich flame zones and hence were more likely to correspond to the emission shown in Figure 5.3. Equally reasonable is the assumption that more than one excited species contributed to the luminescence in the 400 to 600 nm region, particularly so in the hotter flames of the literature. In several experiments of this study, in which constant doping levels of N_2O entered a variety of FPD flames monitored by a grating monochromator, the spectra, too, showed slightly shifting spectral envelopes. The relative and absolute hydrogen and air flows of these FPD flames varied from very hydrogen rich up to almost stoichiometric; and their temperatures from very low to moderately high. At larger air flows and hence hotter conditions, the slight shoulder around 550 nm (see Figure 5.3) became more pronounced and, as a consequence, the emission maximum appeared to shift slightly toward the red. This is consistent with the literature behavior of various types of much hotter flames[83-87], for which visible nitrogen emission occurs at clearly longer wavelengths than in the conventional FPD.

Neither the NH_2 bands[65] nor any of the other nitrogen emissions commonly found in high-energy sources[31,65] could be clearly attributed to the FPD luminescence shown in Figure 5.3. The 300 to 400 nm region (which, in typical spectroscopic flames, contains CN and NH bands) was scanned in separate experiments but contained little radiation short of some flame background (OH). Although the presence of NH_2 and/or NO_2[65] cannot be excluded, this author still prefers to characterize nitrogen response in the FPD as being of unknown (and possibly mixed) origin. Since the spectral range happens to overlap the emission regions of several important elements - though with low intensity - nitrogenous analytes should be considered capable of causing false positives in various types of

FPD-based analyses.

5.5 Antimony

Figure 5.4 shows the spectrum derived from the luminescent response of triphenylstibine. From a low-temperature hydrogen diffusion flame, a similar spectrum was obtained[88] and attributed to the A system of SbO, particularly $A^2\Pi_{3/2}$ - $X^2\Pi_{3/2}$[84].

For comparison only, Figure 5.4 also contains the spectrum derived from triphenylarsine. It appears to be the long-known "arsenic continuum"[31], similar to the emissions recorded from a lab-made FPD[19] and a low-temperature hydrogen diffusion flame[82]. The emitter is generally considered to be unknown (although in some places it is referred to as AsO). We also attempted to check triphenylbismuthine [*c.f.* 20] but, encountering problems of reproducibility and contamination, soon gave up.

5.6 Carbon

Of greater interest are the spectra obtained from carbon compounds themselves, since the latter constitute the major components of many samples wherein trace amounts of organometallics need to be determined. However, to date, no literature source describes such spectra as obtained from an FPD at conventional operating conditions. (Spectra from carbon-containing emitters in much hotter and oxygen-rich H_2/O_2 and H_2/air flames are, however, discussed in various papers[40,84 85 89-91]. Besides, weak FPD responses are particularly likely to vary with differences in detector construction, condition and contamination. And, until the analytically relevant spectra are known, it is difficult to establish conditions for optimal selectivity.

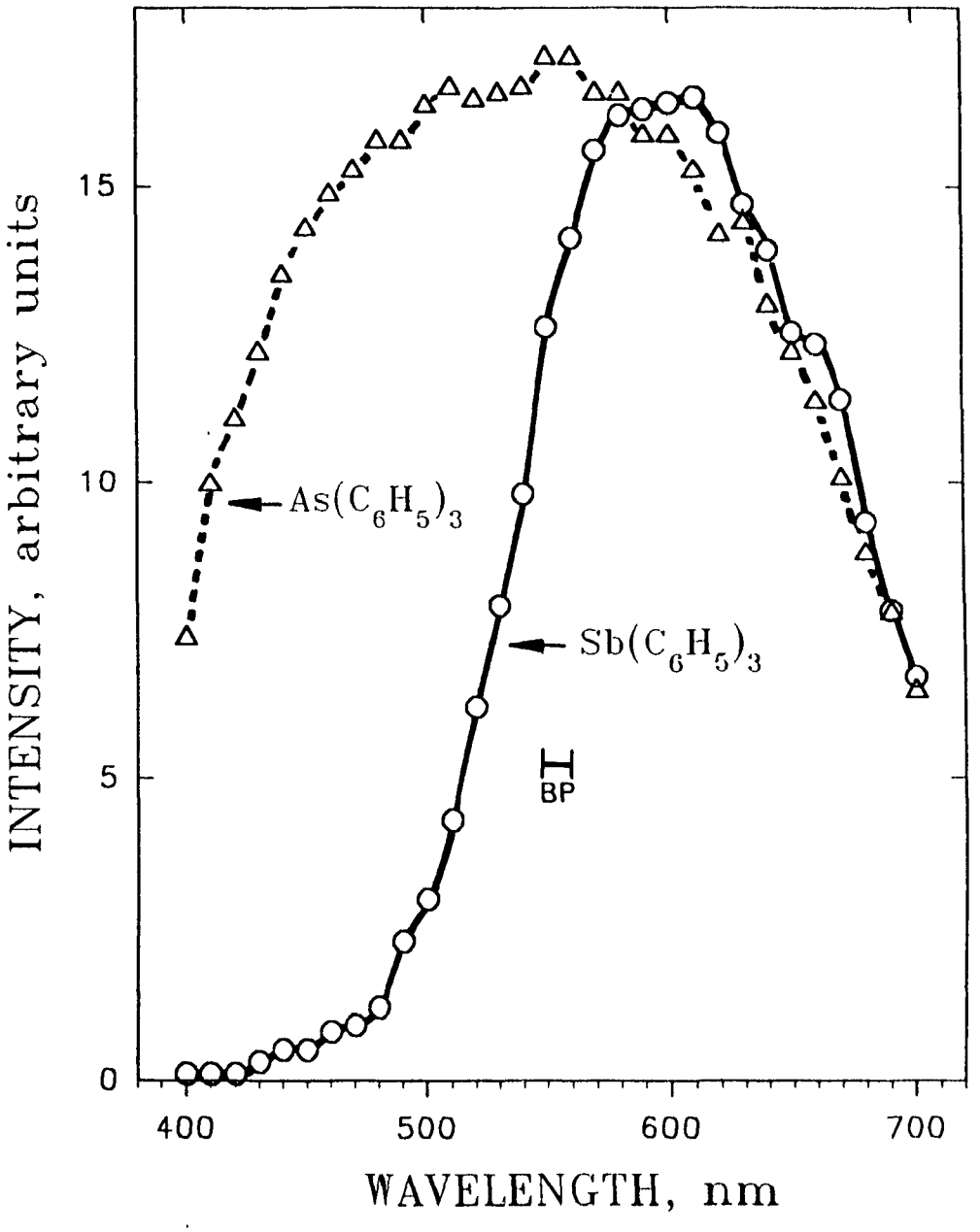

Figure 5.4 *Spectrum from triphenylantimony and triphenylarsenic at flow conditions: 200 mL/min hydrogen, 45 mL/min air. Filter monochromator with R-374 PMT.*

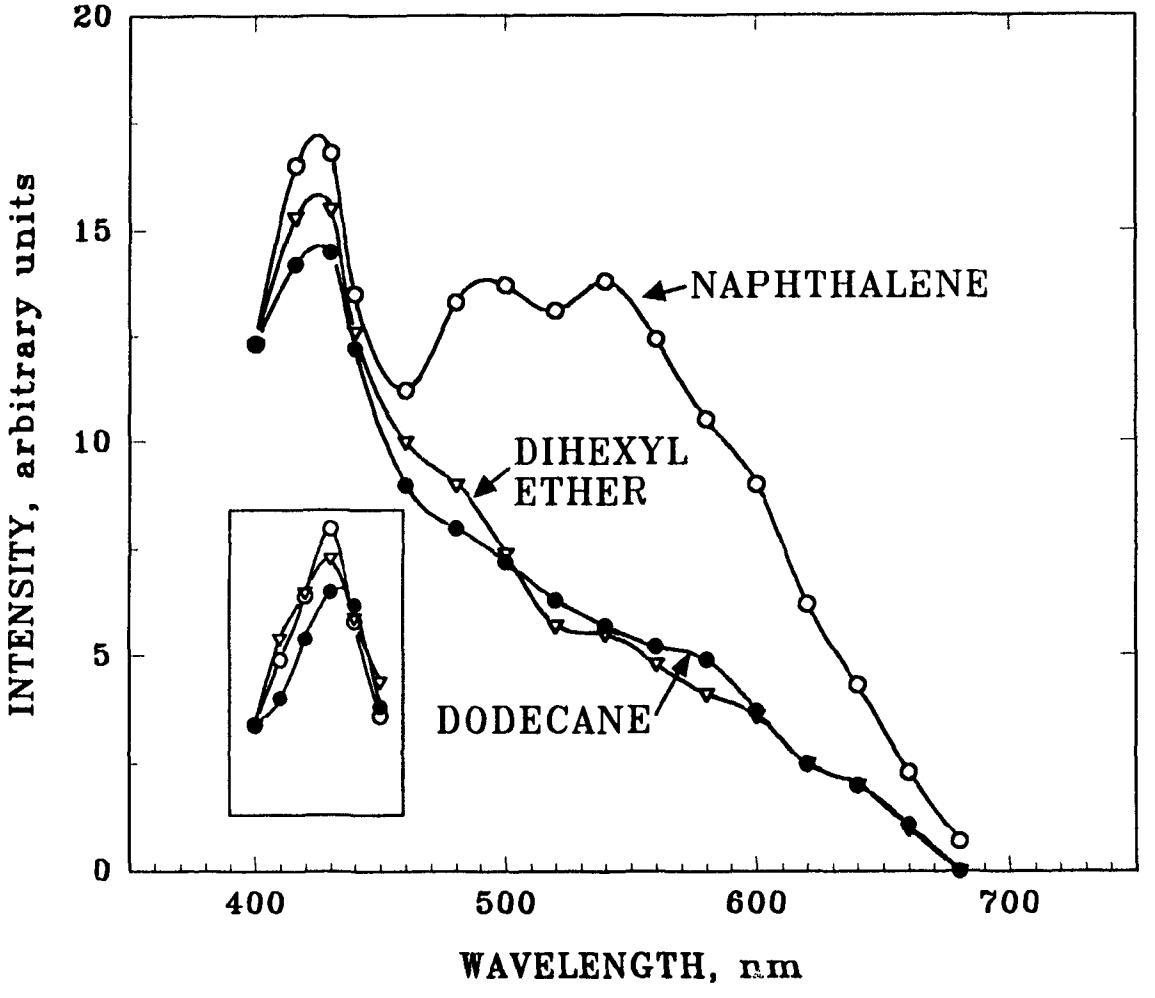

Figure 5.5 *Spectra of naphthalene (-○-), di-n-hexyl ether (-▽-) and dodecane (-●-) obtained on a filter monochromator with 6 mm slit and R-1104 PMT. Flame conditions: 300 mL/min H_2, and 60 mL/min air. Bandpass: 30 nm at 550 nm. Spectrum peaks in the rectangular frame are scanned at precisely the same conditions as the whole spectra, but with narrower bandpass (better resolution): 23 nm at 400 nm (with 4 mm slit).*

Figure 5.5 shows the luminescence spectra obtained from three standard carbon compounds - an alkane, an aliphatic ether, and an aromatic - at regular FPD operating conditions. The three compounds were injected as a mixture in order to keep the relative amounts precisely the same. Similar spectra were obtained from experiments repeated over the course of several months.

It is well known that aromatics respond more strongly in the FPD than aliphatics. The data shown in Figure 5.5 demonstrate that this is due to a partly different (not just a proportionally enhanced) spectrum. There is little agreement between these spectra and the carbon-based emissions from oxyhydrogen flames[40,84,85,89-91], except for the seemingly common peak at 430 nm. In the oxyhydrogen flames this peak clearly represents CH, with the 0,0 transition of $CH(A^2\Delta - X^2\Pi)$ located at 431.42 nm[65]. As shown in Figure 5.5, the peak apex was re-scanned, at the highest resolution obtainable at this low light level. Within the considerable error limits of such a measurement, the maximum is indeed located at that wavelength. The motivation for re-checking the region was related not only to its obvious analytical importance, but also to the suspicion that some or all of the FPD luminescence found there may originate from excited formaldehyde[65]. However, the very low light level characteristic of typical FPD settings prevents an experimental assessment of the relative contributions from CH and CH_2O.

In oxyhydrogen flames, the second most common spectral feature is C_2 ($A^3\Pi_g - X'^3\Pi_u$), *i.e.* the Swan bands[65]. Prominently visible is usually the 0,0 transition (head at 516.52 nm), accompanied by the 0,1 (563.55 nm) and 1,0 (473.71 nm) transitions. Aside from the measurement shown in Figure 5.5, a larger number of spectra were obtained at different times and with different compounds. In none of these did the Swan bands show up unambiguously - although they could, of course, be

present. The low light levels involved, and the differences between different carbon structures at wavelengths longer than, say, 460 nm, make this a difficult question to investigate. Aside from CH - and perhaps CH_2O and C_2 - the luminescence does not appear to fit any other known carbonaceous emitters. While thus not overly revealing in a spectroscopic context, knowledge of the carbon-related spectra is of considerable value for improving analytical selectivity[66].

Chapter 6. FPD NEW SELECTIVE MODE #1 — DIFFERENTIAL OPERATIONS

6.1 Introduction

Selectivity in the flame photometric detector is usually understood to mean the ratio of response from a particular hetero-atom *vs.* the response from carbon. This is in accordance with the most common use of the FPD: to determine gas chromatographic analytes containing one particular hetero-element — *e.g.* sulfur or phosphorus or tin — in sample matrices of a mostly hydrocarbonaceous nature.

While the conventional interference filter-photomultiplier tube combination makes the FPD a very sensitive device (for elements that do produce strong chemiluminescence), its inherently low spectral resolution, and the fact that it often monitors broad molecular bands, raise the question of selectivity. Indeed, one of the FPD's teething problems happened to be the spectral interference of the S_2 bands of sulfur with the HPO signal of phosphorus at 526 nm[54]. Furthermore, the highest sensitivity is often obtained by operating the FPD in the absence of optical dispersion (*i.e.* without interference filter). This "open" mode is particularly suited for monitoring all kinds of FPD-active elements, and for detecting analytes that produce expansive band systems. But it is also the one mode where selectivities are, in general, at their lowest.

Hence it would appear timely to explore the selectivity of various FPD detectable elements against carbon and against each other. And it would appear challenging to improve such selectivities in the low-resolution FPD to the point where they could compete with those obtained in the high-resolution instruments of atomic spectroscopy.

Selectivity ratios in the FPD vary in accordance with its chemical, geometric and spectral conditions. In the present context only spectral conditions are studied, while the same detector chemistry and geometry is imposed on all analytes. The latter is reasonable because the optimum detector gas flows do not change much from one element to the other. In return for this possible minor decrease in sensitivity, the results acquire both general applicability and comparability. The obvious way to start defining selectivity ratios is in the open mode (without any interference filter). At the next stage, filters appropriate for each element can be chosen and the measurements repeated. While such an approach defines neither the best possible sensitivity for each element, nor the best possible selectivity against others, it does provide the most useful overview of the multitude of potential analytes and analytical conditions.

How can selectivity against hydrocarbon - or, for that matter, against other hetero-elements - be further improved? Conventionally, single chromatograms are produced by only one optical channel. Yet, many FPD's have available two channels (a design intended to allow the simultaneous detection of phosphorus and sulfur), and one channel can be subtracted from the other with relative ease to produce a *differential* single output. The principle and some preliminary results of this technique have been discussed in the earlier part of this thesis (Sections 2.9, 3.4.5 and 3.4.6). Briefly: one channel monitored the wavelength at which the analyte element responded best but at which some response from carbon compounds was also seen; the other monitored a wavelength where carbon responded well but response from the analyte element was weak (or, preferably, absent). One of the amplified outputs was then attenuated such that the carbon responses in the two channels became equal - and hence vanished when one channel was subtracted from

the other.

For this approach to be successful, the relevant emission spectra have to be known at the analytical operating conditions of the detector. For some FPD-active analytes (both main-group and transition elements), as well as for different types of carbon compounds, such spectra have been presented in Chapters 4 and 5 of this thesis.

The simple subtraction circuit described earlier (Figure 2.2) would be too cumbersome and time-consuming to use for the measurement and manipulation of a larger number of hetero-element selectivities. It requires multiple runs for establishing an acceptably precise intensity ratio of the two channels, or for subjecting the same sample to different modes of discrimination. On the other hand, such a circuit accepts a wide range of signal levels and, because of its simplicity and on-line operation, does appear preferable for routine analyses.

Two types of signal-processing devices were therefore developed. The first device (shown in Figure 2.3) is a more sophisticated version of the earlier circuit. This "analog interface" is designed to serve in simple tasks where the signals from the two electrometers, after scaling by a given factor, are used to produce a subtraction chromatogram on the recorder chart.

The second device is a computer-based system capable of performing a much wider variety of measurements and manipulations. This "computer system" can store high-quality two-channel detector signals, filter digital data, correct baselines, scale channels with high precision, measure basic selectivity ratios and minimum detectable quantities, establish best analytical conditions, and subject single data sets to sequential algorithms that represent disparate selectivity regimes.

Data-processing capabilities such as these should prove of interest even beyond the confines of this study. For instance, they lend themselves to conventional analytical development and are helpful in the analysis of those environmental samples that are severely limited in supply and highly complex in composition: data from a *single* injection can generate several chromatograms of different selectivity and information content.

6.2 FPD Innate (Filter-less) Selectivities

To present the subject explicitly, this section is being divided into two parts: "main-group elements" and "transition metals".

6.2.1 Main-Group Elements

Table 6.1 presents a listing of "innate" selectivity ratios, *i.e.* the ratios of luminescence intensity from an "open" (filter-less) channel. The data describe how much more light the (red-extended) phototube picks up per atom of a particular element (listed vertically) than per atom of another element (listed horizontally). Sulfur and selenium are included here even though their calibration curves are non-linear, hence inadequately characterized by a single-number selectivity ratio. To compensate in a minor way, their injected amounts are listed in a Table 6.1 footnote.

No untoward surprises lurk in Table 6.1. Clearly, different flow conditions would have lead to a somewhat different set of numbers. Such numbers are valuable for predicting relative elemental responses from a multi-element sample monitored by a *filter-less* FPD channel. Given, in a particular case, knowledge of the prevailing spectra on one hand and specifications of interference filters and photomultiplier tubes on the other, the numbers of Table 6.1 could be further extended to estimate detector performance from a *spectrally selective* channel. As

Table 6.1 INTER-ELEMENT FULL-SPECTRUM FPD SELECTIVITIES* OF MAIN-GROUP ELEMENTS UNDER COMMON CONDITIONS

A\B→ ↓	Sn[a]	Ge[a]	P	S[b]	As	Se[b]	Sb	Pb	B	N	C[c]
Sn[a]	"1"	6	4×10^{1}	9×10^{1}	6×10^{2}	6×10^{2}	2×10^{3}	6×10^{3}	2×10^{4}	3×10^{4}	9×10^{6}
Ge[a]		"1"	8	2×10^{1}	1×10^{2}	1×10^{2}	4×10^{2}	1×10^{3}	4×10^{3}	6×10^{3}	2×10^{6}
P			"1"	2	1×10^{1}	1×10^{1}	6×10^{1}	1×10^{2}	6×10^{2}	7×10^{2}	2×10^{5}
S[b]				"1"	7	7	3×10^{1}	6×10^{1}	2×10^{3}	3×10^{2}	1×10^{5}
As					"1"	1	4	1×10^{1}	4×10^{1}	5×10^{1}	2×10^{4}
Se[b]						"1"	4	1×10^{1}	4×10^{1}	5×10^{1}	2×10^{4}
Sb							"1"	2	1×10^{1}	1×10^{1}	4×10^{3}
Pb								"1"	4	5	2×10^{3}
B									"1"	1	4×10^{2}
N										"1"	3×10^{2}
C[c]											"1"

* *Molar response of element A (column) over molar response of element B (row); both within linear range. "Common" conditions as cited in Experimental section.*

[a] *Mainly MeOH and MeH emissions - the more sensitive blue surface luminescence on quartz is deliberately held to a minimum.*

[b] *Sulfur and selenium have mostly quadratic calibration curves. Values given here refer to 9×10^{-12} or 1×10^{-10} mol/s of S or Se, respectively.*

[c] *Hydrocarbons produce negative response (inverted peaks) at the chosen conditions with a red-extended phototube.*

will become apparent later, the difference between a channel that is equipped with an interference filter and one that is not, is often quite small.

The choice of particular main-group elements for this study is, to a certain extent, arbitrary. Some main-group elements have never been seriously tested for response in the FPD. Others are known to respond - *e.g.* In, Bi, Te - but are excluded here for lack of general importance or analytical interest, or for the commercial scarcity or premature decomposition of the compounds supposed to carry them through the gas chromatographic system. Still others - *e.g.* Cl, Br, I - are disregarded here because they respond adequately only in the presence of another metal (Cu, In, *etc.*).

The choice of conditions, too, is somewhat arbitrary. Different elements do respond best at *different* flow settings. (In addition, absolute and relative elemental responses depend on the construction of the detector.) However, since response variations with flow are rarely exorbitant, and since inter-element selectivity properly comes into play only if two or more FPD-active elements are to be considered, using a *common* set of conditions was both more realistic and of greater value to the analyst than comparing data that were separately optimized for each particular element. Still, in an experimental detour flow optimization was indeed carried out for individual elements - but only to ascertain that their optimized settings did not differ drastically from the "common" conditions selected to accommodate all of them.

Certain elements (*e.g.* boron and arsenic) noticeably increase in signal and, more importantly, also in signal/noise as the air flow increases toward stoichiometric. If such conditions were chosen for a multi-element analysis, the selectivity ratios would change significantly (for instance, B and As response would

become stronger while P, S, and Sn response would become weaker). It should be mentioned in this context that arsenic can produce a vastly superior response in a special detector configuration[19].

6.2.2 Transition Metals

The molar detection limits of metals (in organometallics) - as well as carbon (in three selectivity probes) and nitrogen (in indole) - are listed in Table 6.2 for the same, standard conditions in filter-less, single-channel FPD mode. These numbers can be used to calculate "innate" molar selectivities for atoms of one element against atoms of another. Such selectivities are listed in Table 6.2 for transition elements versus carbon. Inter-metal selectivities can be calculated in the same manner.

The reason that data in Table 6.2 (as in Table 6.1) are reported with one significant digit, is that they are derived from minimum detectable amounts (which, to the purist, admit to only one significant figure). Also, one-digit data are used in awareness of the changes in detector sensitivity that occur with the passage of time, the variation of temperature, the severity of contamination, and the switching of individual photomultiplier tubes. Still, measurements were always taken, and calculations always carried out, on the basis of two or more significant digits.

Minimum detectable amounts and selectivity ratios are recorded here for the two most common types of photomultiplier tubes used with the FPD. These are, in Hamamatsu codes, the R-268 (bialkali, 300-650 nm) and the red-extended R-1104 (multi-alkali, 185-850 nm). Differences between the two sets of results conform to expectations based on analyte spectra. The important fact, however, is that these differences are comparatively small: they do not exceed a factor of five.

Table 6.2 MOLAR DETECTION LIMITS OF ORGANOMETALLICS AND STANDARD CARBON COMPOUNDS IN SINGLE-CHANNEL OPEN MODE WITH R-268 and R-1104 PMT's

Element	Compound	MDL[a]		Selectivity[b]	
		R-268	R1104	R-268	R1104
Ru	$Ru(C_5H_5)_2$	4×10^{-15}	5×10^{-15}	5×10^{5}	8×10^{5}
Ni	$Ni(C_5H_5)_2$ [c]	2×10^{-14}	1×10^{-14}	1×10^{5}	4×10^{5}
Cr	$Cr(CO)_6$	6×10^{-14}	5×10^{-14}	4×10^{4}	8×10^{4}
Os	$Os(C_5H_5)_2$	9×10^{-14}	8×10^{-14}	2×10^{4}	5×10^{4}
Fe	$Fe(C_5H_5)_2$	1×10^{-13}	9×10^{-14}	2×10^{4}	4×10^{4}
Mn	$C_5H_4CH_3Mn(CO)_3$	1×10^{-13}	1×10^{-13}	2×10^{4}	4×10^{4}
Re	$Re_2(CO)_{10}$	5×10^{-13}	2×10^{-13}	4×10^{3}	2×10^{4}
Co	$Co(C_5H_5)_2$	2×10^{-12}	2×10^{-12}	1×10^{3}	2×10^{3}
C	dodecane	2×10^{-9}	4×10^{-9} [d]	1	1
C	naphthalene	2×10^{-9}	2×10^{-9}	1	2
C	di-n-hexyl ether	3×10^{-9}	7×10^{-9}	1	1
N	indole	2×10^{-11}	2×10^{-11}	1×10^{2}	2×10^{2}

[a] *Molar detection limit, in mol of designated metal per second, measured at signal/noise = 2, with noise defined as the peak-to-peak short-term baseline fluctuation. Divide numerical value by 3.7 to obtain approximate detection limit according to the S/σ = 3 IUPAC definition.*

[b] *Minimum detectable mol of carbon in dodecane/minimum detectable mol of metal; (mol C/s)/(mol Me/s).*

[c] *0.5 meter 5% Carbowax 20 M column.*

[d] *Negative (inverted) analyte peak.*

The innate metal-carbon (carbon as in dodecane) selectivities for the clearly responding metals Ru, Ni, Cr, Os, Fe, Mn and Re fall between 7×10^5 and 4×10^3 in filter-less mode, *i.e.* roughly between three and six orders of magnitude. These numbers could be expected to rise in the dispersive (really: wavelength-selective) mode.

The response of a standard compound containing one metal atom (the usual case) could serve to construct a molar calibration curve valid for all analytes containing one atom of that metal. Or, nearer the current context, the selectivity of a particular metal *vis-à-vis* others could be used to define the molar selectivity behavior for all compounds containing these metals. However, that approach requires caution. It cannot be automatically assumed that every response observed is a strictly linear function of the amount of hetero-atom injected, although most of the time this is likely to be the case. For one, different compounds containing the same hetero-atom may be subject to different degrees of on-column decomposition. Also, response may to some extent depend on compound structure.

In those cases where a few compounds of the same metal have actually been tested, *i.e.* in the studies of iron (Section 4.1) and manganese (Section 4.4), response was roughly proportional to metal content. Other transition elements were not examined in that context - owing mainly to the limited commercial availability of suitable test compounds - but they should prove equally well behaved.

In the case of different types of carbon compounds, however, response is not proportional to carbon content. For instance, aromatics respond generally more strongly than aliphatics. There also exists considerable literature on the response of sulfur compounds depending - or, for other authors, not depending - on the type of functional sulfur group present. And, when a particular hetero-element responds but

weakly in the FPD, special caution is called for.

6.3 Selectivities of Transition Elements against Carbon in Single-Channel Filter Mode

Results from wavelength-selective single-channel detection using a variety of filters are listed in Table 6.3 for the R-268 tube, and in Table 6.4 for the R-1104 tube. "Best" selectivities for each metal against carbon (again as in dodecane) now range from 4×10^6 to 1×10^4. That this improvement is surprisingly small should be pointed out to occasional readers of the FPD literature, who are by now accustomed to seeing response in the FPD being described as "specific" and that behaviour being attributed to the choice of a particular interference filter. However, the numbers listed in Tables 6.3 and 6.4 for various transition metals are consistent with their respective spectra, *i.e.* with the location of the chosen metal wavelength in relation to the broad emissions of carbon compounds[63]; as well as with the extent to which the metal spectra are dominated by lines or sharp bands as opposed to broad bands and continua. The factors that describe the improvement (or, occasionally, impairment) in selectivity - from the better suited of the two photomultipliers in the open mode, to the best filter/photomultiplier tube combination in the filter mode - never exceed one order of magnitude. Atomic selectivities *vis-à-vis* carbon (as in dodecane) are thus bettered by a factor of 6 for Ru, 8 for Ni, 5 for Fe, and 3 for Mn; and worsened by a factor of 0.7 for Cr, 0.5 for Re and 0.2 for Os.

6.4 Inter-Element Selectivities in Single-Channel Filter Mode

Enhancement of selectivities among the various transition metals themselves depends on their spectra: how far and in what complexity they cover - in relation to each other - the accessed wavelength range. Some selectivity ratios are

Table 6.3 MOLAR DETECTION LIMITS AND SELECTIVITIES OF TRANSITION METALS AGAINST CARBON IN SINGLE-CHANNEL FILTER MODE, R-268 PMT

Me	Compound	max. (nm)	Filter (nm)	MDA[a] (mol/s)	Selectivity[b] against C_{RH}	C_{ArH}	C_{R2O}	N_{ArN}
Ru	$Ru(C_5H_5)_2$	484	480	8×10^{-15}	1×10^{6}	6×10^{5}	2×10^{6}	3×10^{3}
		528	530	4×10^{-15}	4×10^{6}	5×10^{5}	5×10^{6}	6×10^{3}
Ni	$Ni(C_5H_5)_2$	508	510	1×10^{-14}	3×10^{6}	3×10^{5}	3×10^{6}	2×10^{3}
		542	540	1×10^{-14}	1×10^{6}	2×10^{5}	2×10^{6}	2×10^{3}
		572	570	7×10^{-15}	(3×10^{5})[c]	1×10^{6}	(6×10^{6})[c]	1×10^{4}
Cr	$Cr(CO)_6$	428	430	9×10^{-11}	3×10^{1}	1×10^{1}	7×10^{1}	5×10^{2}
		480	480	2×10^{-13}	5×10^{4}	3×10^{4}	6×10^{1}	1×10^{2}
Os	$Os(C_5H_5)_2$		720 cut-on	no response on R-268 PMT				
Fe	$Fe(C_5H_5)_2$	345	340	8×10^{-13}	2×10^{5}	2×10^{5}	$>4\times10^{5}$	7×10^{2}
Mn	$C_5H_4CH_3$-	403	405	2×10^{-14}	1×10^{5}	9×10^{4}	2×10^{4}	1×10^{1}
	$Mn(CO)_3$	540	540	2×10^{-13}	6×10^{4}	1×10^{4}	1×10^{5}	1×10^{2}
Re	$Re_2(CO)_{10}$		553	1×10^{-12}	(9×10^{3})[c]	2×10^{1}	(3×10^{4})[c]	5×10^{1}

[a] *Molar detection limit, mol metal per second, at S/N = 2.*

[b] *Minimum detectable mol carbon per second in dodecane (RH), naphthalene (ArH), or di-n-hexyl ether (R_2O); or mol nitrogen per second in indole (ArN); divided by minimum detectable mol metal per second.*

[c] *Numbers in parentheses are calculated from negative (reversed peak direction) carbon responses.*

Table 6.4 MOLAR DETECTION LIMITS AND SELECTIVITIES OF TRANSITION METALS AGAINST CARBON IN SINGLE-CHANNEL FILTER MODE, R-1104 PMT

Me	Compound	max. (nm)	Filter (nm)	MDA[a] (mol/s)	Selectivity[b] against			
					C_{RH}	C_{ArH}	C_{R2O}	N_{ArN}
Ru	$Ru(C_5H_5)_2$	484	480	8×10^{-15}	1×10^{6}	5×10^{5}	7×10^{5}	2×10^{3}
		528	530	4×10^{-15}	2×10^{6}	6×10^{5}	4×10^{6}	9×10^{3}
Ni	$Ni(C_5H_5)_2$	508	510	6×10^{-15}	9×10^{5}	5×10^{5}	3×10^{6}	5×10^{3}
		542	540	1×10^{-14}	9×10^{5}	2×10^{5}	1×10^{6}	3×10^{3}
		574	570	9×10^{-15}	2×10^{6}	8×10^{5}	1×10^{7}	6×10^{3}
Cr	$Cr(CO)_6$	428	430	1×10^{-13}	2×10^{4}	2×10^{4}	2×10^{4}	2×10^{2}
		480	480	2×10^{-13}	4×10^{4}	2×10^{4}	3×10^{4}	2×10^{2}
Os	$Os(C_5H_5)_2$		720 cut-on	9×10^{-14}	1×10^{4}	7×10^{3}	2×10^{4}	1×10^{3}
Fe	$Fe(C_5H_5)_2$	345	340	2×10^{-12}	5×10^{4}	5×10^{4}	1×10^{5}	2×10^{2}
Mn	$C_5H_4CH_3$-$Mn(CO)_3$	403	405	3×10^{-14}	9×10^{4}	3×10^{4}	1×10^{5}	2×10^{3}
		540	540	4×10^{-13}	2×10^{4}	4×10^{3}	3×10^{4}	7×10^{1}
Re	$Re_2(CO)_{10}$		553	1×10^{-12}	1×10^{4}	1×10^{4}	4×10^{4}	5×10^{1}

[a] *Molar detection limit, mol metal per second, at S/N = 2.*

[b] *Minimum detectable mol carbon per second in dodecane (RH), naphthalene (ArH), or di-n-hexyl ether (R_2O); or mol nitrogen per second in indole (ArN); divided by minimum detectable mol metal per second.*

Table 6.5 INTER-METAL SELECTIVITIES[a] AT VARIOUS WAVELENGTHS, R-1104 PMT

Me	Filter (nm)	X= Ru	Ni	Cr	Fe	Mn	Os	Re	Co
Ru	480	(1)	1×10^{1}	2×10^{1}		$>1\times10^{2}$			
	530	(1)		1×10^{1}	4×10^{1}	9×10^{1}	1×10^{1}	8×10^{1}	3×10^{3}
Ni	510	2	(1)			9×10^{1}			
Cr	430	2×10^{-1}		(1)	4	6	8	6×10^{1}	8
Fe	340	2×10^{-2}		5×10^{-1}	(1)	$>1\times10^{2}$	$>1\times10^{2}$	$>1\times10^{2}$	$>1\times10^{2}$
Mn	405	3×10^{-1}		7	9	(1)	4×10^{1}	3×10^{2}	3×10^{2}

[a] *Minimum detectable mol X per second divided by minimum detectable mol Me per second; R-1104 PMT.*

Note: selectivity values given as ">" are derived from chromatograms where the peak height of X is smaller than, and is therefore replaced by, the noise level.

listed in Table 6.5; they were chosen for general importance as well as for later reference. These results suggest that the improvement in inter-metal selectivity from filter-less to single-channel filter mode, *i.e.* the improvement obtained from the judicious choice of an interference filter, is rather limited. If the numbers in Table 6.5 are compared with the open-mode metal-metal selectivities easily extracted from Table 6.2, most improvements of selectivity amount to no more than one order of magnitude. For instance, the improvement in selectivity from the best filter-less to the best filter mode involves a factor of 2 for Ru/Ni, Ru/Cr, Ru/Fe, Cr/Ru, Cr/Fe, and Cr/Re; a factor of 3 for Cr/Mn; and a factor of 4 for Cr/Fe, Cr/Os and Ru/Mn (in these analyte/interferent pairs, the first-named element is considered the analyte and hence determines the choice of the interference filter). There are other cases where no improvement - or even some impairment - is noticed in progressing from a filter-less to a filter mode: this happens in the pairs Ru/Os, Ru/Re, Fe/Ru and Fe/Cr. The *significant* improvements occur mainly in cases involving iron - Fe/Mn, Fe/Os, Fe/Re - where factors can exceed two orders of magnitude. This is due to the fact that Fe is monitored at 340 nm, where only a few of the other metals luminesce.

6.5 Selectivities in Dual-Channel Differential Mode

A frequently held perception equates the use of an interference filter in the FPD with "specific" response for the monitored element. Within the confines of this study, such is definitely not the case. In fact, it is in doubt that true specificity (= infinite selectivity) can ever be associated with the use of a particular wavelength. To obtain more significant improvements than single-channel filter operation can offer, *dual*-channel differential modes must be used.

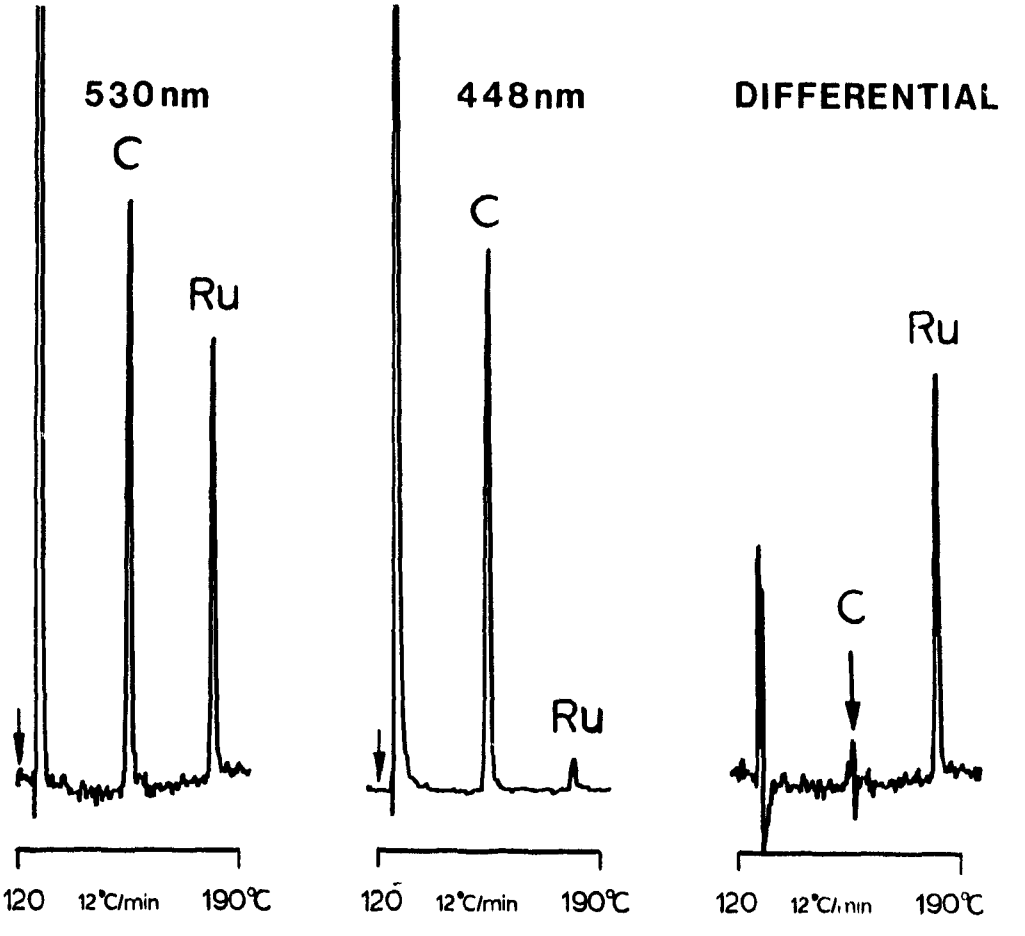

Figure 6.1 *Single channel and dual-channel differential chromatograms of a sample containing 30 μg dodecane ("C") and 300 pg $Ru(C_5H_5)_2$ ("Ru") in acetone.*

A simple example is presented in Figure 6.1, which shows the separation of 30 μg of dodecane and 0.3 ng of ruthenocene. The chromatogram on the left was acquired from a single channel at 530 nm. This monitors a major wavelength of Ru, which yields the best discrimination against carbon. The peaks are almost of the same height, suggesting a compound-to-compound selectivity of 7.4×10^4 (corresponding to an atomic Ru/C selectivity of 1.2×10^6). The chromatogram shown in the middle was taken from a single channel at 448 nm, where the ruthenium emission is fairly weak. The chromatogram captioned "Differential" was obtained from the 530/448 nm dual-channel differential mode tuned for quantitative discrimination against carbon. The amount of dodecane had been deliberately chosen from the upper end of its linear range, where its concentration just becomes large enough to start distorting the Gaussian peak shape. A vacillating, clearly non-Gaussian signal appears in place of the dodecane peak. Even counting the full vertical pen displacement caused by this perturbation, the compound-to-compound selectivity is now in excess of 10^6, the atomic ruthenium-to-carbon selectivity in excess of 10^7. For any reasonable analytical purpose, this seems more than adequate.

If still larger amounts of dodecane are injected, the peak distortion in single-channel mode becomes clearly visible and the characteristic flip-flop pattern of the differential mode intensifies. But does this flip-flop arise from the peak asymmetry (which, after all, is seen by both photomultipliers)?

As will be demonstrated later, purely electronic distortion is likely present in such peak remnants. But limitations of an other than electronic nature can contribute as well. This is not surprising, taking into account the puny and feeble FPD flame. Note for instance that, at the apex of the carbon peak shown in Figure 6.1, the combustion of dodecane already requires more than 3% of the detector's

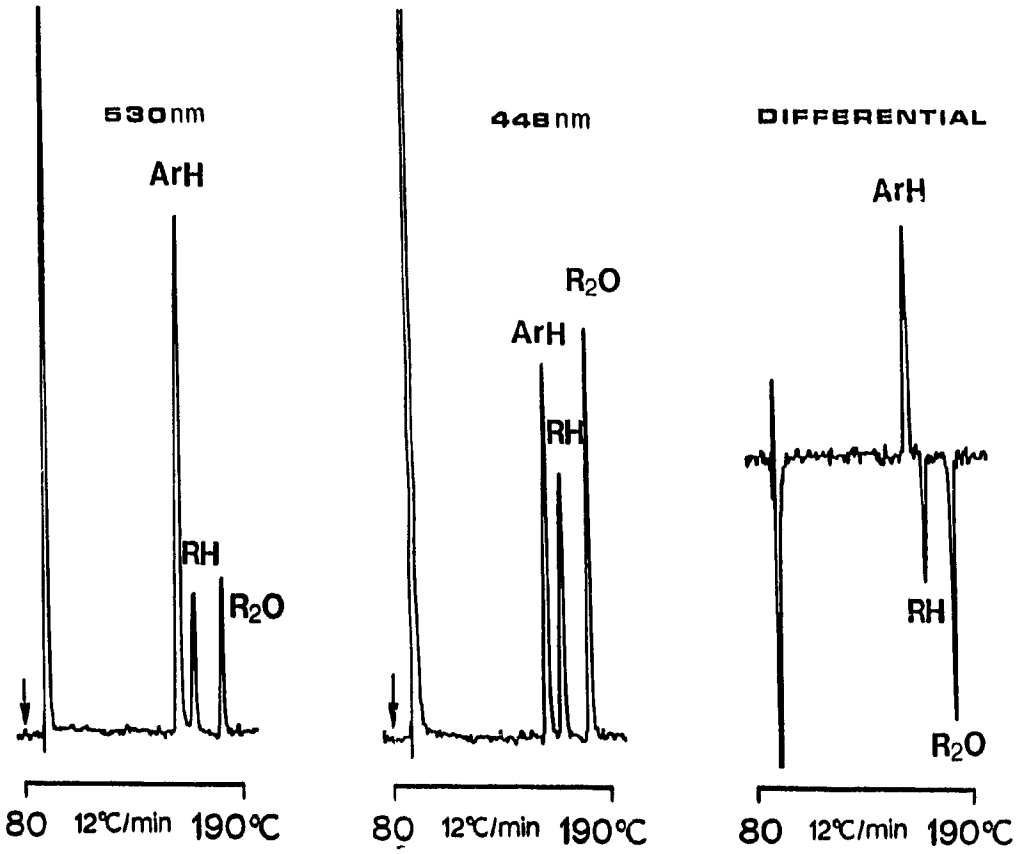

Figure 6.2 *Single channel and dual-channel differential chromatograms of a sample containing 10 μg naphthalene ("ArH"), 10 μg dodecane ("RH"), and 15 μg di-n-hexyl ether ("R_2O") in acetone.*

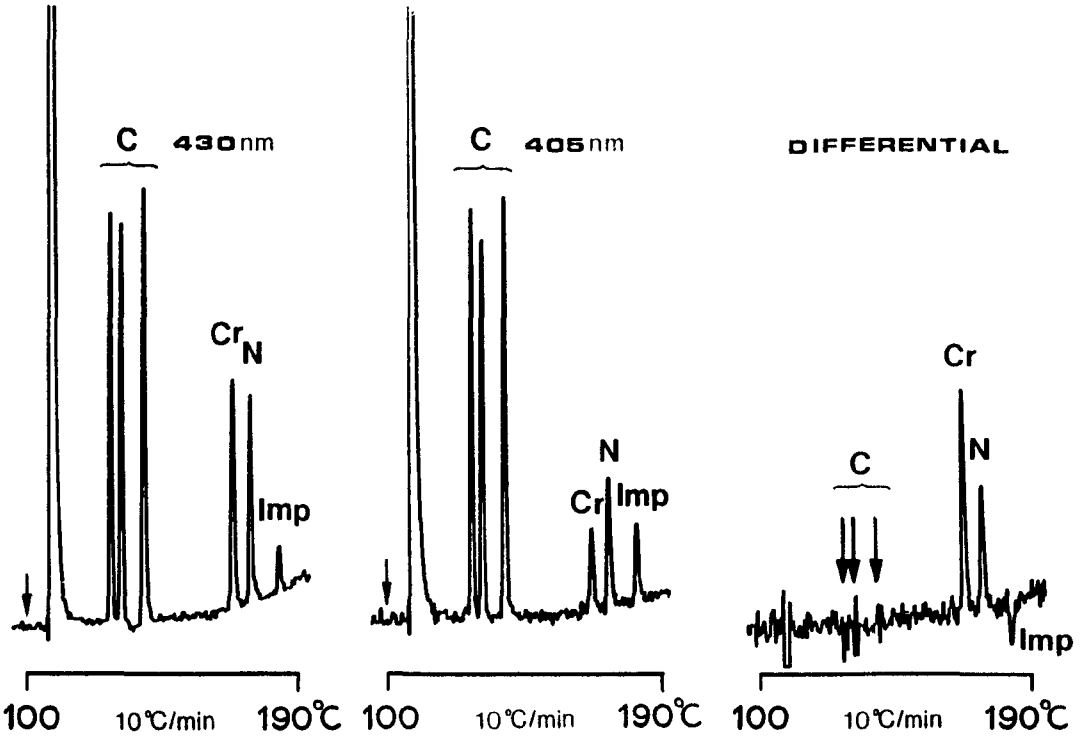

Figure 6.3 *Single channel and dual-channel differential chromatograms of a sample containing 8 μg naphthalene, 8 μg dodecane, and 12 μg di-n-hexyl ether ("C"), together with 4 ng $C_6H_6Cr(CO)_3$ ("Cr") and 600 ng indole ("N") in acetone. "Imp" = impurity of unknown composition.*

oxygen supply, and significant changes in flame size, temperature. chemistry and flicker behaviour could be expected under such severe overload.

Beyond electronic artifacts and flame perturbations, carbon compounds pose special difficulties that stem from the infinite variety of their structures. In particular, the spectra of aromatics are more intense than those of aliphatics in the 480 to 660 nm region (Figure 5.5). This is chromatographically illustrated in Figure 6.2 with a mixture of three carbon compounds. The differential mode, when using two channels at 448 and 530 nm via the computer system, can cancel either the aromatic or the two aliphatics - but it cannot cancel all three at the same time. For producing the right-hand chromatogram in Figure 6.2, the two channels are so tuned that the result distinguishes between aromatics and aliphatics in a qualitative sense, *i.e.* by the direction of response. While this would seem interesting in a general analytical context, it should be noted that the FPD's sensitivity to carbon is very low, and that ambiguous results can be expected from molecules combining different sites/degrees of unsaturation.

Still, it is possible to cancel all three carbon compound types if other wavelengths are used. The relevant spectra (Figure 5.5) suggest that wavelengths up to about 440 nm should be suitable. A chromatogram of the same three carbon compounds shown in Figure 6.2, together with compounds of chromium and nitrogen (plus an impurity of unknown composition) is shown in Figure 6.3. The differential mode, tuned to forestall the appearance of carbon compounds, achieves that objective quite well - despite the fact that the latter are of very different structure and overall spectrum. Thus, if no other circumstances militate against it, 430 nm (or a wavelength close to it) is the preferred choice for the channel used to neutralize the response of carbon compounds. (Obviously, the analyte channel wavelength has to be

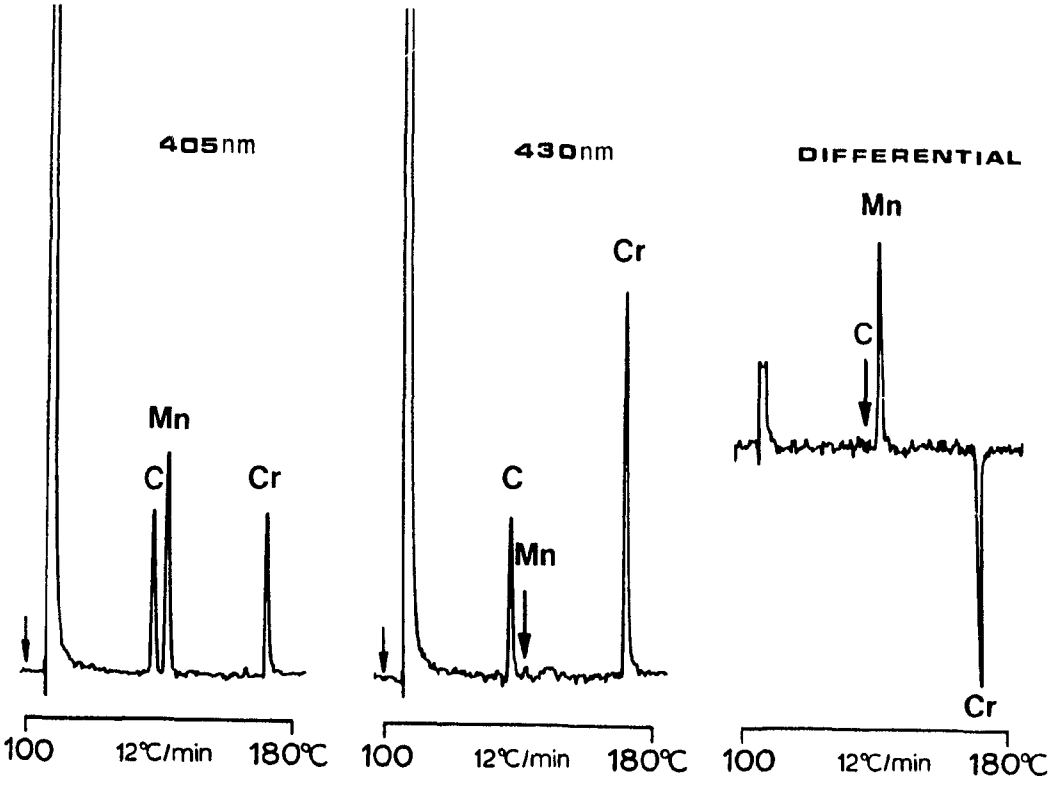

Figure 6.4 *Single channel and dual-channel (carbon-suppressed) differential chromatograms of a sample containing 5 μg dodecane ("C"), 500 pg $C_5H_4CH_3Mn(CO)_3$, and 4 ng $C_6H_6Cr(CO)_3$ in acetone.*

lower than 440 nm as well.)

The eradication of carbon response can also be achieved while, at the same time, the two metals are being qualitatively differentiated by the direction of their peaks. This is shown for manganese and chromium in Figure 6.4. Clearly, this detector mode can be easily extended to most (if not all) FPD-active elements, and should be of particular help in screening-type analyses.

Note that in Figure 6.4 the solvent peak is not completely cancelled in the differential mode. This particular tuning and subtraction process, similar to the one whose results are shown in Figure 6.3, was carried out by the Computer System. In contrast to the "analog interface" (Figure 2.3), the "computer system" (Figure 2.4) is not capable of subtracting a very large peak from its second-channel counterpart. What is shown in Figure 6.4 as a clipped solvent peak merely represents the ratio of the upper limits of the two channels. Similarly, this ratio just happened to coincide with the baseline in Figure 6.3, perhaps falsely suggesting there that the solvent acetone had been entirely suppressed. Obviously, this limitation in range of the "computer system" does not affect peaks that are smaller than two full scales.

The next series of simplified chromatograms is designed to explore and illustrate the degree of control and the improvement of measured selectivity ratios that can be typically expected for two transition metals. This example uses ruthenium and chromium. To set the scene, the series starts with single-channel chromatograms. The left side and the middle of Figure 6.5 show these channels, at preferred wavelengths for the analysis of Ru (480 nm) and Cr (430 nm). Note that the single-channel operation provides only a modest enhancement of selectivity *vis-à-vis* the open mode and that, in a complex "real-life" situation, it might even fail to distinguish between the two metals. The *dual*-channel operation, in its qualitative mode, achieves that distinction quite readily (right side of Figure 6.5). For the more important quantitative mode, the same channels are tuned (scaled) to different ratios,

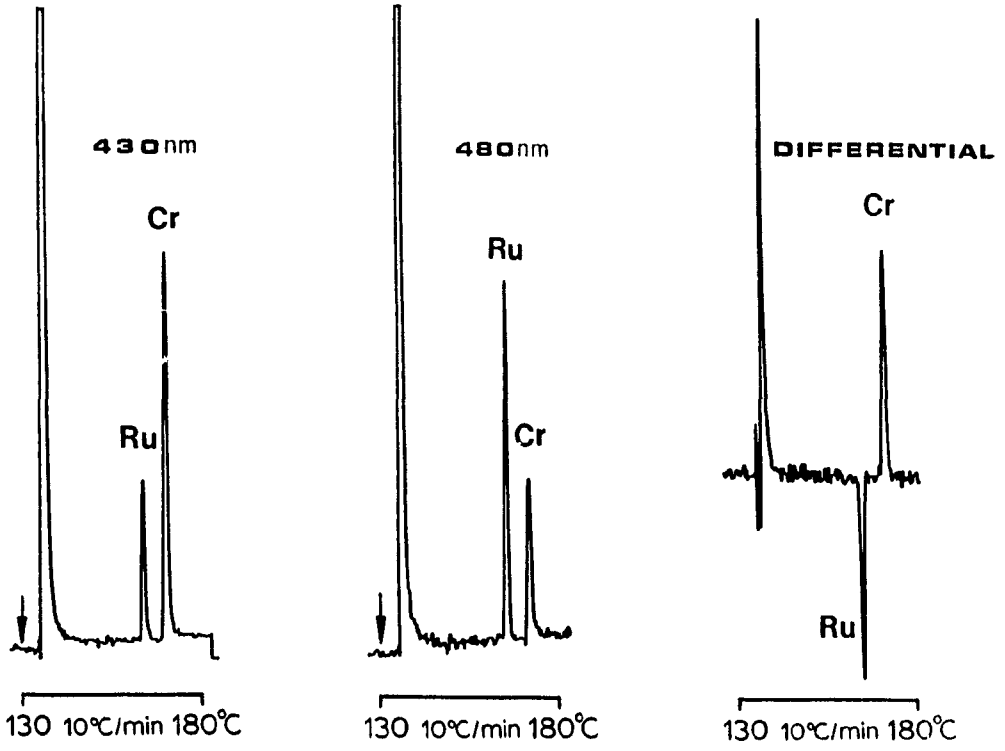

Figure 6.5 *Single channel and dual-channel differential chromatography of a sample containing 500 pg* $Ru(C_5H_5)_2$ *and 4 ng* $C_6H_6Cr(CO)_3$ *in acetone.*

with the result that either Ru or Cr are annulled (Figure 6.6). This absence of any visible trace of interferent begs the question: how large an amount of either of these two species can the system cancel? In other words, how large an improvement in selectivity can the differential modes provide?

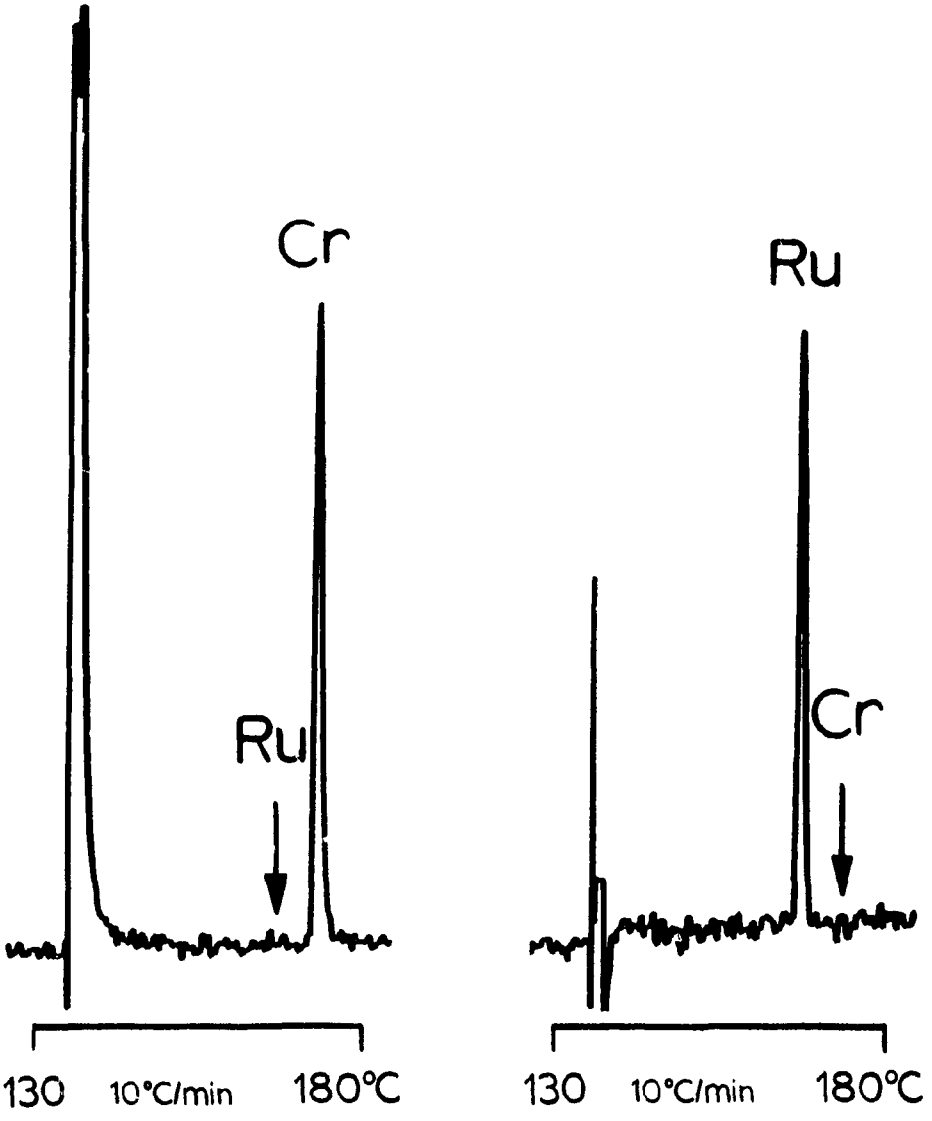

Figure 6.6 *Suppression of ruthenium and chromium by dual-channel differential chromatography in the same sample as in Figure 6.5.*

The original demonstration sample for Figures 6.5 and 6.6 had been mixed so that it would furnish the peaks in comparable sizes in the filter-less mode, and hence produce easily observable peaks for both species in the two single-channel filter modes. Both of these peaks, by having been obliterated in the differential mode, established lower limits to the respective selectivity ratios. For extending the measurement further, however, two mixtures must be made in which either one or the other compound is heavily fortified.

In theory: at ideal conditions and within respective linear ranges, the maximum observable improvement for dual-channel differential as opposed to single-channel operation is given by the linear range of the interferent (on the analyte channel). Thus, no greater a selectivity improvement than two to four orders of magnitude (with the number depending on the elemental nature of the interferent) can be measured by experiments in which the peak resulting from an amount of interferent close to its upper limit of linearity is successfully diminished to an amplitude smaller than the baseline noise of the differential chromatogram.

This theoretical extent of improvement has not been reached by this experiment. The reason is twofold: some of the "ideal" conditions could not be realized and, as is obvious from the fairly typical chromatograms of Figures 6.7 and 6.8, very small remnants of the initially very large interferent peaks tended to persist as non-Gaussian artifacts. Still, in these Figures the gain in selectivity is quite impressive. For a visual comparison, the respective mixtures are also portrayed in their best *single*-channel appearance on the left side of Figures 6.7 and 6.8. The numerical improvement of selectivity from single to dual-channel differential operation is 3×10^2 for Ru/Cr and 2×10^1 for Cr/Ru.

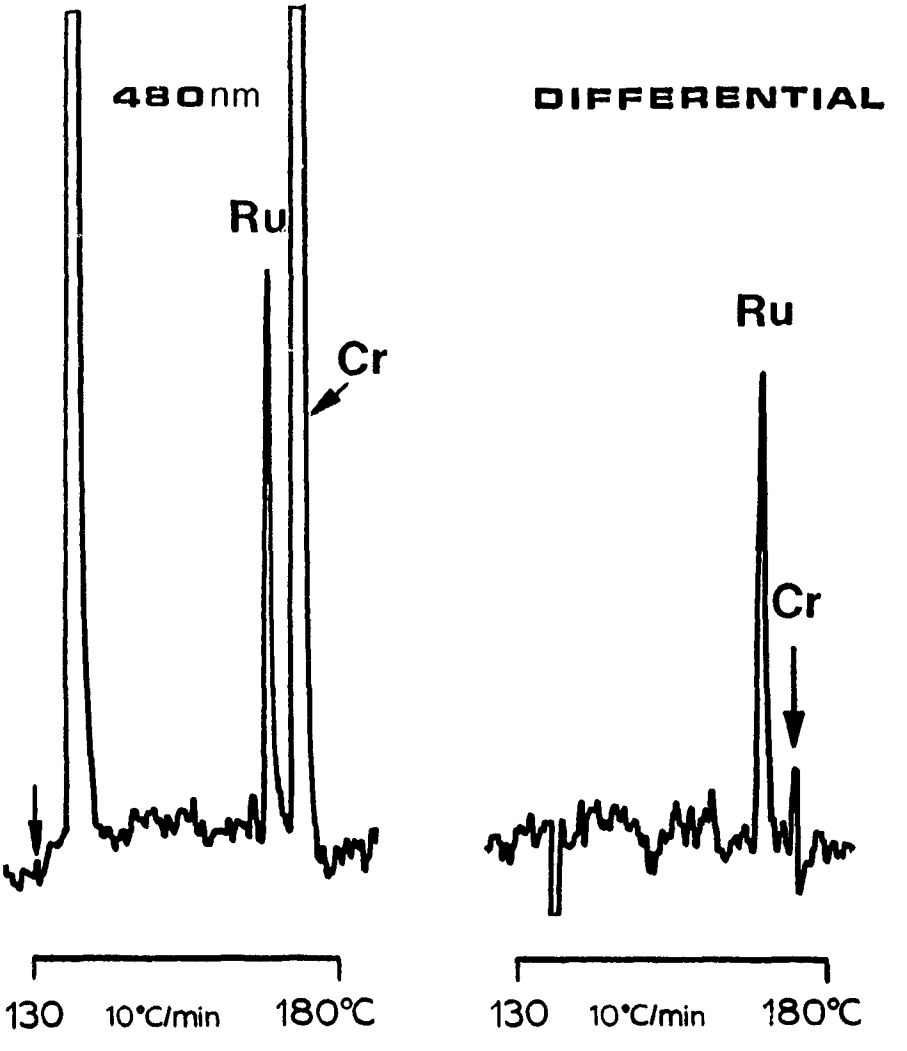

Figure 6.7 *Quantitative suppression of large amounts of chromium in a sample containing 250 ng $C_6H_6Cr(CO)_3$ and 200 pg $Ru(C_5H_5)_2$ in acetone. Other conditions as in Figure 6.5.*

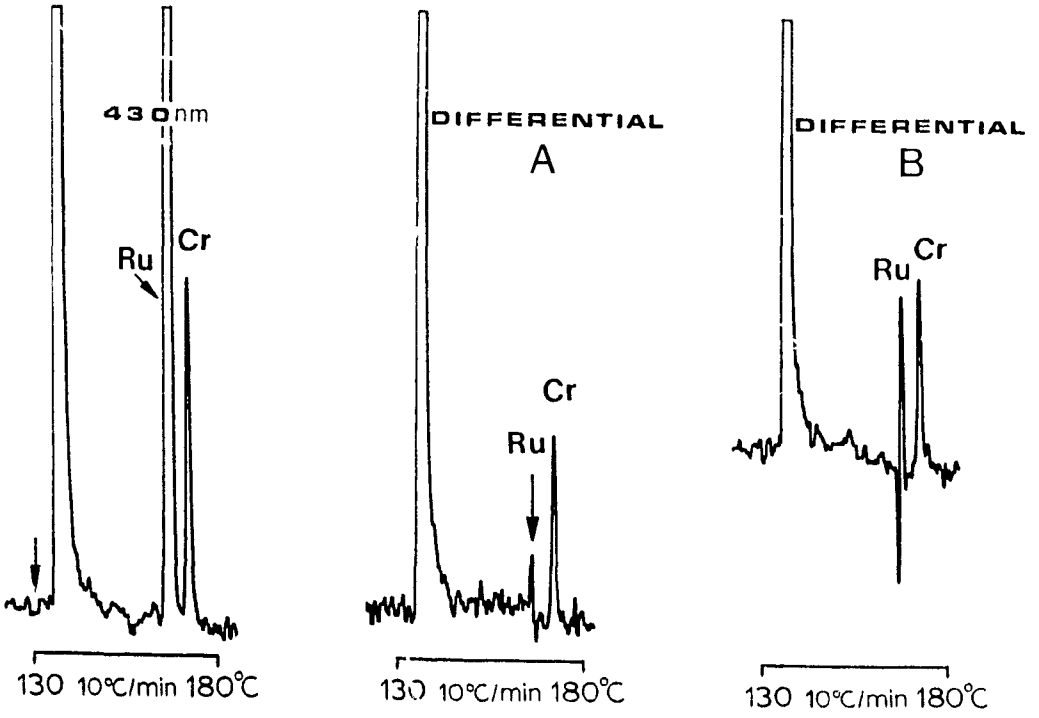

Figure 6.8 *Quantitative suppression of large amounts of ruthenium in a sample containing 10 ng $Ru(C_5H_5)_2$ and 4 ng $C_6H_6Cr(CO)_3$ in acetone. Other conditions as in Figure 6.5.*

Figure 6.8 also contains, on the right-hand side and marked "Differential B", a chromatogram taken under the same chromatographic conditions and overall electronic amplification as the one marked "Differential A". (Note that the Cr peak remains at the same height.) However, different settings are used for the combination of input amplification and output attenuation of the two electrometers (which perform rough scaling on the signals before they reach the "analog interface"). The comparison of the two chromatograms demonstrates that the vacillating signal,

which represents the difference between two very large off-scale peaks, is likely to contain electronic perturbations. The chromatogram labelled "Differential A" is the best, the chromatogram labelled "Differential B" the worse, of a series of matches with the same overall electronic amplification. It is reasonable to expect that more attention to this problem (which, of course, never arises in "regular" chromatography) could reduce the size of the artifacts.

Improvements in selectivity similar to those shown in Figures 6.5 — 6.8 can be realized for other pairs of transition elements as well. How large a number is obtained in each case depends strongly on the relative nature of the two spectra, on the corresponding wavelengths chosen for the two channels and, given the guidelines for measuring valid selectivity ratios, on the extent of the linear ranges.

The dual-channel differential modes work well on systems of two and possibly three different elements, particularly if the latter need to be differentiated with a very high degree of reliability. However, the methodology obviously runs into difficulties if more than two or three luminescing elements participate in the chromatogram. Although real-life samples of this type may be rare, it should be instructive to cast at least a cursory look at a mixture made up of several transition metals, in amounts that produce comparable peak heights in the open mode. The particular standard mixture shown here was also given a compound of sulfur, in recognition of the role that this main-group element plays in many natural samples.

Chromatograms of the mixture are shown in Figure 6.9, first in single-channel, then in dual-channel differential mode. The first channel is open (no interference filter). The second channel at 530 nm was originally chosen for ruthenium. However, it also shows all the other peaks, though with different intensities. This reinforces the point made earlier that spectral discrimination in a

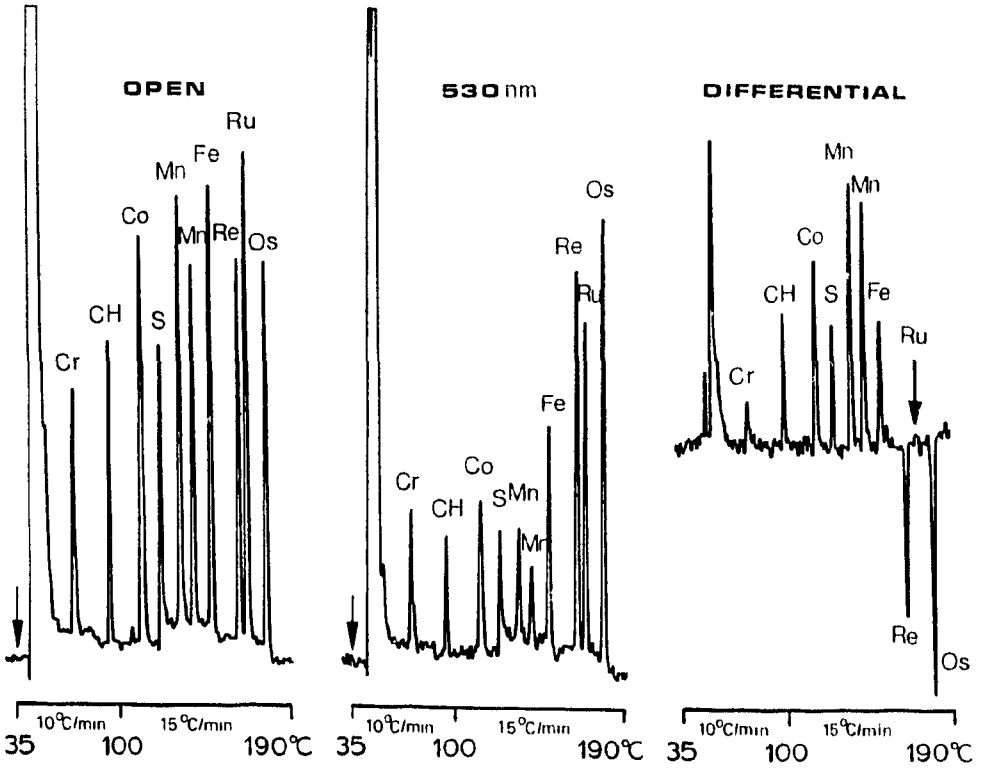

Figure 6.9 *Single channel and dual-channel differential (ruthenium-suppressed) chromatograms of a mixture containing 1.3 ng $Cr(CO)_6$, 1.6 μg nonane(C), 200 ng $Co(C_5H_5)_2$, 17 ng $[(CH_3)_3CS\text{-}]_2$, 3.2 ng $C_5H_5Mn(CO)_3$, 4 ng $C_5H_4CH_3Mn(CO)_3$, 3.2 ng $Fe(C_5H_5)_2$, 24 ng $Re_2(CO)_{10}$, 160 pg $Ru(C_5H_5)_2$ and 4 ng $Os(C_5H_5)_2$ in acetone.*

single channel filter mode - as compared with the open mode - rarely achieves a big increase in selectivity.

The differential-mode chromatogram shown on the right side of Figure 6.9 is obtained by tuning the two channels such that the ruthenium responses cancel. This purpose is well achieved. Thus, a peak vanishing from the chromatogram under

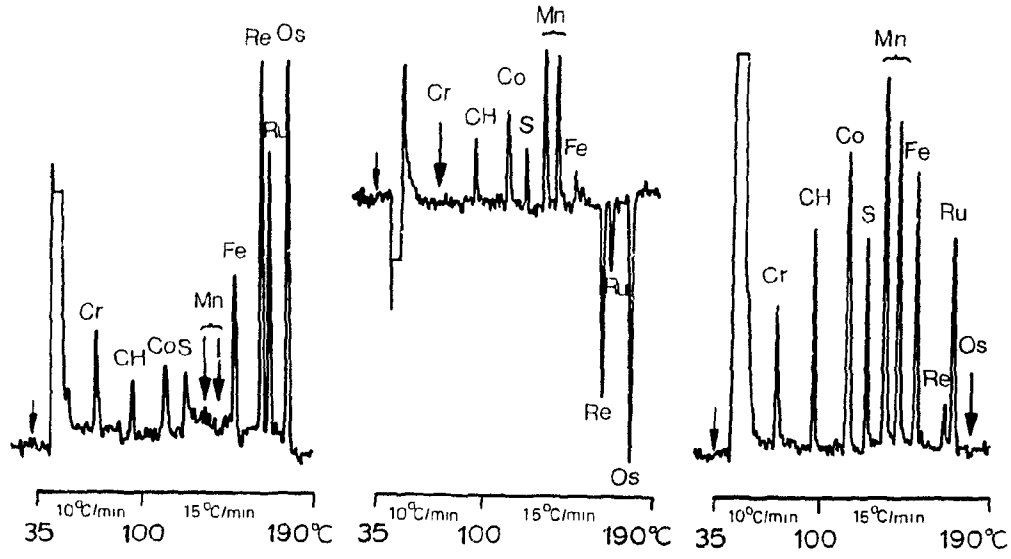

Figure 6.10 *Dual-channel differential chromatograms of the same mixture (and the same chromatographic run) as shown in Figure 6.9, with suppression of — from left to right — manganese, chromium and osmium.*

this particular selectivity regime would alert the analyst to the possible presence of a ruthenium compound. And, other channel (wavelength) combinations could be used to confirm that finding. In addition, clear *qualitative* discrimination is obtained between Cr, C, Co, S, Mn and Fe on one hand, and Re and Os on the other.

The two single channels of data stored in the computer could be used to impose, sequentially, a series of different selectivity regimes on the same chromatographic run. This makes little sense for a routine sample of qualitatively known composition, but it can be quite helpful for a complex sample that contains many components of a chemically disparate nature. For instance, the hypothetical

question could be posed whether there were present in our test mixture any manganese compounds beyond the one "known" to contain Mn. To find the answer, the channels can be tuned for the disappearance of the "known" manganese peak (or of a separately injected manganese standard if the contents of the mixture are truly unknown). If this is carried out, the second, pretendedly "unknown" manganese peak vanishes as well. A demonstration of this is shown on the left-hand side of Figure 6.10.

The middle and right-hand side of Figure 6.10 display two further chromatograms in which the selfsame computer-stored data are used to cancel peaks of chromium and osmium, respectively, while leaving other peaks largely intact. Further elements can be so tested. This is interesting because it demonstrates that several new selectivity criteria can be meaningfully imposed on already existing data. The inter-metal differences in dual-channel response ratios are obviously large enough to allow such approaches - even though the original choice of wavelength had not been made with these additional combinations in mind.

In the high-resolution chromatography of complex samples that include a larger number of compounds containing the same hetero-element, procedures like the one mentioned above can lead to fast and facile early indications which peaks are likely to represent the hetero-element of interest, which represent other hetero-elements, *etc.* Clearly, the underlying assumption - that the spectral response of the metal is independent of analyte amount and organic structure - may need to be ascertained for particular combinations of element and wavelength(s). This assumption has proved to be true in the case of the two manganese compounds discussed above.

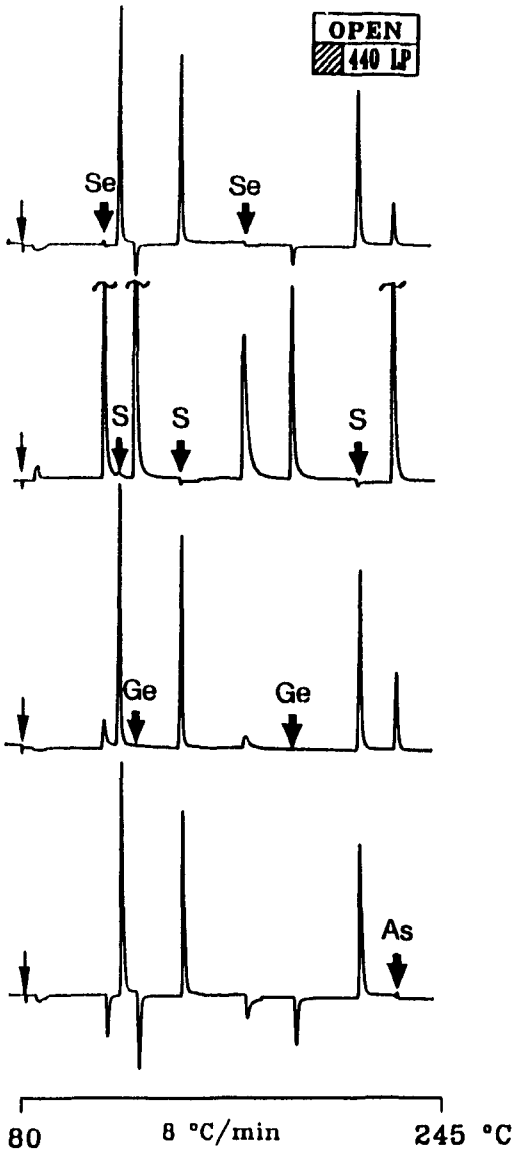

Figure 6.11 *Four subtraction chromatograms of Se, S, Ge and As compounds. Channel 1: open (no filter); channel 2: 440 nm long-pass filter. Compounds in order of elution: 2.9 ng dimethyldiselenide, 5.9 ng diethyldisulfide, 50 ng tetraethylgermane, 6.9 ng di-tert-butyldisulfide, 80 ng methylbenzselenazole, 56 ng tetra-n-butylgermane, 9.6 ng thianthrene, and 480 ng triphenylarsine.*

So far the differential operation has been successful in cancelling chromatographic peaks of transition elements from dual-channel chromatograms of a multi-element mixture. It seems reasonable to assume this routine to work well for any FPD-active element. To examine this assumption, a mixture of compounds containing *main*-group elements is chromatographed with minimal spectral discrimination: one channel is open, the other holds a 440 nm long-pass filter. Figure 6.11 shows the subtraction chromatograms. As anticipated, the computer is successful in suppressing any element among the eight analyte peaks. Figure 6.11 is included here to show not only the capability of the algorithm to manipulate main-group elements, but also its readiness to accept pre-calculated dual-channel "slope ratios". These differential chromatograms are generated according to automatically measured slope ratios, while all other subtractions shown in this chapter had to rely on more complex methods (the "matching" routine of the program CHROM). Details about slope ratios will be discussed in the next chapter.

Still, the situation is less than totally satisfying. What if the analyst wants to see *only* peaks of a particular element, with compounds of all other elements *vanishing* from the chromatogram? While this is possible to achieve, the necessary algorithms are substantially different from the ones covered here and do display limitations of their own[92]. That will be the subject of the next chapter.

Chapter 7. FPD NEW SELECTIVE MODE #2 — CONDAC OPERATIONS

Chapter 6 has demonstrated the potential use of the "differential" mode in achieving better selectivity on the FPD. The method works as expected. However, it is not capable of cancelling several elements at the same time - so that only one element of choice remains, and it never produces specificity (= infinite selectivity). Those are limitations owing to the principle and to various perturbations inherent in the differential mode. We can imagine that in order to cancel an analyte peak completely at any concentration, the signals from the two channels must be exclusively determined by the analyte element. Any chemical interference, fake detector response or electronic defect would cause incomplete subtraction. The CONDAC algorithm is designed to compensate this disadvantage of the differential mode. The principle of CONDAC has been described in "correlation" in Section 2.11.2. This chapter is dedicated to an examination on its performance in dealing with a variety of FPD-active elements in mixtures.

CONDAC uses response ratios to cognize the peaks of *one* species. The values of these response ratios are pre-determined by a separate computer routine. Since these values are critical to CONDAC and themselves contain important qualitative information, it is necessary to discuss the form, meaning, and application of the response ratios as a prerequisite to discussing CONDAC.

7.1 Response Ratios

7.1.1 Introduction

Conventional chromatograms provide the analyst with two physical dimensions of the separated compounds: peak size and peak retention. Response ratios add a third, chemical dimension. They will address peak identity and purity; they will also support derivative chromatograms of significantly higher selectivity.

Response ratios are qualitative indicators of the FPD-active element contained in each peak. They allow the fast perusal of many types of samples; they aid in confirming peak identity; they provide numbers crucial for obtaining CONDAC (or "subtraction") chromatograms; they signal changes in spectral output; they monitor peak purity; and, perhaps most importantly, they draw the attention of the analyst to those peaks in complex environmental or biological samples that contain hetero-elements and are therefore of *prima facie* interest. Below, we shall briefly review four methods for determining response ratios. These are based on the consideration of heights, shapes, areas and slopes of chromatographic peaks.

1 Peak Heights: The simplest and crudest approach is to measure the ratio of peak heights in the two channels (*i.e.* on the two chromatograms). For automated (as opposed to manual) methodology this approach harbors problems - *e.g.* how to define the baseline from which this data pair (the peak apex) is to be measured.

2 Peak Scaling: A far more accurate - and lengthy - approach is to use the CRT screen for amplitudinal scaling of one (or more) peaks from the second channel until their shapes match those of their counterparts in the first channel, *i.e.* until a subtraction chromatogram (the difference of the two signals) shows little or no

evidence of their presence. The final scaling factor is then identical with the sought response ratio. This procedure can deal efficiently with a single or at most with a few peaks. (Its initial and still valid purpose is to provide subtraction chromatograms for their own sake, *i.e.* for cancelling matrix components.) It could turn out unwieldy (and too slow for routine use) when a larger number of peaks need to be evaluated.

3 Peak Area Integration: A simpler approach is to use the digital outputs of two conventional peak integrator modules for continuous calculation of the peak area ratios. The most immediate problem here is the lack of correlation between the two sets of baseline definition and start/stop commands; particularly if the two chromatograms are noisy and differ strongly in their relative peak heights, susceptibilities to interference, and/or drifts in baseline.

4 Peak Slope Ratios: A further possibility is to use the ratios of peak *slopes*. The experimental slope ratio SR_{exp} of the slopes S_A and S_B in channels A and B, ties in particularly well with CONDAC chromatograms:

$$SR_{exp} = \frac{S_A}{S_B}$$

Typical analytical needs suggest three distinct modes of calculating slope ratios. They are: the "manual" mode, in which the analyst slices a single peak into vertical (temporal) segments and lets the computer calculate the response ratios for each; and the two "continuous" modes, in which the computer identifies all peaks and uses them in either "whole" or "split" form for calculating the RR values. The function of each mode and the operation of the computer program have been

described in "Slope Ratios" in Section 2.11.2.

7.1.2 Response Ratio Chromatograms

In order to present the response ratio as a third dimension of chromatographic detection in intuitively acceptable form, the computer generates response ratio chromatograms (RRC's) in addition to numerical data. RRC's are really plots of logarithmic response ratios *vs.* retention time.

Figure 7.1 displays two original "main-group" chromatograms as received from the two FPD channels and stored in the computer. The first channel is "open", *i.e.* no interference filter is used and the spectral range is that of its R-374 photomultiplier. The second channel uses a 440 nm long-pass (cut-on) filter and the same type of photomultiplier. Thus the spectral discrimination is deliberately held to a minimum: on one hand to demonstrate the ease with which further data can be obtained from a very simple optical system, on the other to make use of the fact that broader spectral ranges can accommodate a wider selection of elements with greater sensitivity. The two chromatograms are shown - and will be used - "as received", *i.e.* untouched by digital filtering or baseline correction routines. To allow unfiltered operation, the compounds are used at medium (not low) concentration levels.

Below the two original signal traces in Figure 7.1 is displayed a "split-peak" response ratio chromatogram (RRC). The rectangles shown on the left represent in symbolic form the optical configuration of the two channels. The circular inset depicts the RR values of a split peak in their true shape, *i.e.* as they would appear on the screen (with expanded time axis). As drawn by the sluggish recorder, however, and as reduced by a copier for this particular picture, its resolution appears much worse than that of the original representation.

Figure 7.1 *Individual channels and split-peak response ratio chromatogram of a mixture of main-group compounds. Channel 1: open (no filter); channel 2: 440 nm long-pass filter. Compounds in order of elution: 2.9 ng dimethyldiselenide, 5.9 ng diethyldisulfide, 50 ng tetraethylgermane, 6.9 ng di-tert-butyldisulfide, 80 ng methylbenzselenazole, 56 ng tetra-n-butylgermane, 9.6 ng thianthrene, and 480 ng triphenylarsine. Flow conditions: 200 mL/min hydrogen; 50 mL/min air. No quartz chimney. Note: the same time axis applies to all three chromatograms. The circular insert includes two magnified split peaks to show the true shape of split RRC peaks.*

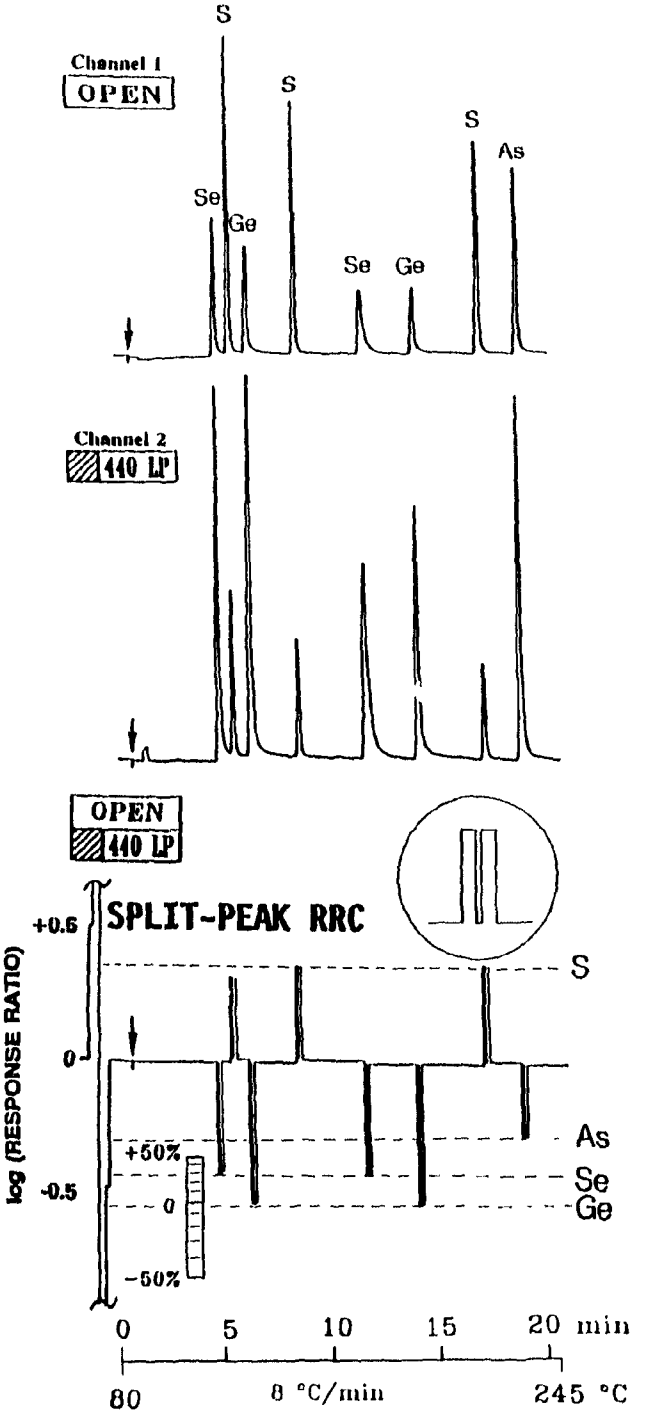
Channel 1
OPEN
S
S
S
As
Se
Ge
Se
Ge
Channel 2
440 LP
OPEN
440 LP
SPLIT-PEAK RRC
+0.5
0
-0.5
log (RESPONSE RATIO)
S
As
Se
Ge
+50%
0
-50%
0
5
10
15
20 min
80
8 °C/min
245 °C

Figure 7.1

Since the range of response ratios (RR's) displayed here is much smaller than the three orders of magnitude the system routinely accepts, the staircase calibration is truncated to save display space. A "percent change" scale has been added (which is valid not just for germanium but, appropriately raised or lowered, for any element). It shows the expected result: response ratios are values that are characteristic of elements and constant within prevailing error bands. An exception is the first sulfur peak that, as the scale indicates, is almost 10% off.

The reason for this clear deviation has not been elucidated. Response ratios among peaks of the same element should vary only if the spectral distribution varies. The most likely explanation is therefore that the immediately preceding Se peak overlapped enough to inject a trace of Se_2 and form a significant amount of the interchalcogen emitter SeS[13]. Other scenarios, based on solvent effects and sulfur emitters with different kinetics[61], also appear possible.

The visual representation of the response ratio chromatogram uses the logarithmic format; however, simultaneous with its appearance on the screen (superimposed there on the two original chromatograms), the same information is sent in antilogarithmic format to the printer. These plain RR values are useful for feeding computer routines (see below), for keeping permanent records, for determining standard deviations, *etc.*. The printout for the split-peak RR's shown in Figure 7.1 is reproduced as an example in Table 7.1. It lists the numerical values for the response ratios, records chromatographic time (start and end of the slope measurement), and indicates whether a particular slope is positive (up the peak) or negative (down the peak). (The elemental designations have been artificially added as the last column for ease of comparison with Figure 7.1.) Obviously, the information could be combined with the initial chromatograms not just on the screen but on a more conventional

record, say one obtained from a plotter. The slight differences between the leading and trailing edges of each peak appear to be random experimental errors. This is in accord with uncompromised peak integrity throughout the RRC.

Table 7.1 PRINT-OUT OF A SPLIT-PEAK RESPONSE RATIO CHROMATOGRAM

Retention (min) (slope start)	Retention (min) (slope end)	Ratio	Slope	(Element)
4:34.6	4:39.4	0.352	POS.	Se
4:39.7	4:48.2	0.361	NEG.	Se
5:13.9	5:18.7	2.122	POS.	S
5:18.9	5:28.8	2.073	NEG.	S
6:01.1	6:06.8	0.280	POS.	Ge
6.07.7	6:16.1	0.279	NEG.	Ge
8:08.6	8:12.7	2.317	POS.	S
8:12.9	8:21.5	2.290	NEG.	S
11:04.8	11:09.7	0.346	POS.	Se
11:12.0	11:18.2	0.357	NEG.	Se
13:24.5	13:29.1	0.277	POS.	Ge
13:30.3	13:37.0	0.276	NEG.	Ge
16:19.3	16:23.7	2.360	POS.	S
16:24.0	16:33.9	2.329	NEG.	S
17:57.7	18:03.1	0.508	POS.	As
18:03.4	18:13.2	0.513	NEG.	As

Note: The separation is the same as shown in Figure 7.1. For easy comparison, the peak designations (the FPD-active elements) have been added; and a one-second computer glitch, which occurred on the tail of the second selenium peak, has been removed.

In contrast to the main-group elements used at medium concentrations in the first example, the second example uses (mainly) transition metals at low concentrations. Here the dual-channel chromatogram, which has been shown before

to produce the differential chromatograms of Figure 6.9, is used again to derive and display as examples the whole-peak and the split-peak response ratio chromatograms. A "reverse-mode" split-peak RRC is also included.

In reverse mode, the algorithm processes the temporally inverted chromatogram. Whether obtained by the algorithm operating forward or backward in time, the resulting RRC's should be identical, given ideal two-channel data. However, if the noise level is high, "spikes" are frequent, and the baseline is subject to drift, there may arise differences between the two. The processing algorithm - just as most chromatographic peaks - is not entirely symmetric with regard to time. Congruity of forward- and backward-run RRC's will thus provide (limited) reassurance of proper electronic function; while incongruity will point to possible trouble spots, and will support estimates of precision. Another example of the usefulness of time-reversed operation will be given later.

Figure 7.2 shows the "open" channel (only) on top of the three RRC's. Note that the original two signal trains (chromatograms) had been run before through digital filtering and baseline correction routines. While these routines ameliorate noise and drift, respectively, they also produce changes in slope and, consequently, introduce some variation of their own into the response ratio chromatograms. Obviously, the selection of processing parameters represents a compromise between suppression of noise/drift and preservation of the "true" response ratios. However, it is necessary to include in this study a separation done at such low analyte concentrations that substantial smoothing/straightening has to be used but that, still,

Figure 7.2 *Open channel and three response ratio chromatograms. The RRC's represent the whole-peak forward-processed, the split-peak forward-processed, and the split-peak backward processed modes for the separation of a mixture containing several transition elements (the same mixture as in Figure 6.9). Second channel (not shown): 430 nm interference filter (bandpass 7.3 nm). Compounds in order of elution: 1.3 ng chromium hexacarbonyl, 1.6 μg n-nonane, 200 ng cobaltocene, 17 ng di-tert-butyldisulfide, 3.2 ng cyclopentadienylmanganese tricarbonyl, 4.0 ng methylcyclopentadienylmanganese tricarbonyl, 3.2 ng ferrocene, 24 ng dirheniumdecacarbonyl, 0.16 ng ruthenocene, and 4.0 ng osmocene. The horizontal arrows in the response ratio chromatograms indicate the direction of computer processing. Note: the log RR value for Ru is close to zero and barely shows up in reproduction.*

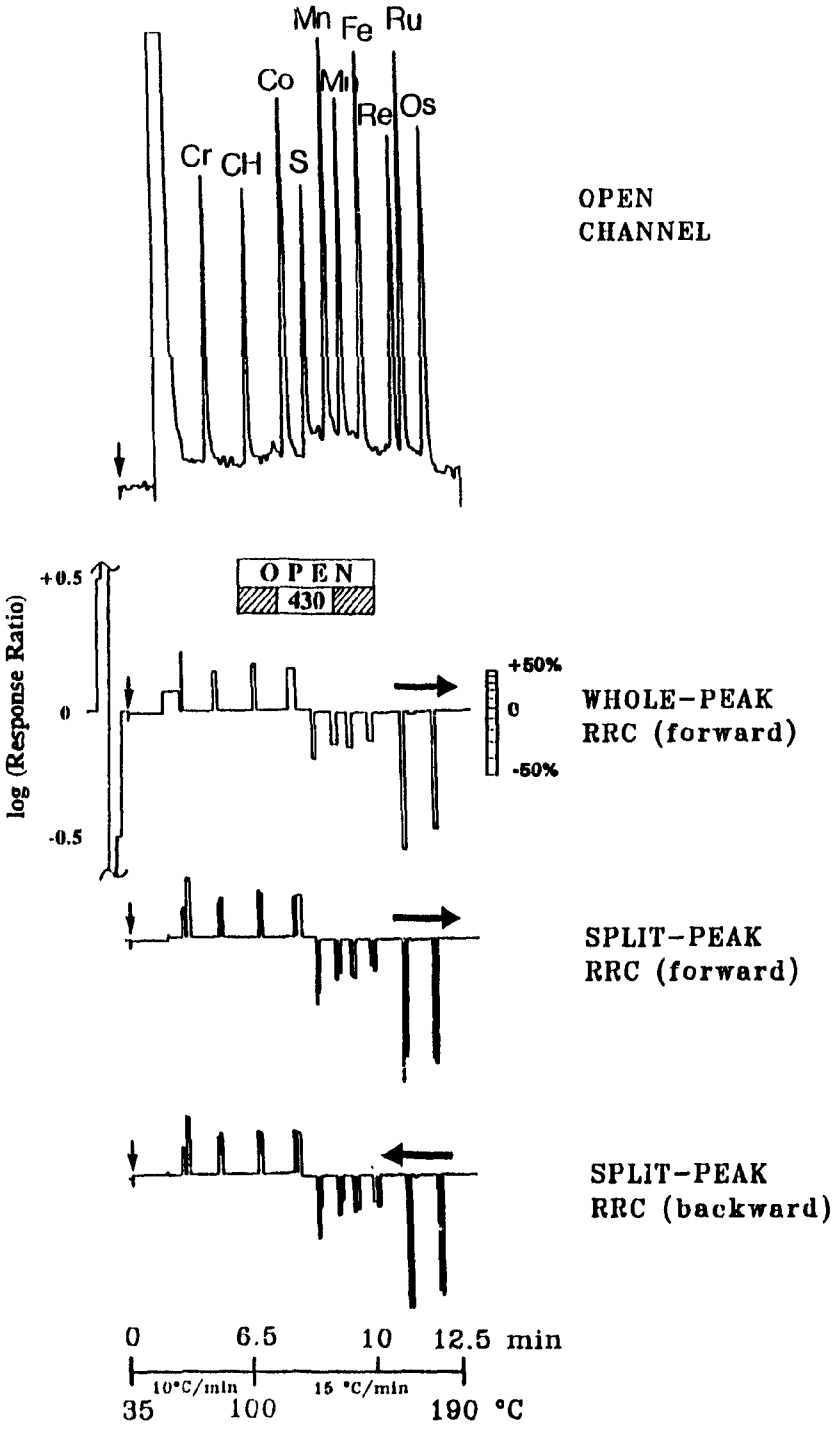
Mn
Fe
Ru
Co
Mi
Re
Os
Cr
CH
S
OPEN
CHANNEL
OPEN
430
+0.5
0
-0.5
log (Response Ratio)
+50%
0
-50%
WHOLE-PEAK
RRC (forward)
SPLIT-PEAK
RRC (forward)
SPLIT-PEAK
RRC (backward)
0
6.5
10
12.5 min
10°C/min
15 °C/min
35
100
190 °C

Figure 7.2

some short-term and long-term fluctuations would continue to persist in the chromatograms. Only this type of challenge can test the robustness and intrinsic suitability of RRC's for trace analysis.

Not surprisingly, then, the variation of response ratios is much more pronounced for the (originally) noise-encrusted peaks of Figure 7.2 than it is for the much cleaner peaks of Figure 7.1. A careful scrutiny of the RRC's suggests that much if not all of this variation is random noise. For this scrutiny, split-peak RRC's processed both forward and backward in chromatographic time prove decidedly helpful. In general, the response ratios remain constant as the analyte concentration is lowered. (Sulfur, due to the quadratic nature of its response, can prove an exception.) This means that the method is as robust as can be hoped for.

In real-life chromatography - particularly of hetero-organic or organometallic trace analytes contained in the complex matrices of environmental or physiological samples - even the best column will fail to bring about complete separation. (Note that all chromatographies of this study were deliberately carried out at low resolution, *i.e.* on just a one-meter packed column.) Hence peak interference must be reckoned with and, as the simplest possible demonstration of how response ratios are determined, let us examine a two-peak overlap.

Figure 7.3 shows on the left the two initial channels of a separation of triphenylphosphine and triphenylarsine. Note that the separation is (deliberately) very poor. "Split-peak" and "whole-peak" response ratio chromatograms appear on the right. The former strongly indicates the need for further scrutiny.

A "manual" examination of response ratios from successive slices of the bimodal concentration profile shows the RR values first remaining relatively constant (and agreeing with the authentic value for phosphorus), then turning

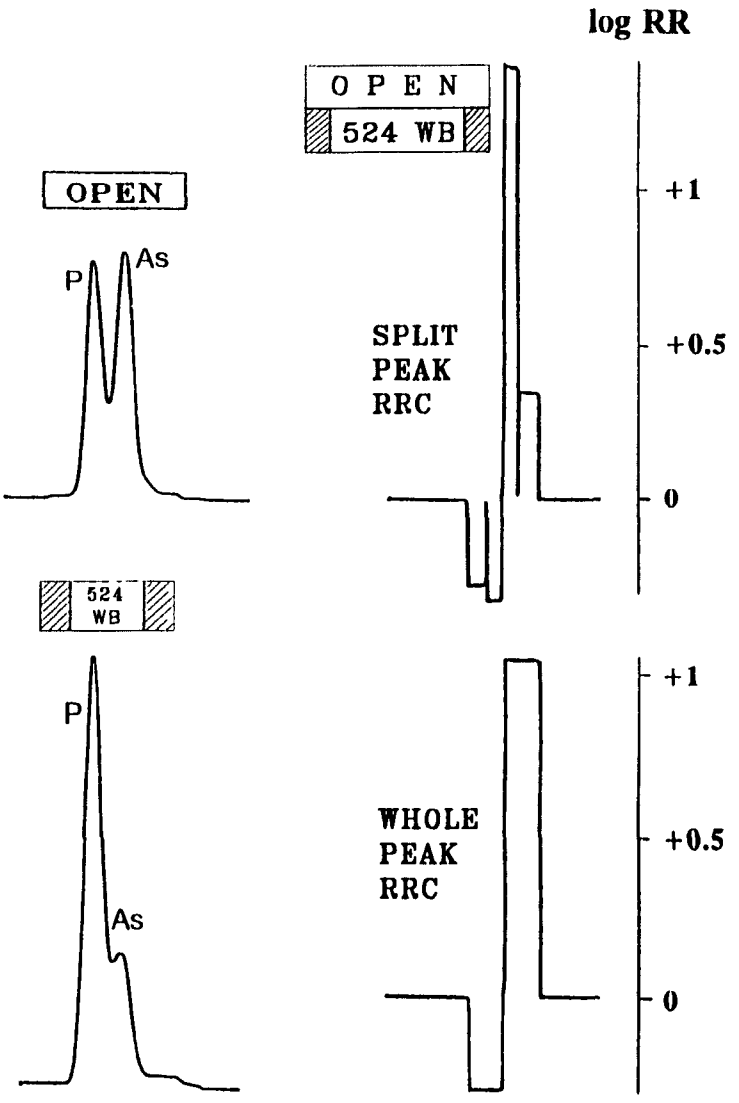

Figure 7.3 *Individual channels, split-peak and whole-peak response ratio chromatograms of overlapping peaks. Compounds in order of elution: triphenylphosphine and triphenylarsine. First channel: open; second channel: 524 nm wide-band filter (40 nm bandpass).*

unjustifiedly high, then again becoming relatively constant (and agreeing with the authentic value for arsenic). The continuous split-peak RRC reflects these changes, although in much coarser fashion. The outer (first and last) RR values are characteristic of phosphorus and arsenic, respectively; the two inner (middle) values are not.

In particular, one very large RR value seems to jut out of nowhere. It is not due to a third species, however. Rather, it arises from the fact that the position on the time axis of the lowest point in the valley between the two peaks is different in the two channels. Slope ratios in the time interval between the two minima are therefore computed from slopes of a different sign. Right at one nadir, the slope ratio is zero; at the other, infinity. This, and the about even mixture of elements present in this most intense region of overlap, renders the inner RR values useless as chemical indicators. The outer RR values, however, still can play that role - provided that peak overlap is not too severe. The whole-peak RR values, which combine the inner and outer RR values, are obviously spurious. Indeed, they could prove downright misleading if consulted in isolation. It is, of course, the very situation of overlapping, interfering, anomalous and/or otherwise interesting peaks, for whose benefit the manual and the split-peak modes have been developed in the first place.

7.2 CONDAC's Specificity

Most of the luminescence monitored by the FPD consists of continua and broad molecular bands, which cover wide wavelength regions. Extensive spectral overlap of emissions from different elements, hence inadequate selectivity in single channel mode, is thus the rule rather than the exception for the FPD. A possible task of CONDAC is to distinguish between two congener elements whose spectra overlap

(*e.g.* S and Se, P and As, *etc.*). Once the relevant FPD spectra are known, the choice of wavelength becomes trivial.

A somewhat more interesting situation is one in which several hetero-atoms appear at different positions in the chromatogram; and in which only one gas chromatographic injection, *i.e.* only one spectral setting, is used. Particularly in the case of samples that are not only in short supply (so that every injection counts) but that are also undefined in regard to the elemental composition of their components (so that a survey-type analysis is called for), the smallest reasonable extent of optical discrimination can ensure that none of the possibly present FPD-active elements is overlooked.

Typical for such a low-resolution mode is the combination of one channel without filter (an "open" channel) with another one using only a wide-band or a long- (or short-)pass filter. Another reasonable mode is the combination of a long-pass with a short-pass filter, whose transmission ranges overlap to a major or minor degree. Even the use of stable color glass filters would seem quite suited to the purpose. Because such configurations are spectrally much less discriminating than, say, two channels equipped with two narrow-band interference filters, they should help to demonstrate how far the optical conditions can be relaxed in the CONDAC approach. Modes that make use of longer sections of the available wavelength range can also produce higher sensitivity for a larger number of elements. Both of these considerations are reflected in the following CONDAC demonstration experiments. A further consideration is to use not just one but several peaks containing the same hetero-element. This tests the reliability of the CONDAC algorithm: all of the peaks that contain the target element (but none of the peaks that do not) must be present in a *bona fide* "element-specific" chromatogram.

Analyte mixtures and spectral conditions designed along these lines are involved in the following three Figures. In each case will the pictorial sequence first show the open (filter-less) channel; then the wavelength-selective channel; then the sequence of (vertically off-set) CONDAC chromatograms derived by the computer from the two original inputs displayed on top.

Figure 7.4 shows a temperature-programmed separation of standard compounds identified by the FPD-active hetero-atom they contain, *i.e.* nitrogen or phosphorus or selenium. Note that the differences in relative peak size between the open and the 40 nm wide-band channel are small (a narrow-band filter centered on the main HPO emission, while increasing selectivity and decreasing sensitivity, would not have changed these correlations by much).

For the CONDAC algorithm to work best, the slope ratios for all peaks of a particular hetero-element should be precisely the same. This, however, is usually not the case. The variance of slope ratios, and some reasons for that variance, have been discussed in the last Section. In an effort to demonstrate applicability to trace analysis, the amounts of the substances used here have been kept deliberately low so that the two baselines, even after some digital filtering, still carried noise. Obviously, a similar band of noise distorts the necessary slope measurements on the peaks (as we have seen from Figure 7.2).

Despite the relatively small amounts of analyte in our experimental mixtures, the noise-induced variation of slope ratios was not large enough to prevent the CONDAC algorithm from identifying all three FPD-active hetero-elements. To demonstrate this, the individual CONDAC chromatograms for nitrogen, phosphorus and selenium are stacked up in the lower part of Figure 7.4. Apparent specificity has been successfully achieved.

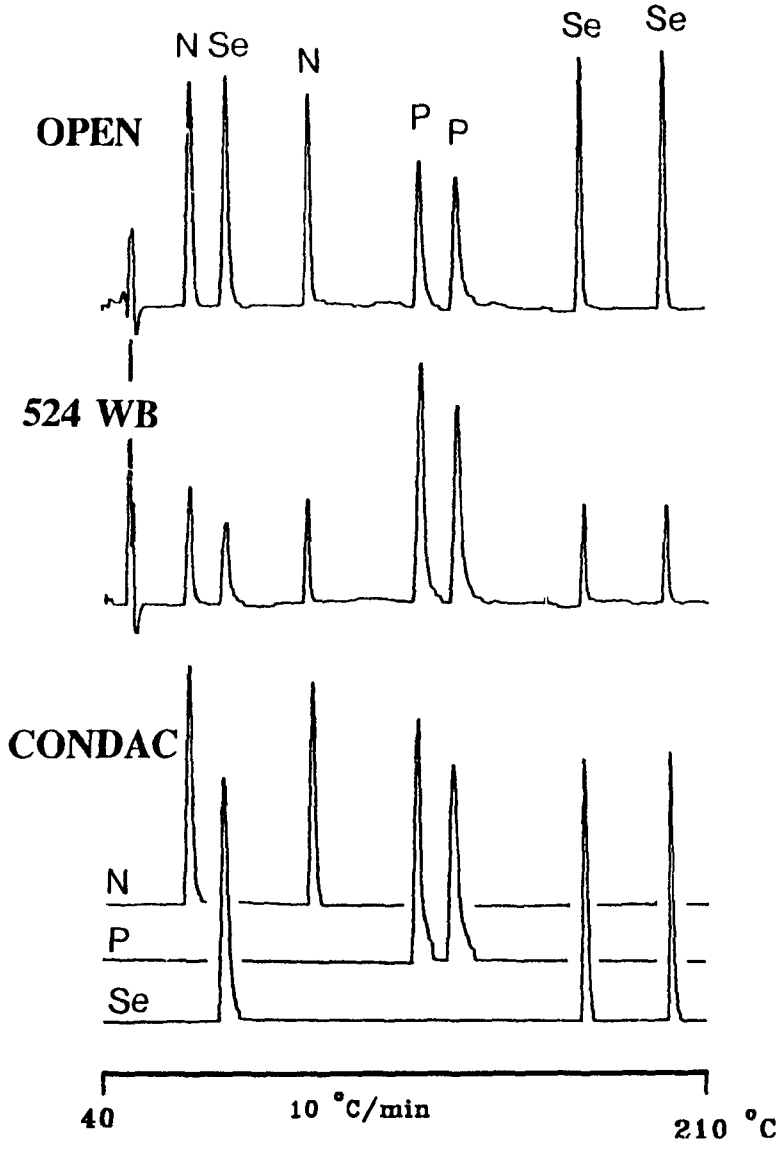

Figure 7.4 *Two-channel and CONDAC chromatograms of main-group elements. The temperature-programmed chromatograms contain (in order of elution): 300 ng triallylamine, 22 ng dimethyldiselenide, 500 ng n-butylamine, 1.0 ng trimethylphosphate, 0.6 ng triethylphosphate, 18 ng methylbenzselenazole, and 20 ng diphenylselenide. One channel open, the other fitted with a 524 nm wide-band interference filter (Ditric, 40 nm bandpass). Flow conditions: 200 mL/min hydrogen; 45 mL/min air. Quartz chimney present.*

One aspect that may make Figures 7.4 to 7.6 confusing, concerns the heights of CONDAC peaks when compared to those of their parent peaks. The explanation of certain size discrepancies is simple: the CONDAC algorithm accepts or rejects peaks but, having two channels at its disposal, allows the operator to choose which version of the accepted peak to send to the recorder (*i.e.* the peak from channel 1, or from channel 2, or from their average; either in original intensity or after multiplication by a convenient scaling factor). In many cases we select the "better" channel, *i.e.* the one in which the particular element displays the larger S/N ratio.

Providing yet another cause for possible confusion, close inspection of any CONDAC chromatogram reveals that the very start and end of most peaks is characterized by a vertical jump of the recorder pen - a jump that forms the visual connection of the "zero" (= no information) line with the first and then the last datum of an algorithmically accepted stretch of signals. A *short* vertical trace normally reflects the position of the signal in relation to the "true" chromatographic baseline. A *long* vertical trace, on the other hand, indicates that the algorithm has rejected a significant part of the peak itself - usually because that part happens to overlap the peak of another FPD-active hetero-element.

Figure 7.5 presents a situation similar to that of Figure 7.4, except that the FPD-active hetero-elements are now sulfur, arsenic, boron and selenium. As demonstrated in the bottom half of the Figure, the CONDAC algorithm is able to distinguish among all four hetero-atoms and provide chromatograms of apparent elemental specificity for each. It should be noted that this is achieved with one wide-band filter as the lone wavelength-selective device present in the system. The choice of the filter's optical characteristics is reasonable but not crucial: several other wavelengths or filter types could have been used as well.

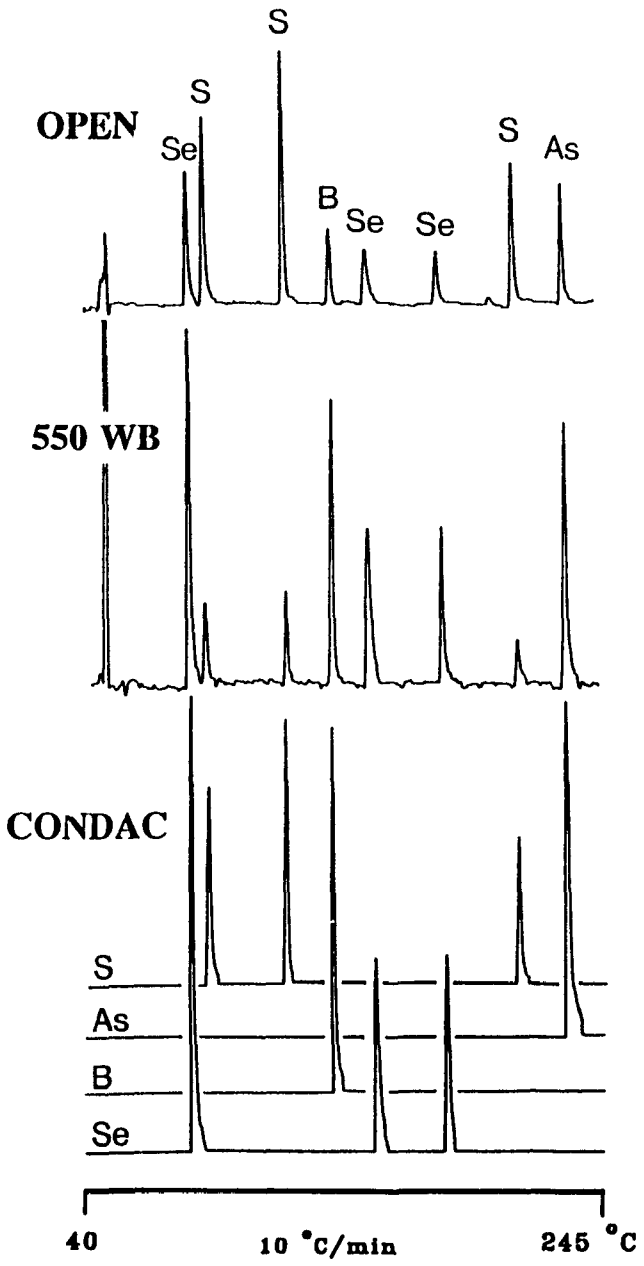

Figure 7.5 *Two-channel and CONDAC chromatograms of main-group elements. In order of elution: 14 ng dimethyldiselenide, 1.0 ng diethyldisulfide, 1.6 ng di-tert-butyldisulfide, 100 ng o-carborane, 20 ng methylbenzselenazole, 15 ng diphenylselenide, 1.0 ng thianthrene, and 10 ng triphenylarsine. Flow conditions: 200 mL/min hydrogen; 45 mL/min air. Quartz chimney present.*

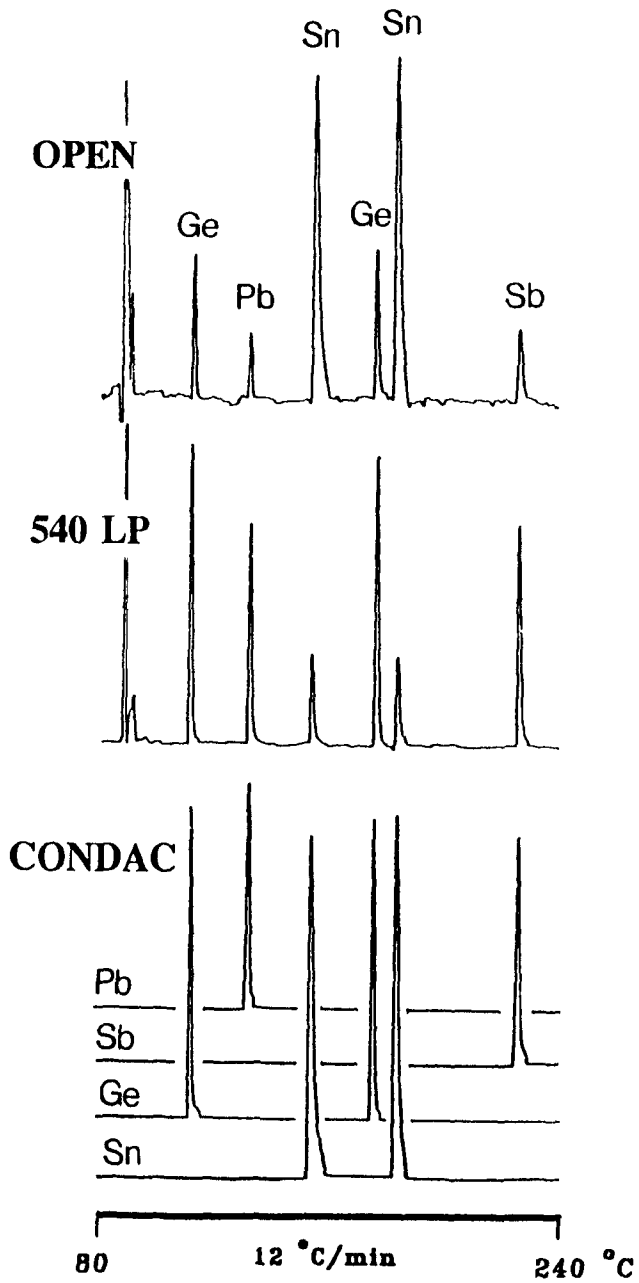

Figure 7.6 *Two-channel and CONDAC chromatograms of main-group elements. In order of elution: 1.8 ng tetraethylgermanium, 12 ng tetraethyllead, 0.20 ng tetra-n-propyltin, 4.8 ng tetra-n-butylgermanium, 0.20 ng tetra-n-butyltin and 24 ng triphenylantimony. Flow conditions: 200 mL/min hydrogen; 50 mL/min air. Quartz chimney absent.*

Figure 7.6 uses CONDAC algorithms on some more main-group elements; namely lead, antimony, germanium and tin. The only spectrally selective device in this configuration is a 540 nm long-pass filter. Again, the CONDAC algorithm successfully separates/identifies the hetero-elements present.

While the numerical slope ratios of the two germanium peaks are practically identical, those of the two tin peaks are slightly different. This may simply be due to experimental noise, but more basic spectrochemical interferences cannot be ruled out. For instance, despite the efforts at suppressing it, some residual surface luminescence of Sn (or Ge) may have been present on, say, the quartz windows shielding the filters/photomultipliers. That type of luminescence is known to be subject to protracted quenching by a variety of elements. If the blue luminescence happened to be present (together with the usual green SnOH and red SnH gas-phase emissions), the potential for changes in slope ratio among tin compounds - eluting at different positions in a temperature-programmed chromatogram and/or following compounds that contain different hetero-elements - cannot be ruled out.

We have drawn attention to certain hypothetical problems that could beset the dealings of CONDAC algorithms with S/Se and Sn/Ge containing samples. This was done for a purpose: by these speculations we wanted to illustrate two general types of processes that can cause variations in slope ratio among peaks containing the same hetero-atom: contamination and multiple spectra. It should be noted that the extent of both effects may depend, *inter alia*, on the concentration of the analyte, or on the temperature, or on the concentration of other species in the gas phase (the temperature program alone causes significant changes in carrier flow and column bleed).

The efficiency of CONDAC in suppressing all but the element of interest is demonstrated in Figure 7.7, which uses gasoline to represent a complex sample matrix. This particular gasoline contains (in addition to the usual aliphatics, aromatics and oxygenates) compounds of sulfur and manganese; and it was doped for this experiment with compounds of lead and phosphorus. The latter elements, as shown in the Figure, can be easily recovered by the algorithm (and so can sulfur and manganese by using different wavelengths). Note that one initial channel - the one shown in the upper part of Figure 7.7 - registers but a very small peak for the phosphorus compound. Yet, this proves good enough for the CONDAC algorithm to retrieve it. The second initial channel, which is not shown here, uses the more effective 524 nm wide-band filter. The phosphorus peak on the CONDAC chromatogram represents the averaged response of the two channels.

Finally, the ability of the "differential mode" and of CONDAC in dealing with overlapping peaks will be demonstrated. In Figure 7.3, we have successfully obtained split-peak slope ratios from the severely overlapped peaks of triphenylphosphine and triphenylarsine. What do subtraction and CONDAC chromatograms look like under such circumstances?

Figure 7.8 repeats the initial single channels for easier orientation, then records the results of the two dual-channel manipulation techniques. The subtraction chromatograms restore (deconvolute) the two peaks that constitute the original doublets. The arsenic peak is shown inverted here, simply because that's how it appears on screen and recorder. It could, of course, be returned to its familiar upright form by using a multiplication factor of -1 on the computer or by flicking a switch on the recorder. The peaks are vertically attenuated but otherwise of the same shape as those of singly injected, pure compounds. They are therefore perfectly

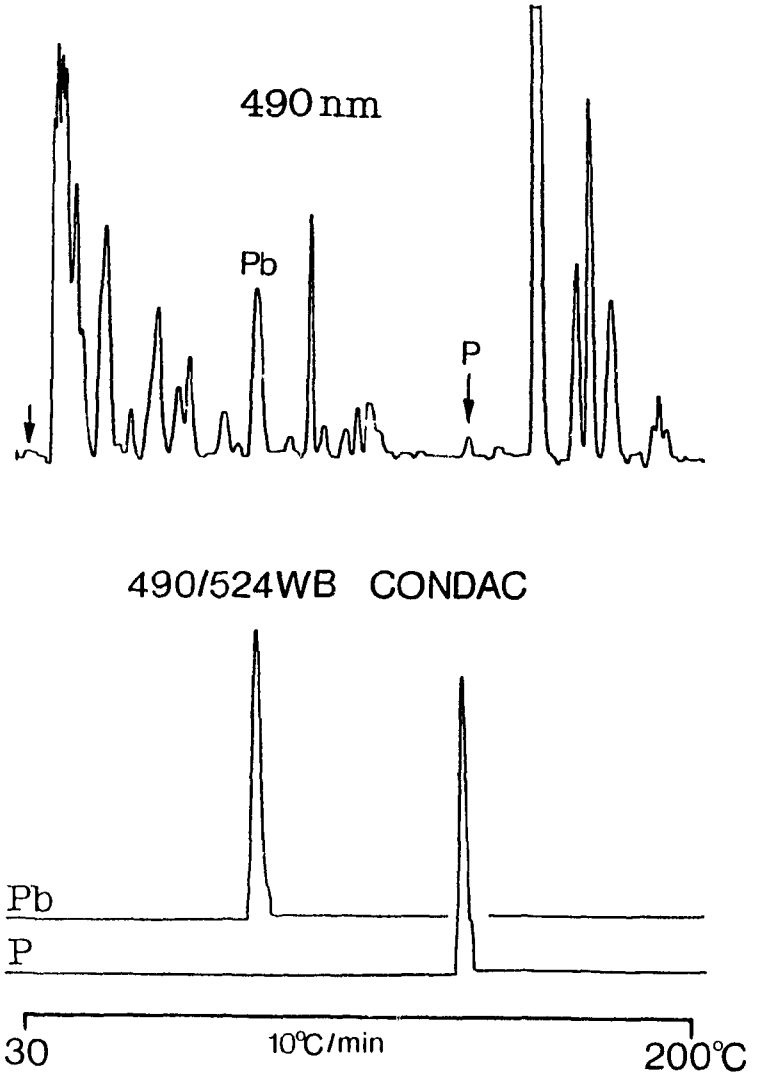

Figure 7.7 *CONDAC chromatograms of gasoline. Upper half: Chromatogram of a local super non-leaded gasoline, doped with 0.65 μg of tetraethyllead and 3.4 ng of triethylphosphate, as seen by a 490 nm interference filter. The second initial channel, equipped with a 524 nm wide-band interference filter, is not shown. Lower half: stacked CONDAC chromatograms for lead and phosphorus. Hydrogen: 220 mL/min. Air: 60 mL/min. 1 meter column packed with 5% Carbowax 20M on 100/120 mesh Chromosorb W AW. Programmed temperature: 30 - 200 °C, with a speed of 10 °C/min.*

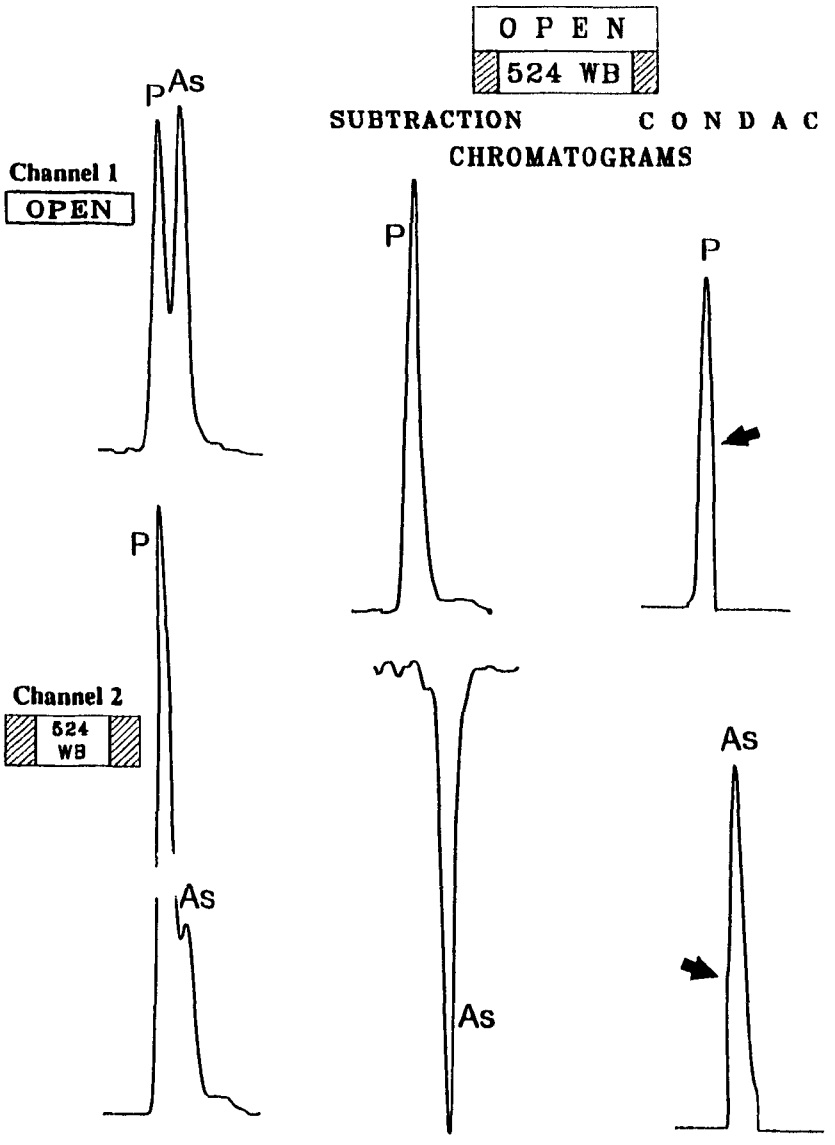

Figure 7.8 *Subtraction and CONDAC chromatograms of overlapping peaks. The individual channels (the same as in Figure 7.3) are repeated on the left for easier orientation.*

suited to height or area quantitation - provided they are compared to peaks of a suitable internal standard, or measured against an external calibration obtained in the subtraction mode based on the same response ratio.

No like area-based quantitation is possible for the CONDAC peaks. These peaks are not fully restored, but are merely parts of peaks imported from (in this case) the first channel. The signals break off (*i.e.* return to the non-committal zero line) when the experimental response ratio strays too far from the theoretical one. In this manner CONDAC peaks with large missing sections simply alert the analyst to the occurrence of peak overlap. In Figure 7.8, the exact location of the two break-off points is marked by arrows.

Beyond the basic SR tolerance band, there are several further conditions involved in CONDAC chromatograms. For instance, the start of a peak is given greater weight for peak definition than the end (a not unreasonable approach for chromatographies with many tailing peaks). A certain number of slopes have to register positive in immediate succession before the algorithm (retroactively) declares the start of a peak. The lack of symmetry implicit in that treatment can be rectified by storing the original signals in both forward and reverse chromatographic time, and then obtaining CONDAC chromatograms for each. The "reverse" mode, although redundant for "clean" chromatograms, is often helpful as a backup or confirmation or averaging technique for doubtful ones. So indeed here: the algorithm experienced some difficulties in declaring the start of the arsenic peak in the forward mode. Channel 2 in Figure 7.8 shows why: the positive slope segment on which the algorithm was supposed to base its assessment is short and ill suited to the task. In the reverse mode, however, two substantial positive slope segments are offered and the CONDAC algorithm easily succeeds. (Note: time-reversed processing can

produce changes in RR or CONDAC chromatograms, but it does not affect subtraction chromatograms.)

It is now obvious that by judicious selection of wavelength in the two channels, the compounds of any selected element can be granted exclusive access to, hence sole presence on, the computer-drawn CONDAC chromatograms. Still, it remains the perceptionally most surprising aspect of this rather primitive algorithm that its output is element-specific.

While the chromatograms do indeed appear specific for any selected element, they are also subject to obvious limitations. The CONDAC version of specificity is neither intrinsic nor inclusive; rather, it is created by computer and confined by circumstances.

It is astonishing how well the CONDAC approach works in practice - particularly in light of the fact that several chromatograms of apparent elemental specificity can be derived from the same injection (*i.e.* from the same set of weak optical discriminants and the same set of stored data).

CONCLUSION

The analytical range of the flame photometric detector (FPD) is far broader than commonly assumed. In this thesis alone, Ru, Ni, Mn, Os, Re, Mo and Co have been added to the roster of elements to which the FPD responds. The sensitivity, selectivity and linearity for Ru, Ni and Mn is excellent and compares favorably with the behavior of these elements in the most advanced high-energy spectroscopic sources.

It is not possible to predict whether or not a particular element will respond in the FPD; this is in accord with chemical - as opposed to thermal - excitation. While some elements responded well (and a few not at all) when tested for this thesis, many elements could not be handled by gas chromatographic means due to the lack of suitably volatile and stable compounds. Future plans of our group therefore include the introduction of *aqueous* solutions into the FPD. This may well lead to a further group of elements being added to the list of potential FPD analytes.

The spectra of various elements in the FPD revealed a richness of features. One interesting feature was the presence of atomic lines that represent transitions to ground state from levels up to 3.6 eV. Some of the most intense emissions were molecular in nature. A few could be assigned to known emitters, but many are reported here for the first time. Very prominent were also continua in the red/infrared, which occurred in the spectra of several metals and whose origin remains an interesting topic for future research.

One of the newly found emitters appears to be of particular analytical value: its intensity is *linearly* related to the concentration of sulfur (sulfur is the pre-eminent FPD analyte, but its conventional determination has to rely on the

quadratic S_2 bands). Although the new linear sulfur mode is slightly less sensitive, its wide-ranging linearity, greater resistance to quenching, and elemental response characteristics should lead to its ready acceptance by the analytical community.

The FPD lends itself well to operations with *two* optical channels. Much of this thesis is therefore concerned with the analytical information that can be obtained by monitoring the same peak at two different wavelengths. For one, a suitably programmed computer can automatically produce "response ratio chromatograms". These add a chemical (i.e. elemental) dimension to the two conventional dimensions of peak retention and amplitude. Response ratio chromatograms, though developed on and for the FPD, should find application in a wider variety of different dual-channel detector systems.

Based on such response ratios, different computer algorithms have been developed that either cancel peaks of one element ("subtraction chromatograms") or cancel peaks of all elements except one ("conditional-access chromatograms"). Both can be used to establish the identity of a peak's luminescing hetero-atom. However, the primary use of subtraction chromatograms lies in the suppression of matrix components or interferents, and in the great increase in selectivity - more than one order of magnitude - this method can provide. In contrast, the primary use of conditional-access chromatograms lies in the scanning of complex, computer-stored records of separations with the purpose of quickly finding the elements of interest.

In this manner, a single chromatographic injection can lead to a larger number of computer-produced chromatograms that reflect the chemical nature of peaks, and thus permit the fast and facile identification - as well as measurement - of most sample components.

Appendix I. SOURCE CODES OF "CHROM" (Version 8)
(Written by B. Millier)

```
DECLARE SUB FindPeakDownSlope ()
DECLARE SUB FindPeakEnd ()
DECLARE SUB DefPeakEnd ()
DECLARE SUB PrintData ()
DECLARE SUB DefCstemp ()
DECLARE SUB ScreenPlotRatio ()
DECLARE SUB RatioExit ()
DECLARE SUB SetRatioMode ()
DECLARE SUB printHeading (za$)
DECLARE SUB FindPeakStart ()
DECLARE SUB DefPeakStart ()
DECLARE SUB FindPeakTop ()
DECLARE SUB contIR ()
DECLARE SUB getParms ()
DECLARE SUB calcIR ()
DECLARE SUB swaparray ()
DECLARE SUB fkeyson ()
DECLARE SUB fkeysoff ()
DECLARE SUB clrl26 ()
DECLARE SUB SNcursorleft ()
DECLARE SUB SNcursorright ()
DECLARE SUB FilterCh (ch%)
DECLARE SUB RedrawSigma ()
DECLARE SUB FilterDiff ()
DECLARE SUB dispRetTime ()
DECLARE SUB windowDRT ()
DECLARE SUB SMDRT ()
DECLARE SUB makegrid ()
DECLARE SUB WaitForKey ()
DECLARE SUB calcSR ()
DECLARE SUB contSR ()
DECLARE SUB loadDac (pa%)
DECLARE SUB userSR ()
DECLARE SUB getslope2 (index!, size!)
DECLARE SUB cursorleft ()
DECLARE SUB cursorright ()
DECLARE SUB SignalToNoise ()
DECLARE SUB correlate2 ()
DECLARE SUB getslope (index!, size!)
DECLARE SUB correlate ()
DECLARE SUB ZeroDac ()
DECLARE SUB plot ()
DECLARE SUB SetRecorderVector ()
DECLARE SUB EnableInts ()
DECLARE SUB disableints ()
DECLARE SUB DifferenceMagnify ()
DECLARE SUB MakeMagCursor ()
DECLARE SUB Getlimits ()
DECLARE SUB subtract ()
DECLARE SUB magnify ()
DECLARE SUB mcursorup ()
DECLARE SUB mcursordown ()
DECLARE SUB wcursorup ()
DECLARE SUB wcursorright ()
DECLARE SUB wcursorleft ()
DECLARE SUB wcursordown ()
DECLARE SUB MainMenu ()
DECLARE SUB DisplayData ()
DECLARE SUB frame (leftcol%, rightcol%, toprow%, bottomrow%)
```

```
DECLARE SUB savedatafile ()
DECLARE SUB titlescreen ()
DECLARE SUB getdatafile ()
DECLARE SUB filterwaveform ()
DECLARE SUB EvaluateCoefs (ntaps!)
DECLARE SUB titles ()
DECLARE SUB redraw ()
DECLARE SUB initialROI ()
DECLARE SUB gencursor ()
DECLARE SUB initscreen ()
DECLARE SUB acquire ()
DECLARE SUB LoadISR ()
DECLARE SUB SetVector3 ()
DECLARE SUB GraphicsScreen ()
DECLARE SUB InitializePit ()

'Hardware constants follow
CONST protobase = &H300
CONST pitd0 = protobase
CONST pitd1 = protobase + 1
CONST pitd2 = protobase + 2
CONST pitc = protobase + 3
CONST daclo = protobase + 4
CONST dachi = protobase + 5

'Program constants follow
CONST int3vect = 4 * &HB
CONST skipfact = 4
CONST cy = 10
CONST scrnymax = 480
CONST scrnxmax = 640
CONST false = 0
CONST true = NOT false
CONST pi = 3.141593
CONST filenotfound = 53
CONST initstep = 4
CONST c1 = 65536

DIM SHARED isr(0 TO 64) AS INTEGER  'storage of v-to-f ISR
DIM SHARED isr2(0 TO 64) AS INTEGER  'storage of recorder ISR
DIM SHARED MaxArraySize AS INTEGER
MaxArraySize = 16001
DIM SHARED Ychan(1 TO 2, 0 TO MaxArraySize) AS INTEGER
DIM SHARED diff(0 TO MaxArraySize) AS INTEGER
DIM SHARED plotout(0 TO MaxArraySize + 1) AS INTEGER
DIM SHARED corr(0 TO MaxArraySize) AS INTEGER
DIM SHARED dist(-99 TO 99)  AS INTEGER

DIM SHARED zj AS LONG
DIM SHARED ptr1 AS INTEGER
DIM SHARED ptr2 AS INTEGER
DIM SHARED ptr3 AS INTEGER
DIM SHARED ptr4 AS INTEGER
DIM SHARED ptr5 AS INTEGER
DIM SHARED cbuf(500) AS INTEGER  'line cursor buffer
DIM SHARED firstpoint, lastpoint, first, last AS INTEGER
DIM SHARED cursx0, cursx1, cursy, cursxsize  AS INTEGER
DIM SHARED numsamples, cursx, deltax AS SINGLE
DIM SHARED SNmode, Windowmode, magmode, Diffmode, SMmode AS INTEGER
DIM SHARED ncutoff  AS SINGLE
DIM SHARED coef(0 TO 128) AS SINGLE
DIM SHARED filter(1 TO 2, 0 TO MaxArraySize) AS INTEGER
DIM SHARED filen$
DIM SHARED magfact, diffmag, amp AS SINGLE
DIM SHARED filefound, horstep  AS INTEGER
DIM SHARED zi, mins, maxs, filtered AS INTEGER
```

```
DIM SHARED dpointer, final AS SINGLE
DIM SHARED tp, rundate$, dataacquired, diskerr
DIM SHARED dc, dcf, freqf
DIM SHARED dcreal, comport, sflag, rdelay
DIM SHARED chan1low, chan1high, chan2low, chan2high, pkleft, pkright AS
INTEGER
DIM SHARED cmode, slope1, slope2, taps, tapsd2, injectionmark AS INTEGER
DIM SHARED sigma, chan1lower, chan2lower, chan1clip, chan2clip AS SINGLE
DIM SHARED i, upct, downct, topct, tpc, csscale, sdir, sm, nsp, nspd2, ncp AS
SINGLE
DIM SHARED cstemp AS INTEGER
DIM SHARED menu1$, mode$
DIM SHARED ch%, lor
DIM SHARED integralerrorflag AS INTEGER

'     ****************************************************************
'     *                  PROGRAM START                                *
'     ****************************************************************
menu1$ = "F1-ZM F2-DF.F3-FUL F5-MAG.F6-PL F7-FIL F8-RES F9-SM F10-COR F11-RT
F12-" + CHR$(229)
CLS
injectionmark = 100
ZeroDac
start: KEY OFF
LoadISR  'load the recorder interrupt service routine
sigma = 1
dataacquired = false
optionloop:
SCREEN 0
MainMenu
rloop: resp$ = INKEY$
resp$ = UCASE$(resp$)
IF resp$ = "" THEN GOTO rloop
IF resp$ = "D" THEN GOTO disp1
IF resp$ = "R" THEN GOTO dispoption
IF resp$ = "Q" THEN END
IF resp$ = "F" THEN CALL savedatafile
IF resp$ = "S" THEN GOTO swapoption
GOTO optionloop

swapoption:
IF dataacquired = false THEN GOTO optionloop
CLS
FOR i = firstpoint TO lastpoint
SWAP Ychan(1, i), Ychan(2, i)
NEXT
PRINT "SWAP COMPLETE"
IF magfact = 0 THEN
   magfact = 1
END IF
magfact = 1 / magfact
GOTO optionloop

dispoption:
SCREEN 0
CALL getdatafile

disp1:
IF dataacquired = false THEN BEEP: CLS : GOTO optionloop
CLS
filtered = false
magmode = false: analysemode = false: Diffmode = false
Windowmode = true
diffmag = 1
CALL initscreen
CALL initialROI
```

```
CALL titles
Windowmode = true
LOCATE 28, 1: PRINT "WINDOW MODE";
LOCATE 28, 53: PRINT "CH2 MAGNIFICATION= ";
PRINT USING "##.###"; magfact;

'activate cursor motion and window def func keys

ON KEY(1) GOSUB Function1
ON KEY(2) GOSUB function2
ON KEY(3) GOSUB Function3
ON KEY(4) GOSUB function4
ON KEY(5) GOSUB function5
ON KEY(6) GOSUB function6
ON KEY(7) GOSUB function7
ON KEY(8) GOSUB function8
ON KEY(9) GOSUB function9
ON KEY(10) GOSUB function10
ON KEY(11) GOSUB cursorup
ON KEY(14) GOSUB cursordown
ON KEY(12) GOSUB cursorleft
ON KEY(13) GOSUB cursorright
ON KEY(30) GOSUB function11
ON KEY(31) GOSUB function12
LOCATE 29, 1
PRINT menu1$;
fkeyson
done = false

DO
 a$ = INKEY$
 IF a$ = CHR$(27) THEN done = true
LOOP UNTIL done
disableints
ZeroDac
clrl26
GOTO optionloop

cursorup:
IF Windowmode THEN wcursorup
IF magmode THEN mcursorup
IF SNmode THEN mcursorup
RETURN

cursordown:
IF Windowmode THEN wcursordown
IF magmode THEN mcursordown
IF SNmode THEN mcursordown
RETURN

cursorleft:
IF Windowmode THEN wcursorleft
IF SMmode THEN cursorleft
IF SNmode THEN SNcursorleft
RETURN

cursorright:
IF Windowmode THEN wcursorright
IF SMmode THEN cursorright
IF SNmode THEN SNcursorright
RETURN

Function1:  'zoom
 IF cursx1 - cursx0 < 20 THEN BEEP: RETURN
 horstep = 1 + INT((cursx1 - cursx0) / scrnxmax)
 firstpoint = 1 + cursx0 OR 1: lastpoint = (cursx1 OR 1) - 1
```

```
 CALL redraw
 filtered = false
 RETURN


function2    'difference mode toggle
IF Diffmode = false THEN
Diffmode = true
LOCATE 28, 1  PRINT 'DIFFERENCE MODE',
LOCATE 28, 53  PRINT 'DIFF MAGNIFICATION=",
PRINT USING "### ##', diffmag,
ELSE
Diffmode = false
LOCATE 28, 1  PRINT "WINDOW MODE",
END IF
CALL titles
RETURN

Function3    'go back to initial screen display
CALL Getlimits
filtered = false
magmode = false
CALL initscreen
CALL initialROI
CALL titles
Windowmode = true
LOCATE 28, 1  PRINT "WINDOW MODE",
LOCATE 28, 53  PRINT 'CH2 MAGNIFICATION= ",
PRINT USING "## ###', magfact,
RETURN

function4    'digital subtraction deleted
RETURN

function5    'magnification mode
IF Diffmode = false THEN CALL magnify ELSE CALL DifferenceMagnify
RETURN

function6    'Output data to a strip chart recorder
CALL plot
RETURN

function7    'do a 'taps' point FIR lowpass filtering of window data
 filtered = false
   clrl26
   PRINT '  # OF SAMPLES TO FILTER = ",
   PRINT USING '#####', lastpoint - firstpoint,
   FOR i = 1 TO 13000  NEXT
   clrl26
   INPUT 'FILTER TAPS   128,64 or 32", taps
   clrl26
   INPUT 'CUTOFF FREQ in Hz  ", n
   clrl26
   tapsd2 = taps \ 2
   ncutoff = n / 10
   CALL EvaluateCoefs(taps)
   CALL filterwaveform
   CALL redraw
   filtered = true
   clrl26
 RETURN


function8    'restore original sample data after filtering
q = 1
IF filtered = false THEN BEEP· RETURN
```

```
IF Diffmode = false THEN
swaparray
ELSE
  FOR i = first TO last
    SWAP diff(i), filter(1, q)
    q = q + 1
  NEXT
END IF
CALL redraw
filtered = false
RETURN

function9:  'Slope Ratio Functions : User selected peak & continuous
DO
 BEEP
 clrl26
 INPUT "1)User-selected  2) Continuous"; resp$
 LOOP UNTIL resp$ = "1" OR resp$ = "2"
 IF resp$ = "1" THEN
   CALL userSR
   RETURN
 ELSE
   clrl26
  INPUT "1) SLOPE  2) INTEGRAL"; resp$
  clrl26
  SetRatioMode
  IF resp$ = "1" THEN
   CALL contSR
  ELSE
   CALL contIR
  END IF
  RETURN
 END IF

function10:  'Correlate
CALL correlate2
RETURN

function11:
CALL dispRetTime
RETURN

function12:
SignalToNoise
RETURN

errhand1:  'filename.d1 (.d2,.d3 ) not found
 BEEP
 LOCATE 18, 22: PRINT SPC(37);
 LOCATE 18, 22
 IF ERR = filenotfound THEN
   PRINT filen$; "; NOT FOUND; ";
 ELSE
  PRINT "DISK ERR"; ERR;
 END IF
 FOR i = 1 TO 20000: NEXT
 LOCATE 18, 22: PRINT SPC(37);
 filefound = false
 RESUME NEXT

errhand2:  'DISK errors during a file save operation
  BEEP
  LOCATE 18, 22: PRINT SPC(37);
  LOCATE 18, 22
  diskerr = ERR
  PRINT "DISK ERR"; diskerr;
```

```
   FOR i = 1 TO 20000: NEXT
   LOCATE 18, 22: PRINT SPC(37);
   CLOSE
   RESUME NEXT

Errhand3:  'Check for existing disk files before file save operation
    diskerr = ERR
    CLOSE #1
RESUME NEXT

ScalingProgress: LOCATE 26, 18
PRINT USING "###"; 100 * (zi / (lastpoint - firstpoint));
RETURN

SUB acquire
BEEP
END SUB

SUB calcIR
 base1left = Ychan(1, pkleft)
 base1right = Ychan(1, pkright)
 base1 = (Ychan(1, pkleft) + Ychan(1, pkright)) / 2   'Find Chan1 average
baseline
 REM Chan2 baselines are 3 point averages based around the same times as
 REM those determined by ContSR routines
 base2left = (Ychan(2, pkleft - 1) + Ychan(2, pkleft) + Ychan(2, pkleft + 1))
/ 3
 base2right = (Ychan(2, pkright - 1) + Ychan(2, pkright) + Ychan(2, pkright
+ 1)) / 3
 base2 = (base2left + base2right) / 2
sigma1 = 0: sigma2 = 0
FOR k = pkleft + 1 TO pkright - 1
 sigma1 = sigma1 + Ychan(1, k) - base1
 sigma2 = sigma2 + Ychan(2, k) - base2
NEXT
IF sigma1 <= 0 OR sigma2 <= 0 THEN
 integralerrorflag = 1
 EXIT SUB
ELSE
sm = sigma1 / sigma2
END IF
END SUB

SUB calcSR
sigmanum = 0: sigmaden = 0
sdir = 0
FOR k = pkleft TO pkright
 CALL getslope2(k, 2)
 IF slope2 <> 0 THEN
   sdir = sdir + slope1
   sigmanum = sigmanum + (slope1 * slope1 / ABS(slope2))
   sigmaden = sigmaden + ABS(slope1)
 END IF
NEXT k
IF sigmaden = 0 THEN
  sm = 999
  BEEP
ELSE
sm = sigmanum / sigmaden
END IF
END SUB

SUB clrl26
LOCATE 26, 1: PRINT SPC(70);
LOCATE 26, 1
END SUB
```

```
SUB contIR
LOCATE 28, 1: PRINT "CONTINUOUS IR MODE";
CALL MakeMagCursor
CALL getParms
makegrid
printHeading ("Integral Ratio")

i = firstpoint - nspd2
IF i < 1 THEN i = 1
FOR j = i TO lastpoint: diff(j) = 8000: NEXT  'preclear the array

  'skip thru until lower thresholds reached   FIND PEAK START

contIRloop:
 cstemp = 8000  'pre-set  to midscale
upct = 0

DO
 FindPeakStart
 IF i = lastpoint THEN GOTO contIRexit
LOOP UNTIL upct = ncp

 'FOUND PEAK START (found # of slopes > than user criteria)
DefPeakStart
topct = 0
DO
 FindPeakTop
 i = i + 1
 IF i = lastpoint THEN GOTO contIRexit
LOOP UNTIL topct = ncp

 'FOUND PEAK TOP ( found # of slopes less < 0)
downct = 0
DO
FindPeakDownSlope
 IF i = lastpoint THEN GOTO contIRexit
LOOP UNTIL downct = ncp

 'FOUND start of Downward portion of peak
downct = 0
DO
 FindPeakEnd
 IF i = lastpoint THEN GOTO contIRexit
LOOP UNTIL downct = ncp
DefPeakEnd
CALL calcIR

IF integralerrorflag = 1 THEN
 cstemp = 8000
 GOTO cir2
END IF

PrintData
LPRINT " "
DefCstemp

cir2:
ScreenPlotRatio
GOTO contIRloop

contIRexit:
RatioExit
END SUB

SUB contSR
LOCATE 28, 1: PRINT "CONTINUOUS SR MODE";
```

```
CALL MakeMagCursor
CALL getParms
INPUT "1) Split peaks  2) Whole peaks"; resp$
IF resp$ = "1" THEN mode$ = "split" ELSE mode$ = "whole"
clrl26
makegrid
printHeading ("Slope Ratio")

i = firstpoint - nspd2
IF i < 1 THEN i = 1
FOR j = i TO lastpoint: diff(j) = 8000: NEXT  'preclear the array

 'FIND PEAK START

contSRloop:
 cstemp = 8000  'pre-set  to midscale
upct = 0
DO
 FindPeakStart
 IF i = lastpoint THEN GOTO contSRexit
LOOP UNTIL upct = ncp

 'FOUND PEAK START (found # of slopes > than user criteria)
DefPeakStart
IF mode$ = "whole" THEN GOTO cswhole

cstemp = 8000
downct = 0
DO
 CALL getslope2(i, nsp)
 IF ABS(slope1) < tpc THEN
   downct = downct + 1
 ELSE
  downct = 0
 END IF
 i = i + 1
 IF i = lastpoint THEN GOTO contSRexit
LOOP UNTIL downct = ncp

 'FOUND PEAK END ( found # of slopes less < user criteria)
GOTO cscalc

cswhole:
topct = 0
DO
 FindPeakTop
 IF i = lastpoint THEN GOTO contSRexit
LOOP UNTIL topct = ncp

 'FOUND PEAK TOP ( found # of slopes less < 0)
downct = 0
DO
 FindPeakDownSlope
 IF i = lastpoint THEN GOTO contSRexit
LOOP UNTIL downct = ncp

 'FOUND start of Downward portion of peak
downct = 0
DO
 FindPeakEnd
 IF i = lastpoint THEN GOTO contSRexit
LOOP UNTIL downct = ncp

cscalc:
DefPeakEnd
CALL calcSR
```

```
PrintData
IF mode$ = "split" THEN
  IF sdir > 0 THEN
    LPRINT " POS "
  ELSE
   LPRINT " NEG "
  END IF
ELSE LPRINT " "
END IF
DefCstemp
ScreenPlotRatio
GOTO contSRloop

contSRexit:
RatioExit
END SUB

SUB correlate2
  clrl26
  INPUT "Enter SM"; sm
  DO
  clrl26
  INPUT "Choose Plot   1) Chan#1  2) Chan#2  3) AVG Ch1&Ch2', cmode
  LOOP UNTIL (cmode = 1) OR (cmode = 2) OR (cmode = 3)
  clrl26
  INPUT "Enter max.deviation,% match, min peak seconds', dev  corrmatch,
mintime
  clrl26
  INPUT "Enter % of PWHH for 'skirt filling'', skirt
  LOCATE 27, 1
  PRINT SPC(79);
  LOCATE 27, 1
  IF cmode = 1 THEN PRINT "PLOTTING CORRELATED CHAN 1'
  IF cmode = 2 THEN PRINT "PLOTTING CORRELATED CHAN 2'
  IF cmode = 3 THEN PRINT "PLOTTING CORRELATED (CH1 +SM*CH2)/2
  clrl26
  PRINT "BASELINE";
  FOR i = firstpoint TO lastpoint· corr(i) = 0  NEXT
  CLS
  WINDOW (firstpoint, 0)-(lastpoint, 20000)
  LOCATE 1, 35: PRINT filen$,
  PSET (0, 0)
  i = firstpoint
     'start of peak finding routine
c0:  numcorr = 0
  IF i > lastpoint THEN GOTO endofdata
  CALL getslope(i, 2)
  IF slope1 <= 0 OR slope2 <= 0 THEN GOTO baseline  'pass by neg slopes
  delta = ABS(slope2 - slope1) / slope1
  IF delta > dev THEN GOTO baseline  'and mismatched slopes
  temp = slope1
  peakstart = i
  peakbottom1 = Ychan(1, i)
  q = 1
c1. IF i + q + 2 > lastpoint THEN GOTO endofdata
  CALL getslope(i + q, 2)
  IF slope1 <= 0 OR slope2 <= 0 THEN GOTO baseline
  delta = ABS(slope2 - slope1) / slope1
  IF delta > dev THEN GOTO baseline
  IF temp >= slope1 THEN GOTO baseline  '2nd deriv not positive
'we have found an area with both matching positive slopes and a positive 2nd
'derivative-indicative of a normal peak
'now go through the points one at a time until top of peak is reached
'and totalize the number of correlations found
numcorr = 1
LOCATE 26, 1: PRINT "PEAK START FOUND",
```

```
c2: q = q + 1
 IF (i + q + 2) > lastpoint THEN GOTO endofdata
 CALL getslope(i + q, 2)
 IF slope1 <= 0 AND slope2 <= 0 THEN GOTO topofpeak
c3: IF slope1 <> 0 THEN
   delta = ABS(slope2 - slope1) / slope1
 ELSE delta = 99999
 END IF
 IF delta < dev THEN numcorr = numcorr + 1
 GOTO c2

topofpeak:
q = q + 1
IF (i + q + 2) > lastpoint THEN GOTO endofdata
CALL getslope(i + q, 2)
IF slope1 > 0 OR slope2 > 0 THEN GOTO c3   'false top of peak

'we have found an area where two consecutive points have
'zero or negative slopes indicating we have gone past peak
'now go through the down-side points one at a time until peak is over
'totalizing the number of correlations found
LOCATE 26, 1: PRINT "TOP OF PEAK FOUND";
topofpeak = i + q
peaktop = Ychan(1, i + q)
c4:
q = q + 1
IF (i + q + 2) > lastpoint THEN GOTO endofdata
CALL getslope(i + q, 2)
IF slope1 <> 0 THEN
  delta = ABS(slope2 - slope1) / slope1
ELSE delta = 99999
END IF
IF delta < dev THEN
 numcorr = numcorr + 1
END IF
IF slope1 < 0 OR slope2 < 0 THEN GOTO c4
c5: q = q + 1
IF (i + q + 2) > lastpoint THEN GOTO endofdata
CALL getslope(i + q, 2)
IF slope1 <> 0 THEN
  delta = (slope2 - slope1) / slope1
ELSE delta = 99999
END IF
IF slope1 < 0 OR slope2 < 0 THEN GOTO c5

'we have found a place where two consecutive points have [illegible] pos slope
peakover:
peakend = i + q
peakbottom2 = Ychan(1, i + q)
IF (numcorr > q * corrmatch / 100) AND q > 10 * mintime THEN
  LOCATE 26, 1: PRINT "PEAK END DETECTED";

  peakbottom = (peakbottom1 + peakbottom2) / 2
  phdiv2 = peakbottom + (peaktop - peakbottom) / 2
  j = peakstart - 1
z1:
  j = j + 1
  IF Ychan(1, j) < phdiv2 THEN GOTO z1
  w1 = j
  j = topofpeak
z2:
  j = j + 1
  IF Ychan(1, j) > phdiv2 THEN GOTO z2
  w2 = j
  PWHH = w2 - w1
  skirt = skirt * PWHH / 100
```

```
  ps = peakstart - skirt
  IF ps < 1 THEN ps = 1
  pe = peakend + skirt
  IF pe > lastpoint THEN pe = lastpoint
  PSET (ps, 0)
  FOR j = ps TO pe
   SELECT CASE cmode
    CASE IS = 1: temp = (Ychan(1, j))
    CASE IS = 2: temp = (Ychan(2, j))
    CASE IS = 3: temp = (Ychan(1, j) + sm * (Ychan(2, j))) \ 2
   END SELECT
   corr(j) = temp
   LINE -(j, temp)
 NEXT
ELSE
LOCATE 26, 1: PRINT "PEAK REJECTED",
 FOR j = peakstart TO peakend
    corr(i) = 0
    LINE -(j, 0)
  NEXT
END IF
i = peakend + 1
LOCATE 26, 1. PRINT "BASELINE",
GOTO c0

endofdata:
BEEP
EXIT SUB

baseline.
 'LINE -(i, 0)
corr(i) = 0
i = i + 1
GOTO c0
END SUB

SUB cursorleft
  LINE (cursx0, 0)-(cursx0, 10000), 0
  'fill in old data points for both channels
  i = cursx0
  LINE (i - 1, 100 + Ychan(1, i - 1))-(i, 100 + Ychan(1, i)), 1
  LINE (i - 1, 4000 + Ychan(2, i - 1))-(i, 4000 + Ychan(2, i)), 2
  i = i + 1
  LINE (i - 1, 100 + Ychan(1, i - 1))-(i, 100 + Ychan(1, i)), 1
  LINE (i - 1, 4000 + Ychan(2, i - 1))-(i, 4000 + Ychan(2, i)), 2
  cursx0 = cursx0 - deltax
  IF cursx0 < firstpoint + 1 THEN
      cursx0 = 1 + firstpoint
  END IF
  LINE (cursx0, 0)-(cursx0, 10000), 4
END SUB

SUB cursorright
  'erase old line
  LINE (cursx0, 0)-(cursx0, 10000), 0
  'fill in old data points for both channels
  i = cursx0
  LINE (i - 1, 100 + Ychan(1, i - 1))-(i, 100 + Ychan(1, i)), 1
  LINE (i - 1, 4000 + Ychan(2, i - 1))-(i, 4000 + Ychan(2, i)), 2
  i = i + 1
  LINE (i - 1, 100 + Ychan(1, i - 1))-(i, 100 + Ychan(1, i)), 1
  LINE (i - 1, 4000 + Ychan(2, i - 1))-(i, 4000 + Ychan(2, i)), 2
  cursx0 = cursx0 + deltax
  IF cursx0 > lastpoint - 1 THEN
      cursx0 = lastpoint - 1
  END IF
```

```
  LINE (cursx0, 0)-(cursx0, 10000), 4
END SUB

SUB DefCstemp
  cstemp = 8000 + csscale * LOG(sm)
IF cstemp > 15200 THEN cstemp = 15200
IF cstemp < 800 THEN cstemp = 800
END SUB

SUB DefPeakEnd
i = i - ncp + nspd2
pkright = i
END SUB

SUB DefPeakStart
i = i - ncp + nspd2
pkleft = i
LINE -(i, cstemp)
END SUB

SUB DifferenceMagnify
  clrl26
  INPUT "ENTER DIFFERENCE MAGNIFICATION FACTOR"; temp
  ON TIMER(1) GOSUB ScalingProgress
  TIMER ON
  CALL Getlimits
  FOR zi = firstpoint TO lastpoint
     diff(zi) = diff(zi) * temp
  NEXT
  TIMER OFF
  LOCATE 27, 1: PRINT "DIFFERENCE ARRAY SCALED";
  diffmag = diffmag * temp
LOCATE 28, 53: PRINT "DIFF MAGNIFICATION= ";
PRINT USING "###.##"; diffmag;
 CALL initscreen
 CALL initialROI
 CALL titles
 Windowmode = true
END SUB

SUB disableints
intstat = INP(&H21)
OUT &H21, intstat OR 8  'stop acquisition
END SUB

SUB DisplayData
  zk = Ychan(1, 0)
  IF zk < 0 THEN zk = zk + c1
  IF zj >= zk THEN EXIT SUB
   IF zi MOD skipfact = 1 THEN
     PSET (zi, 4000! + Ychan(2, zi)), 2
     PSET (zi, Ychan(1, zi)), 3
   END IF
    zi = zi + 1
   zj = zj + 4
END SUB

SUB dispRetTime
IF Windowmode THEN windowDRT
IF SMmode THEN SMDRT
END SUB

SUB EnableInts
intstat = INP(&H21)
intstat = intstat AND 247  'clear the IRQ3 interrupt mask
OUT &H21, intstat
```

```
END SUB

SUB EvaluateCoefs (ntaps)
  DIM m  AS INTEGER
  coef(0) = ncutoff
  FOR m = 1 TO tapsd2
   q = m * pi
   coef(m) = (SIN(ncutoff * q) / q) * (.54 + .46 * COS(q / tapsd2))
  NEXT
END SUB

SUB FilterCh (ch%)
DIM temp1 AS SINGLE
DIM q, j, k AS INTEGER
Diffmode = false
Windowmode = false
SNmode = true
fkeysoff
clrl26
PRINT "FILTER PROGRESS =     %";
ON TIMER(5) GOSUB ScalingProgress
TIMER ON
last = lastpoint
IF firstpoint < 1 + tapsd2 THEN
   first = 1 + tapsd2
   FOR j = 1 TO tapsd2: filter(1, j) = 0: NEXT

   ELSE first = firstpoint - tapsd2
END IF

FOR j = first TO last
   temp1 = 0:
   FOR k = 1 TO tapsd2
     coef = coef(k)
     temp1 = temp1 + (Ychan(ch%, j + k) + Ychan(ch%, j - k)) * coef
   NEXT
   filter(1, j) = temp1 + Ychan(ch%, j) * coef(0)
   IF filter(1, j) > 16000 THEN filter(1, j) = 16000
   zi = j - firstpoint  'for timed progress display purposes
NEXT
LOCATE 27, 1: PRINT SPC(40);
fkeyson
TIMER OFF

CLS
WINDOW (firstpoint, 0)-(lastpoint, 20000)
LOCATE 1, 35: PRINT filen$;
  PSET (firstpoint, Ychan(ch%, firstpoint)), 1: PSET (firstpoint, filter(1,
firstpoint)), 2
  FOR i = firstpoint + 1 TO lastpoint
    LINE (i - 1, 100 + filter(1, i - 1))-(i, 100 + filter(1, i)), 2
    LINE (i - 1, 100 + Ychan(ch%, i - 1))-(i, 100 + Ychan(ch%, i)), 1
  NEXT
LINE (injectionmark, 0)-(injectionmark, 200), 14
CALL titles
CALL initialROI
END SUB

SUB FilterDiff
DIM temp1 AS SINGLE
DIM q, j, k AS INTEGER
fkeysoff
clrl26
PRINT "FILTER PROGRESS =       %";
ON TIMER(5) GOSUB ScalingProgress
TIMER ON
```

```
last = lastpoint
IF firstpoint < 1 + tapsd2 THEN first = 1 + tapsd2 ELSE first = firstpoint -
tapsd2
q = 1
FOR j = first TO last
   temp1 = 0:
   FOR k = 1 TO tapsd2
     coef = coef(k)
     temp1 = temp1 + (diff(j + k) + diff(j - k)) * coef
   NEXT
   filter(1, q) = temp1 + diff(j) * coef(0)
   IF filter(1, q) > 16000 THEN filter(1, q) = 16000
   q = q + 1
   zi = j - firstpoint  'for timed progress display purposes
NEXT
LOCATE 27, 1: PRINT SPC(40);
fkeyson
TIMER OFF
END SUB

SUB filterwaveform
DIM temp1, temp2 AS SINGLE
DIM q, j, k AS INTEGER
fkeysoff
clrl26
PRINT "FILTER PROGRESS =       %";
ON TIMER(5) GOSUB ScalingProgress
TIMER ON
last = lastpoint
IF firstpoint < 1 + tapsd2 THEN first = 1 + tapsd2 ELSE first = firstpoint -
tapsd2
q = 1
IF Diffmode = false THEN
 FOR j = first TO last
   temp1 = 0: temp2 = 0
   FOR k = 1 TO tapsd2
     coef = coef(k)
     temp1 = temp1 + (Ychan(1, j + k) + Ychan(1, j - k)) * coef
     temp2 = temp2 + (Ychan(2, j + k) + Ychan(2, j - k)) * coef
   NEXT
   filter(1, q) = temp1 + Ychan(1, j) * coef(0)
   IF filter(1, q) > 16000 THEN filter(1, q) = 16000
   filter(2, q) = temp2 + Ychan(2, j) * coef(0)
   IF filter(2, q) > 16000 THEN filter(2, q) = 16000
   q = q + 1
   zi = j - firstpoint  'for timed progress display purposes
 NEXT
 swaparray
ELSE
 FOR j = first TO last
   temp1 = 0
   FOR k = 1 TO tapsd2
     coef = coef(k)
     temp1 = temp1 + (diff(j + k) + diff(j - k)) * coef
   NEXT
   filter(1, q) = temp1 + diff(j) * coef(0)
   q = q + 1
   zi = j - firstpoint  'for timed progress display purposes
 NEXT
 q = 1
 FOR j = first TO last  'interchange orig and filtered data
  SWAP diff(j), filter(1, q)
  q = q + 1
 NEXT
END IF
LOCATE 27, 1: PRINT SPC(40);
```

```
fkeyson
TIMER OFF
END SUB

SUB FindPeakDownSlope
 CALL getslope2(i, nsp)
 temp = slope1 * -1
 IF temp > tcp THEN
  downct = downct + 1
 ELSE
 downct = 0
 END IF
 i = i + 1
END SUB

SUB FindPeakEnd
 CALL getslope2(i, nsp)
 IF (Ychan(1, i) < chan1lower) OR (Ychan(2, i) < chan2lower) OR (slope1 * -1)
< tpc THEN
   downct = downct + 1
 ELSE
  downct = 0
 END IF
 i = i + 1
END SUB

SUB FindPeakStart
 CALL getslope2(i, nsp)
 IF (Ychan(1, i) < chan1lower) OR (Ychan(2, i) < chan2lower) OR (ABS(slope1)
< tpc) THEN
   diff(i) = cstemp
   LINE -(i, cstemp)
   upct = 0
 ELSE
  upct = upct + 1
 END IF
 i = i + 1
END SUB

SUB FindPeakTop
 CALL getslope2(i, nsp)
 IF slope1 < 0 THEN
  topct = topct + 1
 ELSE
 topct = 0
 END IF
 i = i + 1
END SUB

SUB fkeysoff
FOR i = 1 TO 14
  KEY(i) OFF
  NEXT
KEY(30) OFF
KEY(31) OFF
END SUB

SUB fkeyson
FOR i = 1 TO 14
  KEY(i) ON
NEXT
KEY(30) ON
KEY(31) ON
END SUB

SUB frame (leftcol%, rightcol%, toprow%, bottomrow%) STATIC
```

```
  LOCATE toprow%, leftcol%  PRINT CHR$(201)
  LOCATE toprow%, rightcol%  PRINT CHR$(187)
  LOCATE bottomrow%, leftcol%  PRINT CHR$(200)
  LOCATE bottomrow%, rightcol%  PRINT CHR$(188),
  FOR vertline% = toprow% + 1 TO bottomrow% - 1
  LOCATE vertline%, leftcol%  PRINT CHR$(186),
  LOCATE vertline%, rightcol%  PRINT CHR$(186)
  NEXT
  horizlength% = rightcol% - leftcol% - 1
  horizline$ = STRING$(horizlength%, 205)
  LOCATE toprow%, leftcol% + 1· PRINT horizline$
  LOCATE bottomrow%, leftcol% + 1  PRINT horizline$,
END SUB

SUB getdatafile

ON ERROR GOTO errhand1
 DO
     LOCATE 19, 22
     PRINT SPC(37),   LOCATE 19, 22
     INPUT 'Filename  (CR to Esc)?", tfilen$
     IF tfilen$ = "" THEN EXIT SUB
     filen$ = tfilen$
     filefound = true  dataacquired = false
     DEF SEG = VARSEG(Ychan(1, 0))
     BLOAD filen$ + " dat", 0  'errhand1 takes care if no file found
 LOOP UNTIL filefound = true
     CLS
     PRINT "FILE LOADED SUCCESSFULLY. RUN WAS",
     CALL Getlimits
     runmins = lastpoint / 600
     PRINT USING "### ##"; runmins,
     PRINT "MINUTES IN DURATION"
     injectionmark = Ychan(2, 0)
     OPEN filen$ + ".par" FOR INPUT AS #1
     INPUT #1, magfact
     CLOSE #1
  FOR i = 1 TO 5000: NEXT
dataacquired = true
ON ERROR GOTO 0
END SUB

SUB Getlimits
 z = Ychan(1, 0)
 IF z < 0 THEN z = z + c1
 lastpoint = z \ 4 - tapsd2
 firstpoint = 1
END SUB

SUB getParms
clrl26
PRINT "Move cursor to LOWER Threshold of Ch1,then hit Enter";
WaitForKey
chan1lower = cursy
PUT (firstpoint, cursy - cy), cbuf, PSET

cursy = 4000
GET (firstpoint, cursy   cy)-(lastpoint, cursy + cy), cbuf
LINE (firstpoint, cursy)-(lastpoint, cursy), 4
clrl26
PRINT "Move cursor to LOWER Threshold of Ch2,then hit Enter";
FOR i = 1 TO 1000: NEXT
WaitForKey
PUT (firstpoint, cursy - cy), cbuf, PSET
chan2lower = cursy - 4000
```

```
cursy = 16000
GET (firstpoint, cursy - cy)-(lastpoint, cursy + cy), cbuf
LINE (firstpoint, cursy)-(lastpoint, cursy), 4
clrl26
PRINT "Move cursor to Clipping level of Ch1,then hit Enter";
FOR i = 1 TO 1000: NEXT
WaitForKey
PUT (firstpoint, cursy - cy), cbuf, PSET
chan1clip = cursy

cursy = 16000
GET (firstpoint, cursy - cy)-(lastpoint, cursy + cy), cbuf
LINE (firstpoint, cursy)-(lastpoint, cursy), 4
clrl26
PRINT "Move cursor to Clipping level of Ch2,then hit Enter";
FOR i = 1 TO 1000: NEXT
WaitForKey
PUT (firstpoint, cursy - cy), cbuf, PSET
chan2clip = cursy - 4000
PSET (firstpoint, 8000)
clrl26
INPUT "# of samples per slope calculation: "; nsp
nspd2 = nsp \ 2
clrl26
INPUT "# of consecutive points required: "; ncp
clrl26
INPUT "Enter Minimum Slope Criteria (%FS/min): "; tpc
tpc = tpc * .266 * nsp  '100% =16000units/60sec =266.6 units/sec
csscale = 7200 / (1.5 * 2.302) '2.302 is Ln to Log: SR=1.5 =7200 units
clrl26
END SUB

SUB getslope (index, size)
    a = Ychan(1, index): b = sm * Ychan(2, index)
    slope1 = Ychan(1, index + size) - a
    slope2 = sm * Ychan(2, index + size) - b
    IF a >= 16000 OR b >= 16000 THEN
      slope1 = 0
      LOCATE 26, 1: PRINT "CLIPPED";
    END IF
END SUB

SUB getslope2 (index, size)
    a = Ychan(1, index): b = Ychan(2, index)
    slope1 = Ychan(1, index + size) - a
    slope2 = Ychan(2, index + size) - b
    IF a >= chan1clip OR b >= chan2clip THEN
      slope1 = 0
    END IF
END SUB

SUB GraphicsScreen
  SCREEN 12
  VIEW (10, 10)-(500, 400), , 15
  WINDOW (0, 0)-(16000, 20000)
  LOCATE 29, 1: PRINT "Elapsed Time: ";
END SUB

SUB InitializePit
   OUT pitc, &H36  'set PIT0 for mode 3 square wave output
   OUT pitd0, 51: OUT pitd0, 51  'set divisor at 51*256 + 51 =13107
   'with 131070 hz clock, pit 0 will put out 10 hz
   OUT pitc, &H70  'set PIT1 for mode 0 pulse accumulator
   OUT pitc, &HB0  'set pit2 for mode 0 pulse accumulator
   OUT pitd1, 255: OUT pitd1, 255  'load 65535  into counter1
   OUT pitd2, 255: OUT pitd2, 255  'load 65535 into counter2
```

```
END SUB

SUB initialROI
cursx0 = INT(firstpoint + .4 * (lastpoint - firstpoint))
cursx1 = INT(firstpoint + .6 * (lastpoint - firstpoint))
cursxsize = cursx1 - cursx0
cursy0 = 0
cursy1 = 16000
deltax = 2 + INT(.04 * (lastpoint - firstpoint))
LINE (cursx0, 0)-(cursx0, 10000), 4
LINE (cursx1, 0)-(cursx1, 10000), 4
END SUB

SUB initscreen
SCREEN 12, 0, 0
CLS
CALL Getlimits
viewx0 = scrnxmax \ 12: viewx1 = scrnxmax * 11 \ 12
viewy0 = 1: viewy1 = scrnymax * 3 \ 4
VIEW (viewx0, viewy0)-(viewx1, viewy1), , 15
WINDOW (firstpoint, 0)-(lastpoint, 20000)
LOCATE 1, 35: PRINT filen$;
IF Diffmode = false THEN
 PSET (1, 100 + Ychan(1, 1)), 1
 PSET (1, 4000 + Ychan(2, 1)), 2
 FOR i = 2 TO lastpoint STEP 4
  LINE -(i, 4000 + Ychan(2, i)), 2
 NEXT
 PSET (1, 4000 + Ychan(2, 1)), 2
  FOR i = 2 TO lastpoint STEP 4
   LINE -(i, 100 + Ychan(1, i)), 1
  NEXT
LINE (injectionmark, 0)-(injectionmark, 200), 14
LINE (injectionmark, 3900)-(injectionmark, 4100), 14
ELSE
 PSET (1, 4000 + diff(1)), 15:
 FOR i = 2 TO lastpoint
  LINE -(i, 4000 + diff(i)), 15
NEXT
LINE (injectionmark, 3900)-(injectionmark, 4100), 14
END IF
END SUB

SUB loadDac (pa%)
temp% = pa% MOD 256
OUT daclo, temp%
temp% = 16 * (pa% \ 256)
OUT dachi, temp%
END SUB

SUB LoadISR
ptr5 = VARSEG(isr2(0))
ptr4 = VARPTR(isr2(0))
DEF SEG = ptr5
BLOAD "int2.sav", ptr4  'load the Recorder interupt service routine
DEF SEG
END SUB

SUB magnify
Windowmode = false
magmode = true
cursy = cy
LOCATE 28, 1: PRINT "MAGNIFICATION MODE";
CALL MakeMagCursor
clrl26
PRINT "Move cursor to LOWER limit of ch1,then hit Enter";
```

```
DO
a$ = INKEY$
LOOP UNTIL a$ = CHR$(13)
chan1lower = cursy - 100
 PUT (firstpoint, cursy - cy), cbuf, PSET
 cursy = 4000
 GET (firstpoint, cursy - cy)-(lastpoint, cursy + cy), cbuf
 LINE (firstpoint, cursy)-(lastpoint, cursy), 4
clr126
PRINT "Move cursor to LOWER limit of ch2,then hit Enter";
FOR i = 1 TO 1000: NEXT
DO
a$ = INKEY$
LOOP UNTIL a$ = CHR$(13)
chan2lower = cursy - 4000
clr126
PRINT "Desired mag factor (or SM )";
INPUT resp$
chan2scale = VAL(resp$)
CALL Getlimits
clr126
PRINT "PLEASE WAIT: Zeroing offsets and SCALING channel 2";
  FOR zi = firstpoint TO lastpoint
    Ychan(1, zi) = Ychan(1, zi) - chan1lower
    temp = (Ychan(2, zi) - chan2lower) * chan2scale
    IF temp > 16000 THEN temp = 16000
    Ychan(2, zi) = temp
    diff(zi) = Ychan(1, zi) - temp
 NEXT
clr126
LOCATE 27, 1: PRINT SPC(70);
filtered = false
magmode = false
magfact = chan2scale
LOCATE 28, 53: PRINT "CH2 MAGNIFICATION= ";
PRINT USING "##.###"; magfact;
CALL initscreen
CALL initialROI
Windowmode = true
LOCATE 28, 1: PRINT "WINDOW MODE";
END SUB

SUB MainMenu
CLS
COLOR 3
CALL frame(20, 60, 10, 20)
LOCATE 11, 22
PRINT "MAIN MENU";
LOCATE 14, 22
PRINT "D-Display data";
LOCATE 15, 22
PRINT "R-Retrieve a data file";
LOCATE 16, 22
PRINT "F-Save current data to disk";
LOCATE 17, 22
PRINT "S- Swap channel 1,channel 2";
LOCATE 18, 22
PRINT "Q- Exit to operating system ( DOS )";
COLOR 7
END SUB

SUB makegrid
  FOR i = 800 TO 15200 STEP 2400
  LINE (firstpoint, i)-(lastpoint, i), 3
  NEXT
  PSET (firstpoint, 8000), 15
```

```
   LOCATE 18, 1: PRINT "      ";
   LOCATE 23, 1: PRINT "      ";

   LOCATE 14, 3
   PRINT " 0.0"
   LOCATE 6, 3
   PRINT "+1.5"
   LOCATE 22, 3
   PRINT "-1.5"
END SUB

SUB MakeMagCursor
'first erase the two window cursors,restore data underneath
 LINE (cursx0, 0)-(cursx0, 10000), 0
 LINE (cursx1, 0)-(cursx1, 10000), 0
  'fill in old data points for both channels
  i = cursx0
  LINE (i - 1, Ychan(1, i - 1))-(i, Ychan(1, i)), 1
  LINE (i - 1, 4000 + Ychan(2, i - 1))-(i, 4000 + Ychan(2, i)), 2
  i = i + 1
  LINE (i - 1, Ychan(1, i - 1))-(i, Ychan(1, i)), 1
  LINE (i - 1, 4000 + Ychan(2, i - 1))-(i, 4000 + Ychan(2, i)), 2
  i = cursx1
  LINE (i - 1, Ychan(1, i - 1))-(i, Ychan(1, i)), 1
  LINE (i - 1, 4000 + Ychan(2, i - 1))-(i, 4000 + Ychan(2, i)), 2
  i = i + 1
  LINE (i - 1, Ychan(1, i - 1))-(i, Ychan(1, i)), 1
  LINE (i - 1, 4000 + Ychan(2, i - 1))-(i, 4000 + Ychan(2, i)), 2

GET (firstpoint, cursy - cy)-(lastpoint, cursy + cy), cbuf
LINE (firstpoint, cursy)-(lastpoint, cursy), 4
END SUB

SUB mcursordown
 PUT (firstpoint, cursy - cy), cbuf, PSET
 cursy = cursy - 40
 IF cursy < cy THEN cursy = cy
 GET (firstpoint, cursy - cy)-(lastpoint, cursy + cy), cbuf
 LINE (firstpoint, cursy)-(lastpoint, cursy), 4
 LOCATE 2, 1: PRINT USING "#####"; cursy;
END SUB

SUB mcursorup
 PUT (firstpoint, cursy - cy), cbuf, PSET
 cursy = cursy + 30
 IF cursy > 20000 - cy THEN cursy = 20000 + cy
 GET (firstpoint, cursy - cy)-(lastpoint, cursy + cy), cbuf
 LINE (firstpoint, cursy)-(lastpoint, cursy), 4
 LOCATE 2, 1: PRINT USING "#####"; cursy;
 END SUB

SUB plot
disableints
plotscale = 1: ticks = false
clrl26
INPUT "PLOT 1) Ch1 2) Ch2 3) Diff 4) Corr 5) ContSR"; resp
clrl26
IF resp = 5 THEN GOTO p1
INPUT "TICKS Y or N"; resp$
IF resp$ = "Y" OR resp$ = "y" THEN ticks = true
LOCATE 26, 1: PRINT "Enter vertical scaling factor";
INPUT plotscale
p1:
clrl26
PRINT "WORKING OUT PLOT DATA"
plotout(0) = 4
```

```
k = 2
FOR i = firstpoint TO lastpoint
 IF resp = 1 THEN temp = 383 + Ychan(1, i) * plotscale
 IF resp = 2 THEN temp = 383 + Ychan(2, i) * plotscale
 IF resp = 3 THEN temp = 8191 + diff(i) * plotscale / 2
 IF resp = 4 THEN temp = 383 + corr(i) * plotscale
 IF resp = 5 THEN temp = 383 + diff(i)

'now clip values to lo and hi limits
 IF temp < 0 THEN temp = 0
 IF temp > 16383 THEN temp = 16383
 IF ticks = true AND i > injectionmark THEN
 IF (i - injectionmark) MOD 100 = 0 THEN temp = temp - 382
 END IF
 IF i = injectionmark THEN temp = temp - 382
 IF temp < 0 THEN temp = 0
 plotout(k) = temp
 k = k + 1
NEXT
IF resp < 5 THEN .  0 p2
REM Make a stairst  ' calib pattern on recorder
clrl26
PRINT "PLOTTING CALIB  STAIRCASE"
zz = TIMER
 CALL loadDac(2096)
DO
LOOP UNTIL TIMER >= zz + 10
zz = TIMER
 CALL loadDac(2696)
DO
LOOP UNTIL TIMER >= zz + 10
zz = TIMER
 CALL loadDac(3296)
DO
LOOP UNTIL TIMER >= zz + 10
zz = TIMER
 CALL loadDac(3896)
DO
LOOP UNTIL TIMER >= zz + 10
zz = TIMER
 CALL loadDac(296)
DO
LOOP UNTIL TIMER >= zz + 10
zz = TIMER
 CALL loadDac(896)
DO
LOOP UNTIL TIMER >= zz + 10
zz = TIMER
 CALL loadDac(1496)
DO
LOOP UNTIL TIMER >= zz + 10
zz = TIMER
 CALL loadDac(2096)
DO
LOOP UNTIL TIMER >= zz + 10

p2:
plotout(1) = 2 * (k - 1)
ptr3 = VARSEG(plotout(0))
isr2(3) = ptr3  'place PLOTOUT segment into ISR2
SetRecorderVector
CALL InitializePit  'start pit going at 10 samples/sec
EnableInts
clrl26
PRINT "PLOTTING DATA"
END SUB
```

```
SUB PrintData
rtm = pkleft \ 600
rts = (pkleft MOD 600) \ 10
rtf = pkleft MOD 10
rtm$ = STR$(rtm)
rts$ = STR$(rts)
rts$ = RIGHT$(rts$, LEN(rts$) - 1)

LPRINT rtm$; ":";
IF rts < 10 THEN LPRINT "0";
LPRINT rts$; "."; rtf;
rtm = pkright \ 600
rts = (pkright MOD 600) \ 10
rtf = pkright MOD 10
rtm$ = STR$(rtm)
rts$ = STR$(rts)
rts$ = RIGHT$(rts$, LEN(rts$) - 1)
LPRINT TAB(25);
LPRINT rtm$; ":";
IF rts < 10 THEN LPRINT "0";
LPRINT rts$; "."; rtf;
LPRINT TAB(50);
LPRINT USING "###.###": sm;
END SUB

SUB printHeading (za$)
LPRINT "Continuous"; za$; "Figures -"; mode$; "peaks"
LPRINT "Filename: "; filen$
LPRINT "DATE: "; DATE$
LPRINT "Ret. Time (slope start)  Ret.Time (slope end) Ratio"
END SUB

SUB RatioExit
clrl26
PRINT "Hit ENTER key to return to Main menu";
WaitForKey
clrl26
Windowmode = true
magmode = false
CALL redraw
CALL titles
LOCATE 14, 3
PRINT "     "
LOCATE 6, 3
PRINT "     "
LOCATE 22, 3
PRINT "     "
END SUB

SUB redraw
CLS
WINDOW (firstpoint, 0)-(lastpoint, 20000)
LOCATE 1, 35: PRINT filen$;
IF Diffmode = false THEN
  PSET (firstpoint, Ychan(1, firstpoint)), 1: PSET (firstpoint, 4000 +
Ychan(2, firstpoint)), 2
  FOR i = firstpoint + 1 TO lastpoint
    LINE (i - 1, 4000 + Ychan(2, i - 1))-(i, 4000 + Ychan(2, i)), 2
    LINE (i - 1, 100 + Ychan(1, i - 1))-(i, 100 + Ychan(1, i)), 1
  NEXT
  LOCATE 28, 53: PRINT "CH2 MAGNIFICATION= ";
  PRINT USING "##.###"; magfact;
LINE (injectionmark, 0)-(injectionmark, 200), 14
LINE (injectionmark, 3900)-(injectionmark, 4100), 14
ELSE
  PSET (firstpoint, diff(firstpoint)), 15
```

```
  FOR i = firstpoint + 1 TO lastpoint
    LINE (i - 1, 4000 + diff(i - 1))-(i, 4000 + diff(i)), 15
  NEXT
  LOCATE 28, 53. PRINT "DIFF MAGNIFICATION=',
  PRINT USING "### ##"  diffmag,
LINE (injectionmark, 3900)-(injectionmark, 4100), 14
END IF
IF Windowmode THEN CALL initialROI
END SUB

SUB savedatafile
     IF dataacquired = false THEN GOTO 111
     LOCATE 18, 22  PRINT SPC(37),
     LOCATE 18, 22
     INPUT "Enter Filename  ", filen$
     IF filen$ = "' THEN EXIT SUB
ON ERROR GOTO Errhand3
     diskerr = 0
     OPEN filen$ + ".par' FOR INPUT AS #1
     IF diskerr = 0 THEN
       CLOSE #1
       BEEP
       LOCATE 18, 22. PRINT SPC(37);
       LOCATE 18, 22
       PRINT "File EXISTS '''",
       GOTO 111
     END IF
     ON ERROR GOTO errhand2
     diskerr = 0
     fsize = Ychan(1, 0)
     Ychan(2, 0) = injectionmark
     IF fsize < 0 THEN fsize = fsize + c1
     DEF SEG = VARSEG(Ychan(1, 0))
     BSAVE filen$ + " dat", 0, fsize
     IF diskerr <> 0 THEN 111
     OPEN filen$ + " par" FOR OUTPUT AS #1
     PRINT #1, magfact
     CLOSE #1
     LOCATE 18, 22: PRINT SPC(37),
     LOCATE 18, 22
     PRINT " FILE SAVED SUCCESSFULLY"
111 :
ON ERROR GOTO 0
END SUB

SUB ScreenPlotRatio
LINE -(pkleft, cstemp)
LINE -(pkright, cstemp)
FOR k = pkleft TO pkright
 diff(k) = cstemp
NEXT
END SUB

SUB SetRatioMode
Windowmode = false
magmode = true
cursy = cy
END SUB

SUB SetRecorderVector
intstat = INP(&H21)   'get existing interrupt mask status
OUT &H21, 255   'disable all interrupts
ptr3 = VARPTR(ptr4)
DEF SEG = VARSEG(ptr4)
a = PEEK(ptr3): b = PEEK(ptr3 + 1)
DEF SEG
```

```
ptr3 = VARPTR(ptr5)
DEF SEG = VARSEG(ptr5)
c = PEEK(ptr3)  D = PEEK(ptr3 + 1)
DEF SEG = 0  'point to interrupt vector segment at 0000
POKE int3vect, a
POKE int3vect + 1, b  'load in new vector
POKE int3vect + 2, c
POKE int3vect + 3, D
OUT &H21, intstat   restore old interrupt mask
DEF SEG
END SUB

SUB SignalToNoise
   clrl26
   cursy = cy
   CALL MakeMagCursor
   PRINT "GENERATING BASELINE FOR',
   PRINT USING '#### #", (lastpoint - firstpoint) / 10,
   PRINT "SECONDS',
   FOR i = 1 TO 20000  NEXT
   clrl26
   INPUT "FILTER TAPS   128,64 or 32", taps
   clrl26
   INPUT "CUTOFF FREQ in Hz  ", n
   LOCATE 26, 1  PRINT SPC(79),
   tapsd2 = taps \ 2
   ncutoff = n / 10
   CALL EvaluateCoefs(taps)
   clrl26
   PRINT "Calculate", CHR$(229), "for 1)Chan 1  2)Chan 2  (3-ESC)",
INPUT resp
clrl26
SELECT CASE resp
  CASE IS = 1  ch% = 1  CALL FilterCh(ch%)
  CASE IS = 2  ch% = 2  CALL FilterCh(ch%)
  CASE ELSE
   EXIT SUB
END SELECT
LOCATE 28, 1  PRINT "S/N MODE",
clrl26
deltax = 1 + INT((lastpoint - firstpoint) / 320)
SNloop
FOR i = -99 TO 99  dist(i) = 0  NEXT
PRINT "Move cursor to LEFT noise boundary, hit Enter to enter it',
lor = 1
FOR i = 1 TO 1000  NEXT
WaitForKey
noiseleft = cursx0
cursx0 = cursx1
clrl26
PRINT "Move cursor to RIGHT noise boundary, hit Enter to enter it',
lor = 75
FOR i = 1 TO 1000· NEXT
WaitForKey
noiseright = cursx0

'Sigma calculation that follows as defined by Walter Aue
'xbar= sum (over interval in window) of [x(i)]/num samples
'x(i)=YCHAN(i)-filteredYchan(i)
'sigma=sqrt    [sigma(x(i)-xbar)^2]
'                ------------------
'                       i-1

IF noiseright < (noiseleft + 1) THEN noiseright = noiseleft + 1

'calculate xbar using raw and filtered data
```

```
xbar = 0:
FOR i = noiseleft TO noiseright
  xbar = xbar + (Ychan(ch%, i) - filter(1, i))
NEXT
xbar = xbar / (noiseright - noiseleft)
ybar = 0. dmin = 16000. dmax = -16000
FOR i = noiseleft TO noiseright
  tmp = Ychan(ch%, i) - filter(1, i) - xbar
  IF tmp < dmin THEN dmin = tmp
  IF tmp > dmax THEN dmax = tmp
  ybar = ybar + (tmp ^ 2)
NEXT
 sigma = SQR(ybar / (noiseright - noiseleft) - 1)
LOCATE 26, 71
PRINT CHR$(229); "=",
PRINT USING '### #"; sigma,
clrl26
 dmax2 = 0. ddiv = 1
 IF ABS(dmin) > dmax2 THEN dmax2 = ABS(dmin)
 IF dmax > dmax2 THEN dmax2 = dmax
 IF dmax2 > 99 THEN ddiv = 1 + (dmax2 - 1) \ 99
 ddiv2 = ddiv / 2
dpeak = 0
FOR i = noiseleft TO noiseright
  tmp = Ychan(ch%, i) - filter(1, i) - xbar
  IF tmp = 0 THEN GOTO 678
  IF tmp > 0 THEN
  tmp = INT((tmp + ddiv2) \ ddiv)
  dist(tmp) = dist(tmp) + 1
  ELSE
  tmp = INT((tmp - ddiv2) \ ddiv)
  dist(tmp) = dist(tmp) + 1
  END IF
678 :
    IF dist(tmp) > dpeak THEN
    dpeak = dist(tmp)
    dcent = tmp
  END IF
NEXT

PRINT "ESC to exit, any other key to continue measurements',
DO
 a$ = INKEY$
LOOP UNTIL a$ <> '"
IF a$ = CHR$(27) THEN GOTO SNexit
GOTO SNloop
SNexit·

OPEN filen$ + ".dst" FOR OUTPUT AS #2
PRINT #2, "Distribution of Noise"
PRINT #2, "76 Y=A1*EXP(-A2*X^2)"
PRINT #2, "2"
PRINT #2, "Screen_Units Occurrances"
PRINT #2, ""
PRINT #2, USING '#.###^^^^", dpeak,
PRINT #2, "  1.0e-4"
PRINT #2, USING '#.###^^^^", 2.77 / (sigma * sigma),
PRINT #2, "  1.0e-9"
PRINT #2, "1 000  1 0e-7"
PRINT #2, "1 000  1 0e-7"
PRINT #2, "1 000  1 0e-7"

FOR i = -99 TO 99
  IF dist(i) > 0 THEN
    PRINT #2, i * ddiv, dist(i)
  END IF
```

```
NEXT
CLOSE #2

SNmode = false
Diffmode = false
Windowmode = true
 go back to original full display
CALL Getlimits
filtered = false
magmode = false
CALL initscreen
CALL initialROI
CALL titles
Windowmode = true
LOCATE 28, 1  PRINT 'WINDOW MODE',
LOCATE 28, 53  PRINT  CH2 MAGNIFICATION- ",
PRINT USING '## ###", magfact
END SUB

SUB SMDRT
  rtm = cursx0 \ 600
  rts = (cursx0 MOD 600) \ 10
  LOCATE 1, 1  PRINT USING "##", rtm,
  PRINT " ",
  PRINT USING "##", rts,
  LOCATE 1  75  PRINT '       ',
END SUB

SUB SNcursorleft
  LINE (cursx0, 0)-(cursx0, 10000), 0
   fill in old data points for both channels
  i = cursx0
  LINE (i - 1  100 + Ychan(ch%, i - 1))-(i, 100 + Ychan(ch%, i)), 1
  LINE (i - 1  100 + filter(1, i - 1))-(i, 100 + filter(1, i)), 2
  LINE (i, 100 + Ychan(ch%, i))-(i + 1, 100 + Ychan(ch%, i + 1)), 1
  LINE (i, 100 + filter(1, i))-(i + 1, 100 + filter(1, i + 1)), 2
  cursx0 = cursx0 - deltax
  IF cursx0 < firstpoint + 1 THEN
      cursx0 = 1 + firstpoint
  END IF
  LINE (cursx0, 0)-(cursx0, 10000), 4

  rtm = cursx0 \ 600
  rts = (cursx0 MOD 600) \ 10
  LOCATE 1, lor  PRINT USING "##", rtm,
  PRINT ' ',
  PRINT USING '##", rts,
END SUB

SUB SNcursorright
  'erase old line
  LINE (cursx0, 0)-(cursx0, 10000), 0
  'fill in old data points for both channels
  i = cursx0
  LINE (i - 1  100 + Ychan(ch%, i - 1))-(i, 100 + Ychan(ch%, i)), 1
  LINE (i - 1, 100 + filter(1, i - 1))-(i, 100 + filter(1, i)), 2
  LINE (i, 100 + Ychan(ch%, i))-(i + 1, 100 + Ychan(ch%, i + 1)), 1
  LINE (i, 100 + filter(1, i))-(i + 1, 100 + filter(1, i + 1)), 2
  cursx0 = cursx0 + deltax
  IF cursx0 > lastpoint - 1 THEN
      cursx0 = lastpoint - 1
  END IF
  LINE (cursx0, 0)-(cursx0, 10000), 4
  rtm = cursx0 \ 600
  rts = (cursx0 MOD 600) \ 10
  LOCATE 1, lor  PRINT USING "##", rtm,
```

```
  PRINT ".";
  PRINT USING "##", rts,
END SUB

SUB subtract
 BEEP
 END SUB

SUB swaparray
 q = 1
 FOR i = first TO last  'interchange orig and filtered data
  SWAP Ychan(1, i), filter(1, q)
  SWAP Ychan(2, i), filter(2, q)
 q = q + 1
 NEXT
END SUB

SUB titles
IF Diffmode = true THEN
 COLOR 7
 LOCATE 18, 1: PRINT "DIFF",
 LOCATE 23, 1: PRINT "      ',
 EXIT SUB
END IF

IF SNmode = true THEN
 COLOR 2
 LOCATE 18, 1: PRINT "FILT",
 COLOR 1
 LOCATE 23, 1· PRINT "RAW',
 COLOR 7
 EXIT SUB
END IF

 COLOR 2
 LOCATE 18, 1: PRINT "Chan2";
 COLOR 1
 LOCATE 23, 1: PRINT "Chan1",
 COLOR 7
END SUB

SUB userSR
Windowmode = false
SMmode = true
magmode = false
sm = 1  'make SM=1 for now as getslope routine uses SM
odx = deltax
oc0 = cursx0: oc1 = cursx1
deltax = INT((lastpoint - firstpoint) / 640)
IF deltax < 0 THEN deltax = 1
LOCATE 28, 1: PRINT "SR MODE",
clrl26
PRINT 'Move cursor to left of peak,hit Enter to enter it",
WaitForKey
pkleft = cursx0
cursx0 = cursx1
clrl26
PRINT 'Move cursor to right of PEAK, hit Enter to enter it',
FOR i = 1 TO 1000  NEXT
WaitForKey
pkright = cursx0
chan1clip = 16000  chan2clip = 16000
CALL calcSR
LOCATE 28, 53. PRINT "Weighted SR= ",
PRINT USING "## ###", sm,
```

```
clrl26
LOCATE 25, 1  PRINT SPC(70),
LOCATE 28, 1  PRINT SPC(40)
  LINE (pkleft, 0)-(pkleft, 10000), 0
   fill in old data points for both channels
  i = pkleft
  LINE (i - 1, Ychan(1, i - 1))-(i, Ychan(1, i)), 1
  LINE (i - 1, 4000 + Ychan(2, i - 1))-(i, 4000 + Ychan(2, i)), 2
  LINE (pkright, 0)-(pkright, 10000), 0
  'fill in old data points for both channels
  i = pkright
  LINE (i - 1, Ychan(1, i - 1))-(i, Ychan(1, i)), 1
  LINE (i - 1, 4000 + Ychan(2, i - 1))-(i  4000 + Ychan(2  i)), 2

deltax = odx
cursx0 = oc0  cursx1 = oc1
SMmode = false
Windowmode = true
CALL initialROI
END SUB

SUB WaitForKey
DO
 a$ = INKEY$
LOOP UNTIL a$ = CHR$(13)
END SUB

SUB wcursordown
 deltax = cursx1 - cursx0
  LINE (cursx0, 0)-(cursx0, 10000), 0
  LINE (cursx1, 0)-(cursx1, 10000), 0
  'fill in old data points for both channels
  i = cursx0
  LINE (i - 1, Ychan(1, i - 1))-(i, Ychan(1, i)), 1
  LINE (i - 1, 4000 + Ychan(2, i - 1))-(i, 4000 + Ychan(2, i)), 2
  i = i + 1
  LINE (i - 1, Ychan(1, i - 1))-(i  Ychan(1, i)), 1
  LINE (i - 1, 4000 + Ychan(2, i - 1))-(i, 4000 + Ychan(2, i)), 2
  i = cursx1
  LINE (i - 1, Ychan(1, i - 1))-(i, Ychan(1, i)), 1
  LINE (i - 1, 4000 + Ychan(2, i - 1))-(i, 4000 + Ychan(2, i)), 2
  i = i + 1
  LINE (i - 1, Ychan(1, i - 1))-(i, Ychan(1, i)), 1
  LINE (i - 1, 4000 + Ychan(2, i - 1))-(i, 4000 + Ychan(2, i)), 2
  deltax = deltax *  1
  IF ((cursx1 - deltax) - (cursx0 + deltax)) > 98 THEN
     cursx0 = cursx0 + deltax
     cursx1 = cursx1 - deltax
  ELSE
    ccenter = (cursx0 + cursx1) \ 2
    cursx0 = ccenter - 49
    cursx1 = ccenter + 49
  END IF

  cursxsize = cursx1 - cursx0
  LINE (cursx0, 0)-(cursx0  10000)  4
  LINE (cursx1, 0)-(cursx1  10000), 4
END SUB

SUB wcursorleft
  LINE (cursx0, 0)-(cursx0  10000), 0
  LINE (cursx1, 0)-(cursx1  10000), 0
  'fill in old data points for both channels
  i = cursx0
  LINE (i - 1, 100 + Ychan(1, i - 1))-(i, 100 + Ychan(1, i)), 1
  LINE (i - 1, 4000 + Ychan(2  i - 1))-(i, 4000 + Ychan(2, i)), 2
```

```
  i = i + 1
  LINE (i - 1, 100 + Ychan(1, i - 1))-(i, 100 + Ychan(1  i)), 1
  LINE (i - 1, 4000 + Ychan(2, i - 1))-(i, 4000 + Ychan(2, i)), 2
  i = cursx1
  LINE (i - 1, 100 + Ychan(1, i - 1))-(i, 100 + Ychan(1  i)), 1
  LINE (i - 1, 4000 + Ychan(2, i - 1))-(i, 4000 + Ychan(2, i)), 2
  i = i + 1
  LINE (i - 1, 100 + Ychan(1, i - 1))-(i, 100 + Ychan(1  i)), 1
  LINE (i - 1, 4000 + Ychan(2, i - 1))-(i, 4000 + Ychan(2, i)), 2
  cursx1 = cursx1 - deltax
  cursx0 = cursx0 - deltax
  IF cursx0 < firstpoint + 1 THEN
      cursx0 = 1 + firstpoint
      cursx1 = cursx0 + cursxsize
   END IF
  LINE (cursx0, 0)-(cursx0, 10000), 4
  LINE (cursx1, 0)-(cursx1, 10000), 4
END SUB

SUB wcursorright
  'erase old line
  LINE (cursx0, 0)-(cursx0, 10000), 0
  LINE (cursx1, 0)-(cursx1, 10000), 0
  'fill in old data points for both channels
  i = cursx0
  LINE (i - 1, 100 + Ychan(1, i - 1))-(i, 100 + Ychan(1  i))  1
  LINE (i - 1, 4000 + Ychan(2, i - 1))-(i, 4000 + Ychan(2, i)), 2
  i = i + 1
  LINE (i - 1, 100 + Ychan(1,   - 1))-(i, 100 + Ychan(1, i)), 1
  LINE (i - 1, 4000 + Ychan(2, i - 1))-(i, 4000 + Ychan(2  i)), 2
  i = cursx1
  LINE (i - 1, 100 + Ychan(1, i - 1))-(i, 100 + Ychan(1, i)), 1
  LINE (i - 1, 4000 + Ychan(2, i - 1))-(i, 4000 + Ychan(2, i))  2
  i = i + 1
  LINE (i - 1, 100 + Ychan(1, i - 1))-(i, 100 + Ychan(1, i)), 1
  LINE (i - 1, 4000 + Ychan(2, i - 1))-(i, 4000 + Ychan(2, i)), 2
  cursx0 = cursx0 + deltax
  cursx1 = cursx1 + deltax
  IF cursx1 > lastpoint - 1 THEN
      cursx1 = lastpoint - 1
      cursx0 = cursx1 - cursxsize
  END IF
  LINE (cursx0, 0)-(cursx0, 10000), 4
  LINE (cursx1, 0)-(cursx1, 10000), 4
END SUB

SUB wcursorup
deltax = INT(deltax * 1 2)
 LINE (cursx0, 0)-(cursx0, 10000), 0
 LINE (cursx1, 0)-(cursx1, 10000), 0
  'fill in old data points for both channels
  i = cursx0
  LINE (i - 1, Ychan(1, i - 1))-(i, Ychan(1, i))  1
  LINE (i - 1, 4000 + Ychan(2, i - 1))-(i, 4000 + Ychan(2, i)), 2
  i = i + 1
  LINE (i - 1, Ychan(1, i - 1))-(i, Ychan(1, i)), 1
  LINF (i - 1, 4000 + Ychan(2, i - 1))-(i, 4000 + Ychan(2, i)), 2
  i = cursx1
  LINE (i - 1, Ychan(1, i - 1))-(i, Ychan(1, i)), 1
  LINE (i - 1, 4000 + Ychan(2, i - 1))-(i, 4000 + Ychan(2, i)), 2
  i = i + 1
  LINF (i - 1, Ychan(1, i - 1))-(i, Ychan(1, i)), 1
  LINE (i - 1, 4000 + Ychan(2, i - 1))-(i, 4000 + Ychan(2  i)), 2

 cursx0 = cursx0 - deltax
 cursx1 = cursx1 + deltax
```

```
 IF cursx0 < firstpoint + 1 THEN cursx0 = firstpoint + 1
 IF cursx1 > lastpoint - 1 THEN cursx1 = lastpoint - 1
 cursxsize = cursx1 - cursx0
  LINE (cursx0, 0)-(cursx0, 10000), 4
  LINE (cursx1, 0)-(cursx1, 10000), 4
END SUB

SUB windowDRT
  rtm = cursx0 \ 600
  rts = (cursx0 MOD 600) \ 10
  LOCATE 1, 1: PRINT USING "##"; rtm;
  PRINT ":";
  PRINT USING "##"; rts;
  rtm = cursx1 \ 600
  rts = (cursx1 MOD 600) \ 10
  LOCATE 1, 75: PRINT USING "##"; rtm;
  PRINT ":";
  PRINT USING "##"; rts;
 END SUB

SUB ZeroDac
 OUT daclo, 0
 OUT dachi, 0
END SUB
```

Appendix II. SOURCE CODES OF "BC"
(Written by B. Millier)

```
'BASELINE correction program for dual channel chromatography interface
'written Nov 23, 1989
'Brian Millier- Dalhousie University Chemistry Department
'revision history

DECLARE SUB wcursu
DECLARE SUB wcursdown ()
DECLARE SUB makespline (x() AS SINGLE, y() AS SINGLE  n!)
DECLARE SUB graphicsScreen ()
DECLARE FUNCTION eval! (v!)
DECLARE SUB getlimits ()
DECLARE SUB wcursorup ()
DECLARE SUB wcursorright ()
DECLARE SUB wcursorleft ()
DECLARE SUB wcursordown ()
DECLARE SUB MainMenu ()
DECLARE SUB frame (leftcol%, rightcol%, toprow%, bottomrow%)
DECLARE SUB savedatafile ()
DECLARE SUB getdatafile ()
DECLARE SUB titles ()
DECLARE SUB initialROI ()
DECLARE SUB initscreen ()
DECLARE SUB graphicsScreen ()

'Program constants follow
CONST scrnymax = 480
CONST scrnxmax = 640
CONST false = 0
CONST true = NOT false
CONST filenotfound = 53
CONST c1 = 65536
CONST maxcp = 50
DIM SHARED cpx(1 TO maxcp) AS SINGLE
DIM SHARED cpy(1 TO maxcp) AS SINGLE
DIM SHARED p(1 TO maxcp) AS SINGLE
DIM SHARED cbvsz, cbhsz AS INTEGER
DIM SHARED MaxArraySize AS INTEGER
MaxArraySize = 16001
DIM SHARED ychan(1 TO 2, 0 TO MaxArraySize) AS INTEGER
DIM SHARED cbuf(100) AS INTEGER  ' box cursor buffer
DIM SHARED firstpoint, lastpoint AS INTEGER
DIM SHARED magfact, ch, cursy AS SINGLE
DIM SHARED numsamples, cursx AS SINGLE
DIM SHARED filen$
DIM SHARED filefound AS INTEGER
DIM SHARED dataacquired, diskerr
DIM SHARED mark, injectionmark, datahug AS INTEGER
DIM SHARED menu1$

'     ***** ************************************************************
'     *                  PROGRAM START                                   *
'     ************************************************************
menu1$ = "F1-MARK CONT POINT F2-GEN  BASELINE F3-DATA FOLLOW ON F4 DATA FOLLOW
OFF"
ch = 1
start: KEY OFF
dataacquired = false

optionloop:
SCREEN 0
```

```
MainMenu
rloop  resp$ = INKEY$
IF resp$ = "" THEN GOTO rloop
IF resp$ = "R" OR resp$ = "r" THEN GOTO dispoption
IF resp$ = "Q" OR resp$ = "q" THEN END
IF resp$ = "F" OR resp$ = "f" THEN CALL savedatafile
IF resp$ = "D" OR resp$ = "d" THEN GOTO disp1
GOTO optionloop

dispoption
SCREEN 0
CALL getdatafile
dataacquired = true

disp1:
IF dataacquired = false THEN BEEP: CLS : GOTO optionloop
CLS
INPUT "Enter channel number to view'; ch
IF ch <> 1 THEN ch = 2
z = 1· mark = false
datahug = true
CALL initscreen
CALL initialROI
CALL titles

'activate cursor motion and window def func keys
ON KEY(1) GOSUB function1
ON KEY(2) GOSUB function2
ON KEY(3) GOSUB Function3
ON KEY(4) GOSUB function4
ON KEY(5) GOSUB function5
ON KEY(6) GOSUB function6
ON KEY(7) GOSUB function7
ON KEY(8) GOSUB function8
ON KEY(9) GOSUB function9
ON KEY(10) GOSUB function10
ON KEY(14) GOSUB cursordown
ON KEY(11) GOSUB cursorup
ON KEY(12) GOSUB cursorleft
ON KEY(13) GOSUB cursorright

LOCATE 29, 1
PRINT menu1$;
LOCATE 25, 50  PRINT "CONTROL POINT";
COLOR 11
LOCATE 25, 70· PRINT "NONE";
COLOR 7
FOR i = 1 TO 14
  KEY(i) ON
NEXT
done = false

DO
a$ = INKEY$
IF a$ = CHR$(27) THEN done = true
LOOP UNTIL done
GOTO optionloop

cursorup
CALL wcursup
RETURN

cursordown:
CALL wcursdown
RETURN
```

```
cursorleft:
CALL wcursorleft
RETURN

cursorright:
CALL wcursorright
RETURN

function1:  'place a control point
  mark = true
  IF z > maxcp THEN
     z = maxcp
  END IF
  COLOR 11
  LOCATE 25, 70: PRINT USING "####"; z;
  COLOR 7
  cpx(z) = cursx
  cpy(z) = cursy - 100
  z = z + 1
  BEEP
RETURN

function2:  'generate a cubic spline curve with operator's control points
 z = z - 1
 CALL makespline(cpx(), cpy(), z)
 FOR i = cpx(1) TO cpx(z)
   q = eval(i)
   PSET (i, q + 100), 4
 NEXT
 LOCATE 26, 1: PRINT SPC(70);
 LOCATE 26, 1: INPUT "OK to Subtract this baseline"; resp$
 LOCATE 26, 1: PRINT SPC(70);
 IF resp$ = "Y" OR resp$ = "y" THEN
   LOCATE 26, 1: PRINT SPC(70);
   LOCATE 26, 1: PRINT "PLEASE WAIT- correcting baseline";
   i = cpx(1)
   q = eval(i)  'get the first control point
   FOR j = 1 TO i  'and evaluate for use with data points preceeding it
   ychan(ch, j) = ychan(ch, j) - q
   NEXT
   k = cpx(z)  'get the last control point
   FOR j = i + 1 TO k  ' do all points in the spline fitted region
     ychan(ch, j) = ychan(ch, j) - eval(j)
   NEXT
   q = eval(k)  'get last baseline correction
   FOR j = k + 1 TO lastpoint  ' do all points from end of spline to end of
data
     ychan(ch, j) = ychan(ch, j) - q
   NEXT
   LOCATE 26, 1: PRINT "BASELINE CORRECTION DONE";
   CALL initscreen
   CALL initialROI
   CALL titles
  END IF
 RETURN

Function3:  'enable cursor data follow mode
datahug = true
RETURN

function4:  'disable cursor data follow mode
datahug = false
RETURN

function5:
RETURN
```

```
function6:
RETURN
function7:
RETURN

function8:
RETURN

function9:

RETURN
function10:
RETURN

ErrHand1:  'filename.dat not found
 BEEP
 LOCATE 18, 22: PRINT SPC(37);
 LOCATE 18, 22
 IF ERR = filenotfound THEN
   PRINT filen$; "; NOT FOUND; ";
 ELSE
  PRINT "MISC DISK ERROR"; ERR;
 END IF
 FOR i = 1 TO 20000: NEXT
 LOCATE 18, 22: PRINT SPC(37);
 filefound = false
 RESUME NEXT

ErrHand2:  'DISK errors during a file save operation
  BEEP
  LOCATE 18, 22: PRINT SPC(37);
  LOCATE 18, 22
  diskerr = ERR
  SELECT CASE diskerr
  CASE IS = 61
  PRINT "DISK IS FULL- INSERT ANOTHER DISK";
  CASE IS = 52
  PRINT "ILLEGAL DOS FILENAME - TRY AGAIN";
  CASE IS = 64
  PRINT "BAD FILE NAME";
  CASE IS = 71
  PRINT "DISK NOT IN DRIVE OR UNFORMATTED-TRY AGAIN";
  CASE IS = 72
  PRINT "DISK ERROR DURING WRITE";
  CASE ELSE
  PRINT "MISC ERROR # "; ERR;
  END SELECT
  FOR i = 1 TO 20000: NEXT
  LOCATE 18, 22: PRINT SPC(37);
  CLOSE
  RESUME NEXT

FUNCTION eval (v AS SINGLE)
  DIM t, u AS SINGLE
  DIM i AS INTEGER

  i = 0
  DO
  i = i + 1  'Find spline segment to interpolate between
  LOOP UNTIL v <= cpx(i + 1)

  u = cpx(i + 1) - cpx(i)
  t = (v - cpx(i)) / u
  eval = t * cpy(i + 1) + (1 - t) * cpy(i) + u * u * (t * t * t - t) * p(i +
1) + ((1 - t) ^ 3 - (1 - t)) * p(i)
END FUNCTION
```

```
SUB frame (leftcol%, rightcol%, toprow%, bottomrow%) STATIC
  LOCATE toprow%, leftcol%  PRINT CHR$(201)
  LOCATE toprow%, rightcol%  PRINT CHR$(187)
  LOCATE bottomrow%, leftcol%  PRINT CHR$(200),
  LOCATE bottomrow%, rightcol%  PRINT CHR$(188)
  FOR vertline% = toprow% + 1 TO bottomrow% - 1
  LOCATE vertline%, leftcol%  PRINT CHR$(186),
  LOCATE vertline%, rightcol%  PRINT CHR$(186),
  NEXT
  horizlength% = rightcol% - leftcol% - 1
  horizline$ = STRING$(horizlength%, 205)
  LOCATE toprow%, leftcol% + 1  PRINT horizline$
  LOCATE bottomrow%, leftcol% + 1  PRINT horizline$,
END SUB

SUB getdatafile
ON ERROR GOTO ErrHand1
1000 filefound = true
     PRINT
     LOCATE 18, 22
     PRINT SPC(37),   LOCATE 18, 22
     INPUT "Enter Filename  ', filen$
     DEF SEG = VARSEG(ychan(1, 0))
     BLOAD filen$ + " dat", 0'errhand1 takes care if no file found
     IF filefound = false THEN 1000
     CLS
     PRINT "FILE LOADED SUCCESSFULLY  RUN WAS',
     CALL getlimits
     runmins = lastpoint / 600
     PRINT USING "### ##", runmins,
     PRINT "   MINUTES IN DURATION'
     injectionmark = ychan(2, 0)
     sigma = 0
     OPEN filen$ + " par" FOR INPUT AS #1
     INPUT #1, magfact
     CLOSE #1
  FOR i = 1 TO 5000  NEXT
ON ERROR GOTO 0
END SUB

SUB getlimits
 z = ychan(1, 0)
 IF z < 0 THEN z = z + c1
 lastpoint = z \ 4 - tapsd2
 firstpoint = 1
END SUB

SUB graphicsScreen
  SCREEN 12
  VIEW (10, 10)-(500, 400), , 15
  WINDOW (0, 0)-(16000, 20000)
  LOCATE 29, 1  PRINT 'Elapsed Time  ',
END SUB

SUB initialROI
cursx = firstpoint + cbhsz
cursy = ychan(ch, cursx)
GET (cursx - cbhsz, cursy - cbvsz)-(cursx + cbhsz, cursy + cbvsz), cbuf
LINE (cursx, cursy - cbvsz + 1)-(cursx, cursy + cbvsz - 1), 14
LINE (cursx - cbhsz + 1, cursy)-(cursx + cbhsz - 1, cursy), 9
END SUB

SUB initscreen
SCREEN 12, 0, 0
CLS
CALL getlimits
```

```
viewx0 = scrnxmax \ 12  viewx1 = scrnxmax * 11 \ 12
viewy0 = 1  viewy1 = scrnymax * 3 \ 4
VIEW (viewx0, viewy0)-(viewx1, viewy1), , 15
WINDOW (firstpoint, 0)-(lastpoint, 17000)
 PSET (1, 100 + ychan(ch, 1)), 1
  FOR i = 2 TO lastpoint STEP 2
   LINE -(i, 100 + ychan(ch, i)), 1
  NEXT
LINE (injectionmark, 0)-(injectionmark, 300), 14
cbvsz = 17000 / 100  cbhsz = (lastpoint - firstpoint) \ 150
END SUB

SUB MainMenu
CLS
COLOR 3
CALL frame(20, 60, 10, 20)
LOCATE 11, 30
PRINT 'BASELINE CORRECT',
LOCATE 12, 35
PRINT "MAIN MENU",
LOCATE 13, 22
PRINT "R-Retrieve a data file ,
LOCATE 14, 22
PRINT "F-Save current data to disk',
LOCATE 15, 22
PRINT 'D-display current data",
LOCATE 16, 22
PRINT "Q- Exit to operating system ( DOS )',
COLOR 7
END SUB

SUB makespline (x() AS SINGLE, y() AS SINGLE, n)
 DIM i AS INTEGER
 DIM d(1 TO maxcp), w(1 TO maxcp), u(1 TO maxcp) AS SINGLE
   FOR i = 2 TO n - 1   form TRI-DIAGONAL matrix
     d(i) = 2 * (x(i + 1) - x(i - 1))
   NEXT
   FOR i = 1 TO n   1
     u(i) = x(i + 1) - x(i)
   NEXT
   FOR i = 2 TO n - 1
   w(i) = (y(i + 1) - y(i)) / u(i) - (y(i) - y(i - 1)) / u(i - 1)
   NEXT
   FOR i = 2 TO n - 2   Gaussian Elimination
     d(i + 1) = d(i + 1) - u(i) * u(i) / d(i)
     w(i + 1) = w(i + 1) - w(i) * u(i) / d(i)
   NEXT
   p(1) = 0  p(n) = 0   'natural spline condition
   FOR i = n - 1 TO 2 STEP -1  'back substitution
   p(i) = (w(i) - u(i) * p(i + 1)) / d(i)
   NEXT
END SUB

SUB savedatafile
ON ERROR GOTO ErrHand2
     IF dataacquired = false THEN GOTO 111
     LOCATE 18, 22  PRINT SPC(37),
     LOCATE 18, 22
     fsize = ychan(1, 0)
     ychan(2, 0) = injectionmark
     IF fsize < 0 THEN fsize = fsize + c1
     INPUT 'Enter Filename  ', filen$
     DEF SEG = VARSEG(ychan(1, 0))
     BSAVE filen$ + ' dat', 0, fsize
     IF diskerr <> 0 THEN 111
     OPEN filen$ + ' par" FOR OUTPUT AS #1
```

```
      PRINT #1, magfact
      CLOSE #1
      LOCATE 18, 22  PRINT SPC(37),
      LOCATE 18, 22
      PRINT "FILE SAVED SUCCESSFULLY';
111:
ON ERROR GOTO 0
END SUB

SUB titles
  COLOR 1
  LOCATE 23, 1· PRINT "Chan";
  PRINT USING "##", ch,
  COLOR 11
  LOCATE 28, 1· PRINT "CAUTION- ";
  COLOR 9: PRINT "Place control points from LEFT to RIGHT !",
  COLOR 7
END SUB

SUB wcursdown
  FOR i = 10 TO 14  KEY(i) OFF: NEXT
  IF mark = false THEN
  PUT (cursx - cbhsz, cursy - cbvsz), cbuf, PSET
  END IF
 cursy = cursy - 20
 IF cursy < cbvsz THEN cursy = cbvsz
GET (cursx - cbhsz, cursy - cbvsz)-(cursx + cbhsz, cursy + cbvsz), cbuf
LINE (cursx, cursy - cbvsz + 1)-(cursx, cursy + cbvsz - 1), 14
LINE (cursx - cbhsz + 1, cursy)-(cursx + cbhsz - 1, cursy), 9
 IF mark = true THEN mark = false
FOR i = 10 TO 14· KEY(i) ON  NEXT
END SUB

SUB wcursorleft
  FOR i = 10 TO 14: KEY(i) OFF  NEXT
  IF mark = false THEN
  PUT (cursx - cbhsz, cursy - cbvsz), cbuf, PSET
  END IF
 cursx = cursx - 10
 IF cursx < cbhsz THEN cursx = cbhsz
IF datahug = true THEN cursy = ychan(ch, cursx)
GET (cursx - cbhsz, cursy - cbvsz)-(cursx + cbhsz, cursy + cbvsz), cbuf
LINE (cursx, cursy - cbvsz + 1)-(cursx, cursy + cbvsz - 1), 14
LINE (cursx - cbhsz + 1, cursy)-(cursx + cbhsz - 1, cursy), 9
 IF mark = true THEN mark = false
FOR i = 10 TO 14: KEY(i) ON  NEXT
END SUB

SUB wcursorright
  FOR i = 10 TO 14: KEY(i) OFF. NEXT
  IF mark = false THEN
  PUT (cursx - cbhsz, cursy - cbvsz), cbuf, PSET
  END IF
 cursx = cursx + 10
 IF cursx + cbhsz > lastpoint THEN cursx = lastpoint - cbhsz
 IF datahug = true THEN cursy = ychan(ch, cursx)
GET (cursx - cbhsz, cursy - cbvsz)-(cursx + cbhsz, cursy + cbvsz), cbuf
LINE (cursx, cursy - cbvsz + 1)-(cursx, cursy + cbvsz - 1), 14
LINE (cursx - cbhsz + 1, cursy)-(cursx + cbhsz - 1, cursy), 9
 IF mark = true THEN mark = false
FOR i = 10 TO 14: KEY(i) ON  NEXT
END SUB

SUB wcursup
  FOR i = 10 TO 14: KEY(i) OFF· NEXT
  IF mark = false THEN
```

```
   PUT (cursx - cbhsz, cursy - cbvsz), cbuf, PSET
   END IF
  cursy = cursy + 20
  IF cursy > 16000 - cbvsz THEN cursy = 16000 - cbvsz
GET (cursx - cbhsz, cursy - cbvsz)-(cursx + cbhsz, cursy + cbvsz), cbuf
LINE (cursx, cursy - cbvsz + 1)-(cursx, cursy + cbvsz - 1), 14
LINE (cursx - cbhsz + 1, cursy)-(cursx + cbhsz - 1, cursy), 9
  IF mark = true THEN mark = false
FOR i = 10 TO 14: KEY(i) ON: NEXT
END SUB
```

REFERENCES

1 V. D. Smissen, C. Ernst, U.S. Patent 3,213,747 (Oct. 26, 1965).

2 S. S. Brody and J. E. Chaney, J. Gas Chromatogr., 4 (2), 42 (1966).

3 M. C. Bowman and M. Beroza, Anal. Chem. 40, 1448 (1968).

4 R. R. Watts, J. AOAC, 53, 787 (1970).

5 G. Winnett, J. Chromatogr. Sci., 8, 554 (1970).

6 C. A. Burgett and L. E. Green, J. Chromatogr. Sci., 12, 356 (1974).

7 C. A. Burgett and L. E. Green, Spectrochim. Acta, 30B, 55 (1975).

8 P. L. Patterson, R. L. Howe and A. Abu-Shumays, Anal. Chem., 50, 339 (1978).

9 P. L. Patterson, Anal. Chem., 50, 345 (1978).

10 W. E. Dale and C. C. Hughes, J. Gas Chromatogr., 6, 603 (1968).

11 M. Dressler, J. Chromatogr., 262, 77 (1983).

12 A. Attair, R. Forgey, J. Horn, and W. H. Corocoran, J. Chromatogr. Sci., 15, 222 (1977).

13 W. A. Aue and C. G. Flinn, J. Chromatogr., 158, 161 (1978).

14 M. Maruyama and M. Kakemoto, J. Chromatogr. Sci., 16, 1 (1978).

15 T. Sugiyama, Y. Suzuki and T. Takeuchi, J. Chromatogr. 80, 61 (1973).

16 E. Mangani, F. Bruner, and N. Penna, Anal. Chem., 55, 2193 (1983).

17 S. Fredriksson and A. Cedergren, anal. Chem., 53, 614 (1981).

18 G. H. Liu and P. R. Fu, Chromatographia, 27, 159 (1989).

19 S. Kapila and C. R. Vogt, J. Chromatogr. Sci., 17, 327 (1979).

20 W. A. Aue and C. R. Hastings, J. Chromatogr., 87, 232 (1973).

21 W. A. Aue and C. G. Flinn, Anal. Chem., 52, 1537 (1980).

22 E. Atar, S. Cheskis and A. Amirav, Anal. Chem., 63, 2064 (1991).

23 C. H. Muller III. K. Schofield and M. Steinberg, Int. Symp. Combust., 17, 867 (1979).

24 T. Sugiyama, Y. Suzuki and T. Takeuchi, J. Chromatogr. Sci., 11, 639 (1973).

25 S. Kapila, D. O. Duebelbeis and S. E. Manahan, Flame Photometric Detectors, in Environmental Analysis Using Chromatography Interfaced with Atomic Spectroscopy, R. M. Harrison and S. Rapsomanikis, Eds.; Ellis Horwood Series in Analytical Chemistry, John Wiley & Sons: Chichester, 1989.

26 M. L. Selucky, Chromatographia, 4, 425 (1971).

27 T. Sugiyama, Y. Suzuki and T. Takeuchi, J. Chromatogr., 77, 309 (1973).

28 T. J. Caldwell and P. J. Marriott, J. Chromatogr. Sci., 20, 83 (1982).

29 S. O. Farwell and C. J. Barinaga, J. Chromatogr. sci., 24, 483 (1986).

30 A. Syty and J. A. Dean, Appl. Optics, 7, 1331 (1968).

31 P. T. Gilbert, in Analytical Flame Spectroscopy, ed. by R. Mavrodineanu, MacMillan, London, 1970.

32 E. J. Sowinski and I. H. Suffet, J. Chromatogr. Sci., 9, 632 (1971).

33 R. Ross and T. Shafik, J. Chromatogr. Sci., 11, 46 (1973).

34 W. A. Aue and C. G. Flinn, J. Chromatogr., 142, 145 (1977).

35 C. G. Flinn and W. A. Aue, J. Chromatogr., 186, 299 (1979).

36 C. G. Flinn and W. A. Aue, J. Chromatogr. Sci., 18, 136 (1980).

37 C. G. Flinn and W. A. Aue, Can. J. Spectr., 25, 141 (1980).

38 C. G. Flinn and W. A. Aue, J. Chromatogr., 153, 49 (1978).

39 E. J. Sowinski and I. H. Suffet, Anal. Chem., 46, 1218 (1974).

40 F. M. Zado and R. S. Juvet, Jr., Anal. Chem., 38, 571 (1966).

41 M. C. Bowman and M. Beroza, J. Chromatogr. Sci., 7, 484 (1969).

42 F. A. Gunther, A. Lopez-Roman, R. I. Asai and W. E. Westlake, Bull. Envir. Contam. Toxicol., 4, 202 (1969).

43 Y.-Z. Tang and W. A. Aue, J. Chromatogr., 408, 69 (1987).

44 M. C. Bowman, M. Beroza and G. Nickless, J. Chromatogr. Sci., 9, 44 (1971).

45 B. Versino and H. Vissers, Chromatographia, 8, 5 (1975).

46 B. Versino and G. Rossi, Chromatographia, 4, 331 (1971).

47 W. A. Aue and R. E. Moseman, J. Chromatogr., 61, 35 (1971).

48 A. V. Novak and H. V. Malmstadt, Anal. Chem., 40, 1108 (1968).

49 X.-Y. Sun and W. A. Aue, J. Chromatogr., 467, 75 (1989).

50 X.-Y. Sun and W. A. Aue, Can. J. Chem., 67, 897 (1989).

51 X.-Y. Sun and W. A. Aue, Mikrochim. Acta, I, 1 (1990).

52 W. A. Aue, B. Millier and X.-Y. Sun, Anal. Chem., 62, 2453 (1990).

53 W. A. Aue, B. Millier and X.-Y. Sun, Anal. Chem., 63, 2951 (1991).

54 V. A. Joonson and E. P. Loog, J. Chromatogr., 120, 285 (1976).

55 M. Dressler, Selective gas chromatographic detectors, J. Chrom. Library, Vol. 36, Elsevier, Amsterdam, 1986.

56 R. S. Hutte, R. E. Sievers and J. W. Birks, J. Chromatogr. Sci. 1986, 24, 499-505.

57 R. L. Benner and D. H. Stedman, Anal. Chem., 61, 1266 (1989).

58 B. D. Quimby and J. J. Sullivan, Anal. Chem. 1990, 62, 1027-1034.

59 S. E. Eckert-Tilotta, S. B. Hawthorne and D. J. Miller, J. Chromatogr. 1992,

591, 313-323.

60 H. G. Eckhardt, M. B. Denton and J. L. Moyers, J. Chromatogr. Sci., 13, 133 (1975).

61 W. A. Aue, B. Millier and X.-Y. Sun, Response Ratios in Chromatography", 75th CIC Conference, Edmonton, Alberta, Canada; June 1992.

62 Y.-Z. Tang, Ph.D. thesis, Dalhousie University, 1987.

63 X.-Y. Sun, B. Millier and W. A. Aue, Can. J. Chem., 70, 1129 (1992).

64 W. A. Aue, X.-Y. Sun and B. Millier, J. Chromatogr., 606, 73 (1992).

65 R. W. B. Pearse and A. G. Gaydon, The Indentification of Molecular Spectra, Chapman & Hall, London, 4th ed., 1976.

66 W. A. Aue, B. Millier and X.-Y. Sun, Can. J. Chem., 70, 1143 (1992).

67 W. F. Meggers, C. H. Corliss and B. F. Scribner, Tables of Spectral-Line Intensities, Part 1, NBS Monograph 145, National Bureau of Standards, U.S. Government Printing Office, Washington, DC, 2nd ed., 1975.

68 M. L. Parsons and P. M. McElfresh, Flame Spectroscopy: Atlas of Spectral Lines, IFI/Plenum, New York, 1971, p. 53.

69 P. C. Uden, D. E. Henderson, F. P. DiSanzo, R. J. Lloyd and T. Tetu, J. Chromatogr., 196, 403 (1980).

70 S. A. Estes, P. C. Uden and R. M. Barnes, Anal. Chem., 53, 1829 (1981).

71 T. R. Crompton, Comprehensive Organometallic Analysis, Plenum Press, New York, 1987, p. 418-423, 763-765.

72 G. W. Smith and A. K. Palmby, Anal. Chem., 31, 1798 (1959).

73 M. D. DuPuis and H. H. Hill Jr., Anal. Chem., 51, 292 (1979).

74 B. D. Quimby, P. C. Uden and R. M. Barnes, Anal. Chem., 50, 2112 (1978).

75 P. C. Uden, R. M. Barnes and F. P. DiSanzo, Anal. Chem., 50, 852 (1978).

76 M. Coe, R Cruz and J. C. VanLoon, Anal. Chem. Acta, 120, 171 (1980).

77 M. C. B. Hotz, Alternatives to Lead in Gasoline, The Royal Society of Canada. Commission on Lead in the Environment, Minister of Supply and Services Canada, Ottawa, Ontario, 1986.

78 Anonymous, Manganese, Environmental Health Criteria 17, World Health Organization, Geneva, Switzerland, 1981.

79 D. S. Lee, Anal. Chem., 54, 1182 (1982).

80 D. H. Stedman, D. A. Tammaro, 1976 Pittsburgh Conference Abstract #189, Anal. Letters, 9, 81 (1976).

81 R. E. Smith, Proc. R. Soc. Lond, A 332, 113 (1973).

82 R. S. Juvet, Jr. and R. P. Durbin, Anal. Chem., 38, 565 (1966).

83 R. S. Braman and E. S. Gordon, Proc. Ann. Inst. Autom. Conf. Exhibit 17, 13 (1962); C.A. 1964, 4754c.

84 R. S. Braman, Anal. Chem., 38, 734 (1966).

85 R. M. Dagnall, D. J. Smith, K. C. Thompson and T. S. West, Analyst 94, 871 (1969).

86 R. Belcher, S. L. Bogdanski, A. C. Calokerinos and A. Townshend, Analyst, 106, 625 (1981).

87 J. M. S Belcher and G. F. Kirkbright, Analyst, 103, 1104 (1978).

88 R. M. Dagnall, B. Fleet, T. H. Risby and D. R. Deans, Talanta, 18, 155 (1971).

89 P. F. McCrea and T. S. Light, Anal. Chem., 39, 1731 (1967).

90 J. W. Robinson and V. Smith, Anal. Chim. Acta, 36, 489 (1966)

91 J. J. Kroeten, H. W. Moody and M. L. Parsons, Anal. Chim , Acta 52, 101 (1970).

92 W. A. Aue, B. Millier and Sun, Abstract #36, 73rd CIC Conference, Halifax, N. S. (July 1990).